



Geneeskundige **S**tichting **K**oningin **E**lisabeth
Fondation **M**édicale **R**eine **E**lisabeth
Königin-**E**lisabeth-**S**tiftung für **M**edizin
Queen **E**lisabeth **M**edical **F**oundation

Verlag – Rapport – Bericht – Report

2017

G.S.K.E. – F.M.R.E. – K.E.S.M. – Q.E.M.F.

www.fmre-gske.be
www.fmre-gske.eu
www.fmre-gske.com

Geneeskundige Stichting Koningin Elisabeth 2017

Inleiding verslag activiteiten van de GSKE – FMRE

Zestien onderzoeksploegen werden in 2016 geselecteerd om financiële steun te ontvangen van de Stichting voor de volgende drie jaren (2017-2019).

De Wetenschappelijke dag in mei 2017, onder het erevoorzitterschap van H.K.H. Prinses Astrid, begon met een eerbetoon aan Prof de Barys overleden in 2016.

Het publiek luisterde emotioneel naar de toespraak van de Prinses ter nagedachtenis van Prof. de Barys. Zij heeft hem gedurende vele jaren gekend aan het hoofd van Stichting als wetenschappelijk directeur en nadien als voorzitter.

De voorzitter H. Deprez leidde de zitting in tijdens dewelke de onderzoeksploegen die financiële steun ontvangen van de Stichting werden voorgesteld en de wetenschappelijke prijzen 2017 werden uitgereikt.

De onderzoekers en hun onderzoeksprojecten werden kort voorgesteld door de Wetenschappelijk directeur: het betreft de Prof. dr. V. Baekelandt, PhD (KU Leuven), Prof. dr. Ir. S. De Meyer (KU Leuven-KULAK), Prof. dr. B. De Strooper, MD, PhD (KU Leuven), Prof. dr. A. Goris, PhD (KU Leuven), Prof. dr. W. Vandenberghe, MD.,PhD (KU Leuven), Prof. dr. P. Vangheluwe, PhD (KU Leuven), Prof. Dr. C. Verfaillie (KU Leuven), Prof. dr. T.Voets (KU Leuven), Prof. dr. V. Timmerman, PhD (UA), Prof. dr. L. Leybaert, PhD (UGent), Prof. dr. G. van Loo (UGent), Prof. dr. K. Vonck (UGent), Prof. dr.D. De Bundel, PhD (VUB). Prof. F. Tissir, PhD (UCL), Prof. dr. B. Vanhollebeke, PhD (ULB), Dr. L. Nguyen, PhD (ULg).

Tijdens de zitting werden vier prijzen uitgereikt:

- Prijs UCB in aanwezigheid van de heer H. Klitgaard aan Prof. P. Vanderhaeghen voor zijn onderzoekswerk: *“How to make cortical neurons : mechanism, evolution and diseases”* en aan Prof. F. Tissir voor zijn onderzoekswerk : *“Shaping the nervous system: role of the planar cell polarity genes”*
- Prijs Ernest Solvay, in aanwezigheid van de heer D. Solvay aan Prof. Julie Duqué voor haar onderzoekswerk: *“Parkinson’s disease revisited: a new vision of basal ganglia functions in the context of the Parkinson’s disease.”*
- Prijs CBC Banque, in aanwezigheid van de heer J-P Jansen aan Prof. G. van Loo, voor zijn onderzoekswerk: *“Endoplasmic reticulum stress in autoimmune central nervous system inflammation and demyelination.”*
- Prijs Janine et Jacques Delruelle in aanwezigheid van Baron en Barones Delruelle aan Prof. SN. Schiffmann voor zijn onderzoekswerk: *“Basal ganglia’s functions and disorders: from specific genes and signalling pathways to neuronal sub-populations.”*

De zitting werd afgesloten met een receptie, een ideaal moment voor de onderzoekers om onderling van gedachten te wisselen, de genodigden en de aanwezige gezagsdragers te ontmoeten.

De onderzoeksploegen hebben hun projecten ontwikkeld in 2017 en in 2016 verschenen 55 publicaties met de steun van de Stichting. Deze werken werden gepubliceerd in gerenommeerde tijdschriften en waren de aanleiding tot het geven van verschillende presentaties op nationale en internationale wetenschappelijke bijeenkomsten.

Op 23 november 2017 bracht H.K.H. Prinses Astrid een bezoek aan twee laboratoria van de KU Leuven: de laboratoria van Prof T. Voets en P. Vangheluwe.

Zij was vergezeld van de Voorzitter, de heer H. Deprez, de Afgevaardigd bestuurder N. De Bruyne, de Wetenschappelijk directeur en de secretaris van de Geneeskundige Stichting.

Zij werd ontvangen door de autoriteiten van de KU Leuven, de Rector, de Decaan en verschillende personaliteiten.

Dit bezoek startte met wetenschappelijke presentaties, gevolgd door een bezoek aan de laboratoria en eindigde met een aangename receptie.

Het Wetenschappelijk Comité ontving de publicaties en de activiteitsrapporten 2017 van de onderzoeksgroepen die zullen gebruikt worden om de drie prijzen toe te kennen tijdens de wetenschappelijke dag op 26 april 2018.

Wij danken zeer hartelijk H.K.H. Prinses Astrid voor Haar steun en Haar aanwezigheid op de activiteiten, georganiseerd door de Stichting.

Wij danken ook de leden van de Raad van Bestuur en het Wetenschappelijk Comité voor hun werk dat zij doen ten voordele van de onderzoekers in het domein van de neurowetenschappen in ons land en dank zij de steun van mecenasen kunnen de onderzoekers hun innovatieve projecten verder ontwikkelen.

Prof. dr. Jean-Marie Maloteaux,
wetenschappelijk directeur
Brussel, 30 december 2017

Seize équipes de recherches furent sélectionnées en 2016 pour bénéficier du soutien financier de la Fondation pour les trois ans à venir (2017-2019).

La journée scientifique de mai 2017, placée sous la présidence d'honneur de S.A.R. la Princesse Astrid, débuta par un hommage au Professeur de Barys décédé en 2016. C'est avec beaucoup d'émotion que le public a écouté le discours de la Princesse à propos du Professeur de Barys qu'elle a connu durant de nombreuses années à la tête de la Fondation en tant que Directeur scientifique puis Président.

Le président H. Deprez introduisit la réunion qui fut l'occasion de présenter les équipes de recherche qui bénéficieront du soutien de la Fondation et aussi de remettre les Prix scientifiques. Les chercheurs et leurs projets de recherche ont été présentés brièvement par le Directeur scientifique : il s'agit des Prof. dr. V. Baekelandt, PhD (KU Leuven), Prof. dr. Ir. S. De Meyer (KU Leuven-KULAK), Prof. dr. B. De Strooper, MD, PhD (KU Leuven), Prof. dr. A. Goris, PhD (KU Leuven), Prof. dr. W. Vandenberghe, MD., PhD (KU Leuven), Prof. dr. P. Vangheluwe, PhD (KU Leuven), Prof. Dr. C. Verfaillie (KU Leuven), Prof. dr. T. Voets (KU Leuven), Prof. dr. V. Timmerman, PhD (UA), Prof. dr. L. Leybaert, PhD (UGent), Prof. dr. G. van Loo (UGent), Prof. dr. K. Vonck (UGent), Prof. dr. D. De Bundel, PhD (VUB), Prof. F. Tissir, PhD (UCL), Prof. dr. B. Vanhollebeke, PhD (ULB), Dr. L. Nguyen, PhD (ULg).

Au cours de la séance, quatre prix furent décernés :

- Prix UCB en présence de monsieur H. Klitgaard au Prof. P. Vanderhaeghen pour son travail *"How to make cortical neurons : mechanism, evolution and diseases"* et au Prof. F. Tissir pour son travail : *"Shaping the nervous system: role of the planar cell polarity genes"*.
- Prix Ernest Solvay, en présence de monsieur D. Solvay au Prof. J. Duqué pour son travail *"Parkinson's disease revisited: a new vision of basal ganglia functions in the context of the Parkinson's disease."*
- Prix CBC Banque, en présence de monsieur J-P Jansen au Prof G. van Loo, pour son travail : *"Endoplasmic reticulum stress in autoimmune central nervous system inflammation and demyelination."*
- Prix Janine et Jacques Delruelle en présence du Baron et la Baronne Delruelle au Prof. S. N. Schiffmann pour son travail : *"Basal ganglia's functions and disorders: from specific genes and signalling pathways to neuronal sub-populations."*

La séance s'est terminée par une réception qui a permis aux chercheurs de discuter et de rencontrer les mécènes, les membres du public et les autorités présentes.

Les équipes ont développé leurs projets en neurosciences durant l'année 2017 et 55 publications furent réalisées en 2016 avec le soutien de la Fondation. Ces travaux furent publiés dans des revues de haut niveau et permirent aussi de nombreuses présentations dans des réunions nationales et internationales.

Le 23 novembre 2017, S.A.R. la Princesse Astrid a visité deux laboratoires de la KU Leuven: les laboratoires des Professeurs T. Voets et P. Vangheluwe. Accompagnée par le Président H. Deprez, l'Administrateur délégué N. De Bruyne, le Directeur scientifique et le secrétaire de la Fondation Médicale, elle fut accueillie par les autorités de la KU Leuven, le Recteur, le Doyen et de nombreuses personnalités. Cette visite débuta par des exposés scientifiques et fut suivie d'une visite des laboratoires et d'une agréable réception.

Le Comité scientifique a reçu les publications et rapports d'activités des groupes de recherche de l'année 2017 et ceux-ci serviront à décerner trois prix lors de la prochaine journée scientifique du 26 avril 2018.

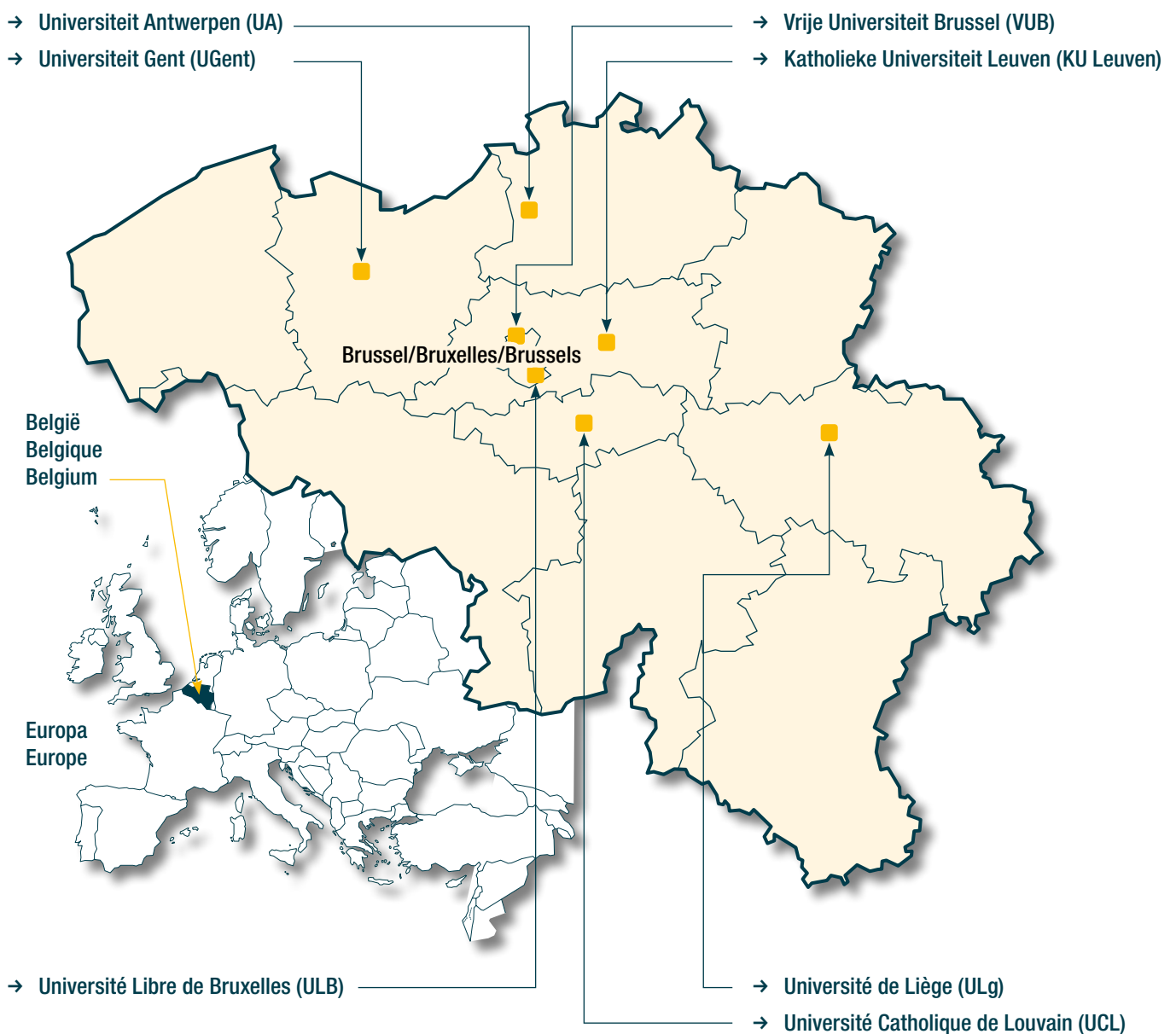
Nous remercions vivement S.A.R. la Princesse Astrid pour Son soutien et Sa présence aux évènements organisés par la Fondation. Nous remercions également les membres du Conseil d'Administration et du Comité scientifique pour le travail qu'ils accomplissent au bénéfice des chercheurs en neurosciences de notre pays qui grâce aux mécènes peuvent développer leurs projets innovants.

Prof. dr. Jean-Marie Maloteaux,
directeur scientifique
Bruxelles, 30 décembre 2017

Universiteiten met onderzoeksprogramma's die gesteund worden door de G.S.K.E.

Universités ayant des programmes de recherche subventionnés par la F.M.R.E.

Universities having research programs supported by the Q.E.M.F.



Onderzoeksprogramma's gefinancierd door de G.S.K.E. -
Programma 2017-2019

Programmes de recherche subventionnés par la F.M.R.E. -
Programme 2017-2019

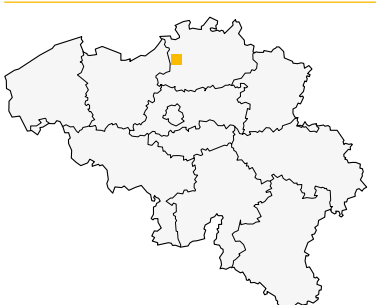
Q.E.M.F. funded research projects -
Program 2017-2019

KU Leuven



- **Prof. dr. Baekelandt Veerle, PhD**
The role of alpha-synuclein aggregation, spreading and neuroinflammation in Parkinson's disease and related disorders.
- **Prof. dr. Ir De Meyer Simon**
Neutrophil extracellular traps: novel targets for neuroprotection in stroke.
- **Prof. dr. De Strooper Bart, MD. PhD**
The study of the initial cellular phase of Alzheimer's disease.
- **Prof. Goris An, PhD**
Unraveling the BAFF pathway towards targeted treatment of multiple sclerosis.
- **Prof. dr. Vandenberghe Wim, MD. PhD**
LRRK2, Rab10 and mitochondrial quality control in Parkinson's disease.
- **Prof. dr. Vangheluwe Peter, PhD**
Neuroprotection by lysosomal transport mechanisms in Parkinson's disease.
- **Prof. dr. Verfaillie Catherine**
Unraveling the role of TREM2 mutations in Alzheimer's disease using human Pluripotent Stem Cells.
- **Prof. Voets Thomas**
Unraveling the role of TRMP3 in neuropathic and inflammatory pain.

UA



- **Prof. dr. Timmerman Vincent, PhD**
Unravelling the novel molecular pathways contributing to distal hereditary motor neuropathy caused by mutant HSPB8 with the aim to identify potential therapeutic targets.

UCL



- **Prof. Fadel Tissir, PhD**
Development and malformations of the cerebral cortex: role of the diaphanous 3 gene.

UGent



- **Prof. dr. Leybaert Luc, MD. PhD**
Exploring the role of astroglial Cx43 hemichannels as therapeutic targets in stroke.
- **Prof. dr. Geert van Loo, PhD**
Microglia, inflammasomes and multiple sclerosis.
- **Prof. dr. Vonck Kristl**
The role of locus coeruleus noradrenergic neurons in the mechanism of vagus nerve stimulation and the effect of selective activation of these neurons in epilepsy.

ULB



- **Prof. Vanhollebeke Benoit, PhD**
Organ-wide analysis of brain neurovascular communication in real-time and at single-cell resolution.

ULg



- **Dr. Nguyen Laurent, PhD**
Deciphering the role of protein ubiquitination in human cortical malformation and hearing impairment.

VUB



- **Prof. dr. De Bundel Dimitri, PhD**
Chemogenetic interrogation of neuromedin U involvement in stress-induced psychopathology.

Progress reports of the university research groups, supported by the Queen Elisabeth Medical Foundation in collaboration with the following professors and doctors (2017)

Prof. dr. Baekelandt Veerle, PhD	11
Prof. dr. De Bundel Dimitri, PhD	21
Prof. dr. Ir. De Meyer Simon	31
Prof. dr. De Strooper Bart, MD. PhD	47
Prof. Goris An, PhD	55
Prof. dr. Leybaert Luc, MD. PhD	67
Dr. Laurent Nguyen, PhD & dr. Brigitte Malgrange	77
Prof. dr. Timmerman Vincent, PhD	87
Prof. Fadel Tissir, PhD	95
Prof. dr. Vandenberghe Wim, MD. PhD	109
Prof. dr. Vangheluwe Peter, PhD	127
Prof. Vanhollebeke Benoit, PhD	135
Prof. dr. Geert van Loo, PhD	149
Prof. dr. Verfaillie Catherine	159
Prof. Voets Thomas	167
Prof. dr. Vonck Kristl	175



Geneeskundige Stichting Koningin Elisabeth
Fondation Médicale Reine Elisabeth
Königin-Elisabeth-Stiftung für Medizin
Queen Elisabeth Medical Foundation

Progress report
of the research group of

Prof. dr. Baekelandt Veerle, PhD

Katholieke Universiteit Leuven (KU Leuven)

Principal investigator

Prof. dr. Baekelandt Veerle, PhD
Laboratory for Neurobiology and Gene Therapy
Division of Molecular Medicine K.U.Leuven –
Faculty of Medicine Kapucijnenvoer 33 VCTB+5
B-3000 Leuven
Belgium
Tel.: +32 16 37 40 61
Fax: +32 16 33 63 36
E-mail: Veerle.Baekelandt@kuleuven.be

The role of α -synuclein aggregation, spreading and neuroinflammation in Parkinson's disease and related disorders

WP1. Characterization of seeding and spreading properties of patient-derived α -SYN assemblies

In this WP1 we aim to bridge the gap between preclinical studies using recombinant protein and the human pathology. To this end, we will test patient-derived *in vitro* amplified α -SYN assemblies in the rodent brain and compare those to recombinant α -SYN assemblies for disease-inducing properties in terms of α -SYN spreading and pathology.

1.1. Isolation and characterization of patient-derived α -SYN assemblies

Brain samples of patients with PD (Parkinson's Disease), MSA (Multiple System Atrophy) and DLB (Dementia with Lewy bodies) obtained from the UK Brain Bank via Prof. S. Gentleman (Imperial College London, UK; n=8-10/group) have been extensively characterized from a clinicopathological point of view. These samples have been transferred to the group of our collaborator Prof. R. Melki (CNRS, France) who has isolated, purified and characterized the different α -SYN assemblies present. As a result, WP 1.1 has been completed successfully.

1.2. *In vivo* characterization of patient-derived α -SYN strains

Patient-derived homogenates as well as *in vitro* amplified α -SYN assemblies have been injected into the substantia nigra (SN) of BAC transgenic rats expressing human full-length wild-type α SYN. These injected animals are subjected to the cylinder test on a monthly basis and statistical analyses on this behavioral assay are ongoing. We will sacrifice the injected BAC transgenic rats at 8 months post injection based on their behavioral performance. We will perform immunohistochemical analysis on the isolated rat brains to assess the effect of the different α -SYN species on dopaminergic neurodegeneration by stereological quantification of tyrosine hydroxylase (TH) positive cell bodies and nerve terminals. This assessment will be complemented with neuropathological characterization based on stainings for α -SYN, phosphorylated α -SYN (which is a pathology-related form of the protein) and the aggresome marker p62. We plan to finish the immunohistochemical analysis by June 2018. In conclusion, WP 1.2 is on track and the proposed timelines are met so far.

WP2. Elucidation of the role of the innate immune system in α -SYN spreading and neurotoxicity

Evidence is emerging that α -SYN can adopt distinct conformations, also referred to as 'strains', which are characterized by remarkable differences in structural and phenotypic features (Bousset et al. 2013, Peelaerts et al. 2015). Therefore, presentation of different α -synuclein assemblies (monomers, oligomers or fibrils) to the innate immune system and the subsequent immune response might be a driving force in the disease, although the exact α -SYN strains which might trigger this inflammatory response have not yet been identified (Hansen et al. 2011).

2.1. Characterization of the microglial response to different α -SYN assemblies

In this part of the WP, we have studied the phenotype of BV2 cells (immortalized murine microglial cell line) in response to exogenous administration of recombinant α -SYN assemblies including oligomers and two different fibrillar α -SYN strains, called fibrils and ribbons (**Fig. 1, B-D**). Fibrils and ribbons display distinct structural properties and present different toxicity and propagation propensity in cell culture

(Bousset et al. 2013). The different α -SYN assemblies were administered to BV2 cells for 24 hours and the microglial cell response was assessed by qPCR. Untreated and BSA-treated cells were included as negative controls, whereas lipopolysaccharide (LPS) and IL4 treated cells were used as positive control for the pro-inflammatory and anti-inflammatory profile, respectively.

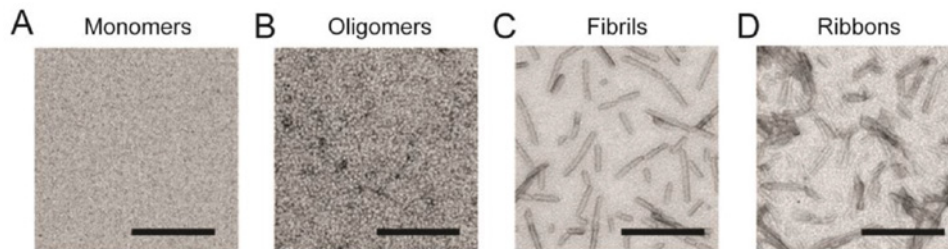


Figure 1 – Different recombinant α -SYN assemblies. A-D, Electron micrographs of α -SYN monomers (A), oligomers (B), fibrils (C) and ribbons (D) used throughout this study. The scale bars represent 200 nm.

As a result, the pro-inflammatory microglial markers iNOS, TNF α , IL1 β and IL6 were significantly elevated in response to fibrils and ribbons, whereas the expression of these markers remained stable upon treatment with oligomeric α -SYN (**Fig. 2 E-H**). In contrast, microglial anti-inflammatory markers (i.e., Arg1 and Fizz1) were remarkably downregulated after administration of both fibrillar α -SYN assemblies compared to the BSA control. However, these anti-inflammatory markers remained stable upon treatment with oligomeric α -SYN (**Fig. 2 I, J**). From these results, we conclude that both α -SYN fibrils and ribbons induce the classical pro-inflammatory microglial phenotype and suppress the alternative repair state, characterized by the expression of anti-inflammatory markers.

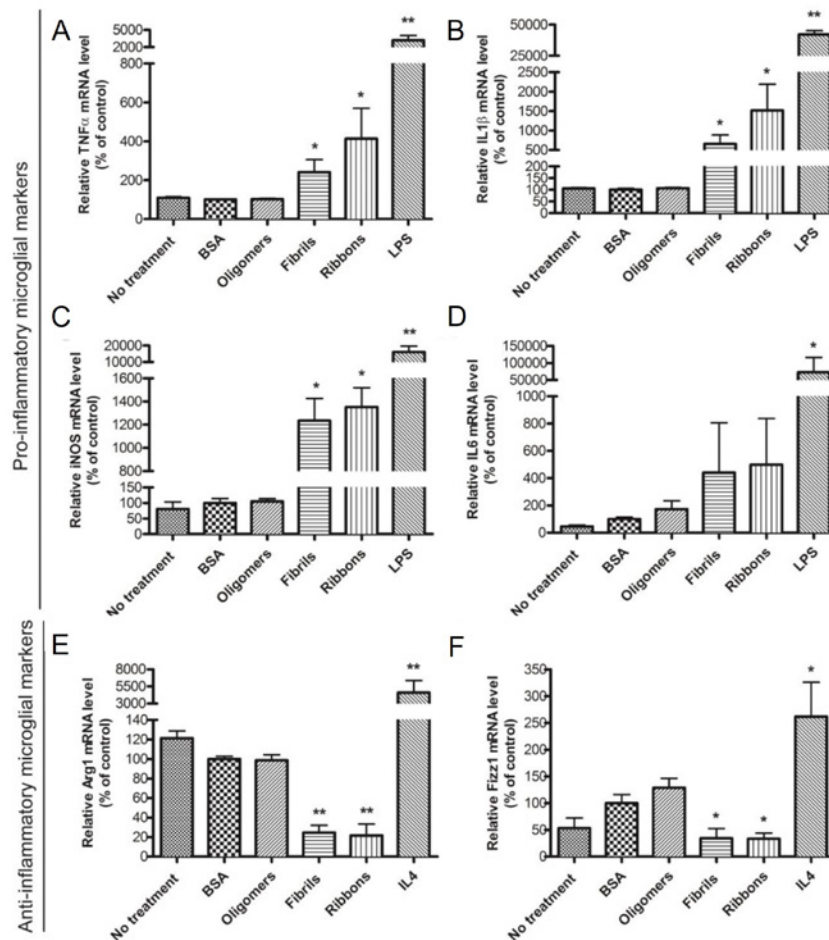


Figure 2 – Microglial phenotype of BV2 cells after treatment with different α -SYN assemblies. E-J, Quantification of mRNA levels of TNF α (E), IL1 β (F), iNOS (G), IL6 (H), Arg1 (I) and Fizz1 (J) in BV2 cells upon administration of the two different fibrillar forms of α -SYN (fibrils and ribbons, 1 μ M each) or oligomeric α -SYN (1 μ M). LPS (2.5 mg/ml) and IL4 (20 ng/ml) treatments were used as a positive control for the pro-inflammatory and anti-inflammatory profile, respectively. Untreated cells and cells treated with BSA (1 μ M) were used as negative controls. Mean \pm SEM are shown (n=3). * p < 0.05, ** p < 0.01 (Van der Perren *et al.*, unpublished results).

To further define the microglial inflammatory response with respect to the different α -SYN assemblies, we extended our study to primary microglia isolated from mouse brain. We administered the two distinct fibrillar α -SYN strains (fibrils and ribbons), as well as α -SYN monomers and oligomers to primary microglia (**Fig. 3**). Treatment with BSA was used as a negative control, while administration of LPS and IL4 was included as positive control for the pro- and anti-inflammatory profile, respectively. First, in order to assess the uptake of the different α -SYN assemblies, we performed double immunocytochemistry for α -SYN and the microglial marker Iba1, 24 hours after administration of the α -SYN strains. As shown in Fig. 3, the different α -SYN assemblies were taken up by primary microglia. However, α -SYN fibrils and ribbons seemed to be internalized by microglial cells more efficiently than oligomeric and monomeric α -SYN based on qualitative analysis of confocal images. To confirm these findings, we are currently analyzing in detail both the uptake and degradation of the different α -SYN assemblies over time.

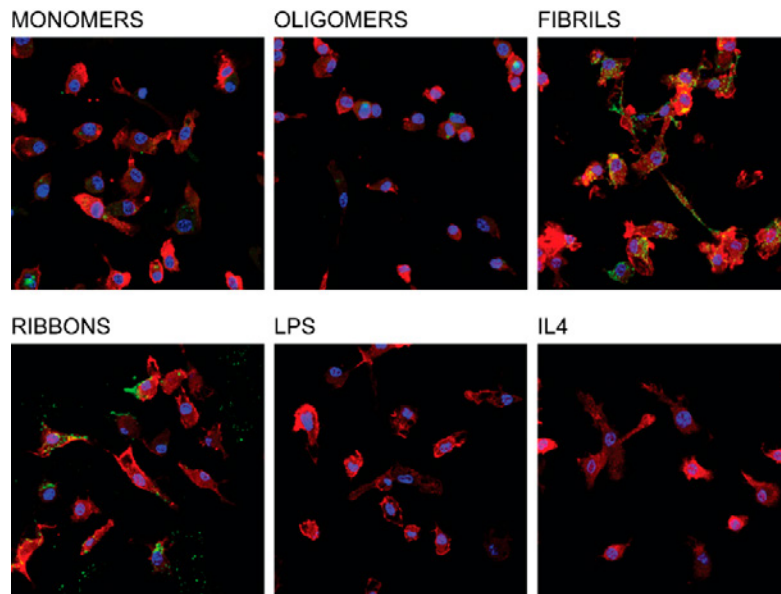


Figure 3 - Uptake of different α -SYN assemblies by murine primary microglia.

Double immunofluorescent staining for human α -SYN (green) and murine Iba1 (red) of primary microglia treated with different α -SYN strains for 24 hours. α -SYN fibrils and ribbons are taken up more efficiently by microglial cells. LPS and IL4 treatment were included as positive control for the pro-inflammatory and anti-inflammatory profile, respectively. Scale bar = 50 μ m (Van der Perren *et al.*, unpublished results).

Further, we analyzed the microglial pro-inflammatory response in reaction to the different α -SYN assemblies. We found that the expression of TNF α , IL1 β and IL6 was strongly upregulated upon administration of α -SYN fibrils and ribbons, but remained stable after treatment with monomeric and oligomeric α -SYN (Fig. 4). In line with the results obtained in BV2 cells, primary microglia showed a pronounced pro-inflammatory response but only towards the fibrillar forms of α -SYN.

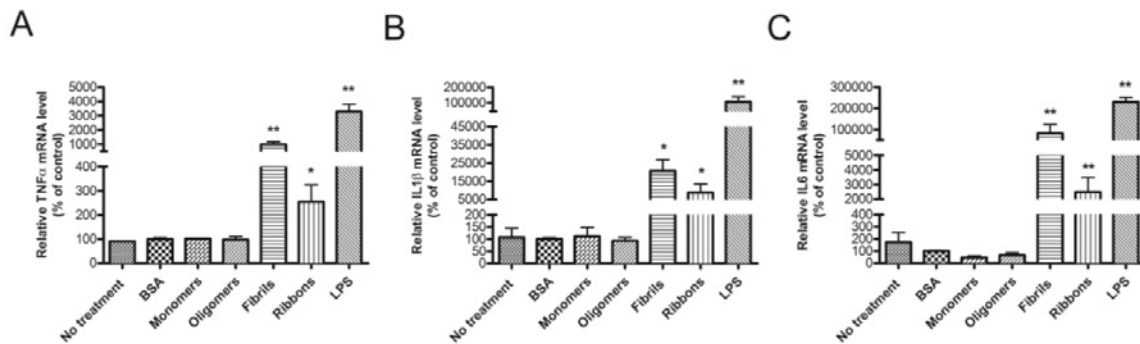


Figure 4 - Characterization of the pro-inflammatory response in primary microglia upon treatment with different α -SYN assemblies. Quantification of mRNA levels of TNF α (A), IL1 β (B) and IL6 (C) in murine primary microglia upon administration of the two different fibrillar α -SYN forms (fibrils and ribbons, 1 μ M each) or oligomeric α -SYN (1 μ M). LPS treatment (2.5 mg/ml) was used as positive control. Untreated cells and cells treated with BSA (1 μ M) were included as negative controls. Mean \pm SEM are shown (n=3). * p < 0.05, ** p < 0.01 (Van der Perren *et al.*, unpublished results).

In a next step, primary neurons will be exposed to the microglial supernatant or microglia-neuron co-cultures will be used to investigate the effect of microglia priming, in response to α -SYN, on neuronal toxicity. We are currently optimizing our primary neuronal cultures with regard to purity in order to co-culture them with microglia (Fig. 5). As a quality control for the purity of our primary cortical neurons, we have transduced these cultures with a lentiviral vector expressing eGFP under control of the CMV (cytomegalovirus) promoter. Double immunofluorescent stainings for eGFP and GFAP (glial fibrillary acidic protein) revealed that there are few glial cells present in our neuronal cultures. Finally, we will

also perform a triple staining for eGFP/NeuN/GFAP and eGFP/NeuN/Iba1 to assess the number of astrocytes and microglia present in the cultures. Once optimized, neuronal integrity will be assessed through functional live cell imaging, immunocytochemistry and western blot analysis.

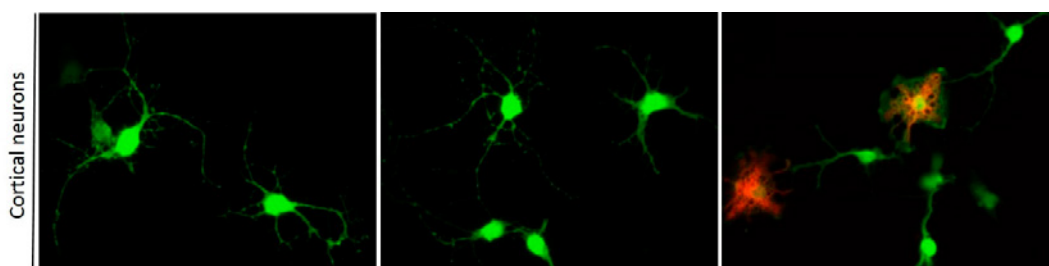


Figure 5 – Evaluation of the purity of primary cortical neurons. Immunofluorescent staining for eGFP (green) and GFAP (red) of primary cortical neurons after transduction with a lentiviral vector expressing eGFP under control of the CMV promoter.

In order to study the microglial immune response in reaction to different α -SYN assemblies *in vivo*, we have stereotactically injected α -SYN monomers, oligomers and the two fibrillar α -SYN strains into the SN of adult mice. Mice injected with BSA were included as a negative control. Two days post injection, we sacrificed the animals and performed immunohistochemical analysis using the CD11b antibody in order to visualize the microglial cells (**Fig. 6**). As a result, we observed an increase in the number of CD11b positive cells in the injected side of the brain upon exposure to α -SYN fibrils and ribbons compared to control animals injected with BSA. A less pronounced microglial response was detected upon administration of α -SYN oligomers, while CD11b positive cells were almost undetectable in animals injected with α -SYN monomers. These results suggest that the fibrillar α -SYN assemblies are more prone to induce microglial activation *in vivo* compared to oligomeric and monomeric species. We are currently analyzing the brains from mice injected with the different α -SYN assemblies, which were sacrificed six months post injection, using immunohistochemical analysis for phosphorylated α -SYN, Iba1, Arg, CD68, and YM1 in order to study possible alterations in the microglial immune response over time.

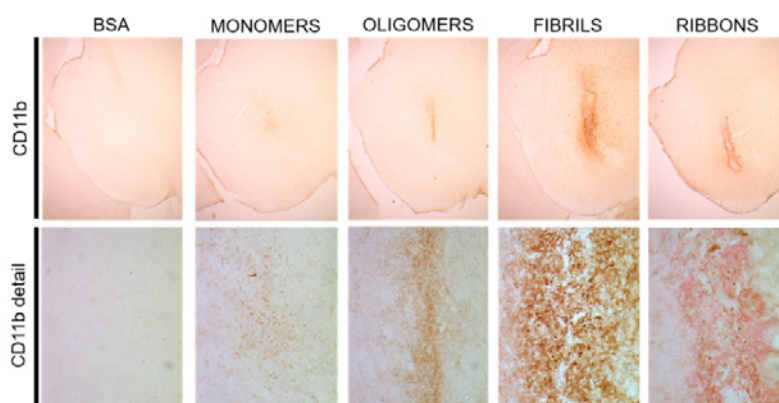


Figure 6 – Characterization of the microglial response upon stereotactic injection of different α -SYN assemblies in the mouse SN. Immunohistochemical staining for CD11b showing the presence of microglia, two days after injection of recombinant α -SYN strains in the SN. BSA was injected as a negative control (Van der Perren *et al.*, unpublished results).

We have chosen to use mice for these experiments instead of rats as the experiments in the next WP will be mainly performed in transgenic mice. However, we will perform immunohistochemical stainings for different inflammatory markers in the animals used in WP 1.2. We did not start the experiments with patient-derived α -SYN assemblies in this WP, we preferred to start studying the microglial response towards well-characterized recombinant α -SYN assemblies. In a later stage in the project, we will assess the microglial response towards patient-derived samples. In conclusion, WP 2.1 is currently ongoing.

2.2. Analysis of the origin of inflammatory cells

To gain insights into the involvement of inflammatory cells in α -SYN spreading and neurotoxicity, we will use a double transgenic reporter mouse model (CX3CR1^{GFP}/CCR2^{RFP}) to distinguish microglia from peripheral macrophages. At the moment, we are breeding CX3CR1^{GFP}/CCR2^{RFP} transgenic mice and have already obtained relevant groups of young mice (n=6-8/group) for our experiments. We have started optimizing the immunohistochemical analysis in the CX3CR1^{GFP}/CCR2^{RFP} mice after stereotactic injection with LPS (**Fig. 7**). In a next step, we will inject the distinct α -SYN assemblies and perform confocal fluorescent microscopic analysis as well as FACS analysis to analyze the innate immune response.

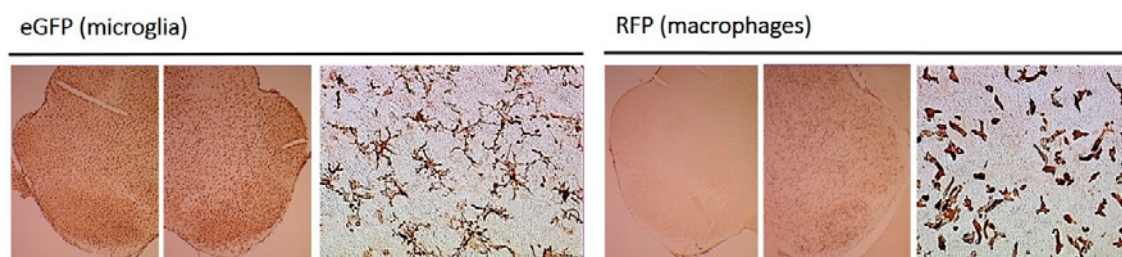


Figure 7 – Characterization of microglial response upon stereotactic injection of LPS in mouse SN of CX3CR1^{GFP}/CCR2^{RFP} mice. Immunohistochemistry for eGFP showing the presence of microglia two days after injection of LPS in the SN. Immunohistochemistry for RFP (red fluorescent protein) showing the presence of infiltrating macrophages two days after injection of LPS in the SN (Van der Perren *et al.*, unpublished results).

2.3. Manipulation of the microglial response

To better understand the role of the innate immune system in α -SYN spreading and neurotoxicity, we will experimentally deplete the microglia using a CSF1R inhibitor (PLX3397) in the CX3CR1^{GFP}/CCR2^{RFP} transgenic mice. To investigate the effect of microglial depletion on α -SYN induced neuronal cell death, CX3CR1^{GFP}/CCR2^{RFP} transgenic mice will be stereotactically injected with rAAV α -SYN vector into the SN. In this experimental set-up, we will analyze the impact of microglial cell depletion on neurodegeneration as well as motor behavior, six weeks post injection. In a second approach, we will assess the involvement of the innate immune system in α -SYN spreading. Therefore, recombinant α -SYN assemblies (fibrils or ribbons), will be administered to CX3CR1^{GFP}/CCR2^{RFP} transgenic mice through different routes: directly into the brain or peripherally into the blood stream. Subsequent pathology will be assessed using immunohistochemical analysis to examine α -SYN aggregation and spreading. Moreover, we will study the effect of microglia depletion on other cell types present in the central nervous system (neurons and astrocytes) and in the periphery (macrophages) via immunocytochemistry and flow cytometry. Finally, we will investigate whether the absence of microglia alters the adaptive immune response by analyzing and quantifying T cell infiltration in the brain by immunohistochemistry and flow cytometry. We plan to initiate this WP in the second year as planned in the project.

3. Scientific communication

We have presented our intermediate results at international conferences and meetings. We are writing down our results and plan to publish in highly-ranked peer-reviewed scientific journals.

3.1. Publications

Gelders G, Baekelandt V and Van der Perren A, **Linking Neuroinflammation and Neurodegeneration in Parkinson's disease**, Journal of Immunology Research, Special Issue: "Immune and Inflammatory-Mediated Disorders: From Bench to Bedside". Review paper submitted

3.2. List of conferences and meetings

- **Alzheimer Disease & Parkinson's Disease (ADPD) meeting**, Vienna, Austria, March 29 - April 2 2017. Poster presentation
- **Venusberg Meeting on Neuroinflammation**, Bonn, Germany, May 11-15 2017. Poster presentation
- **12th National Congress of the Belgian Society for Neuroscience**, Ghent, Belgium, May 22 2017. Poster presentation
- **20 years of alpha-synuclein in Parkinson's disease and other related synucleinopathies. "From the bedside to the bench and back to the patient"**. Athens, Greece, September 7-10 2017. Poster presentation
- **Neuroscience meeting (SFN)**, Washington DC, US, November 9-15 2017. Selected for dynamic poster presentation

4. References

- Bousset, L., L. Pieri, G. Ruiz-Arlandis, J. Gath, P. H. Jensen, B. Habenstein, K. Madiona, V. Olieric, A. Böckmann, B. H. Meier, and R. Melki. 2013. "Structural and functional characterization of two alpha-synuclein strains." *Nat Commun* 4:2575. doi: 10.1038/ncomms3575.
- Hansen, C., E. Angot, A. L. Bergström, J. A. Steiner, L. Pieri, G. Paul, T. F. Outeiro, R. Melki, P. Kallunki, K. Fog, J. Y. Li, and P. Brundin. 2011. "α-Synuclein propagates from mouse brain to grafted dopaminergic neurons and seeds aggregation in cultured human cells." *J Clin Invest* 121 (2):715-25. doi: 10.1172/JCI43366.
- Peelaerts, W., L. Bousset, A. Van der Perren, A. Moskalyuk, R. Pulizzi, M. Giugliano, C. Van den Haute, R. Melki, and V. Baekelandt. 2015. "α-Synuclein strains cause distinct synucleinopathies after local and systemic administration." *Nature* 522 (7556):340-4. doi: 10.1038/nature14547.



Geneeskundige Stichting Koningin Elisabeth
Fondation Médicale Reine Elisabeth
Königin-Elisabeth-Stiftung für Medizin
Queen Elisabeth Medical Foundation

Progress report
of the research group of

Prof. dr. De Bundel Dimitri, PhD

Vrije Universiteit Brussel (VUB)

Principal investigator

Prof. dr. Dimitri De Bundel

Co-investigators

Prof. dr. Ilse Smolders

Prof. dr. Ann Van Eeckhaut

Research Group Experimental Pharmacology, Center for Neurosciences
Department of Pharmaceutical and Pharmacological Sciences
Vrije Universiteit Brussel
Laarbeeklaan 103
1090 Brussels

Neuromedin U involvement in stress-induced psychopathology

1. Stress and the hypothalamus-pituitary-adrenal axis

The brain is the central organ for adaptation to psychobiological stressors because it determines what is threatening, stores relevant memories, and regulates physiological and behavioural responses (1). These allostatic responses enable an organism to actively adapt to its changing environment and achieve stability. Activation of the hypothalamus-pituitary-adrenal-axis (HPA axis) is a key physiological allostatic process characterized by release of corticotropin-releasing hormone (CRH) from the hypothalamic paraventricular nucleus (PVH), adrenocorticotrophic hormone (ACTH) from the pituitary and glucocorticoids such as cortisol and corticosterone (CORT) from the adrenal cortex (1). Release of glucocorticoids initiates a series of cardiovascular, metabolic and behavioural coping mechanisms. However, when allostatic load exceeds the physiological regulatory capacity, due to the unpredictable or uncontrollable nature of stressors, HPA axis activity can become maladaptive, leading to inappropriate physiological and behavioural responses that may impede coping and recovery (1, 2). Not surprisingly, stress has been identified as a major risk factor for the development of cardiovascular, metabolic and mental disorders (3-5). More specifically, excessive HPA axis activation following stress exposure is associated with alterations in neuronal activity, changes in spine morphology, dendritic remodelling, suppression of dentate gyrus neurogenesis, and inappropriate behavioural responses that are proposed to be core features in the aetiology of psychiatric disorders such as post-traumatic stress disorder and major depression (6). Neuropeptides are typically released by discrete neuronal populations and may enable diversified physiological and behavioural responses to a wide range of stressors through their specific projections in the brain.

Position	1	2	3	4	5	6	7	8	9	10	11	12	13	14	15	16	17	18	19	20	21	22	23	24	25
Human NMU-25	Phe	Arg	Val	Asp	Glu	Glu	Phe	Gln	Ser	Pro	Phe	Ala	Ser	Gln	Ser	Arg	Gly	Tyr	Phe	Leu	Phe	Arg	Pro	Arg	Asn -NH ₂
Rat NMU-23	Tyr	Lys	Val	Asn	Glu	*	Tyr	Gln	Gly	Pro	*	Val	Ala	Pro	Ser	Gly	Gly	Phe	Phe	Leu	Phe	Arg	Pro	Arg	Asn -NH ₂
Mouse NMU-23	Phe	Lys	Ala	*	Glu	*	Tyr	Gln	Ser	Pro	Ser	Val	Gly	Gln	Ser	Lys	Gly	Tyr	Phe	Leu	Phe	Arg	Pro	Arg	Asn -NH ₂

Figure 1. The structure of NMU in distinct species. The highly conserved C-terminus is shown in bold. Structural homology between human, rat and mouse sequences is emphasized by elongation with gaps represented by an asterix (*). Adapted from (7)

2. Neuromedin U and the stress response

Neuromedin U (NMU) is a neuropeptide coded by the *Nmu* gene showing a remarkable amino acid sequence homology across mammals (7), suggesting a strong evolutionary pressure to maintaining its structure and function (Figure 1). The C-terminal amidated heptapeptide is entirely conserved in mammals and the C-terminal amidated octapeptide NMU-8 exerts the same biological effects as its longer endogenous isoforms, NMU-25 in humans or NMU-23 in rodents (7). NMU-like immunoreactivity has been detected in neurons of the brain, spinal cord and mesenteric plexus (7). NMU activates two G-protein coupled receptors: NMUR1 receptors that are mainly expressed in the periphery and NMUR2 receptors that mainly expressed in the brain and spinal cord (8, 9). NMU was previously demonstrated to modulate food intake and stress responsiveness through activation of hypothalamic NMUR2 receptors (8, 10-13). Nevertheless, precise anatomical knowledge remains lacking and in-depth insight in the role of NMU systems in the brain remains hampered by the lack of specific and sensitive research tools. For this reason, we developed a knock-in mouse model expressing Cre recombinase under the *Nmu* promotor to enable a highly specific expression of proteins for anatomical and physiological characterisation of NMU-producing cells based on tools exploiting Cre-lox recombination.

3. Results obtained in 2017

3.1. Neuroanatomical characterization of NMU-expressing cells in the central nervous system

We generated a B6.NmuCre-IRES-Nmu knock-in mouse model constitutively expressing a Cre recombinase in NMU-producing cells in collaboration with Dr. Peter Boyd (GeneOway, France). This was achieved by insertion of Cre-IRES-Nmu cDNA in frame with the ATG coding sequence of the *Nmu* gene on chromosome 5qC3.3. This strategy was designed to minimize the risk of interfering with regulatory elements while inserting exogenous elements and to avoid deregulating the targeted *Nmu* gene and the neighbouring genes. We encountered a delay in the final stages of the project due to small litter sizes and initial failure in excision of the Neo-selection cassette. These issues were resolved by mid-2017 and heterozygous B6.NmuCre-IRES-Nmu mice were delivered. We are now crossing these heterozygous B6.NmuCre-IRES-Nmu mice with homozygous B6.*ROSA26RCL-ZsGreen1* reporter mice that harbour a targeted mutation of the *ROSA26* gene locus with a loxP-flanked STOP cassette preventing transcription of a CAG promoter-driven enhanced green fluorescent protein (*ZsGreen1*). Cre recombination should lead to the expression of *ZsGreen1* NMU-producing cells. We will validate the appropriate expression of Cre recombinase in our mouse model using fluorescence in-situ hybridization (FISH) in collaboration with Dr. Eve Seuntjens (Katholieke Universiteit Leuven). Hereto, we have cloned three antisense RNA probes based on distinct designed primer pairs that hybridize to NMU of the mouse. Essentially, RNA was extracted from mouse tissue, RNA was reverse transcribed to copy DNA, inserted into a PCRII-topo vector and transformed into DH5a E.coli bacterial cells for selection of clones with correct insertion of the appropriate DNA sequence (Figure 2).

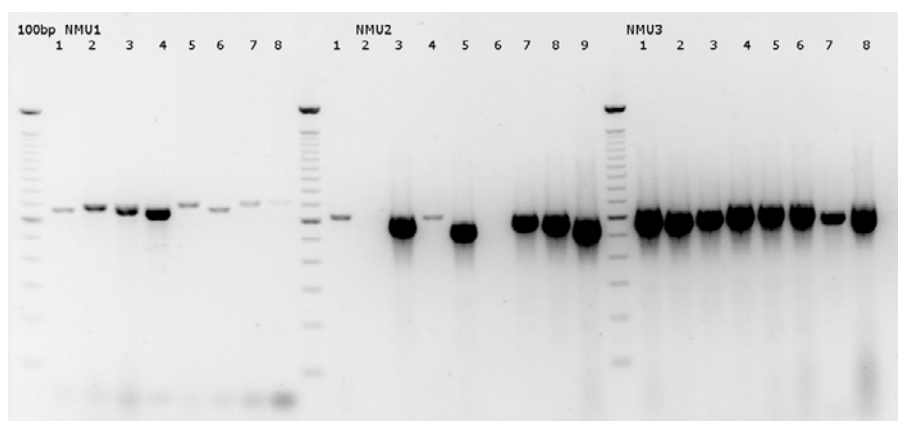


Figure 2. PCR for detection of correct DNA insertion in eight colonies for three different NMU probes based on distinct designed primer pairs.

Vectors containing the DNA insertion in the correct orientation were purified, linearized and transcribed to antisense RNA probes with digoxigenin-11-UTP tag for detection. Validation of the B6.NmuCre-IRES-Nmu will be finished in the first trimester of 2018. We expect to obtain our results for the neuroanatomical characterization of NMU expressing cells in the central nervous system as outlined in our application by the end of 2018.

3.2. Neuroanatomical activity mapping following central administration of NMU

We proposed to investigate how direct manipulation of NMU-expressing cells in B6.NmuCre-IRES-Nmu knock-in mice affects stress-responsiveness. Given the delay in the production of our mouse model, we carried out preliminary experiments in C57BL6/J mice to validate our proof of concept that NMU increases activity in the HPA axis in mice. We used an immunohistochemical approach to map neuronal activation following intracerebroventricular (i.c.v.) administration of NMU-8 using c-Fos immunoreactivity as a marker for antibodies against the immediately early gene c-Fos, a marker for neuronal activation.

We found that NMU-8 significantly increased c-Fos expression in the arcuate nucleus (ARC) and in the paraventricular hypothalamus (PVH) (Figure 3).

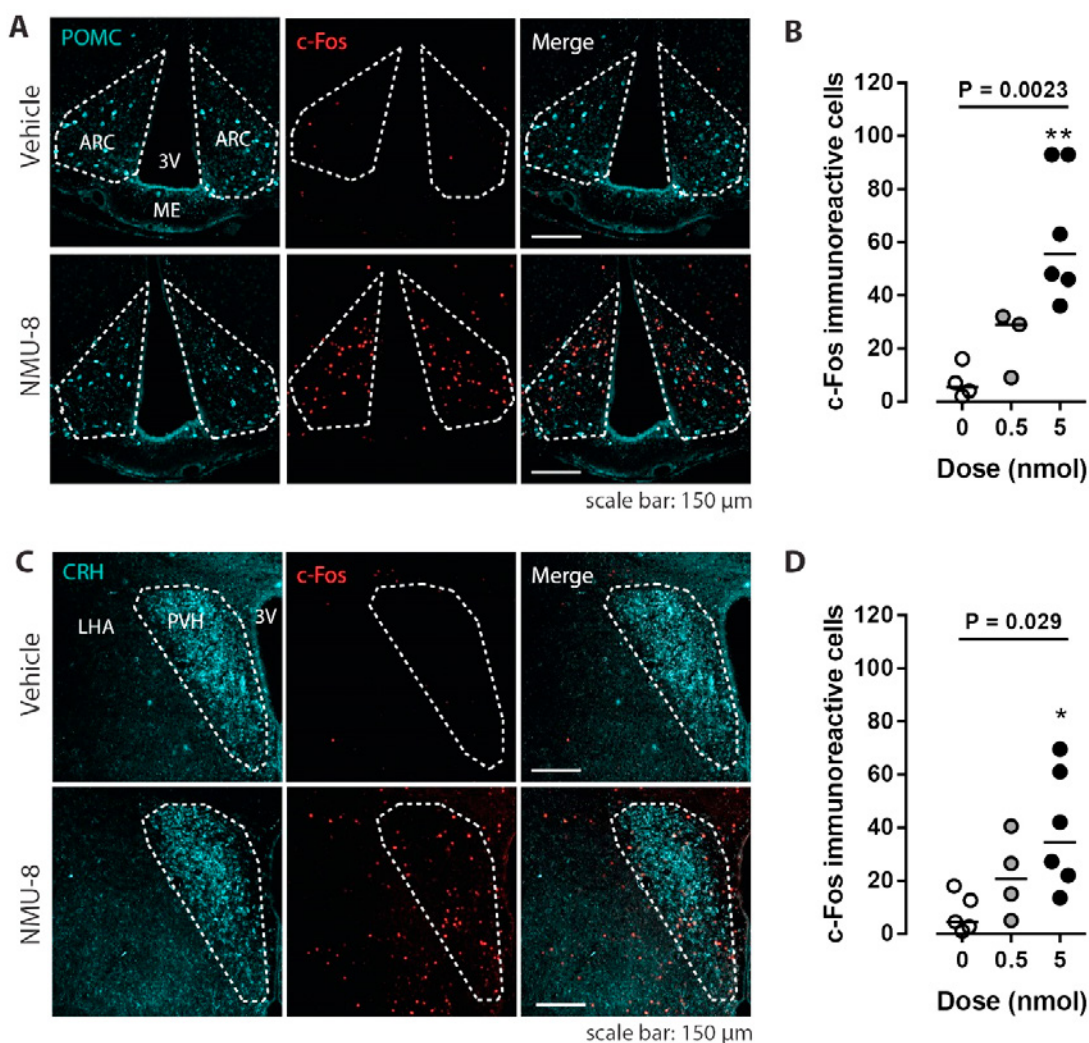


Figure 3. Effects of central administration of NMU-8 on expression of the immediately early gene *c-Fos* in the arcuate nucleus (ARC), identified using antibodies against pro-opiomelanocortin (POMC), and the paraventricular hypothalamus (PVH), identified using antibodies against corticotropin-releasing hormone (CRH), in C57BL6/J mice. Representative confocal images (A,C) and quantification by an observer blinded to treatment (B,D) show that intracerebroventricular (i.c.v.) administration of the highest dose of NMU-8 (5 nmol) significantly increases the number of *c-Fos* immunoreactive cells in both the ARC and PVH. Data are represented as a dot plot for individual values with designation of the median value and $N=3-6$ per group. * $P<0.05$ and ** $P<0.01$ versus vehicle (0 nmol) analysed by Kruskal-Wallis followed by Dunn's post-hoc test. ARC: arcuate nucleus, ME: medial eminence, LHA: lateral hypothalamus, PVH: paraventricular hypothalamus, 3V: third ventricle.

Activation of these brain regions has been proposed to underlie the effects of NMU on food intake and stress-responsiveness (8, 13-15). In addition, we are presently investigating *c-Fos* immunoreactivity in putative target brain areas regulating stress-responsiveness such as the paraventricular thalamus, the bed nucleus stria terminalis and the central amygdala.

3.3. Behavioural effects of central administration of NMU

In line with the effects of central administration of NMU-8 on *c-Fos* immunoreactivity in the hypothalamus of C57BL6/J mice, we observed a significant increase in grooming behaviour following i.c.v. administration of NMU-8 but no effects on digging activity or overall locomotor activity (Figure 4). NMU-induced grooming behaviour was previously observed in rats and was attributed to activation of the HPA axis (13). To substantiate this observation, we next investigated whether NMU-8 administration affects stress-responsiveness in the forced swim test.

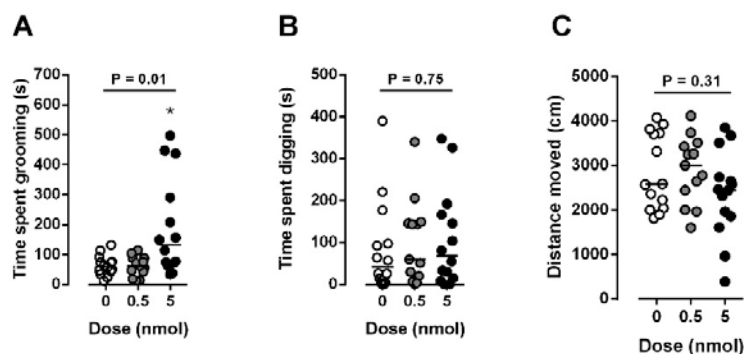


Figure 4. Effects of central administration of NMU-8 on home cage activity in C57BL6/J mice. Intracerebroventricular (i.c.v.) administration of vehicle or NMU-8 was carried out at the onset of a 20 min observation period. The total time spent grooming (A), time spent digging (B), and total distance moved (C) were scored by an observer blinded to treatment. Mice treated with the highest dose of NMU-8 (5.0 nmol) showed significantly higher grooming activity compared to control mice. Data are presented as a dot blot for individual values with designation of the median and N=10-11 per group. * $P < 0.05$ versus vehicle controls analysed by Kruskal-Wallis followed by Dunn's post-hoc test.

In line with our hypothesis, i.c.v. administration of NMU-8 increased behavioural despair in the forced swim test (Figure 5). This suggests that blocking NMU-8 function may suppress depression-like behaviour. We will further investigate this using a silencing approach in B6.NmuCre-IRES-Nmu knock-in mice after their in-depth characterization.

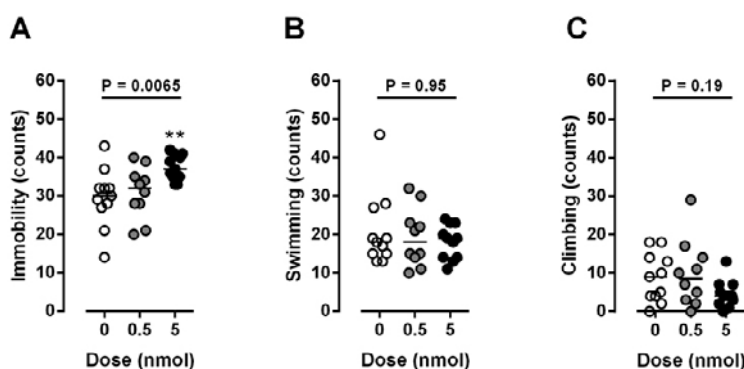


Figure 5. Effects of central administration of NMU-8 on behavioural despair in C57BL6/J mice. Intracerebroventricular (i.c.v.) administration of vehicle or NMU-8 was carried out 20 minutes before the 5 min forced swim test. Immobility (A), swimming (B), and climbing (C) were scored over 5 second bins. Mice treated with the highest dose of NMU-8 (5.0 nmol) showed significantly higher immobility compared to control mice. Data are presented as a dot blot for individual values with designation of the median and N=13-14 per group. * $P < 0.05$ versus vehicle controls analysed by Kruskal-Wallis followed by Dunn's post-hoc test.

3.4. Optimization of nanoUHPLC-MS/MS parameters for NMU quantification

We proposed to investigate NMU release in targeted brain areas following direct manipulation of NMU-containing neurons. We will adopt an optogenetic approach using Cre-dependent expression of channel rhodopsin (ChR2), a yellow light-sensitive cation channel, in B6.NmuCre-IRES-Nmu mice. ChR2 expression will permit stimulating NMU-containing cells at a specific frequency (1-20 Hz) using an implanted optical fibre connected to an appropriate light-source. NMU release will be determined by intracerebral microdialysis and nanoUHPLC-MS/MS. For this purpose we have investigated parameters that influence the loss of peptide caused by adsorption to the *in vivo* microdialysis setup. Our results clearly showed that the perfusion solvent exerts an important effect on peptide recovery. Moreover, the separation of four neuromedin-like peptides was investigated on four different core-shell stationary phases. In addition, the effect of the mobile phase composition, i.e. organic modifier (acetonitrile and methanol) and additive (trifluoroacetic acid, formic acid, acetic acid, ammonium formate and ammonium acetate) on the chromatographic performance was studied. An improvement in chromatographic performance was observed when using the ammonium salt instead of its corresponding acid as additive,

except for the column containing a positively charged surface (C18+). In general, the RP-Amide column provided the highest separation power with different mobile phases. However, for the neuromedin-like peptides of interest, the C18+ column in combination with a mobile phase containing methanol as organic modifier and acetic acid as additive provided more efficient peaks. A three-factor, three-level design was applied to further optimize the method in terms of increased peak height and reduced solvent consumption, without loss in resolution. The optimized method was subsequently used to assess the *in vitro* microdialysis recovery of the peptides of interest. Recovery values between 4 and 8% were obtained using a perfusion flow rate of 2 $\mu\text{L}/\text{min}$. These results were recently published in the Journal of Pharmaceutical and Biomedical Analysis (16) and in Chromatographia (17).

3.5. Development of NMU receptor ligands

In parallel with the experiments in the B6.NmuCre-IRES-Nmu knock-in mouse model, we also aim to develop subtype-selective, stable and blood-brain-barrier permeable pharmacological NMU receptor ligands. In collaboration with Prof. Dr. Steven Ballet (Vrije Universiteit Brussel) and Dr. Brigitte Holst (University of Copenhagen) we have now developed a set of novel NMU-analogues based on NMU-8 ($\text{Tyr}^1\text{-Phe}^2\text{-Leu}^3\text{-Phe}^4\text{-Arg}^5\text{-Pro}^6\text{-Arg}^7\text{-Asn}^8\text{-NH}_2$), by introducing unnatural amino acids into the native sequence. This approach shows that it is possible to generate molecules with increased potency and improved plasma stability without major changes of the peptidic nature or the introduction of large conjugates. The developed ligands showed agonist activity for NMU receptors and substitution of Phe^4 or Pro^6 respectively changed selectivity towards NMUR1 or NMUR2. To study the effect of the modifications on the proteolytic stability of the molecules, an *in vitro* stability assay in human plasma at 37 °C was performed. All analysed analogues possessed an increased resistance against enzymatic degradation in human plasma resulting in half-lives from 4 min for NMU-8, up to more than 23 h for compound 42 (Figure 6). These results were recently published in the European Journal of Medicinal Chemistry (18)

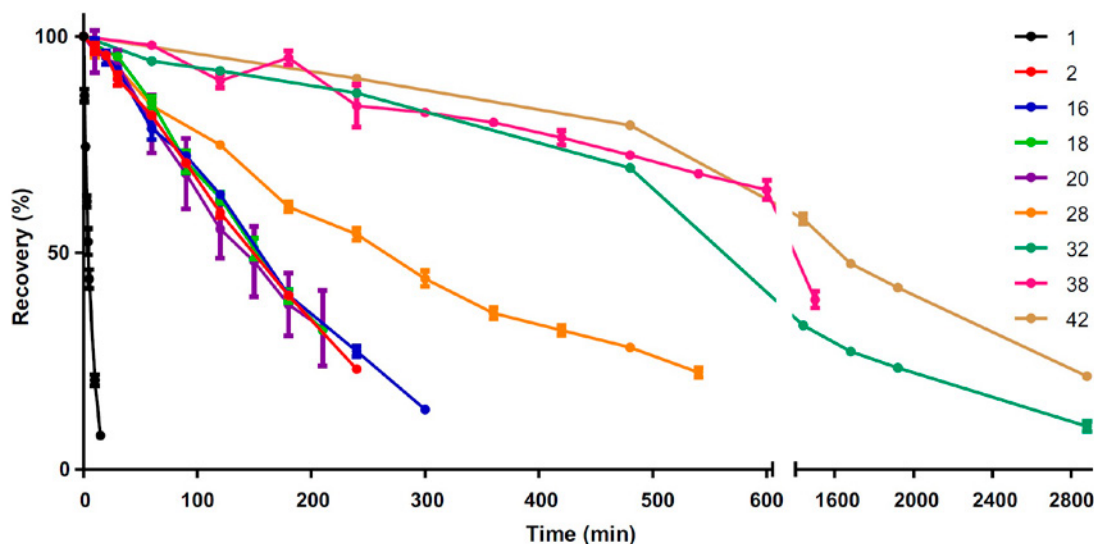


Figure 6. Percentage of recovery of NMU-analogues in human plasma incubated at 37 °C. The experiments were performed in triplicate and the results are presented as mean \pm SEM ($n = 3$).

4. References

1. B. S. McEwen, N. P. Bowles, J. D. Gray, M. N. Hill, R. G. Hunter, I. N. Karatsoreos, C. Nasca, Mechanisms of stress in the brain. *Nature neuroscience* **18**, 1353-1363 (2015); published online EpubOct (10.1038/nn.4086).
2. J. M. Koolhaas, A. Bartolomucci, B. Buwalda, S. F. de Boer, G. Flugge, S. M. Korte, P. Meerlo, R. Murison, B. Olivier, P. Palanza, G. Richter-Levin, A. Sgoifo, T. Steimer, O. Stiedl, G. van Dijk, M. Wöhr, E. Fuchs, Stress revisited: a critical evaluation of the stress concept. *Neuroscience and biobehavioral reviews* **35**, 1291-1301 (2011); published online EpubApr (10.1016/j.neubiorev.2011.02.003).
3. A. Steptoe, Diabetes: Stress resilience and risk of type 2 diabetes mellitus. *Nature reviews. Endocrinology* **12**, 189-190 (2016); published online EpubApr (10.1038/nrendo.2016.17).
4. A. Steptoe, M. Kivimäki, Stress and cardiovascular disease. *Nature reviews. Cardiology* **9**, 360-370 (2012); published online EpubJun (10.1038/nrcardio.2012.45).
5. C. Pittenger, R. S. Duman, Stress, depression, and neuroplasticity: a convergence of mechanisms. *Neuropsychopharmacology : official publication of the American College of Neuropsychopharmacology* **33**, 88-109 (2008); published online EpubJan (10.1038/sj.npp.1301574).
6. B. S. McEwen, C. Nasca, J. D. Gray, Stress Effects on Neuronal Structure: Hippocampus, Amygdala, and Prefrontal Cortex. *Neuropsychopharmacology : official publication of the American College of Neuropsychopharmacology* **41**, 3-23 (2016); published online EpubJan (10.1038/npp.2015.171).
7. P. J. Brighton, P. G. Szekeres, G. B. Willars, Neuromedin U and its receptors: structure, function, and physiological roles. *Pharmacological reviews* **56**, 231-248 (2004); published online EpubJun (10.1124/pr.56.2.3).
8. A. D. Howard, R. Wang, S. S. Pong, T. N. Mellin, A. Strack, X. M. Guan, Z. Zeng, D. L. Williams, Jr., S. D. Feighner, C. N. Nunes, B. Murphy, J. N. Stair, H. Yu, Q. Jiang, M. K. Clements, C. P. Tan, K. K. McKee, D. L. Hreniuk, T. P. McDonald, K. R. Lynch, J. F. Evans, C. P. Austin, C. T. Caskey, L. H. Van der Ploeg, Q. Liu, Identification of receptors for neuromedin U and its role in feeding. *Nature* **406**, 70-74 (2000); published online EpubJul 6 (10.1038/35017610).
9. J. Gartlon, P. Szekeres, M. Pullen, H. M. Sarau, N. Aiyar, U. Shabon, D. Michalovich, K. Steplewski, C. Ellis, N. Elshourbagy, M. Duxon, T. E. Ashmeade, D. C. Harrison, P. Murdock, S. Wilson, A. Ennaceur, A. Atkins, C. Heidebreder, J. J. Hagan, A. J. Hunter, D. N. Jones, Localisation of NMU1R and NMU2R in human and rat central nervous system and effects of neuromedin-U following central administration in rats. *Psychopharmacology* **177**, 1-14 (2004); published online EpubDec (10.1007/s00213-004-1918-3).
10. H. Zeng, A. Gragerov, J. G. Hohmann, M. N. Pavlova, B. A. Schimpf, H. Xu, L. J. Wu, H. Toyoda, M. G. Zhao, A. D. Rohde, G. Gragerova, R. Onrust, J. E. Bergmann, M. Zhuo, G. A. Gaitanaris, Neuromedin U receptor 2-deficient mice display differential responses in sensory perception, stress, and feeding. *Molecular and cellular biology* **26**, 9352-9363 (2006); published online EpubDec (10.1128/MCB.01148-06).
11. A. Peier, J. Kosinski, K. Cox-York, Y. Qian, K. Desai, Y. Feng, P. Trivedi, N. Hastings, D. J. Marsh, The antiobesity effects of centrally administered neuromedin U and neuromedin S are mediated predominantly by the neuromedin U receptor 2 (NMUR2). *Endocrinology* **150**, 3101-3109 (2009); published online EpubJul (10.1210/en.2008-1772).
12. E. S. Graham, Y. Turnbull, P. Fotheringham, K. Nilaweera, J. G. Mercer, P. J. Morgan, P. Barrett, Neuromedin U and Neuromedin U receptor-2 expression in the mouse and rat hypothalamus: effects of nutritional status. *Journal of neurochemistry* **87**, 1165-1173 (2003); published online EpubDec (
13. R. Hanada, M. Nakazato, N. Murakami, S. Sakihara, H. Yoshimatsu, K. Toshinai, T. Hanada, T. Suda, K. Kangawa, S. Matsukura, T. Sakata, A role for neuromedin U in stress response. *Biochemical and biophysical research communications* **289**, 225-228 (2001); published online EpubNov 23 (10.1006/bbrc.2001.5945).
14. M. Yokota, Y. Ozaki, F. Sakamoto, S. Yamada, J. Saito, H. Fujihara, Y. Ueta, Fos expression in CRF-containing neurons in the rat paraventricular nucleus after central administration of neuromedin U. *Stress* **7**, 109-112 (2004); published online EpubJun (10.1080/10253890410001727370).
15. E. L. Thompson, K. G. Murphy, J. F. Todd, N. M. Martin, C. J. Small, M. A. Ghatei, S. R. Bloom, Chronic administration of NMU into the paraventricular nucleus stimulates the HPA axis but does not influence food intake or body weight. *Biochemical and biophysical research communications* **323**, 65-71 (2004); published online EpubOct 8 (10.1016/j.bbrc.2004.08.058).
16. Y. Van Wanseele, J. Viaene, L. Van den Borre, K. Dewachter, Y. Vander Heyden, I. Smolders, A. Van Eeckhaut, LC-method development for the quantification of neuromedin-like peptides. Emphasis on column choice and mobile phase composition. *J Pharm Biomed Anal* **137**, 104-112 (2017); published online EpubApr 15 (10.1016/j.jpba.2017.01.014).
17. Y. Van Wanseele, K. Maes, K. Lanckmans, J. Van Schoors, I. Smolders, A. Van Eeckhaut, Surface and Solvent Dependent Adsorption of Three Neuromedin-Like Peptides in Glass and Plastic Syringes. *Chromatographia*, (2017); published online EpubOctober 12 (10.1007/s10337-017-3397-9).
18. A. De Prins, C. Martin, Y. Van Wanseele, L. J. Skov, C. Tomboly, D. Tourwe, V. Caveliers, A. Van Eeckhaut, B. Holst, M. M. Rosenkilde, I. Smolders, S. Ballet, Development of potent and proteolytically stable human neuromedin U receptor agonists. *Eur J Med Chem* **144**, 887-897 (2017); published online EpubDec 14 (10.1016/j.ejmech.2017.12.035).

5. Publications acknowledging support from G.S.K.E.

- Y. Van Wanseele, J. Viaene, L. Van den Borre, K. Dewachter, Y. Vander Heyden, I. Smolders, A. Van Eeckhaut, LC-method development for the quantification of neuromedin-like peptides. Emphasis on column choice and mobile phase composition. *J Pharm Biomed Anal* 137, 104-112 (2017); published online EpubApr 15 (10.1016/j.jpba.2017.01.014).
- Y. Van Wanseele, K. Maes, K. Lanckmans, J. Van Schoors, I. Smolders, A. Van Eeckhaut, Surface and Solvent Dependent Adsorption of Three Neuromedin-Like Peptides in Glass and Plastic Syringes. *Chromatographia*, (2017); published online EpubOctober 12 (10.1007/s10337-017-3397-9).
- A. De Prins, C. Martin, Y. Van Wanseele, L. J. Skov, C. Tomboly, D. Tourwe, V. Caveliers, A. Van Eeckhaut, B. Holst, M. M. Rosenkilde, I. Smolders, S. Ballet, Development of potent and proteolytically stable human neuromedin U receptor agonists. *Eur J Med Chem* 144, 887-897 (2017); published online EpubDec 14 (10.1016/j.ejmech.2017.12.035).



Geneeskundige Stichting Koningin Elisabeth
Fondation Médicale Reine Elisabeth
Königin-Elisabeth-Stiftung für Medizin
Queen Elisabeth Medical Foundation

Progress report
of the research group of

Prof. dr. Ir. De Meyer Simon

Katholieke Universiteit Leuven (KU Leuven)

Principal investigator

Prof. dr. ir. Simon De Meyer
Laboratory for Thrombosis Research
IRF Life Sciences Department of Cardiovascular Sciences
KU Leuven Kulak
E. Sabbelaan 53
8500 Kortrijk
Belgium
Tel.: +32 56 24 62 32
Fax: +32 56 24 69 97
E-mail: simon.demeyer@kuleuven-kortrijk.be
www.kuleuven-kulak.be/irf/thrombosis

Table of contents

1. Summary of project
2. Progress and next steps
 - WP1: NETs in thrombi from stroke patients
 - WP2: Prothrombolytic capacity of DNase-1
 - WP3: NETs in a mouse model of tMCAO
 - WP4: NETs markers in plasma of stroke patients
3. Novel opportunities and impact of 1-year progress
4. Output
 - papers
 - awards
 - invited lectures
 - conference communications
 - new collaborations and networks
5. References

Translocator protein expression in temporal lobe epilepsy: picturing a Janus face?

1. Summary of the project

Ischemic stroke is one of the leading causes of death and sustained disability worldwide. Blockade of blood flow to the brain by an occlusive thrombus leads to irreversible damage of the associated brain tissue. The **enormous clinical, economic and social burden** of ischemic stroke is in strong contrast with the **limited treatment options** that are currently available. Despite the huge clinical need, only one pharmacological intervention is currently approved: early thrombolysis using the fibrinolytic agent tissue plasminogen activator (t-PA). However, t-PA can only be administered in the limited time window of 4.5 hours post-stroke onset due to the unacceptable risk of cerebral bleeding when treatment is delayed. As a consequence, t-PA treatment is available to less than 10% of patients.¹ Most remarkably, t-PA results in recanalization only in less than half of the patients that receive it and factors that contribute to this so-called '**t-PA resistance**' are not well understood.² Furthermore, although timely recanalization of the occluded cerebral artery is fundamental to salvage threatened ischemic brain tissue, reperfusion of the ischemic territory itself can also seriously exacerbate tissue damage by **reperfusion injury**. This problem does not only occur after successful thrombolysis but also often complicates stroke outcome after successful mechanical thrombectomy. Even though reperfusion injury significantly accelerates neurodegeneration, the underlying cellular and molecular interactions are still poorly understood.

It has become clear that both thrombotic and inflammatory pathways are involved in ischemic brain damage, known as "thrombo-inflammation".³ Without a doubt, neutrophils and especially **neutrophil extracellular traps (NETs)** have recently led to a paradigm shift in various fields. NETs have been discovered by Brinkmann et al. as a novel mechanism by which neutrophils contribute to the innate immune response.⁴ Indeed, as a result of a unique form of cell death, dubbed "NETosis", neutrophils **release their chromatin** that is lined with granular components, creating fibrous nets with antimicrobial properties that prevent microorganisms from spreading (Figure 1). Although much of the cell biological mechanisms of NETosis are still being characterized, one essential step is histone citrullination by peptidylarginine deiminase 4 (PAD4).

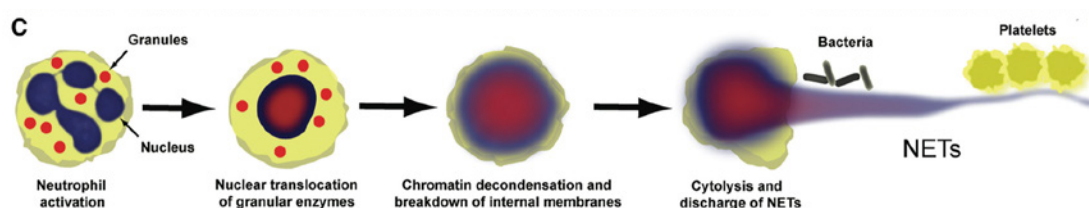


Figure 1: Scheme of NET formation (NETosis) ⁵ Enzymes such as PAD4 from granules (red) translocate to the nucleus (blue) and facilitate chromatin decondensation. Internal membranes break down and cytolysis releases NETs.

PAD4 enters the nucleus to modify histones via hypercitrullination of specific arginine residues on histones H3 and H4. This results in a loss of positive charge from the transformed arginine residues allowing chromatin decondensation (figure 1). Apart from their role in immunity, it has become clear that NETs are also strongly implicated in various thrombotic and thrombo-inflammatory pathologies.⁶

To date, nothing is known yet about the potential effect of NETs in stroke-associated brain damage. Yet, our hypothesis is that, on the one hand, NETs could contribute to cerebral thrombus stabilization preventing fast restoration of cerebral blood flow and, on the other hand, that NETs could further aggravate brain damage by promoting thrombo-inflammatory reperfusion injury after restoration of

blood vessel patency. The general objective of this research project was to identify NETs as potential new players in the pathophysiology of ischemic stroke in order to develop novel neuroprotective strategies in stroke management.

2. Progress and next steps

In order to successfully complete this project, four delineated work packages (WP) were defined:

- WP1: Nets in thrombi obtained from stroke patients
- WP2: Prothrombolytic capacity of DNase-1
- WP3: NETs in a mouse model of tMCAO
- WP4: NETs markers in plasma of stroke patients

In this section, the 1-year progress for each work package is detailed, as well as the planned next steps for the following years.

WP 1: NETs in thrombi obtained from stroke patients

The goal of this work package was to assess the presence of NETs in thrombi retrieved from ischemic stroke patients. Recent studies demonstrate that NETs can form a scaffold for platelets and prothrombotic plasma proteins and consequently participate in both arterial and venous thrombus formation.⁷⁻¹⁰ It is surprising how little is known about the exact composition of thrombi that cause ischemic stroke. Yet, such information is crucial for designing efficient and safe thrombolytic strategies. To investigate the presence of NETs in thrombi from ischemic stroke patients, we take advantage of the unique opportunity offered by the emergence of cerebral thrombectomy in the clinic. In collaboration of AZ Groeninge hospital in Kortrijk (Prof. Tommy Andersson and Dr. Olivier Francois), more than 150 thrombi retrieved from stroke patients have been collected.

In this work package we already completed and published a first important study.¹¹ A first set of 68 thrombi retrieved from ischemic stroke patients undergoing endovascular treatment were characterized by immunostaining using neutrophil markers (CD66b and neutrophil elastase) and NETs markers (citrullinated histones H3 (H3Cit) and extracellular DNA).

Observation 1: Neutrophils are abundant in ischemic stroke thrombi

Classically, blood clots are thought to be formed mainly by platelets, fibrin and trapped red blood cells. Upon examination of the stroke thrombi, however, H&E stainings revealed a large number of leukocytes, visible as nucleated cells in all thrombus specimens (Fig. 2A, 2B and 2E). To specifically assess the presence of neutrophils, we stained thrombi samples for the granulocyte marker CD66b (Fig. 2A, 2C and 2F) and for neutrophil elastase (NE, Fig. 2A, 2D and 2G). Neutrophils were abundant in all 68 thrombi, with varying amounts (Fig. 2J and 2K). No differences in neutrophil counts were observed between thrombi with different etiology (Fig. 2J). Interestingly, older thrombi (> 1 day) contained significantly higher amounts of neutrophils (8726 ± 4493 per mm^2) compared to fresh thrombi (< 1 day) (5292 ± 2551 per mm^2 , $p < 0.001$, Fig. 2K). In conclusion, these results clearly show a high cellular load of ischemic stroke thrombi with a specific abundance of neutrophils.

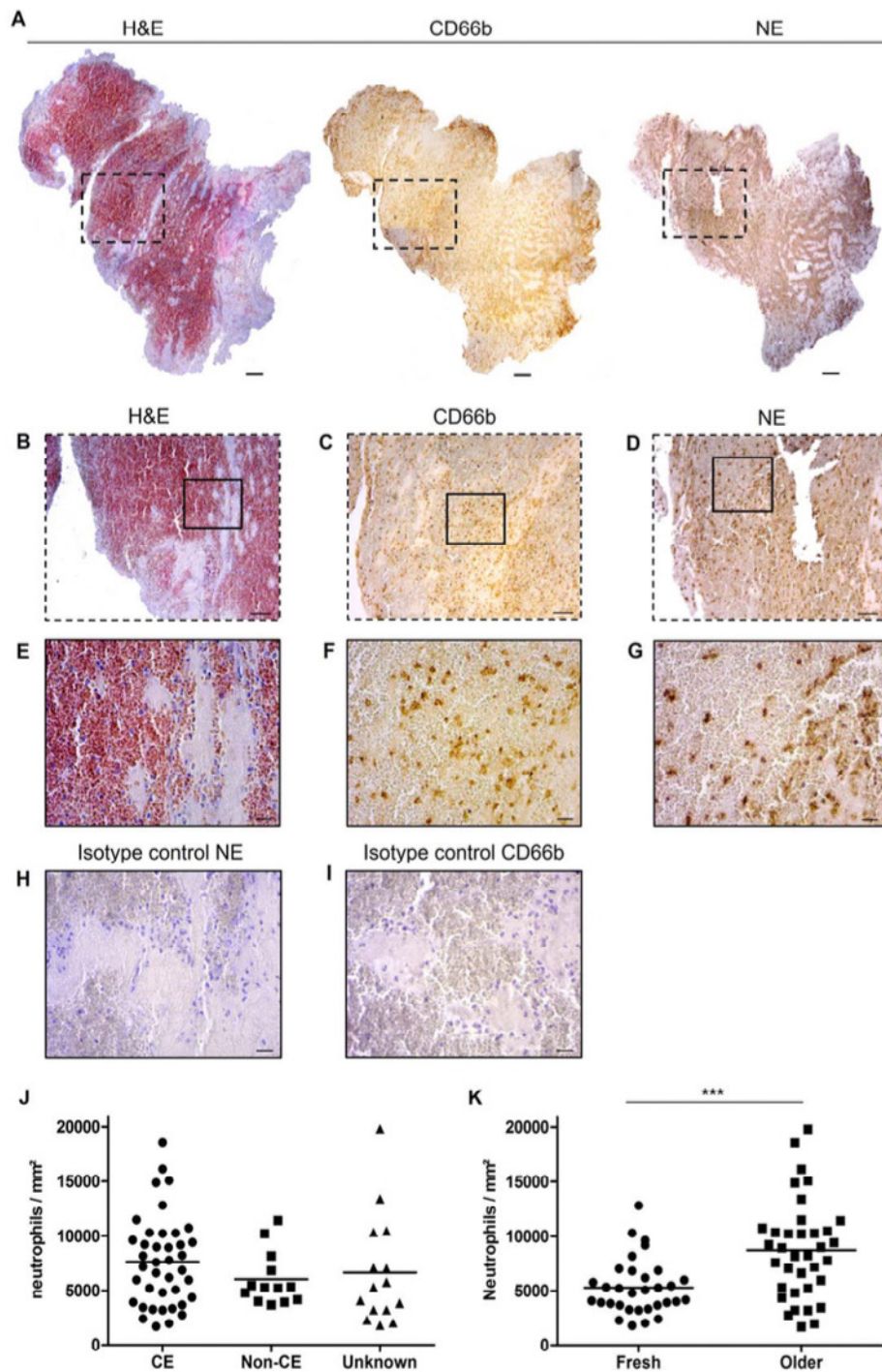


Figure 2: Neutrophils are abundant in ischemic stroke thrombi. To visualize the presence of neutrophils, sections of thrombi retrieved from ischemic stroke patients were stained with H&E and with antibodies against CD66b and neutrophil elastase (NE). Panel (A) shows representative composite images of one thrombus stained for H&E (left), CD66b (middle) and NE (right) (scale bar: 100 μ m.). Magnifications show the presence of leukocytes on H&E staining (B) and in particular neutrophils via either CD66b (C) or NE (D) staining. Scale bar: 50 μ m. Larger magnifications of these areas are shown for H&E (E), CD66b (F) and NE (G). Scale bar: 10 μ m. Isotype control staining is shown for NE (H) and CD66b (I). Scale bar: 10 μ m. Neutrophil numbers in thrombi were quantified and are presented according to stroke etiology (J) (CE: cardioembolic, non-CE: non-cardioembolic) and thrombus age (K) (fresh: < 1 day, older: > 1 day). *** $p < 0.001$. Published in *Annals of Neurology*.¹¹

Observation 2: NETs are present in ischemic stroke thrombi

Careful analysis of H&E staining sometimes revealed prominent extracellular nucleic acid rich areas that were located in neutrophil-rich zones (Fig. 3A). We hypothesized that these structures could be NETs. To confirm this hypothesis, thrombus sections were also stained for citrullinated H3 histones (H3Cit), a defining marker of NETs. These stainings revealed that the areas containing extracellular nucleic acids visible by H&E indeed are rich in citrullinated histones (Fig. 3B). These extensive networks typically also stained positive for NE, further demonstrating their neutrophil origin (Fig. 3C).

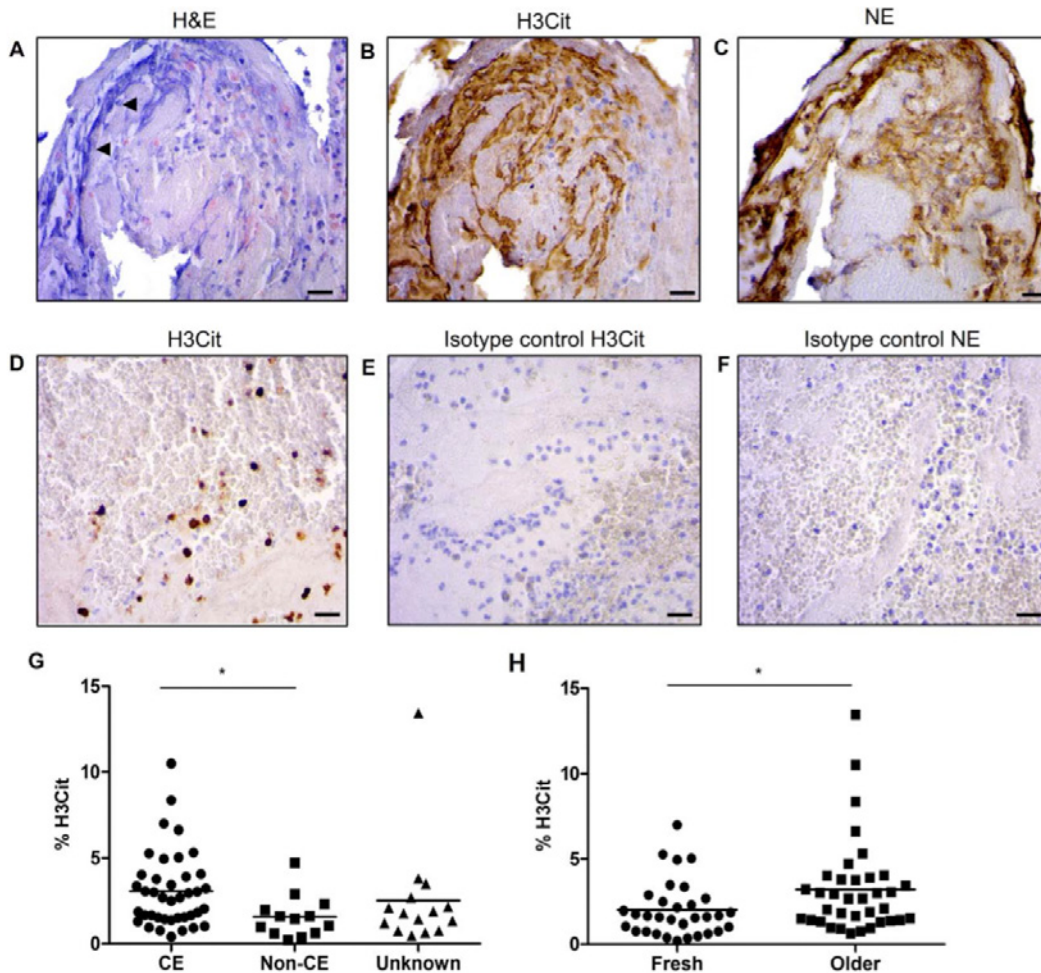


Figure 3: Citrullinated histones reveal the presence of NETs in ischemic stroke thrombi. The presence of citrullinated histones was analyzed via immunohistochemistry using an antibody against H3Cit. Extracellular zones of nuclear material were often observed on H&E stainings (A, arrow heads). These chromatin strands corresponded with areas staining positive for H3Cit (B, brown staining) and NE (C, brown staining). In other places, no extracellular structures were visible and H3Cit-positive signal was observed only intracellularly, indicative of early NETosis processes (D). No H3Cit nor NE signal was present on isotype control stainings (E and F). Scale bars: 10 μ m. H3Cit-positive signal was present in all thrombi and quantification of H3Cit staining per thrombus is shown according to stroke etiology (G) (CE: cardioembolic, non-CE: non-cardioembolic) or thrombus age (H) (fresh: < 1 day, older: > 1 day). * $p < 0.05$. Published in *Annals of Neurology*.¹¹

H3Cit-positive signal was found in all thrombi, indicating that NETs are a common component of ischemic stroke thrombi. Besides the presence of neutrophils that had already formed extracellular fibrous NET structures (as e.g. shown in Fig. 3B), thrombi typically also contained neutrophils in the initiation phase of NETosis. These neutrophils show H3Cit-positive chromatin that was still inside cells that had not bursted yet, hence the term intracellular (Fig. 3D). H3Cit quantification showed a broad range of NET amounts among different thrombi (Fig 3G and 3H). Of note, thrombi of cardioembolic origin contained nearly double the amount of NETs compared to non-cardioembolic thrombi ($p < 0.05$, Fig. 3G). Furthermore, older thrombi showed significantly higher amounts of H3Cit compared to fresh thrombi (Fig. 3H).

Observation 3: fluorescent stainings confirm the presence of NETs in ischemic stroke thrombi and further illustrate the presence of various stages of NETosis

To further confirm the presence of NETs and origin of citrullinated histones, immunofluorescent stainings were performed combining H3Cit with the granulocyte marker CD66b and a DNA dye (DAPI). Fluorescent co-staining of H3Cit together with CD66b and extracellular DNA further corroborate the abundance of decondensed DNA networks containing citrullinated histones that originate from CD66b positive cells (Fig. 4). In line with the immunohistochemical stainings, fluorescent staining also showed neutrophils in the initial stages of NETosis (Fig. 4A), with sometimes even only one nuclear lobe containing H3Cit positive chromatin (middle row of Fig. 4A) and neutrophils that had already fully ejected their decondensated chromatin into the extracellular space (Fig. 4B). Neutrophil origin of extracellular DNA was also confirmed by immunofluorescent co-staining with neutrophil elastase (not shown, see publication). In conclusion, these results clearly show the abundant presence of NETs in ischemic stroke thrombi.

Next steps for WP1

As a conclusion of the previous results on 68 thrombi, we show that neutrophils are an important constituent of thrombo-embolic occlusions in ischemic stroke. We demonstrated for the first time the presence of NETs in ischemic stroke thrombi and found that their presence is correlated with cardioembolic etiology as well as with thrombus organization. This work was published in the leading journal 'Annals of Neurology' with GSKE acknowledgement.¹¹ We now want to expand this study to a larger set of samples. In the meantime, we have more than 150 thrombi via our collaboration with the AZ Groeninge hospital. In the meantime we have expanded our network and also receive ischemic stroke thrombi from the CHRU in Lille (France), Bruges and Leuven. We also plan to receive thrombi from other hospitals in Belgium and abroad. Large numbers are needed (we aim van >500 thrombi) as we plan to match NETs presence with more clinical patient data (MRI, CT, thrombus origin, stroke etiology, patient recovery, thrombectomy success rates...). Large numbers will make stronger conclusions. Such correlations could potentially help to stratify stroke treatments and to design optimal secondary prevention treatment.

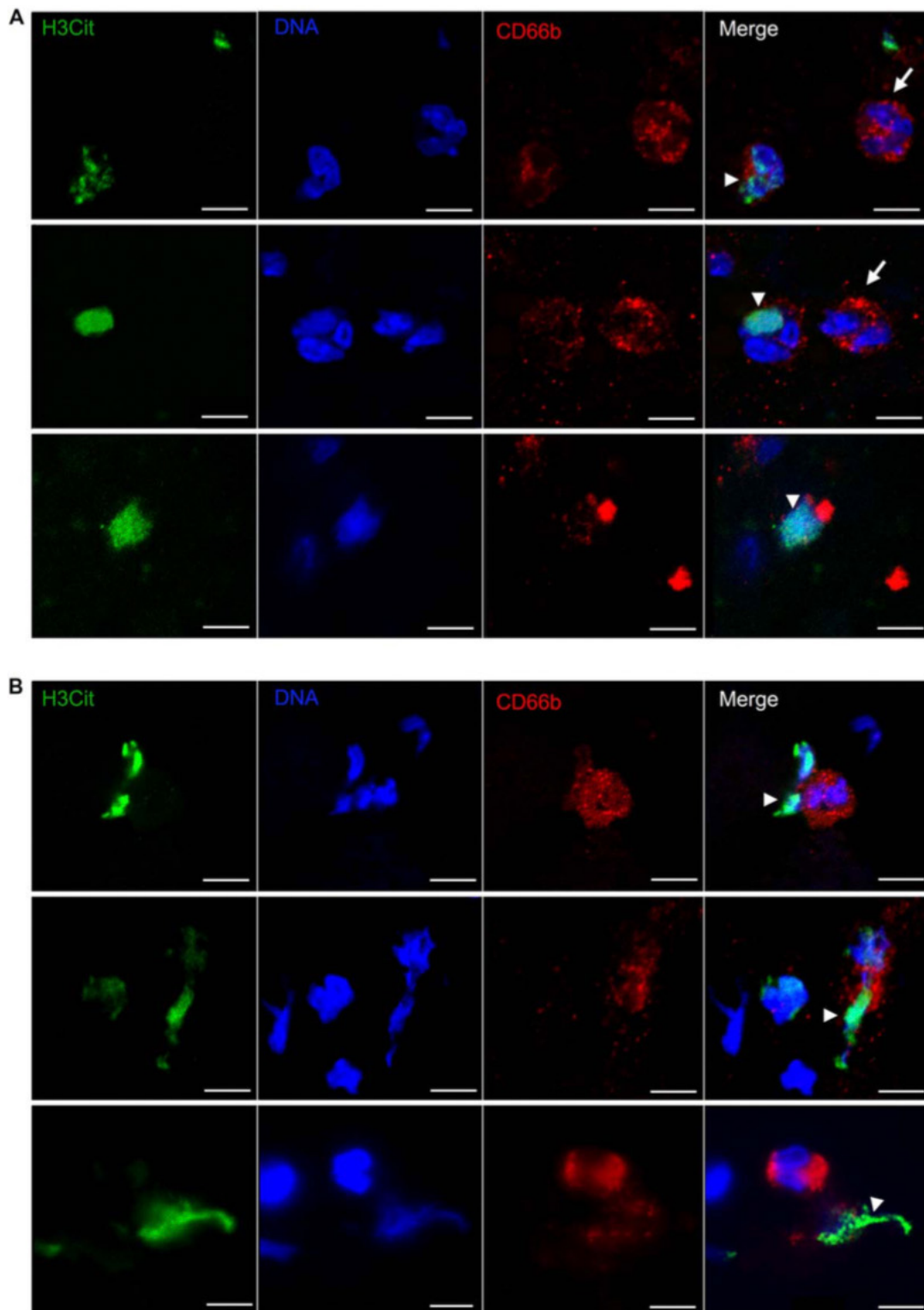


Figure 4: Immunofluorescent identification of NETs in stroke thrombi. NETs were visualized in human ischemic stroke thrombi by co-staining of the granulocyte marker CD66b (red) with H3Cit (green) and DNA (DAPI, blue). (A) Three representative images of neutrophils at the initial stage of NET formation. H3Cit positive signal is only detected inside the cell (arrowhead). Neutrophils without citrullinated histones are also shown (arrows). (B) Three representative images of neutrophils that underwent complete NETosis. Neutrophils released their decondensated chromatin in the extracellular space. Arrowheads indicate extracellular co-staining of DNA with H3Cit. Scale bar: 5 μ m. Published in *Annals of Neurology*.¹¹

WP 2: Prothrombolytic capacity of DNase-1

Since use of t-PA leads to the dissolution of occluding thrombi in some cases, but not in others, we believe that factors other than fibrin are involved in thrombus stability. Such newly identified factors can become promising targets for thrombolytic therapy. We recently showed that von Willebrand confers tPA-resistance to cerebral thrombi and that the von Willebrand factor-cleaving protease ADAMTS13 has a prothrombolytic activity that may become useful in stroke.¹² Similarly, we hypothesize that extracellular DNA traps are likely candidates as stabilizers of thrombi. Strikingly, the co-distribution of fibrin and extracellular DNA traps is apparent in arterial thrombi and a fascinating study showed that these DNA traps change the structure of fibrin, rendering it resistant to mechanical and enzymatic destruction.¹³ The goal of this work package therefore is to test the capacity of DNase-1 to support acute thrombolytic activity by disassembling extracellular DNA traps in stroke thrombi. In the first year of this project, we already obtained promising results, showing exactly our hypothesis.

Observation: DNase 1 promotes ex vivo lysis of ischemic stroke thrombi

Given our observations (described in the progress section of WP1) that NETs can form extensive DNA networks in stroke thrombi, we reasoned that pharmacological breakdown of NETs could enhance thrombus dissolution. To test this, two equal parts of fresh patient thrombi (n=8) were submitted to ex vivo lysis by t-PA (1 µg/ml) or by a combination of t-PA (1 µg/ml) and DNase 1 (100 IE/ml) for 120 min at 37°C. Thrombus lysis was calculated in function of time as percentage of thrombus weight compared to the original weight (Figure 5). Standard t-PA alone induced gradual, partial lysis of the thrombi (residual weight at 120 min was 62.84 % ± 20.59 % of original thrombus weight). Strikingly, addition of DNase 1 to t-PA significantly accelerated ex vivo lysis compared to t-PA alone, reducing the thrombus weight at 120 min to 40.65 % ± 27.25 % (p < 0.01). These findings show that DNase 1 can promote ex vivo stroke thrombus dissolution and provide proof-of-concept to target NETs as a novel prothrombolytic strategy.

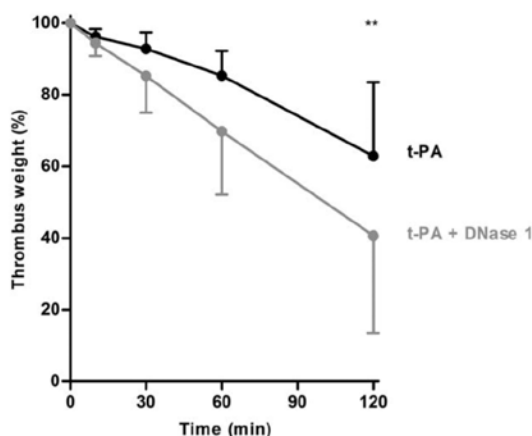


Figure 5: DNase 1 promotes ex vivo lysis of ischemic stroke thrombi. For ex vivo lysis of thrombi (n=8) retrieved from ischemic stroke patients, 2 equal parts were used. The thrombus parts were incubated for 120 min at 37°C in the presence of either t-PA alone (black) or t-PA plus DNase 1 (grey). Thrombus weight % of original weight) was measured at time points 0, 10, 30, 60 and 120 minutes. Data are represented as mean with SD (** p < 0.01). Published in *Annals of Neurology*.¹¹

Next steps for WP2

Our first results show already the potential of DNase-1 to promote thrombus dissolution on human material retrieved from stroke patient via endovascular procedures. In a next step we want to extend these findings in an established and pathophysiologically relevant mouse stroke model in which an occlusive thrombus is formed at the origin of the middle cerebral artery (MCA) after local administration of thrombin or FeCl₃. Using this model, we recently showed a novel thrombolytic activity of ADAMTS13 in stroke.¹² Important for clinical translation, we will also investigate the additional benefit of combining DNase-1 together with t-PA (or even ADAMTS13).¹² This model is currently being set up for DNase-1 experiments.

WP 3: NETs-formation in a mouse model of transient middle cerebral artery occlusion

In this WP, the goal is to assess the involvement of NETs in progressive ischemic brain damage during ischemia and reperfusion in mice. Pathogenic mechanisms underlying this reperfusion injury are not completely understood but involve a complex interplay of thrombo-inflammatory processes.³ We recently showed that NET formation worsened outcome in mouse models of myocardial ischemia/reperfusion.¹⁴ The role of NETs in (mouse models of) cerebral ischemia/reperfusion brain damage has never been investigated. To clarify the potential involvement of NETs in we will use an established model of cerebral ischemia/reperfusion injury¹⁵, which in the past year has been learned and acquired the researcher on this GSKE WP. In the past year, we also developed a new mouse strain that will be of great value for this WP. Indeed, we have been intercrossing specific mouse strains to obtain neutrophil-specific PAD4 knock-out mice. We made good progress and expect to have this new mouse-strain available in year 2 of this GSKE program.

Next steps for WP3

At different time points after induction of ischemia (up to 48 hours), mice will be sacrificed and brain histology for NETs will be performed. In addition 3D imaging via confocal microscopy will also be used to visualize cerebral NETosis. To directly compare the impact of NET formation in experimental stroke outcome, we will use specific mouse strains: PAD4^{-/-} mice (which cannot form NETs), DNase^{-/-} mice (which lack the NETs degrading enzyme DNase-1) and the newly developed neutrophil-specific PAD4^{-/-} mice. Stroke outcome will be assessed by measuring cerebral infarct volume and functional behavior of the mice 24h after induction of ischemia.

WP 4: NETs markers in plasma of stroke patients

In this WP, the goal was to investigate the presence of established circulating biomarkers of NETs (cell-free DNA, nucleosomes, DNA-MPO complexes) in stroke patients. Such NETs -markers were recently shown to be increased in a variety of pathological conditions, such as sepsis, small vessel vasculitis, venous thrombosis and coronary atherosclerosis^{6,16} but almost nothing is known yet about circulating NETs markers in stroke patients. Plasma of different groups of stroke patients (and healthy controls) will be assessed and levels of NETs biomarkers will be measured.

Observation: Cell-free DNA is elevated in stroke patients

We already obtained a large cohort of stroke patients (and healthy volunteers) through our collaboration with Prof. C. Kleinschnitz (Würzburg, now Essen in Germany).¹⁷ As a first marker, we already tested our cohort for cell-free DNA as an indication of NETs in stroke. In total, 104 patients with stroke (AIS or TIA) and 85 healthy volunteers (HV) were included in the study. Trisodium citrate anticoagulated blood was collected on day 0, 1, and 3 in patients with stroke, and once in HV between 08.00 and 12.00 hours from an antecubital vein using a 21-gauge butterfly needle. Cell-free DNA in plasma was analyzed using PicoGreen and quantified via a DNA standard curve. Interestingly, patients with ischemic stroke presented with significantly higher levels of circulating DNA (compared to healthy volunteers) and this was true for day 0, 1 and 3 of stroke (Figure 6). These results are line with our previous data showing that plasma nucleosome levels are elevated in mice after stroke, which could potentially be derived from NETs that are formed in the ischemic area.¹⁸

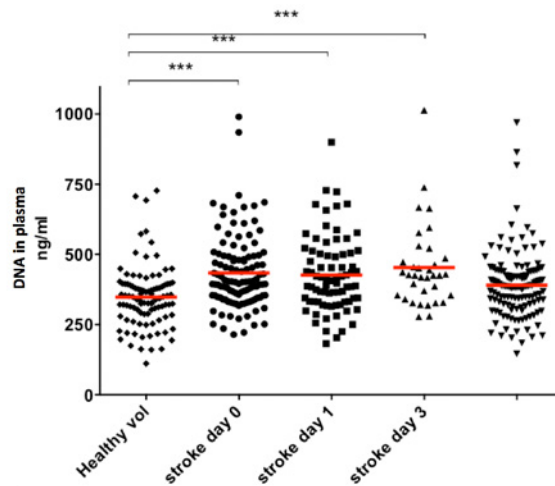


Figure 6: Plasma DNA levels are increased in patients with ischemic stroke. In total, 104 patients with stroke and 85 healthy volunteers were included in the study. Trisodium citrate anticoagulated blood was collected on day 0, 1, and 3 in patients with stroke, and once in HV. Cell-free DNA in plasma was analyzed using PicoGreen and quantified via a DNA standard curve. Unpublished results.

Next steps for WP4

Along the same lines of our results on DNA, we plan to also measure other established markers of NETs, including DNA, MPO, S100A8/S100A9, soluble H3cit and DNA-MPO complexes. Since all clinical data of our patient cohort is available, we will be able to correlate levels of circulating NETs markers with clinical parameters such as treatment success, morbidity, disability and mortality.

3. Novel opportunities and impact of 1-year progress

As shown by the progress in the first year of this GSKE project, some important findings have been achieved. As main discovery of this year, we demonstrated for the first time the presence of NETs in ischemic stroke thrombi and found that their presence is correlated with cardioembolic etiology as well as with thrombus organization. Targeting NETs with DNase-1 successfully improved ex vivo thrombolysis, calling for further investigation of DNase-1-based strategies to improve thrombus dissolution and prevent excessive neurodegeneration in acute ischemic stroke.

Given the serious limitations in current stroke therapy, the clinical implications of our findings could be of high relevance for acute ischemic stroke management. Our results provide new insights into the clinical generation and pathology of ischemic stroke thrombi. More importantly, these results provide perspectives for novel thrombolytic treatment strategies. Serving as a thrombotic scaffold, NETs most likely contribute to overall thrombus stability and might confer resistance to fibrinolytic therapy thereby exacerbating ischemic stroke neurodegeneration. In vivo settings, as planned in WP2, will be crucial to further investigate the physiological potential of DNase-1 activity in ischemic stroke. Importantly, DNase-1 already is a safe, low-cost, FDA-approved drug routinely used for cystic fibrosis to clear extracellular DNA in the lungs. Combination of DNase-1 with t-PA could potentially allow decreasing the dose of t-PA utilized, limiting its side effects and potentially increasing its therapeutic time window. Even a small prolongation of the therapeutic window for safe thrombolytic therapy would already help hundreds of thousands of patients each year. This would allow a drastic reduction of the current burden caused by the negative side-effects of t-PA. Additional studies are needed to further assess this hypothesis and are planned in the future.

Importantly, use of DNase-1 could become a therapeutic strategy that kills two birds with one stone. We previously demonstrated that DNase-1 also had a protective effect in a mouse model of cerebral

ischemia/reperfusion injury.¹⁸ Hence, besides its potential prothrombolytic activity that could promote fast restoration of blood vessel patency, DNase-1 could additionally reduce subsequent reperfusion injury and thus improve neurological outcome in ischemic stroke.

Apart from the direct potential therapeutic opportunities, the progress described in this progress report also led to multiple new networks and collaborations that will be valuable for the future research on this topic (see further).

4. Output

The results that were obtained with support of the GSKE already led to significant output, visibility and novel collaborations. In the following section an overview of the most important output achievements of 2017 is given.

Papers with GSKE acknowledgement:

- Laridan, E., Denorme, F., Desender, L., François, O., Andersson, T., Deckmyn, H., Vanhoorelbeke K, De Meyer SF. (2017). Neutrophil extracellular traps in ischemic stroke thrombi. *Annals of Neurology*, 313, 1451–10. (Impact factor 9.89)
- Laridan E., Martinod K., De Meyer SF, Neutrophil extracellular traps in thrombosis, Invited review for *Seminars in Thrombosis and Haemostasis* (in preparation - to be submitted February 2018)

Awards:

The work described in WP1 and WP2 has already led to several awards, including:

- *2017 Eberhard F. Mammen Young Investigator Award (to my PhD student Elodie Laridan)*.
The Eberhard F. Mammen Young Investigator Awards (up to a total of six in any year) are given for the “Best presentation or meeting abstract by a young investigator — as presented or delivered to an international or large regional meeting on a topic related to the fields of thrombosis and hemostasis and whose subject matter is determined to be in the spirit of Dr. Mammen.” (Dr Mammen was the Founding Editor of ‘**Seminars in Thrombosis & Hemostasis**’ (STH)). The award carries a cash prize of US\$1000 and awardees are expected to prepare a review or other article related to the topic of their presentation for publication in STH.
- *ISTH Young Investigator Award (to my PhD student Elodie Laridan)*.
The Young Investigator Awards of the International Society of Thrombosis and Hemostasis are given to the highest scored abstracts of the bi-annual international meeting of the ISTH. Elodie Laridan received this awards for her presentation “Neutrophil extracellular traps in thrombi retrieved from ischemic stroke patients” during the 2017 ISTH meeting in Berlin.
- Two travel grants (to Elodie Laridan and granted by the Belgian Society on Thrombosis and Hemostasis) to present this work at the ESOC meeting in Prague (2017) and the ISTH meeting in Berlin (2017).

Invited lectures:

The first results that we obtained on the presence of NETs in ischemic stroke thrombi (and the potential prothrombolytic capacity of DNase-1) has been well received in the international community as is reflected by the many invitations I received to present this work at international conferences. These invitations include:

- 2nd Thrombosis Meeting, February 2017 Freiburg, Germany ([invited speaker](#))
- Haematology Lectures Program, Erasmus Medical Center, May 2017, Rotterdam, The Netherlands ([invited speaker](#))
- International Society on Thrombosis and Hemostasis Congress, July 2017, Berlin, Germany ([invited speaker](#))
- The 9th Bari International Conference, September 2017, Bari, Italy ([invited speaker](#))
- GFHT meeting, October 2017, Caen, France ([invited speaker - Plenary Lecture](#))
- 14th Congress of the World Federation of Interventional and Therapeutic Neuroradiology, October 2017, Budapest, Hungary ([invited speaker - Plenary Lecture](#))
- 3rd Neuravi Clot summit, December 2017, Amsterdam, The Netherlands ([invited speaker](#))
- ECMINT 1.3 European Course on Minimally Invasive Neurological Therapy, December 2017, Oxford, UK ([invited speaker](#))
- 2017 meeting of the Belgian Society of Interventional and Therapeutic Neuroradiology, December 2017, Brussels, Belgium ([invited speaker](#))
- 4th European Stroke Organisation Conference, May 2018, Göteborg, Sweden ([invited speaker](#))

- International Society on Thrombosis and Hemostasis SSC meeting, 2018, Dublin, Ireland ([invited speaker](#))
- 11th World Stroke Congress, October 2018, Montreal, Canada ([invited speaker, co-convenor](#))

Conference communications in national and international meetings:

Apart from the above invited lectures (given by myself), the GSKE work was also presented during the following oral communications (give by my PhD student Elodie Lardian):

- Interuniversity Belgian Stroke Meeting, June 2017, Antwerp, Belgium (oral presentation)
- 3rd European Stroke Organisation Conference, May 2017, Prague, Czech Republic (oral presentation)
- International Society on Thrombosis and Hemostasis Congress, July 2017, Berlin, Germany (oral presentation)

New collaborations and networks:

The progress made in the GSKE project opened new research avenues (as described above) and, in particular, also led to novel research collaborations. The most important include:

- Participation in the EU HORIZON2020 INSIST consortium (In Silico Clinical Trials for Acute Ischemic Stroke) (<http://www.insist-h2020.eu>). Start in 2018.
- New research contacts with technology companies Neuravi (Galway, Ireland), Sensome (Paris, France) and Matisse Pharmaceuticals (Geleen, The Netherlands)
- New research collaborations with academic partners and hospitals (AZ Sint Jan in Bruges, UZ Antwerp, UZ Gasthuisberg Leuven in Belgium and CHRU in Lille, France, NUI in Galway Ireland)

5. References

1. Hacke W, Kaste M, Bluhmki E, et al. Thrombolysis with alteplase 3 to 4.5 hours after acute ischemic stroke. *N. Engl. J. Med.* 2008;359(13):1317–1329.
2. Rha J-H, Saver JL. The impact of recanalization on ischemic stroke outcome: a meta-analysis. *Stroke.* 2007;38(3):967–973.
3. De Meyer SF, Denorme F, Langhauser F, et al. Thromboinflammation in Stroke Brain Damage. *Stroke.* 2016;47(4):1165–1172.
4. Brinkmann V, Reichard U, Goosmann C, et al. Neutrophil extracellular traps kill bacteria. *Science.* 2004;303(5663):1532–1535.
5. Fuchs TA, Brill A, Wagner DD. Neutrophil extracellular trap (NET) impact on deep vein thrombosis. *Arteriosclerosis, Thrombosis, and Vascular Biology.* 2012;32(8):1777–1783.
6. Martinod K, Wagner DD. Thrombosis: tangled up in NETs. *Blood.* 2014;123(18):2768–2776.
7. Fuchs TA, Brill A, Duerschmied D, et al. Extracellular DNA traps promote thrombosis. *Proc. Natl. Acad. Sci. U.S.A.* 2010;107(36):15880–15885.
8. Brill A, Fuchs TA, Savchenko AS, et al. Neutrophil extracellular traps promote deep vein thrombosis in mice. *J Thromb Haemost.* 2012;10(1):136–144.
9. Oklu R, Albadawi H, Watkins MT, et al. Detection of extracellular genomic DNA scaffold in human thrombus: implications for the use of deoxyribonuclease enzymes in thrombolysis. *J Vasc Interv Radiol.* 2012;23(5):712–718.
10. Brühl von M-L, Stark K, Steinhart A, et al. Monocytes, neutrophils, and platelets cooperate to initiate and propagate venous thrombosis in mice in vivo. *Journal of Experimental Medicine.* 2012;209(4):819–835.
11. Laridan E, Denorme F, Desender L, et al. Neutrophil extracellular traps in ischemic stroke thrombi. *Ann Neurol.* 2017;313:1451–10.
12. Denorme F, Langhauser F, Desender L, et al. ADAMTS13-mediated thrombolysis of t-PA-resistant occlusions in ischemic stroke in mice. *Blood.* 2016;127(19):2337–2345.
13. Longstaff C, Varjú I, Sótónyi P, et al. Mechanical stability and fibrinolytic resistance of clots containing fibrin, DNA, and histones. *J. Biol. Chem.* 2013;288(10):6946–6956.
14. Savchenko AS, Borissoff JI, Martinod K, et al. VWF-mediated leukocyte recruitment with chromatin decondensation by PAD4 increases myocardial ischemia/reperfusion injury in mice. *Blood.* 2014;123(1):141–148.
15. Verhene S, Denorme F, Libbrecht S, et al. Platelet-derived VWF is not essential for normal thrombosis and hemostasis but fosters ischemic stroke injury in mice. *Blood.* 2015;126(14):1715–1722.
16. Fuchs TA, Hovinga JAK, Schatzberg D, Wagner DD, Lämmle B. Circulating DNA and myeloperoxidase indicate disease activity in patients with thrombotic microangiopathies. *Blood.* 2012;120(6):1157–1164.

17. Kraft P, Drechsler C, Gunreben I, et al. Von Willebrand Factor Regulation in Patients with Acute and Chronic Cerebrovascular Disease: A Pilot, Case–Control Study. *PLoS ONE*. 2014;9(6):e99851.
18. De Meyer SF, Suidan GL, Fuchs TA, Monestier M, Wagner DD. Extracellular chromatin is an important mediator of ischemic stroke in mice. *Arteriosclerosis, Thrombosis, and Vascular Biology*. 2012;32(8):1884–1891.



Geneeskundige Stichting Koningin Elisabeth
Fondation Médicale Reine Elisabeth
Königin-Elisabeth-Stiftung für Medizin
Queen Elisabeth Medical Foundation

Progress report
of the research group of

Prof. dr. De Strooper Bart, MD. PhD

Katholieke Universiteit Leuven (KU Leuven)

Principal investigator

Prof. dr. De Strooper Bart, MD. PhD
VIB Center for Brain and Disease Research
Herestraat 49
3000 Leuven
Belgium
Tel.: +32 495 77 10 44
E-mail: Bart.Destrooper@vib.be

Hilde Govaert
Administrative Director
hilde.govaert@kuleuven.vib.be

Wei-Ting Chen
Postdoctoral Researcher
weiting.chen@kuleuven.vib.be

Mark Fiers
VIB Expert Technologist
mark.fiers@kuleuven.vib.be

Katleen Craessaerts
Staff employee
katleen.craessaerts@kuleuven.vib.be

Ashley Lu
PhD student
ashley.lu@kuleuven.vib.be

Carlo Sala Frigerio
Staff scientist
carlo.salafrigerio@kuleuven.vib.be

Benjamin Pavie
Imaging Analysis Expert
benjamin.pavie@kuleuven.vib.be

The study of the initial cellular phase of Alzheimer's Disease

1. Overall summary of the report:

In the first year of this grant we have performed a pilot single cell analysis as initially proposed in the application and have obtained data on 362 cells. However, it turns out that single cell isolation of mature brain is a major technical hurdle (discussed in detail below) and results in unacceptable biases in the cells isolated. The work shows that only microglia can be isolated from adult brain in an unbiased way and we have therefore refocused this part of the project on an effort to characterize microglia only. We have secured additional funding from AbbVie to support that part of the project, allowing generating a database of ten thousand of microglia expression profiles over different stages of AD. In the meantime, we have changed protocols and are now performing single nuclei isolation that works excellently even with adult brain and human brain. We have therefore refocused this part of the project on characterization of AD patients which we plan to initiate in 2018. We report on a feasibility experiment with single nuclei RNA seq below, and plan to initiate a full blown experiment later this year when the drop seq line is fully established in our single cell core (see below for further discussion). In the meantime the costs per cell and the throughput is tremendously improved, and it is likely that we will be able to provide an order of magnitude more cell sequencing data in the course of the next year using the renewed protocols that are currently elaborated.

Finally, to make progress, we have accelerated the spatial transcriptomics project that was mentioned as complementary to the single cell-sequencing project. We report in more detail on the generation of several databases of mice at 3.5, 6, 12 and 18 months of age allowing to overview the changes in the brain associated with incipient amyloid pathology and late amyloid pathology. We report on the successful implementation of that work below. We expect to finalize a manuscript on this in the course of the second half of this year when all analyses on the databases will have been executed.

In summary, the first year of this project has forced us to rethink our strategy for single cell analysis, but provides us now with a higher throughput and very efficient protocols that allows us to catch up very rapidly with promised sample size. In the meantime, we started a complementary collaboration with AbbVie to analyze the expressomes of thousands of microglia, demonstrating the leverage of funding we obtained from GSKE. Finally, we made strong progress with our spatial transcriptomics approaches and are working on innovative bioinformatics to analyze the complex cellular phase of Alzheimer's disease.

2. Details of achievement:

2.1. Spatial Transcriptomics (ST):

Amyloid plaque has been identified as a pathogenic hallmark in AD brain since 1911. Since then, gliosis and neurodystrophy have been characterized as features surrounding amyloid plaques. However, there is few findings on the molecular alterations around plaques beyond this cellular description. Amyloid plaque deposition starts from 3 months of age in the cortex of APP^{NL-G-F} KI mice and sequentially spreads out to thalamus, hypothalamus and then to hippocampus as the disease progressed (Figure 1). Astrocytes react to plaques in the very early stage and this cellular reaction is different in-between brain regions. There is a positive correlation of astrocyte cell number with the plaque size in cortex but not in hippocampus. This indicates a different cellular and molecular reaction toward amyloid plaques in-between brain regions. Here, we applied the advanced technology, spatial transcriptomics, to explore the alteration of gene expression around amyloid plaques in the coronal sections from APP^{NL-G-F} KI mice.

We established spatial transcriptomics in our lab in Leuven, Belgium. Twenty databases from C57BL/6J and *APP^{NL-G-F}* KI mice at 3.5, 6, 12, and 18 months of age have been successfully generated (Table 1). Each database is generated from a sandwich of coronal sections (in-between bregma staging -2.0 to -2.2, Figure 2) to get the gene count table from the middle section and the metadata with amyloid and cellular information from the two adjacent sections. The thickness of a section is 10 μ m. The middle section was mounted onto a ST array which contains 1007 spots (100 μ m in diameter per spot). We thus have an *in situ* global transcriptomic profile per spot. The two adjacent sections were immunostained by anti-amyloid-beta (6E10), anti-NeuN, anti-Gfap and DAPI. The average size of dense-core plaque is 10 μ m and the diffuse plaque is various from 10-100 μ m in diameter. Therefore, the resolution of spot is reasonable to get the gene expression profiles around plaques.

Data collection is completed with good quality. Satisfying numbers of spot per region for each genotype allow statistical comparisons (Figure 3A). Satisfying numbers of unique molecules are detected in each spot (30K UMIs and 7K genes per spot on average, Figure 3B). This number allows us to recapture the brain hierarchy by unbiased clustering on the transcriptomic profiles, indicating that brain regions have distinguishable molecule expression (Figure 3D). We also show the expression of landmark genes in the restricted area (Figure 3C). This provides confidence on the reliability of our strategy to detect gene expression with precise spatial localization. We realize that the transcriptomic profiles from the brain are highly heterogeneous (Figure 3D), which is logical given the highly organized cellular structure (e.g. multiple layers in the hippocampus) or the diverse functions in-between brain regions. Regional effects must be taken into consideration for proper normalization and comparison. To annotate the brain region for each spot, we aligned our HE images with the atlas templates from Allen Brain Atlas and collect information in our metadata. Dimensional reduction via t-distributed stochastic neighbor embedding (t-SNE) on our full databases shows that transcriptomic profiles are reasonably segregated by experimental groups and brain regions (Figure 4).

We are now setting up a thorough analysis of all databases. The first level of analysis is akin to bulk analysis that we take all spots within cortex, hippocampus or brain stem for comparison. The second level of analysis has higher resolution on 13 regions in the brain. The third level of analysis is a fine region analysis within hippocampus which is subdivided into 11 sub-regions. We will analyze the plaque reactive genes by two approaches: differential expression analysis and random forest. Differential gene expression around plaques will be explored. Random forest is an ensemble learning method to predict relevant genes on a specific index (eg. amyloid burden). Several plaque reactive genes with significance have been found (Figure 5). We will compare the plaque reactive genes via different approaches and validate the target genes by RNAscope. Functional alteration (eg. inflammation or neurogenesis) and cellular reaction to plaques will also be predicted by bioinformatics packages (eg. GSEA, Gorilla, AUCell). We hope to provide a hypothesis and molecular mechanism on how does different brain regions react differentially to amyloid plaques in the early stage or the late stage of AD.

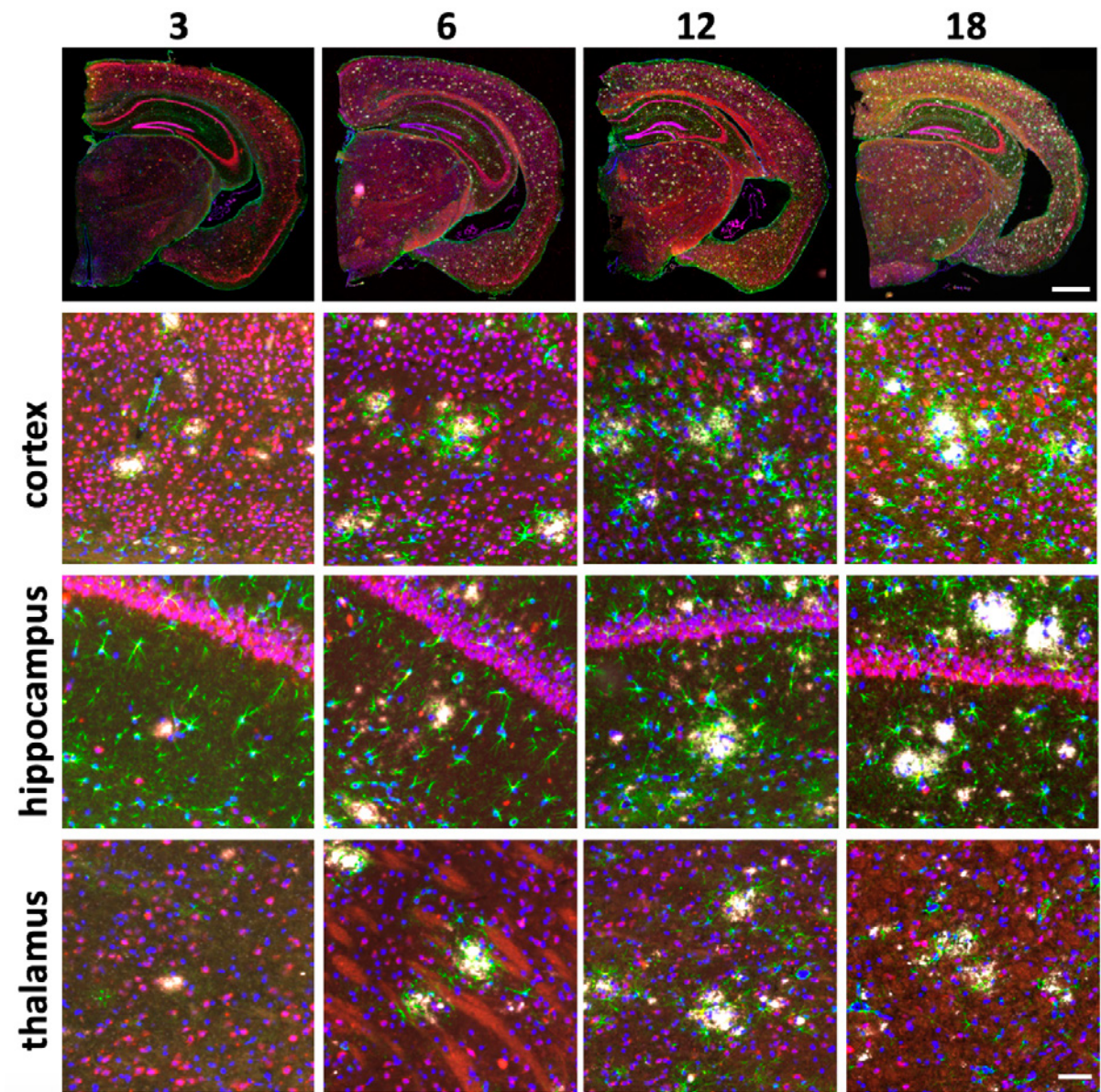


Figure 1. Immunostaining on coronal sections of APPNL-G-F KI mice at 3, 6, 12, and 18 months of age. Colors: DAPI (blue), anti-NeuN (red), anti-Gfap (green), anti-amyloid beta (6E10, white). Scale bar: 1 mm (coronal sections, upper panels) and 100 μ m (zoom-ins, lower panels)

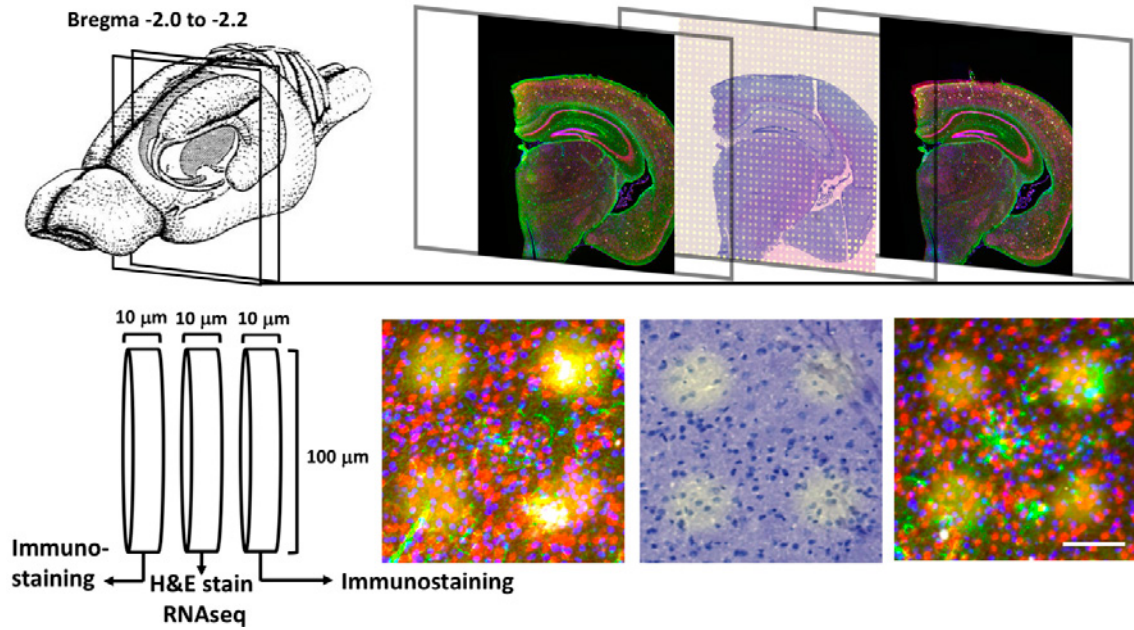


Figure 2. Experimental design. Three adjacent coronal sections (a sandwich) were sliced from brains at bregma staging -2.0 to -2.2. The middle section was mounted onto ST array with 1007 spots to generate gene expression table. The two adjacent sections were immunostained to get amyloid and cellular information. Each mouse has two sandwiches to get two independent databases. Resolution of each transcriptomic profile: tissue cylinder with 10 mm of thickness and 100 mm in diameter. Colors: DAPI (blue), anti-NeuN (red), anti-Gfap (green), anti-amyloid beta (6E10, white), spot (yellow). Scale bar: 100 µm

	WT: C57Black6J				AD: APP ^{NL-G-F}			
Age (month)	3	6	12	18	3	6	12	18
Mouse	2	1	1	2	2	1	1	2
Sandwich	4	1	1	4	4	1	1	4
Spot	2277	537	447	2057	2015	478	488	2028

Table 1. Sample size

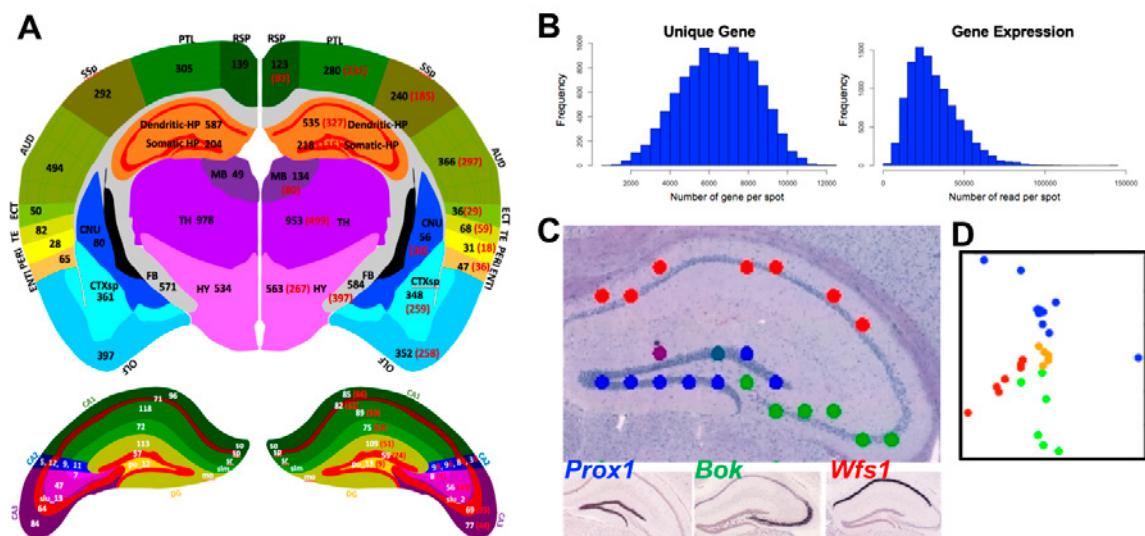


Figure 3. Quality of our databases. (A) Number of spot per region. Coronal section is sub-divided into 17 regions. Hippocampus is sub-divided into 15 regions. (B) Number of gene per spot and number of read per spot. (C) Upper panel: If a spot is detected by expression with *Prox1* (blue), *Bok* (green), or *Wfs1* (red), it will show the corresponding color. Lower panel: *In situ* hybridization from Allen brain atlas. (D) PCA plot of 28 spots in somatic layer of hippocampus shows spot segregation by brain regions: DG (blue), CA1 (red), and CA3 (green).

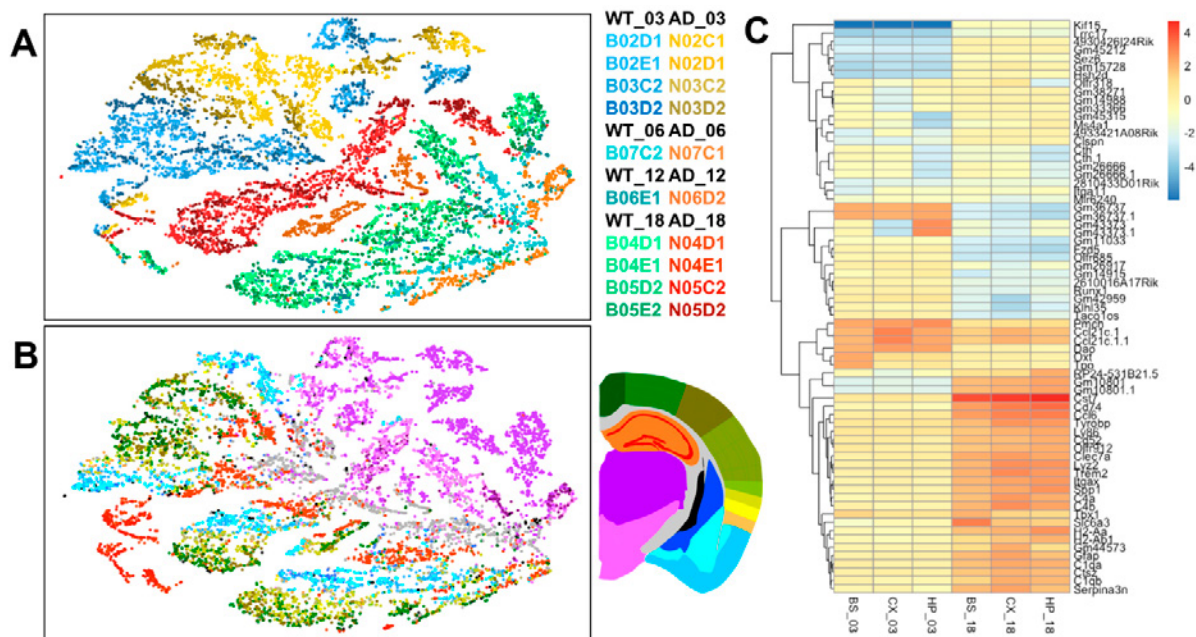


Figure 4. Preliminary analysis (A) t-SNE plot on full databases colored by samples. (B) t-SNE plot colored by brain regions. (C) Heatmap of significant genes and colored by log fold-changes. FDR<0.0005, logFC >2



Geneeskundige Stichting Koningin Elisabeth
Fondation Médicale Reine Elisabeth
Königin-Elisabeth-Stiftung für Medizin
Queen Elisabeth Medical Foundation

Progress report
of the research group of

Prof. Goris An, PhD

Katholieke Universiteit Leuven (KU Leuven)

Principal investigator

Prof. Goris An, PhD
KU Leuven
Department of Neurosciences
Laboratory for Neuroimmunology
Tel.: +32 16 33 07 72
E-mail: an.goris@kuleuven.be

Table of contents

1. Summary and current status of research program
2. Achievements
3. Networking and collaborations
4. Relevance and future perspectives
5. Financial report
6. Publications under GSKE support
7. Team publications
8. References

Unraveling the BAFF pathway towards targeted treatment of multiple sclerosis

1. Summary and current status of research program

Multiple sclerosis (MS) is one of the most common neurological disorders in young adults, affecting around 10,000 people in Belgium and 2.5 million worldwide. The disease can lead to important physical as well as cognitive disability at a time that is crucial in the personal and professional development of patients. MS is characterized by three hallmarks: inflammation, demyelination and neuronal loss¹. The aetiology is unknown but the past few years have seen exciting progress in the field.

The International Multiple Sclerosis Genetics Consortium (IMSGC), of which I am the Belgian representative, has recently identified 200 genetic susceptibility factors for MS (IMSGC, *Science*, revision in preparation, preprint available on <http://dx.doi.org/10.1101/143933>). These risk factors highlight the role not only of T cells, but increasingly also of B cells in the pathogenesis of MS. In a systems immunology approach comparing multiple immunomodulatory treatments, we have previously demonstrated a unique B cell pathway, including B cell activation factor (BAFF) and transitional B cells, as shared across treatments². This shared B-cell related mechanism has recently been extended to other novel treatments in the literature^{3,4} and in recent conference presentations (European Charcot Symposium, November 2017). The combination of these data point to a key role for B cells not only in the pathogenesis but also in the treatment of MS⁵.

In the project supported by GSKE, we set out to build on these data supporting the role of a specific B cell pathway in the treatment of MS with two aims.

1. We unravel the role of the B cell pathway in detail, investigating the different contributions of known splice-forms, soluble and membrane-bound forms of BAFF and the different receptors and co-stimulatory molecules on transitional B cells. The role of B cells in the treatment of MS is emerging, but successful and failed B-cell related clinical trials indicate that a better understanding of the B cell pathway in treatment is required to develop targeted new treatments.

Experimental results for this project have been obtained, analysis is ongoing and [a manuscript is in preparation](#).

Ide Smets, Teresa Prezzemolo, Josselyn E. Garcia-Perez, Klara Mallants, James Dooley, Stephanie Humblet-Baron, Bénédicte Dubois, Adrian Liston*@, An Goris*@, The role of BAFF and BAFF receptors in the treatment of multiple sclerosis. manuscript in preparation

2. We correlate the B cell pathway with genetic and clinical factors in order to better understand how these contribute to patient-to-patient heterogeneity in pathogenesis and response to treatment. This outcome would provide a rationale for personalized medicine.

[The correlation between genetic factors and the B cell pathway has led one publication in press and one manuscript under peer review.](#)

Ide Smets*, Barnaby Fiddes*, Josselyn E. Garcia-Perez*, Di He*, Klara Mallants, Wenjia Liao, James Dooley, George Wang, Stephanie Humblet-Baron, Bénédicte Dubois, Alastair Compston, Joanne Jones, Alasdair Coles, Adrian Liston, Maria Ban, An Goris@, Stephen Sawcer@. Multiple sclerosis risk variants alter expression of co-stimulatory genes in B cells. *Brain*, in press

Vasiliki Lagou, Josselyn E. Garcia-Perez, Ide Smets, Lies Van Horebeek, Marijne Vandeborgh, Liye Chen, Klara Mallants, Teresa Prezzemolo, Kelly Hilven, Stephanie Humblet-Baron, Matthieu Moisse, Philip Van Damme, Guy Boeckxstaens, Paul Bowness, Bénédicte Dubois, James Dooley, Adrian Liston*[@], An Goris*[@]. Interrelationship between genetic control of human immune system variation and disease susceptibility. *Nature Immunology*, under peer review

2. Achievements

2.1. Achievement 1. Multiple sclerosis risk variants alter expression of co-stimulatory genes in B cells (Smets et al., *Brain*, in press)

1. Summary

The increasing evidence supporting a role for B cells in the pathogenesis of multiple sclerosis prompted us to investigate the influence of known susceptibility variants on the surface expression of co-stimulatory molecules in these cells. Using flow cytometry we measured surface expression of CD40 and CD86 in B cells from 68 patients and 162 healthy controls that were genotyped for the multiple sclerosis associated single nucleotide polymorphisms (SNPs) rs4810485, which maps within the CD40 gene, and rs9282641, which maps within the CD86 gene. We found that carrying the risk allele at rs4810485*T lowered the cell-surface expression of CD40 in all tested B cell subtypes (in total B cells $p \leq 5.10 \times 10^{-5}$ in patients and $\leq 4.09 \times 10^{-6}$ in controls), while carrying the risk allele rs9282641*G increased the expression of CD86, with this effect primarily seen in the naïve B cell subset ($p = 0.048$ in patients and 5.38×10^{-5} in controls). In concordance with these results analysis of RNA expression demonstrated that the risk allele rs4810485*T resulted in lower total CD40 expression ($p = 0.057$) but with an increased proportion of alternative splice-forms leading to decoy receptors ($p = 4.00 \times 10^{-7}$). Finally, we also observed that the risk allele rs4810485*T was associated with decreased levels of interleukin-10 ($p = 0.020$), which is considered to have an immunoregulatory function downstream of CD40. Given the importance of these co-stimulatory molecules in determining the immune reaction that appears in response to antigen our data suggest that B cells might have an important antigen presentation and immunoregulatory role in the pathogenesis of multiple sclerosis.

2. Situation in the GSKE project

This study unraveled the mechanism of action of established MS susceptibility genes CD40 and CD86, which fall within the B-cell pathway that is the topic of this GSKE project. The study demonstrates that the CD40 MS risk variant acts through a deficit in the protective role of immunoregulatory B cells. These immunoregulatory B cells are enriched amongst early (transitional) B cells, respond to the growth factor B cell activating factor (BAFF) and produce the immunoregulatory cytokine interleukin10.

3. Future perspectives and clinical implications

Blocking CD40 with monoclonal anti-CD40 antibodies has been proposed as a therapy for MS based on animal models and is currently considered by pharmaceutical companies. However, the results from our study suggest that decreasing or blocking CD40 is associated with increased risk for MS instead of protection. Whereas anti-CD40 may be beneficial for more antibody-driven autoimmune diseases such as lupus erythematosus, it calls for extreme caution in applying this treatment for MS. This is completely in line with the anti-BAFF therapies, which are successful in other autoimmune diseases but failed clinical trials in MS and even worsened instead of improved MS. Both anti-CD40 and anti-BAFF limit the important role of immunoregulatory B cells in MS.

Results also suggest that if limiting the role of immunoregulatory B cells worsens disease, enhancing the protective role of immunoregulatory B cells in MS may instead be beneficial. We have previously demonstrated that several currently used and efficacious MS treatments share this as a unique mechanism of action². This shared B-cell related mechanism has recently been extended to other novel

treatments in the literature^{3,4} and in recent conference presentations (European Charcot Symposium, November 2017). Our results especially suggest that current, promising B cell depletion therapies may increase the efficacy/safety balance if they would deplete B cells more selectively, i.e. deplete likely pathogenic B cells such as memory B cells, but spare beneficial B cells such as the immunoregulatory B cells. Our research group is currently working towards a scientific basis for this aim.

2.2. Achievement 2. Interrelationship between genetic control of human immune system variation and disease susceptibility (Lagou et al., manuscript under peer review)

1. Summary

The immune system is characterized by enriched polymorphism in genetic control factors, coupled to a high degree of cellular plasticity and sensitivity to environmental drivers. This diversity is an important control mechanism for infections but also contributes to susceptibility to a broad set of sterile diseases. Despite this, characterization of the genetic architecture of the immune system has lagged behind the vast progress made by genome-wide association studies (GWAS) of emergent diseases. Our GWAS for 54 functionally relevant immune phenotypes in 489 healthy individuals identifies eight novel genome-wide significant associations explaining 6-20% of variance. Results implicate novel variant pathways as key immune regulators in humans, in particular controlling B and T cell differentiation and pro-inflammatory cytokine response. Suggestive associations reveal new mechanisms of disease associations. Pinpointing key human immune regulators offers therapeutic perspectives.

2. Situation in the GSKE project

The recent advent of in-depth immune phenotyping across large sample sizes has enabled characterization of the extent and identification of the factors shaping variation in the human immune profile⁶. Longitudinal studies have reported high levels of inter-individual variation, with low longitudinal variation and a highly elastic structure, where transient antigen-induced changes are followed by a return to the individual's unique baseline^{7,8}. Twin and family-based studies provide heritability estimates of 20-40% on average, but covering a wide range across individual traits^{7,9,10}. Aging contributes up to 5% of variation^{7-9,11}, and environmental factors include obesity, cohabitation and chronic viral infections^{8,9,11}. Identification of genetic factors controlling variation in the immune system is still in the initial discovery phase, with novel and strong associations emerging from pioneer studies^{7,10,11}. We performed a GWAS of up to 10,246,977 autosomal variants in 489 healthy Caucasian individuals for 54 immune phenotypes established as part of our previous study⁸. The 54 functionally relevant immune phenotypes for which genetic determinants were identified in this study include B cells and B cell subsets. We identified eight regions reaching genome-wide significance ($P < 5 \times 10^{-8}$) to at least one immune phenotype. Amongst these genome-wide significant results, we identify genetic determinants controlling B cell immunophenotypes that are of relevance for the pathogenesis of MS. In particular, one association was seen for memory B cells, a cell type we previously implicated in the immune profile of MS². A second association was observed for KREC excision circles. KREC is a marker for the early B cells which are enriched for the immunoregulatory B cells that form the topic of this GSKE project. The genetic variant associated with KREC influences the expression of a gene that previously shown to control early B cells in mice. Our data provide the first evidence translating the key importance of these genes and pathways from animals to humans, and highlight that in humans these pathways are variable in vivo in a physiological range.

3. Future perspectives and clinical implications

We have previously demonstrated that KREC is increased upon treatment with current efficacious MS treatments². We currently investigate whether KREC and/or the genetic determinant associated with KREC is associated with the efficacy of MS treatments and can be used as a biomarker for treatment response. Such biomarkers are much needed to ensure that each patient is treated as early as possible with the best possible treatment ("precision medicine") in the current context where the clinician is

faced with the choice between a whole range of MS treatments, each with their own efficacy and safety profile. Further understanding of the role of how these novel genes and pathways control B cell numbers and B cell differentiation may additionally offer novel leads for rational treatment design in the context of targeting B cells as a promising therapeutic strategy for MS.

2.3. Achievement 3. The role of BAFF and BAFF receptors in the treatment of multiple sclerosis (Smets et al., manuscript in preparation)

1. Summary

We have collected peripheral blood mononuclear cells (PBMCs) from a cohort of 114 MS patients, with three subsets of untreated patients, patients treated with interferon-beta and patients treated with fingolimod. For comparison, we include 40 patients suffering from autoimmune thyroid disease (AITD). The characteristics of the study population are summarized in **Table 1**. We used the PBMCs of this cohort for a large flow cytometry experiment focusing on total B cells and five different B cell subsets. The B cell marker definitions have been outlined in **Table 2**. A representative experiment for one patient including gating strategy is illustrated in **Figure 1**. All flow cytometry experiments have been completed, RNA expression analyses are ongoing, and the data are under analysis. A manuscript from this work is under preparation.

Number of MS patients	114	Number of AITD patients	40
Female/Male	72/42	Female/Male	33/7
Age (years), mean (\pm SD)	49 (\pm 13.3)	Age (years), mean (\pm SD)	46 (\pm 15.0)
Age at onset (years), mean (\pm SD)	33 (\pm 11.6)	Hashimoto/Graves	9/31
Disease course, RR/PP	104/9		
MSSS, mean (\pm SD)	2.8 (\pm 2.5)		
Treatment			
None	43		
Fingolimod	29		
Interferon beta	42		

Table 1: Study demographics

AITD = autoimmune thyroid disease, MS = Multiple sclerosis, MSSS = Multiple Sclerosis Severity Score, RR = relapsing remitting, PP = primary progressive, SD = standard deviation

Marker definition	Subset name
CD19 ⁺	B
CD19 ⁺ TACI ⁺	B_TACI
CD19 ⁺ BAFF-R ⁺	B_BAFFR
CD19 ⁺ CD80 ⁺	B_CD80
CD19 ⁺ CD86 ⁺	B_CD86
CD19 ⁺ CD40 ⁺	B_CD40
CD19 ⁺ CD27 ⁺ IgD ⁻	Naive
CD19 ⁺ TACI ⁺	Naive_TACI
CD19 ⁺ BAFFR ⁺	Naive_BAFFR
CD19 ⁺ CD80 ⁺	Naive_CD80
CD19 ⁺ CD86 ⁺	Naive_CD86
CD19 ⁺ CD40 ⁺	Naive_CD40
CD19 ⁺ CD27 ⁺ IgD ⁺	Memory
CD19 ⁺ CD27 ⁺ IgD ⁺ TACI ⁺	Memory_TACI
CD19 ⁺ CD27 ⁺ IgD ⁺ BAFFR ⁺	Memory_BAFFR
CD19 ⁺ CD27 ⁺ IgD ⁺ CD80 ⁺	Memory_CD80
CD19 ⁺ CD27 ⁺ IgD ⁺ CD86 ⁺	Memory_CD86
CD19 ⁺ CD27 ⁺ IgD ⁺ CD40 ⁺	Memory_CD40
CD19 ⁺ CD27 ⁺ IgD ⁻	Switched Memory
CD19 ⁺ CD27 ⁺ IgD ⁻ TACI ⁻	Switched_TACI
CD19 ⁺ CD27 ⁺ IgD ⁻ BAFFR ⁺	Switched_BAFFR
CD19 ⁺ CD27 ⁺ IgD ⁻ CD80 ⁺	Switched_CD80
CD19 ⁺ CD27 ⁺ IgD ⁻ CD86 ⁺	Switched_CD86
CD19 ⁺ CD27 ⁺ IgD ⁻ CD40 ⁺	Switched_CD40
CD19 ⁺ CD24 ^{hi} CD38 ^{hi}	Transitional
CD19 ⁺ CD24 ^{hi} CD38 ^{hi} TACI ⁺	Tr_TACI
CD19 ⁺ CD24 ^{hi} CD38 ^{hi} BAFFR ⁺	Tr_BAFFR
CD19 ⁺ CD24 ^{hi} CD38 ^{hi} CD80 ⁺	Tr_CD80
CD19 ⁺ CD24 ^{hi} CD38 ^{hi} CD86 ⁺	Tr_CD86
CD19 ⁺ CD24 ^{hi} CD38 ^{hi} CD40 ⁺	Tr_CD40
CD19 ⁺ CD24 ⁻ CD38 ⁺	Plasmablast
CD19 ⁺ CD24 ⁻ CD38 ⁺ TACI ⁺	PB_TACI
CD19 ⁺ CD24 ⁻ CD38 ⁺ BAFFR ⁺	PB_BAFFR
CD19 ⁺ CD24 ⁻ CD38 ⁺ CD80 ⁺	PB_CD80
CD19 ⁺ CD24 ⁻ CD38 ⁺ CD86 ⁺	PB_CD86
CD19 ⁺ CD24 ⁻ CD38 ⁺ CD40 ⁺	PB_CD40

Table 2: B cell marker definition

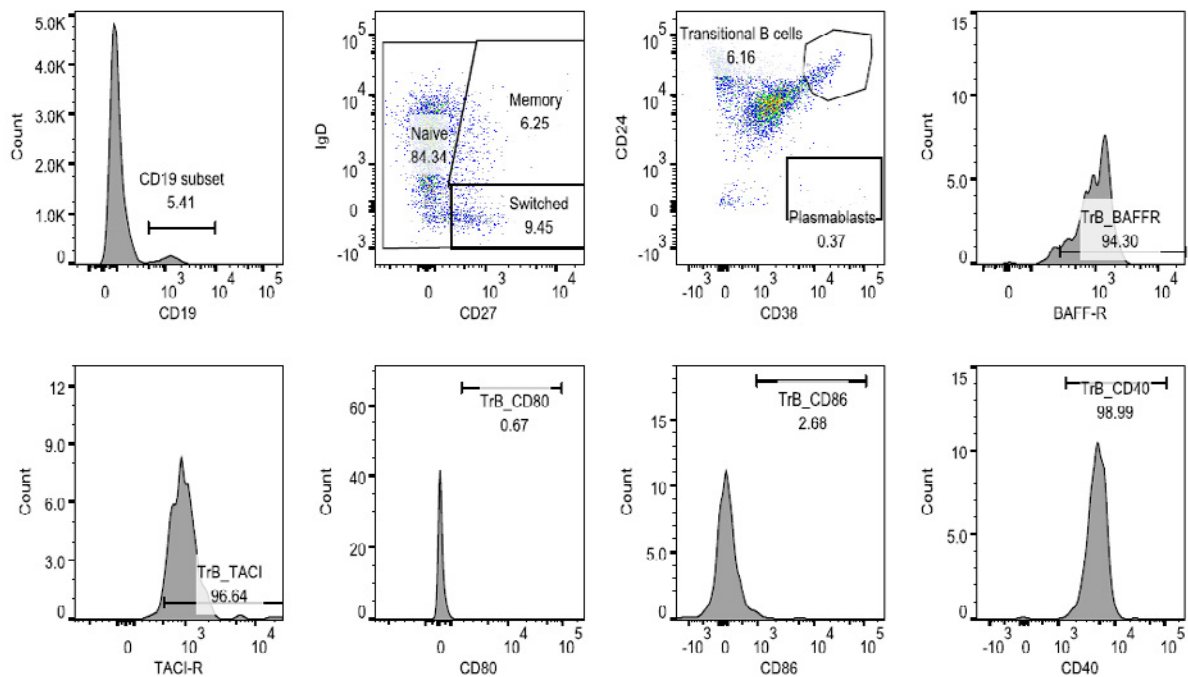


Figure 1: B cell flow cytometry gating strategy in one untreated MS patient.

2. Situation in the GSKE project

We previously compared 245 individuals, including untreated MS patients as well as four common immunomodulatory treatments (interferon-beta, glatiramer acetate, natalizumab, fingolimod), on the same large-scale platform². An increase in memory CD8⁺ T cells and B cells was observed in untreated MS patients. Interferon-beta and fingolimod have significant impacts upon multiple aspects of the peripheral immune system, and overall push the immune system in different directions. We identified a unique B cell related pathway shared across these treatments: an increase in transitional B cells driven by elevated B cell activating factor (BAFF) levels. Whereas this pathway may be therapeutic in MS through a regulatory B cell function¹², it is thought to be pathogenic in other autoimmune diseases by inducing auto-antibody production¹³. By comparing treatment groups with untreated patients and controls, as well as AITD patients (where this pathway may be pathogenic), we refine in detail the B cell pathway upregulated during treatment of MS and the specific markers involved.

3. Future perspectives and clinical implications

An improved understanding of how BAFF has a protective role in MS, likely through regulatory B cells, but contributes to the pathogenesis of other autoimmune diseases where auto-antibody production is a hallmark, will provide novel leads for B cell related therapeutic strategies in MS. This would allow the development of more specific B cell therapies instead of the current promising but non-selective B cell therapies, which deplete all B cells with potential safety concerns.

3. Networking and collaborations

Achievement 1 was realized in collaboration with Prof. Stephen Sawcer of Cambridge University (UK). Importantly, concordant results and conclusions were reached in both the Belgian case and UK control study populations, independent of experimental design, providing replication and robustness of our results. Our research group is a member of the Research Foundation Flanders Research Community Multiple Sclerosis, is the Belgian representative in the International Multiple Sclerosis Genetics Consortium (www.imsgc.org), and is a member of the EU Horizon2020 Consortium MultipleMS (www.multiplems.eu).

Over the past year, members of my research group and I attended the European Conference on the Treatment and Research in Multiple Sclerosis (ECTRIMS) in Paris, France and the European Charcot Foundation Meeting in Baveno, Italy. Results from the achievements above were presented at the following occasions:

- 24-October-2017: Research Community “Multiple Sclerosis” of the Research Foundation Flanders, Hasselt, Belgium
- 26-October-2017: European Conference on the Treatment and Research in Multiple Sclerosis (ECTRIMS), Paris
- 24-November-2017: Belgian Immunological Society, Leuven, Belgium
- 9-November-2017: Department of Human Genetics, KU Leuven, Belgium
- 6-December-2017: Neurology Department UZ Leuven, Belgium

4. Relevance and future perspectives

In summary, results obtained so far strongly indicate a role of B cells in the pathogenesis as well as the treatment of MS. Our genetic and immunological studies indicate, however, that not all B cell subsets contribute equally. Whereas the memory B cell subset is thought to exert a pathogenic role, the subset of immunoregulatory B cells appears protective in the disease process and contributes to the mechanism of action of current treatments. B cell depletion therapies, in which all B cells are wiped out, are the most promising novel treatment for MS that has entered the Belgian market. B cell depletion therapies highly reduce disease activity but their long-term safety, for example with respect to susceptibility to infections, remains to be evaluated. Our data indicate that a more selective or a more targeted B cell depletion, wiping out only pathogenic B cells but sparing beneficial B cells may increase the efficacy/safety balance of MS treatment. Whereas B cell depletion therapies are promising overall, there is a group of patients for whom the treatment is not effective but may even worsen disease. B-cell related biomarkers may indicate the subset of MS patients who are most likely to benefit from B cell therapies. Our research group currently continues on these two lines: understanding the precise role of B cell subsets towards a more targeted therapy and identifying possible B-cell related biomarkers for precision medicine. Support from GSKE is instrumental in this B-cell research line within our research group, and any additional financial support would allow us to build maximally on the promising results obtained in the first year. Please see the section “Future perspectives” for each of the manuscripts described above on how we would specifically extend this research line in future. We expect to translate our research results to the much-anticipated and much-needed development of precision medicine in the clinical care for MS patients.

5. Financial report

As foreseen, GSKE support has been assigned for 50% to staff and 50% to consumable costs. The KU Leuven Financial Department will provide a detailed report. Current achievements are part of the PhD thesis of Ide Smets, first author of two of the GSKE supported manuscripts, who plans to defend her PhD thesis in September 2018. Marijne Vandebergh, graduated *magna cum laude* in Biomedical Sciences at the KU Leuven in June 2017, recently joined the project and will - together with expert technical assistance by Klara Mallants - ensure continuity over the following years. Continued support from GSKE would in particular allow us to cover part of staff and consumable costs for research building on current results outlined under future perspectives.

6. Publications under GSKE support

* indicates shared first/senior authors and @ indicates corresponding author

- Ide Smets*, Barnaby Fiddes*, Josselyn E. Garcia-Perez*, Di He*, Klara Mallants, Wenjia Liao, James Dooley, George Wang, Stephanie Humblet-Baron, Bénédicte Dubois, Alastair Compston, Joanne Jones, Alasdair Coles, Adrian Liston, Maria Ban, An Goris@, Stephen Sawcer@. Multiple sclerosis risk variants alter expression of co-stimulatory genes in B cells. *Brain*, in press
- Vasiliki Lagou, Josselyn E. Garcia-Perez, Ide Smets, Lies Van Horebeek, Marijne Vandeborgh, Liye Chen, Klara Mallants, Teresa Prezzemolo, Kelly Hilven, Stephanie Humblet-Baron, Matthieu Moisse, Philip Van Damme, Guy Boeckxstaens, Paul Bowness, Bénédicte Dubois, James Dooley, Adrian Liston*@, An Goris*@. Interrelationship between genetic control of human immune system variation and disease susceptibility. *Nature Immunology*, under peer review

7. Team publications

* indicates shared first/senior authors and @ indicates corresponding author

- The International Multiple Sclerosis Genetics Consortium. The Multiple Sclerosis Genomic Map: Role of peripheral immune cells and resident microglia in susceptibility. *Science*, revision in preparation. Available on <http://dx.doi.org/10.1101/143933>
- Lagou V., Garcia-Perez J.E., Smets I., Van Horebeek L., Vandeborgh M., Chen L., Mallants K., Prezzemolo T., Hilven K., Humblet-Baron S., Moisse M., Van Damme P., Boeckxstaens G., Bowness P., Dubois B., Dooley J., Liston A.*@, Goris A.*@. Interrelationship between genetic control of human immune system variation and disease susceptibility. *Nature Immunology*, under peer review
- Smets I.*, Fiddes B.*, Garcia-Perez J.E.*, He D.*, Mallants K., Liao W., Dooley J., Wang G., Humblet-Baron S., Dubois B., Compston A., Jones J., Coles A., Liston A., Ban M., Goris A.@, Sawcer S.@. Multiple sclerosis risk variants alter expression of co-stimulatory genes in B cells. *Brain*, in press
- Hilven K.*, Vandeborgh M.*, Smets I., Mallants K., Goris A.@, Dubois B.. Genetic basis for relapse rate in multiple sclerosis: association with *LRP2* genetic variation. *Multiple Sclerosis Journal*, in press
- Put K., Vandenhaute J., Avau A., Van Nieuwenhuijze A., Brisse E., Dierckx T., Rutgeerts O., Garcia-Perez J., Toelen J., Waer M., Leclercq G., Goris A., Van Weyenbergh J., Liston A., De Somer L., Wouters C., Matthys P.@ (2017). Inflammatory gene expression profile and defective IFN- γ and granzyme K in natural killer cells of systemic juvenile idiopathic arthritis patients. *Arthritis & Rheumatology*, 69, 213-224.
- McLaughlin R.*, Schijven D.*, van Rheenen W., van Eijk K., O'Brien M., Project MinE GWAS Consortium, Schizophrenia Working Group of the Psychiatric Genomics Consortium, Kahn R., Ophoff R., Goris A., Bradley D., Al-Chalabi A., van den Berg L., Luykx J.@, Hardiman O.@, Veldink J.# (2017). Genetic correlation between amyotrophic lateral sclerosis and schizophrenia. *Nature Communications*, 8, 14774-14774.

8. References

1. Dendrou, C. A., Fugger, L. & Friese, M. A. Immunopathology of multiple sclerosis. *Nat Rev Immunol* **15**, 545-558, doi:10.1038/nri3871 (2015).
2. Dooley, J. *et al.* Immunological profiles of multiple sclerosis treatments reveal shared early B cell alterations *Neurology(R) neuroimmunology & neuroinflammation* **3**, e240 (2016).
3. Miyazaki, Y. *et al.* Suppressed pro-inflammatory properties of circulating B cells in patients with multiple sclerosis treated with fingolimod, based on altered proportions of B-cell subpopulations. *Clin Immunol* **151**, 127-135, doi:10.1016/j.clim.2014.02.001 (2014).
4. Schubert, R. D. *et al.* IFN-beta treatment requires B cells for efficacy in neuroautoimmunity. *J Immunol* **194**, 2110-2116, doi:10.4049/jimmunol.1402029 (2015).
5. Krumbholz, M., Derfuss, T., Hohlfeld, R. & Meinl, E. B cells and antibodies in multiple sclerosis pathogenesis and therapy. *Nat Rev Neurol* **8**, 613-623, doi:10.1038/nrneuro.2012.203 (2012).
6. Liston, A., Carr, E. J. & Linterman, M. A. Shaping Variation in the Human Immune System. *Trends in immunology* **37**, 637-646, doi:10.1016/j.it.2016.08.002 (2016).
7. Orru, V. *et al.* Genetic variants regulating immune cell levels in health and disease. *Cell* **155**, 242-256, doi:10.1016/j.cell.2013.08.041 (2013).
8. Carr, E. J. *et al.* The cellular composition of the human immune system is maintained in multiple stable equilibriums shaped by age and cohabitation *Nat Immunol* **417**, 461-468 (2016).
9. Brodin, P. *et al.* Variation in the human immune system is largely driven by non-heritable influences. *Cell* **160**, 37-47, doi:10.1016/j.cell.2014.12.020 (2015).
10. Roederer, M. *et al.* The genetic architecture of the human immune system: a bioresource for autoimmunity and disease pathogenesis. *Cell* **161**, 387-403, doi:10.1016/j.cell.2015.02.046 (2015).
11. Aguirre-Gamboa, R. *et al.* Differential Effects of Environmental and Genetic Factors on T and B Cell Immune Traits. *Cell Rep* **17**, 2474-2487, doi:10.1016/j.celrep.2016.10.053 (2016).
12. Bouaziz, J. D., Yanaba, K. & Tedder, T. F. Regulatory B cells as inhibitors of immune responses and inflammation. *Immunol Rev* **224**, 201-214, doi:10.1111/j.1600-065X.2008.00661.x (2008).
13. Vossenkamper, A., Lutalo, P. M. & Spencer, J. Translational Mini-Review Series on B cell subsets in disease. Transitional B cells in systemic lupus erythematosus and Sjogren's syndrome: clinical implications and effects of B cell-targeted therapies. *Clin Exp Immunol* **167**, 7-14, doi:10.1111/j.1365-2249.2011.04460.x (2012).



Geneeskundige Stichting Koningin Elisabeth
Fondation Médicale Reine Elisabeth
Königin-Elisabeth-Stiftung für Medizin
Queen Elisabeth Medical Foundation

Progress report
of the research group of

Prof. dr. Leybaert Luc, MD. PhD

Universiteit Gent (UGent)

Principal investigator

Prof. dr. Leybaert Luc, MD. PhD
Dept. Basic Medical Sciences
Faculty of Medicine and Health Sciences
Ghent University
Belgium
Tel.: +32 9 332 33 66
Fax: +32 16 33 09 39
E-mail; Luc.Leybaert@UGent.be

Exploring the role of astroglial Cx43 hemichannels as therapeutic targets in stroke.

1. Introduction

Stroke is, like cancer, associated with a major mortality risk and is the second important cause of death, next to ischemic heart disease. The majority of strokes are caused by blood vessel obstruction, either by a clot (thrombus) or an embolism, resulting in decreased perfusion of certain brain areas and rapid development of ischemia, leading to cell injury and neuronal cell death. Current therapeutic possibilities include clot lysis by means of tissue plasminogen activator (tPA) administration within 3 hours or endovascular clot removal (endarterectomy) within 6 hours after the insult. As a result of these limited time windows and possible side effects of these treatments, a majority of patients fall outside the selection criteria to receive these treatments. Hence, there is an urgent need for further research towards identifying novel therapeutic targets and developing new treatments. The work performed in this project aims to investigate connexin proteins as potential targets to protect the brain against ischemic cell injury. Brain cells not only encompass neurons but also glial cells that are in fact more numerous than neurons (at least 3 times more numerous depending on the species). Research over the past 20 years has demonstrated that astrocytes (star shaped glial cells), which form a bridge between neurons and blood vessel cells, exert crucial functions in substrate delivery to the neurons (energy substrate, neurotransmitter precursors) and removal of end products of metabolism as well as ions, which are transferred away from active zones and transferred to the blood. This crucial role of astrocytes is, in part, facilitated by connexin proteins that form channels, called gap junctions, that connect cells to form a large glial network, called the glial syncytium. Gap junctions are formed by two half gap junction channels called 'hemichannels'; these hemichannels are also present in the plasma membrane in their free form, i.e. not as part of a gap junction. As such, hemichannels form non-selective pores that, when open, pass ions and molecules up to ~1.5 kDa, which may disturb cell function and lead to cell injury/cell death. The purpose of the present work is to investigate whether blocking hemichannels protects the neural tissue against post-ischemic cell injury. Over the past 10 years, the Leybaert group has provided a detailed characterization of hemichannel control by cytoplasmic Ca^{2+} and developed, based on these insights, a peptide toolset that allows to specifically modulate hemichannel function; one of these compounds is Gap19 that inhibits hemichannels composed of Cx43, the most abundant connexin in the brain that is largely present in astrocytes. Interestingly, Gap19 does not inhibit gap junctions and as such leaves the crucial physiological functions of the junctional channels intact. The work presented below reports on the first year research activities performed in the context of investigating connexin hemichannels as a potential target to protect the brain against ischemic injury. We also started up work directed at investigating the role of connexin hemichannels as a vascular target to prevent blood-brain barrier dysfunction, thereby providing brain protection at the blood-brain interface. The work related to this second aim will be presented in the next report when the dataset is more complete.

Summary results of the first year research activities. In this first year, we characterized a mutant Cx43 with a 'phospho-dead' MAP kinase domain and found it to phenotypically present with a loss of hemichannel function in brain astrocytes. In an animal model of permanent occlusion of the mid-cerebral artery, Cx43 MAP kinase mutant animals had significantly smaller brain infarcts and less cell death compared to WT animals. We tested other Cx43 phosphorylation sites (PKC, CK1) but those did not protect against permanent brain ischemia. We also tested whether blocking hemichannels with Gap19 could provide protection in WT animals and found that this peptide gave a similar reduction in brain infarct size as observed in the Cx43 MAP kinase mutants. Interestingly, this protection was obtained by a single i.p. administration of Gap19 2 hours after vessel occlusion, mimicking a therapeutic

setting. Further work is underway to characterize the protective effect at the level of functional post-ischemic deficits. The paper concerning this work will be submitted in 2018 when all experimental work including functional characterization is finalized. Another paper on protection at the blood-brain interface will also be submitted in 2018; results regarding this work will be discussed in the next report.

2. Targeting connexin hemichannels to protect the brain against ischemic injury.

Hemichannels are composed of six connexin subunits, which are tetraspan proteins that contain two extracellular loops, one intracellular loop and N- and C-terminal domains located inside the cell (Fig. 1). Opening of Cx43 hemichannels necessitates an interaction of the C-terminal tail with the intracellular loop as demonstrated by previous work from our group (1). We started the present work from the observation that the C-terminal tail of Cx43 has two different domains that interact with the intracellular loop: the CT9 domain composed of the last 9 amino acids (2-4) of the C-terminal and the Src homology-3 (SH3) binding domain located ~100 amino acids upstream in N-terminal direction (5). This SH3 domain is part of a larger stretch of amino acids that contain 4 Ser residues from a MAP-kinase (MAPK) domain, further called the MK4 domain (Fig. 1).

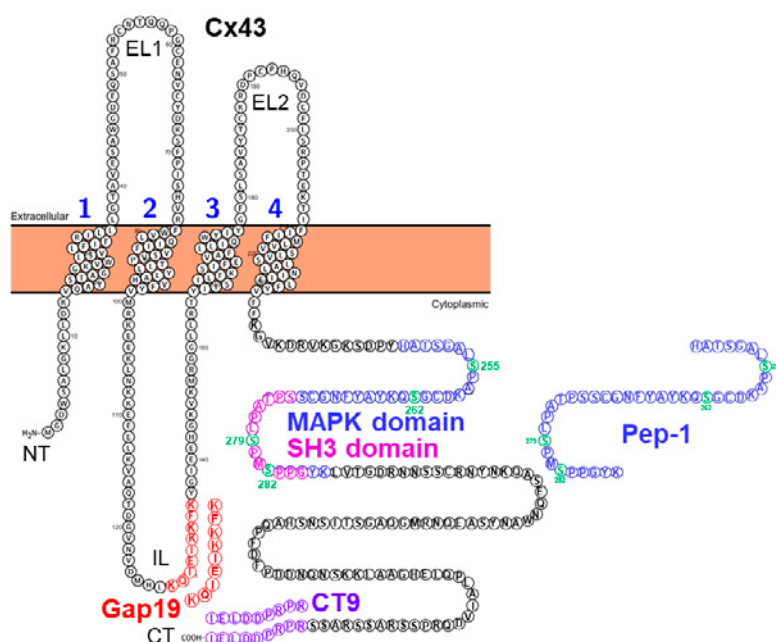


Fig. 1. Cx43 topology with indication of the CT9, SH3 and MAPK domains, and the peptides Gap19, Pep-1 and CT9.

To investigate whether the MK4 domain, which is larger than the SH3 domain, is also involved in hemichannel regulation, we performed experiments on Cx43 in which the 4 Ser residues in the MK4 domain (S255, S262, S279 & S282 – marked green in Fig. 1) were each modified to Ala making the MK4 domain ‘phospho-dead’. In collaboration with the group of Dr. P. Lampe (Translational Research Program, Fred Hutchinson Cancer Research Center, Seattle, USA) we obtained transgenic animals expressing mutant Cx43 with a phospho-dead MK4 domain (Cx43 phosphorylation null mutants) and performed single channel patch-clamp experiments on Cx43 hemichannel function. In astrocytes isolated from WT animals, hemichannel openings were triggered by a small increase of the intracellular Ca^{2+} concentration ($[Ca^{2+}]_i$) from 50 to 200 nM (Fig. 2A). Gap19, a nonapeptide derived from the cytoplasmic loop of Cx43 (Fig. 1), which was previously shown to inhibit hemichannel activity without inhibiting gap junctions (6), abolished the unitary current activities (Fig. 2A). All-point histograms furthermore indicated a unitary conductance in the range of 230-245 pS, i.e. in the range of ~220 pS reported for Cx43 hemichannels (7, 8) (Fig. 2B). As illustrated in Fig. 2C, charge transfer mediated by hemichannels was negligible at

50 nM $[Ca^{2+}]_i$, but was significantly enhanced at 200 nM $[Ca^{2+}]_i$ and was reduced to the basal level by Gap19 (Fig. 2C). Remarkably, in astrocytes isolated from MK4 Cx43 phosphorylation null mutant animals, 200 nM $[Ca^{2+}]_i$ stimulation did not trigger any hemichannel current activity indicating loss of hemichannel function (Fig. 2D). We next tested whether supplying MK4 mutant astrocytes with a cell-penetrating peptide called Pep-1 composed of His-248 to Lys-287 on the Cx43 CT encompassing the 4 Ser residues modified in MK4 mice (Fig. 1), could rescue hemichannel activity. Strikingly, preincubating astrocytes isolated from MK4 mutant animals with Pep-1 rescued hemichannel activities at 200 nM $[Ca^{2+}]_i$ (Fig. 2D). As illustrated in Fig. 2E, the unitary conductance of restored hemichannel currents in MK4 mutant astrocytes was in the range of 220-240 pS, not different from the conductance in WT astrocytes. We further quantified the effect of Pep-1 on charge transfer associated with hemichannel openings and demonstrated significantly increased charge transfer at 200 nM $[Ca^{2+}]_i$ in MK4 mutant astrocytes exposed to Pep-1 peptide as compared to those in non-treated MK4 mutants (Fig. 2F).

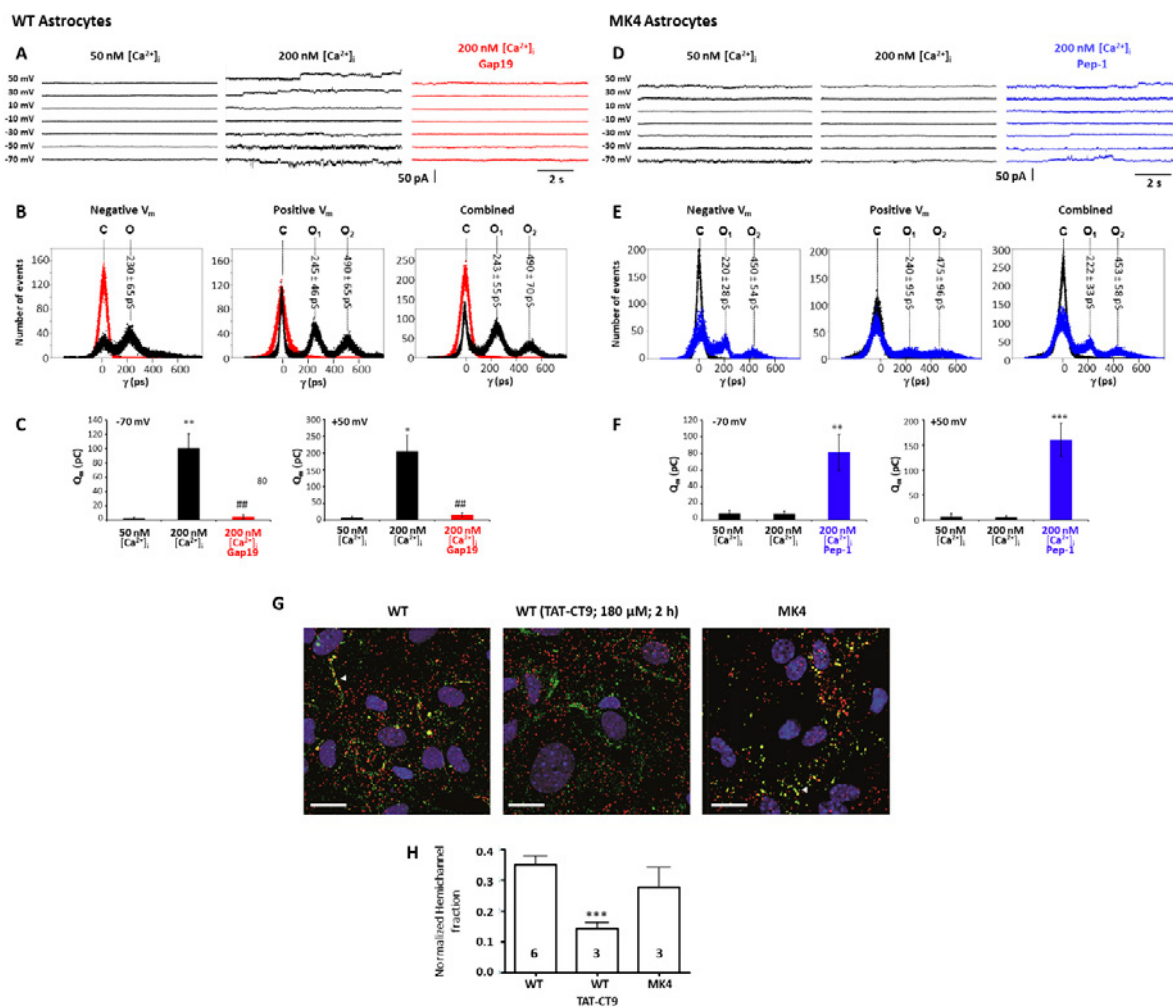


Fig. 2. Hemichannel activity is reduced in MK4 Cx43 phosphorylation null mutant astrocytes. **A.** Current traces in WT astrocytes for voltage steps indicated left. Unitary current activity appeared at both negative and positive V_m when $[Ca^{2+}]_i$ was elevated from 50 nM to 200 nM. Gap19 (100 μ M, added via the pipette) suppressed unitary activity (red traces). **B.** All-point histogram of current activities at negative, positive and combined V_m . Unitary conductance of one (O₁) or two open hemichannels (O₂) are indicated above each peak (mean \pm s.d.). Gap19 abolished all current activity (red peak at baseline). **C.** Charge transfer (Q_m) associated with unitary current activities for recordings at -70 and +50 mV ($n = 6$). * $P < 0.05$ vs 50 nM $[Ca^{2+}]_i$; ** $P < 0.01$; ##, $P < 0.01$ vs 200 nM $[Ca^{2+}]_i$. **D.** Current traces in MK4 mutant astrocytes. Unitary activity was absent at 200 nM $[Ca^{2+}]_i$ but pre-treatment with Pep-1 peptide (35 μ M, 1 h) restored activity (blue traces). **E.** All-point histogram showing that currents restored by Pep-1 had a single channel conductance similar to WT. **F.** Q_m charge transfer data illustrating restoration of opening activities with Pep-1 ($n = 6$). ** $P < 0.01$ compared to 200 nM $[Ca^{2+}]_i$; *** $P < 0.001$. **G.** Confocal images of Duolink (red) and Cx43 (green) stainings in WT and MK4 mutant astrocytes; yellow co-localization signal corresponds to hemichannels. WT astrocytes (left) displayed clear hemichannel signal (arrowhead) that was decreased after TAT-CT9 treatment; hemichannel signal was also present in MK4 mutant astrocytes (right). **H.** Summary data of normalized yellow signal, demonstrating that the signal from MK4 mutant astrocytes was not different from WT. *** $P < 0.001$ WT vs WT (TAT-CT9). Scale bars are 20 μ m. All error bars represent s.e.m.

To exclude the possibility that the lower unitary hemichannel activity is due to a smaller pool of plasma membrane hemichannels in MK4 mutants, we performed Duolink in situ proximity ligation assays in isolated WT and MK4 mutant astrocytes. This assay reports the spatial hemichannel organization relative to gap junctions through amplification of Cx43/ZO-1 complexes that represent hemichannels (9). As illustrated in Fig. 2G, red Duolink fluorescence occurred throughout the cells while the yellow signal produced by red-green co-localized spots at GJs (arrowhead), representing hemichannels underway to GJs as reported for other cell types (10). We next tested TAT-CT9, a peptide composed of the last 9 amino acids of the Cx43 C-terminal end fused to the TAT membrane translocation sequence; this peptide promotes incorporation of hemichannels into gap junctions by competing for ZO-1 binding for which the 4 last amino acids of the C-terminal tail are crucial (11). WT astrocytes treated with TAT-CT9 (180 μ M, 2 hr) displayed markedly less Duolink fluorescence signal, in line with its promoting effect on hemichannel assembly into GJs (Fig. 2G). Quantification of the yellow signal relative to the green Cx43 signal corresponding to the normalized plasma membrane hemichannel fraction, showed that the signal in MK4 mutant astrocytes was not different from the signal in WT cells (Fig. 2H). Thus, the lower hemichannel activity in MK4 mutant astrocytes is the consequence of altered gating and not the result of a decreased hemichannel pool.

The results discussed above demonstrated that MK4 Cx43 phosphorylation null mutant animals have a loss of hemichannel function in brain astrocytes. In a next step, we tested whether this is associated with a protective effect following ischemic stroke. To that purpose we collaborated with Dr. C.C. Naus (Cellular & Physiological Sciences, Faculty of Medicine, The University of British Columbia, Vancouver, Canada) and made use of various Cx43 phosphorylation null mutants generated by and Dr. P. Lampe (Translational Research Program, Fred Hutchinson Cancer Research Center, Seattle, USA). These mutants included the MK4 mutant but also a CK1 and PKC mutant; MAPK, CK1 and PKC kinases have all been shown to be active in ischemic conditions (12-15). To test whether disrupting CK1, PKC or MAPK phosphorylation sites of the C43 C-terminal tail impacts stroke outcome, a cohort of male and female WT and Cx43 phosphorylation null mutants for CK1, PKC and MAPK (MK4) mice were subjected to permanent occlusion of the mid-cerebral artery (pMCAO). Four days after pMCAO the CK1 and PKC Cx43 phosphorylation null mutant mice did not show significant changes in infarct volume with respect to WT controls (Fig. 3b and c). However, MK4 mutant mice exhibited a significant ($P = 0.0181$) 58.3% reduction in infarct volume compared with WT counterparts (Fig. 3b and c). In light of the compelling phenotype observed in MK4 mutant ischemic mice, a larger cohort of WT and MK4 mutant male and female animals were subjected to pMCAO. Consistent with our initial study, MK4 mutant mice exhibited a significant ($P = 0.0053$) 40.2% reduction in infarct volume compared with WT counterparts (Fig. 3d). Apoptosis triggered by an ischemic event may occur over several days and contribute to delayed neuronal death and loss of viable peri-infarct tissue (16). To investigate whether the difference in infarct volume found in WT and MK4 mutant ischemic mice is correlated with differences in the level of apoptosis, WT and MK4 brain sections from ischemic mice were subjected to TUNEL immunostaining. In contrast to WT mice, TUNEL staining exhibited a significant ($P = 0.0337$) 70.0% reduction in the number of apoptotic TUNEL+ cells within the infarct region of MK4 mutant brain tissue sections, 4-days after pMCAO (Fig. 3e and f).

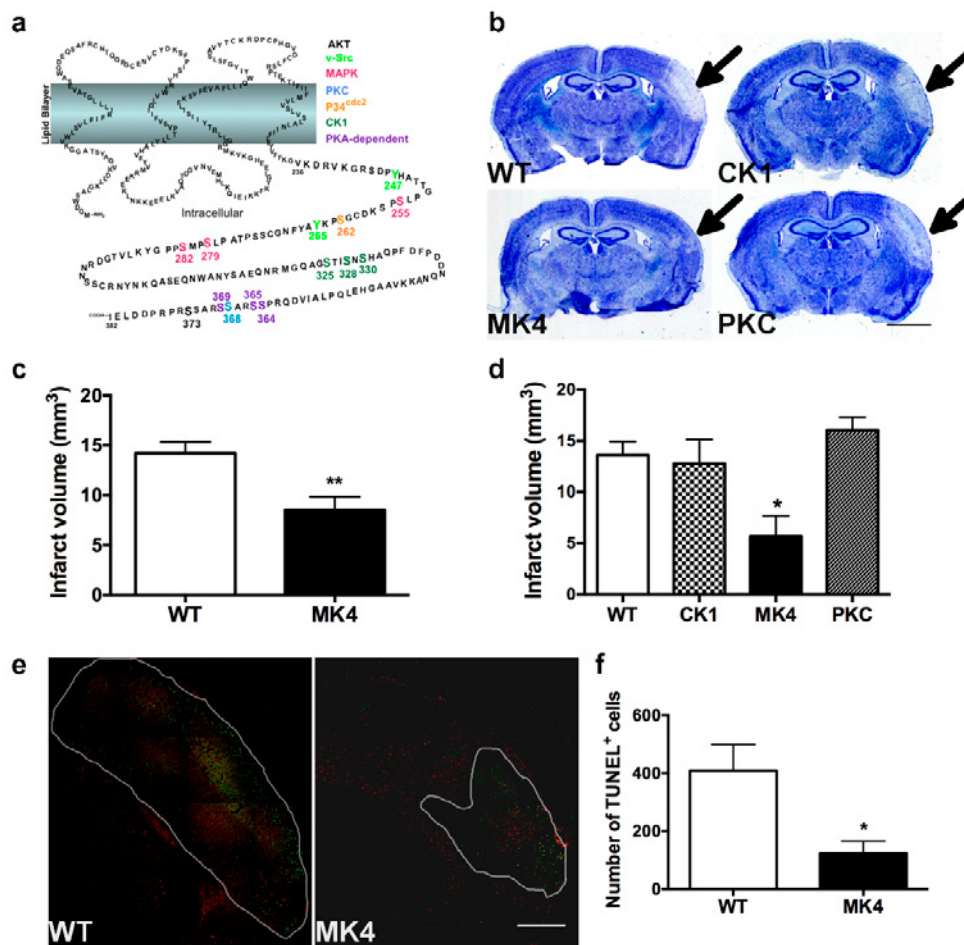


Fig. 3. Disrupting the MAPK phosphorylation sites of Cx43 C-terminus results in both a decrease in infarct volume and TUNEL staining 4-days after pMCAO. (a) Schematic depicting Cx43 secondary structure and phosphorylation sites in the C-terminal domain (modified from (76)). (b) Representative photomicrographs of thionin-stained sections from WT and Cx43 null phosphorylation mutant CK1, PKC and MAPK (MK4) mutant mice, 4-days post-pMCAO. Scale bar = 2 mm. (c) Quantification of infarct volume from WT and Cx43 null phosphorylation mutant CK1, PKC and MAPK (MK4) thionin-stained brain sections, 4-days post-pMCAO (One-way ANOVA followed by Bonferroni post-test; * $P = 0.0181$; WT: $n = 5$ mice; CK1: $n = 4$; PKC: $n = 4$; MK4: $n = 4$). (d) Quantification of infarct volume from WT and MK4 thionin-stained brain sections, 4 days post-pMCAO (unpaired Student's t -test; ** $P = 0.0053$; WT: $n = 10$ mice; MK4: $n = 11$ mice). (e) Co-immunofluorescence staining of cerebral cortex from WT (left micrograph) and MK4 (right micrograph) mice, 4 days after pMCAO, using the astrocyte marker GFAP (red) with TUNEL apoptosis marker (green). White outline on WT and MK4 micrographs delineates infarct area. Scale bar = 500 μm . (f) Quantification of average number of TUNEL⁺ cells in brain sections from WT and MK4 mice 4 days after pMCAO (unpaired Student's t -test; * $P = 0.0337$; WT: 4 sections, $n = 5$ mice; MK4: 4 sections, $n = 4$ mice). All error bars represent s.e.m.

We next asked whether the decreased hemichannel activity exhibited in MK4 astrocytes is a key factor in the neuroprotective phenotype of these animals subjected to pMCAO. To test this hypothesis, we subjected WT animals to pMCAO followed by pharmacological administration of either the hemichannel blocker TAT-Gap19 (6) or its scrambled form TAT-GAP19^{scrambled}. Fusion of Gap19 to the TAT (transactivator of transcription) sequence facilitates cellular uptake of the peptide, allowing it to cross the blood-brain barrier (17). Intraperitoneal (i.p.) injection of 0.75 $\mu\text{mol/Kg}$ or 7.5 $\mu\text{mol/Kg}$ TAT-Gap19 2hrs after pMCAO, significantly reduced infarct volume by 47.8 %, and 77.6 %, respectively 4-days after pMCAO, compared with those mice that received saline or scrambled alone (Fig. 4a and b). Mice treated with the negative control TAT-gap19^{scrambled} did not show significant changes with respect to saline controls (Fig. 4a and b). Mice treated with 7.5 $\mu\text{mol/Kg}$ TAT-Gap19 showed a significant reduction in infarct volume compared to mice treated with 0.75 $\mu\text{mol/Kg}$ of TAT-Gap19 (Fig. 4b).

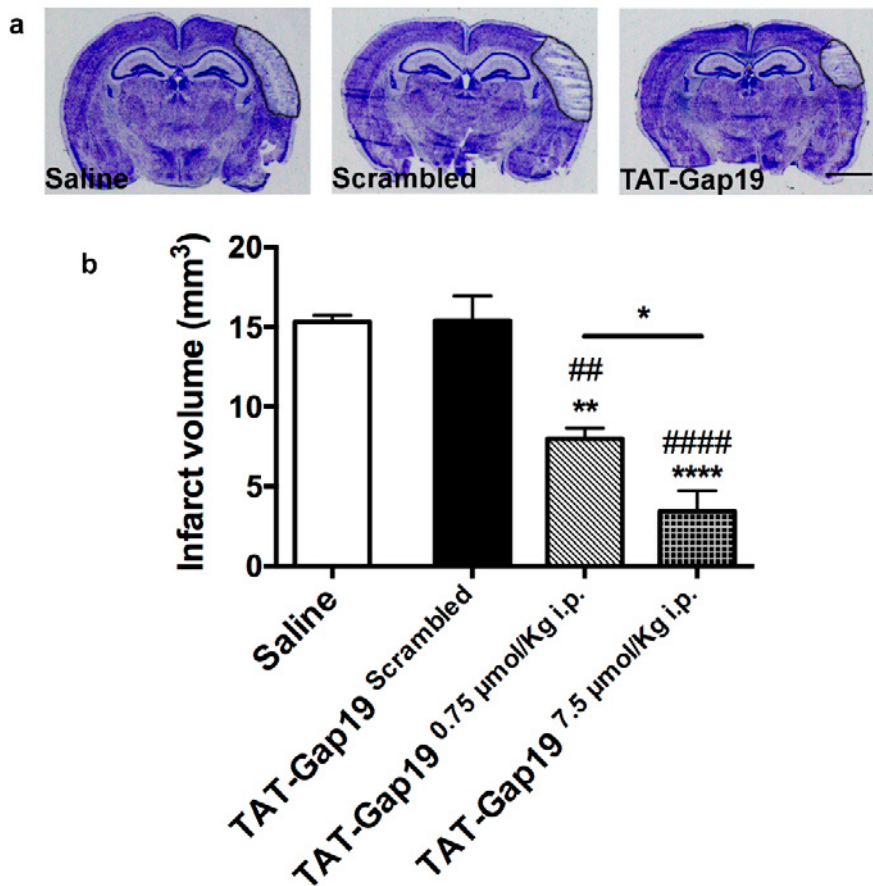


Fig. 4. TAT-Gap19 Cx43 hemichannel blocker is neuroprotective in mice subjected to pMCAO. (a) Representative photomicrographs of thionin-stained sections, 4 days after pMCAO, in WT mice treated with either saline (left micrograph), 7.5 μmol/Kg i.p. scrambled TAT-GAP19 Scrambled (center micrograph), or 0.75 μmol/Kg i.p. hemichannel blocker TAT-GAP19 (right micrograph), 2 hrs after pMCAO. Black outline highlights infarct. Scale bar = 2 mm. **(b)** Quantification of infarct volume, 4 days after pMCAO, from WT mice treated with either saline, 7.5 μmol/Kg i.p. scrambled TAT-GAP19 Scrambled, 0.75 μmol/Kg i.p. or 7.5 μmol/Kg i.p.. TATGAP19, 2 hrs after pMCAO. (One-way ANOVA followed by Tukey's multiple comparisons test; Saline vs Scrambled: $P = > 0.9999$; Saline vs 0.75 μmol/Kg TAT-GAP19: $**P = 0.0021$; Saline vs 7.5 μmol/Kg TAT-GAP19: $****P = < 0.0001$; Scrambled vs 0.75 μmol/Kg TAT-GAP19: $## P = 0.0019$; Scrambled vs 7.5 μmol/Kg TAT-GAP19: $##### P = < 0.0001$; 0.75 μmol/Kg TAT-GAP19 vs 7.5 μmol/Kg TAT-GAP19: $* P = 0.0484$; Saline: $n = 4$ mice; 7.5 μmol/Kg TATGAP19Scrambled: $n = 4$ mice; 7.5 μmol/Kg TAT-GAP19: $n = 4$ mice; 0.75 μmol/Kg TAT-GAP19: $n = 4$). All error bars represent s.e.m.

3. References

1. L. Leybaert, P. D. Lampe, S. Dhein, B. R. Kwak, P. Ferdinandy, E. C. Beyer, D. W. Laird, C. C. Naus, C. R. Green, R. Schulz, Connexins in Cardiovascular and Neurovascular Health and Disease: Pharmacological Implications. *Pharmacol Rev* **69**, 396-478 (2017).
2. R. Ponsaerts, E. De Vuyst, M. Retamal, C. D'Hondt, D. Vermeire, N. Wang, H. De Smedt, P. Zimmermann, B. Himpens, J. Vereecke, L. Leybaert, G. Bultynck, Intramolecular loop/tail interactions are essential for connexin 43-hemichannel activity. *FASEB J* **24**, 4378-4395 (2010).
3. M. Bol, N. Wang, M. De Bock, B. Wacquier, E. Decrock, A. Gadicherla, K. Decaluwe, B. Vanheel, H. V. van Rijen, D. V. Krysko, G. Bultynck, G. Dupont, J. Van de Voorde, L. Leybaert, At the cross-point of connexins, calcium, and ATP: blocking hemichannels inhibits vasoconstriction of rat small mesenteric arteries. *Cardiovasc Res* **113**, 195-206 (2017).
4. C. D'Hondt, J. Iyyathurai, N. Wang, R. G. Gourdie, B. Himpens, L. Leybaert, G. Bultynck, Negatively charged residues (Asp378 and Asp379) in the last ten amino acids of the C-terminal tail of Cx43 hemichannels are essential for loop/tail interactions. *Biochem Biophys Res Commun* **432**, 707-712 (2013).
5. J. Iyyathurai, N. Wang, C. D'Hondt, J. X. Jiang, L. Leybaert, G. Bultynck, The SH3-binding domain of Cx43 participates in loop/tail interactions critical for Cx43-hemichannel activity. *Cell Mol Life Sci*, (2017).
6. N. Wang, E. De Vuyst, R. Ponsaerts, K. Boengler, N. Palacios-Prado, J. Wauman, C. P. Lai, M. De Bock, E. Decrock, M. Bol, M. Vinken, V. Rogiers, J. Tavernier, W. H. Evans, C. C. Naus, F. F. Bukauskas, K. R. Sipido, G. Heusch, R. Schulz, G. Bultynck, L. Leybaert, Selective inhibition of Cx43 hemichannels by Gap19 and its impact on myocardial ischemia/reperfusion injury. *Basic Res Cardiol* **108**, 309 (2013).

7. J. E. Contreras, J. C. Saez, F. F. Bukauskas, M. V. Bennett, Gating and regulation of connexin 43 (Cx43) hemichannels. *Proc Natl Acad Sci U S A* **100**, 11388-11393 (2003).
8. N. Wang, M. De Bock, G. Antoons, A. K. Gadicherla, M. Bol, E. Decrock, W. H. Evans, K. R. Sipido, F. F. Bukauskas, L. Leybaert, Connexin mimetic peptides inhibit Cx43 hemichannel opening triggered by voltage and intracellular Ca²⁺ elevation. *Basic Res Cardiol* **107**, 304 (2012).
9. J. M. Rhett, J. Jourdan, R. G. Gourdie, Connexin 43 connexon to gap junction transition is regulated by zonula occludens-1. *Mol Biol Cell* **22**, 1516-1528 (2011).
10. J. A. Palatinus, J. M. Rhett, R. G. Gourdie, The connexin43 carboxyl terminus and cardiac gap junction organization. *Biochim Biophys Acta* **1818**, 1831-1843 (2012).
11. C. Jin, K. D. Martyn, W. E. Kurata, B. J. Warn-Cramer, A. F. Lau, Connexin43 PDZ2 binding domain mutants create functional gap junctions and exhibit altered phosphorylation. *Cell Commun Adhes* **11**, 67-87 (2004).
12. N. Kaneko, J. Y. Hwang, M. Gertner, F. Pontarelli, R. S. Zukin, Casein kinase 1 suppresses activation of REST in insulted hippocampal neurons and halts ischemia-induced neuronal death. *J Neurosci* **34**, 6030-6039 (2014).
13. S. V. Demyanenko, S. N. Panchenko, A. B. Uzdensky, Expression of neuronal and signaling proteins in penumbra around a photothrombotic infarction core in rat cerebral cortex. *Biochemistry (Mosc)* **80**, 790-799 (2015).
14. M. Freitas-Andrade, P. Carmeliet, D. B. Stanimirovic, M. Moreno, VEGFR-2-mediated increased proliferation and survival in response to oxygen and glucose deprivation in PIGF knockout astrocytes. *J Neurochem* **107**, 756-767 (2008).
15. Z. Jiang, Y. Zhang, X. Chen, P. Y. Lam, H. Yang, Q. Xu, A. C. Yu, Activation of Erk1/2 and Akt in astrocytes under ischemia. *Biochem Biophys Res Commun* **294**, 726-733 (2002).
16. T. Nakase, G. Sohl, M. Theis, K. Willecke, C. C. Naus, Increased apoptosis and inflammation after focal brain ischemia in mice lacking connexin43 in astrocytes. *Am J Pathol* **164**, 2067-2075 (2004).
17. V. Abudara, J. Bechberger, M. Freitas-Andrade, M. De Bock, N. Wang, G. Bultynck, C. C. Naus, L. Leybaert, C. Giaume, The connexin43 mimetic peptide Gap19 inhibits hemichannels without altering gap junctional communication in astrocytes. *Front Cell Neurosci* **8**, 306 (2014).

4. Publications under GSKE support

- **L. Leybaert**, P. D. Lampe, S. Dhein, B. R. Kwak, P. Ferdinandy, E. C. Beyer, D. W. Laird, C. C. Naus, C. R. Green, R. Schulz, 2017. "Connexins in cardiovascular and neurovascular health and disease: pharmacological implications." *Pharmacological Reviews*. 69(4): 396-478.

Impact factor: 17.893, category: PHARMACOLOGY & PHARMACY, rank: 2/256, Vigintile: 1.



Geneeskundige Stichting Koningin Elisabeth
Fondation Médicale Reine Elisabeth
Königin-Elisabeth-Stiftung für Medizin
Queen Elisabeth Medical Foundation

Progress report
of the research group of

Dr. Laurent Nguyen, PhD &
dr. Brigitte Malgrange

Université de Liège (ULg)

Dr. Laurent Nguyen, PhD

Laboratoire de régulation moléculaire de la neurogenèse
GIGA-Neurosciences
ULiège
4000 Liège
Belgium
Tel.: 32 4 366 59 87
Fax: 32 4 366 59 12
E-mail: Nguyen@ulg.ac.be
www.giga.ulg.ac.be

Dr. Brigitte Malgrange

Unité de Neurobiologie du développement
GIGA-Neurosciences
ULiège
4000 Liège
Belgium
Tel.: 32 4 366 59 87
Fax: 32 4 366 59 12
E-mail: bmalgrange@ulg.ac.be
www.giga.ulg.ac.be

Deciphering the role of protein ubiquitination in human cortical malformation and hearing impairment

1. State of the art and objectives

The cerebral cortex is an evolutionary advanced brain structure that contains different classes of neurons distributed within layers that are regionally organized into sensory, motor and association areas¹. Cortical layering arises inside-out as progenitors give birth to successive waves of pyramidal projection neurons in the dorsal telencephalon² and, GABAergic interneurons in the ventral forebrain³. Projection neurons migrate radially to settle in appropriate cortical layers and they grow axonal projections towards cortical or sub-cortical targets. Interneurons migrate from the ganglionic eminences along multiple tangential paths to integrate local cortical networks. More generally, the development of the cortex implies a continuous rearrangement of a primordial structure that progresses through successive steps including, proliferation, specification, migration, and neuronal differentiation. Disrupting the completion of one or several of these events often lead to Malformations of Cortical Development (MCD). MCDs correspond to a heterogeneous group of focal or diffuse anatomical brain abnormalities with wide spectrum of clinical presentations, developmental delay or motor and intellectual disabilities. They usually occur during the first two trimesters of human pregnancy and involve cells that contribute to the formation of the cortex^{4,5}. They are frequently associated with drug-resistant epilepsy, and more surprisingly, to neuro-sensory deafness and treatments are generally limited to symptom relief (reviewed in⁶). Most MCD are believed to have a genetic origin and their classification arises from diagnoses established by histopathological analyses, magnetic resonance imaging (MRI), electro-clinical studies and further identification of mutation in genes involved in cortical development.

Ubiquitination is a biochemical process that affect proteins in many ways: it can act as a signal for their degradation via the proteasome, change their cellular location, or modify their activity⁷. This process involves the covalent attachment of ubiquitin to a target protein, and is carried out by three enzymes: ubiquitin activating enzyme, E1, ubiquitin conjugating enzyme, E2, and ubiquitin ligase, E3. Each E3 enzyme targets a small number of proteins for ubiquitin modification but the exact substrates are mostly unknown and their identification continues to be a challenge. Regulation of protein turnover is essential for cellular homeostasis in all tissues, including the brain and the inner ear⁸⁻¹⁰; therefore the mutation of any enzyme involved in this process may affect brain and inner ear development. Along this line, our collaborator, Professor Jamel Chelly (IGBMC, Strasbourg, France), has identified novel human NEDD4-2 (a E3 ubiquitin ligase) mutations (c.2690G>A, p.Glu893Lys and c.2677G>A, p.Glu893Lys) in patients suffering from intellectual disabilities, MCD (the main feature being periventricular nodular heterotopia), epilepsy as well as hearing impairment (manuscript under revision at Nature Genetics). Identification of this novel MCD gene is important for diagnosis and genetic counselling of patients and their families, but also to better understand the molecular processes of corticogenesis and cochlear development in health and disease.

1.1. Outstanding questions and objectives

The aim of our proposal is to characterise the physiological functions of E3 ubiquitin ligases in the development of the cerebral cortex (WP1) and the formation of the cochlea, the auditory portion of the inner ear (WP2). For this purpose, we will focus on the pathophysiological mechanisms trigger by novel mutations in the HECT domain of *Nedd4-2* that lead to MCD and hearing impairment in patients. The Nguyen laboratory will focus on cortical interneurons whose contribution to MCD remains poorly understood and the Malgrange laboratory will study the mechanisms of deafness associated with *Nedd4-2* mutations. The project will combine mouse genetics with molecular and cell biology to decipher the physiological functions of *Nedd4-2*, as well as its closely related gene *Nedd4-1*, and to further untangle the pathomechanisms downstream its patient-related mutations.

WP1. Deciphering the role of Nedd4-1/2 in the developing cerebral cortex in health and disease

The molecular connections existing between MCD and ubiquitination defects remain largely unknown. *Nedd4-2* codes for a HECT-domain E3-ubiquitin ligase, a protein involved in substrate ubiquitination whose mutation is associated with some MCD.

Our current project uncovers both the physiological role of *Nedd4-2* and the impact of its MCD-associated mutations on the biology of cortical interneurons using the mouse as a model.

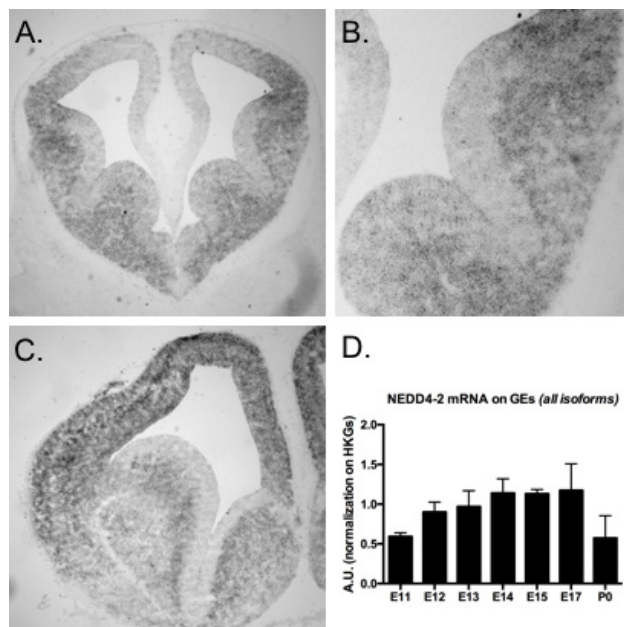


Fig.1. *Nedd4-2* expression pattern **A, B.** E12.5 MF1 mouse, whole brain coronal slice (A) and higher magnification focusing on medial (MGE) and lateral (LGE) ganglionic eminences (B), ISH. *Nedd4-2* mRNAs are expressed in the subventricular zone of both MGE and LGE, **C.** E14.5 MF1 mouse, one hemisphere coronal slice, ISH. Expression of *Nedd4-2* now expands towards the cortex **D.** qRT-PCR performed on whole GE extracts. *Nedd4-2* is expressed throughout embryonic stages in the brain and drops at birth.

We have first established the spatial (using ISH) and temporal (by qRT-PCR) expression patterns of *Nedd4-2* messengers (Fig.1A-1D). Our findings are consistent with the expression of *Nedd4-2* in post-mitotic interneurons during their tangential migration into the cortex (Fig. 1A, 1B). Our collaborators demonstrated earlier a role of *Nedd4-2* in projection neuron migration (Broix et al. Nat Genet. 2016 Nov;48(11):1349-1358). According to its expression pattern in the ventral forebrain (Fig.1B), *Nedd4-2* is likely also expressed by newborn migrating cortical interneurons (cINs). This will be confirmed by IHC on brain section from WT mouse embryos. While impaired migration or maturation of cINs can contribute to the physiopathology of epilepsy (several mutations carriers suffer from seizure), poor migration and differentiation of cINs in MCD remains to be assessed. In order to address this question, we generated a conditional knockout (cKO) mouse model to genetically invalidate *Nedd4-2* in newborn cINs. For this purpose, we crossed *Nedd4-2*^{flox/flox} mice (collaboration with H. Kawabe, Max Planck Institute of Experimental Medicine, Göttingen, Germany) with *Dlx5,6:CRE-GFP* mice (available in our laboratory) to generate cKO embryos. Due to high sequence homology between *Nedd4-2* and *Nedd4-1*, the ancestral member of the NEDD family, and to exclude any compensatory mechanisms, we also generated and analyzed cKO cINs, using *Nedd4-1*^{flox/flox} and *Nedd4-1*^{flox/flox}/*Nedd4-2*^{flox/flox}.

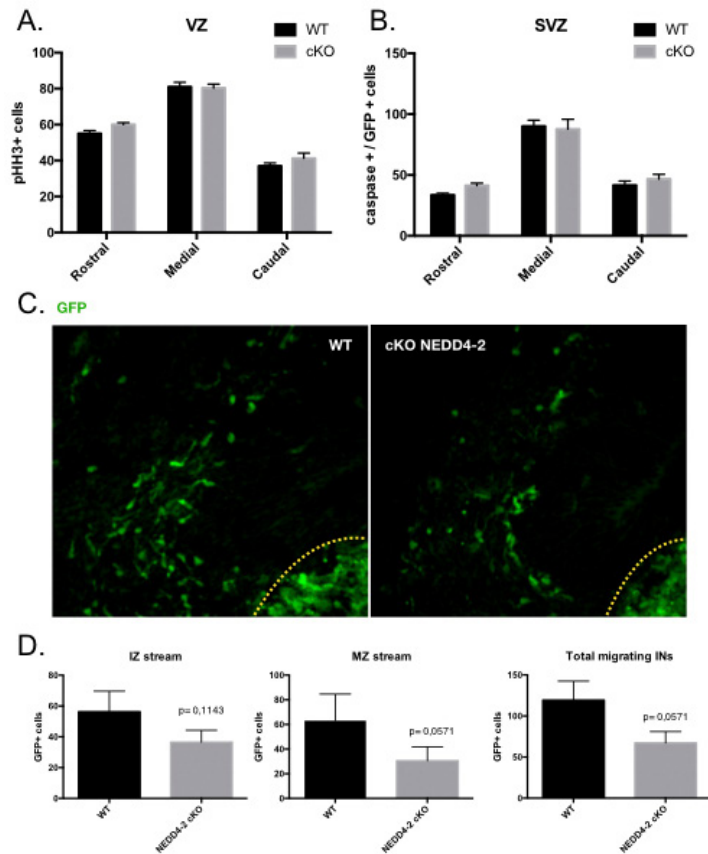


Fig. 2. Analysis of cell biological parameters in the cerebral cortex of *Nedd4-2* cKO and WT mouse embryos **A.** IHC quantification. No significant difference in number of phospho-histone H3 positive cells in the ventricular zone of E14.5 embryos GE. **B.** IHC quantification. No significant difference in number of caspase/GFP double positive cells in the subventricular zone of E14.5 embryos GE. **C.** Confocal microscopy analyses of the cerebral cortex of E13.5 mice. Yellow dotted lines delineate GE/cortex border. **D.** Quantification of data shown in C. Non-parametric tests were applied due to too low a number of animal in each group. Number of animals needs to be increased to perform parametrical t-test.

The analyzes of these different cKO mouse lines did not revealed any developmental impairment of proliferation or survival of cINs and their progenitors (Fig. 2A, 2B). We next performed time lapse recording on cultured brain slices from embryonic day (E14.5) mice to further explore the migration of the cINs in the cortical wall. We observed a trend for a defect of migration marked at early stages by a decreased number of cIN exiting the ganglionic eminences (GEs ; Fig. 2C, 2D). The positioning of the migration front of cINs at later stages was also affected upon loss of *Nedd4-2* expression (preliminary data not shown).

In order to perform a fine analysis of the morphological remodelings of cINs during migration, we performed time lapse recordings on explants culture of medial GEs (MGEs) Migrating cINs exhibit a peculiar migratory pattern known as nucleokinesis. The cell develops an expansion known as the leading process, senses the environnement and then, upon correct positioning of this leading process, the nucleus jumps forward. During those recordings, many parameters of migration were measured: average cell migration speed (Fig. 3B, 3C), frequency (Fig. 3D) and amplitude of nucleokinesis (Fig. 3E) as well as migration persistence - the ability to follow a straight line - of migrating cINs (Fig. 3.F). Neither nucleokinesis amplitude nor migration persistence were affected by the genetical loss of *Nedd4-2* expression. However, our results underline a decreased frequency of nukleokinesis in *Nedd4-2* cKO cINs resulting in a reduced speed of migration. This defect may account for the migration phenotype observed in brain slices (Fig. 2C, 2D) Importantly, we couldn't find any migration defects in *Nedd4-1* cKO cINs.

We will further analyze the migration of cINs from WT and *Nedd4-2* cKO mouse embryos using genetic tools to assess microtubule remodeling and actomyosin dynamics, which both contribute to cell movement. Ultimately, genetic replacement experiments integrating MCD-related mutated proteins into *Nedd4-2* cKO cINs will be performed in order to decipher their pathophysiological implication. Since *Nedd4-2* is an E3 ligase, we will next study the level of expression of relevant proteinic substrates, by first focussing on ion channels (as impaired membrane depolarization defect may explain why cINs are not migrating properly).

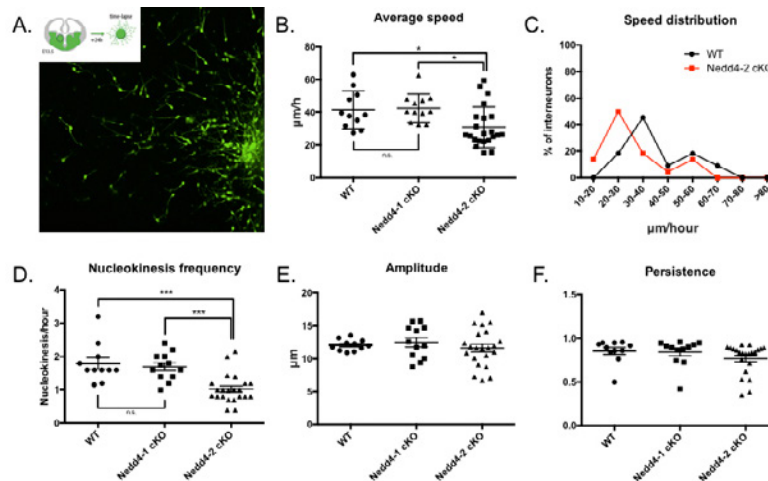


Fig. 3. *Ex vivo* imaging **A.** GE explants of E13.5 embryos are micro-dissected and cultured on cortical feeder. Five-hour recordings are held 24 to 48 hours later under controlled conditions. **B-F.** Quantification of migration features (see text). (*) P value < 0.05 (***) P value < 0.001

For this purpose, we will combine UbiScan on FACS-isolated cells with western-blot and IHC in the developing mouse cortex in both WT and *Nedd4s* cKO mice. Co-immunoprecipitation between *Nedd4-2* and the strongest candidates will be assessed in cell culture.

In conclusion and to further contextualize our work, identification of novel genes whose mutations lead to MCD is not only important for diagnosis and genetic counselling of patients and their families, but also to better understand the molecular processes of cerebral cortical development. Here, we could originally underline the involvement of both ubiquitination and interneurons migration defects in neurodevelopmental disorders characterized by MCD.

WP2. Deciphering the role of *Nedd4-1/2* in the developing inner ear and age-related hearing loss

Our preliminary data indicate that *Nedd4-1* and *Nedd4-2* mRNAs are expressed in the developing cochlea (starting at E14.5 in mice). While both are expressed at E17.5 in the organ of Corti, the stria vascularis and in the spiral ganglion (Appendix 2, Figure 2B), *Nedd4.2* is not any more present postnatally. We next performed preliminary experiments at the cellular level. We start in the organ of Corti and performed immunohistochemistry in E17.5 cochlea (Fig.5). We found that *Nedd41/2* are more specifically expressed at cellular junctions between hair cells and supporting cells.

We will confirm these data by studying the expression pattern of *Nedd4-1/2* mRNAs and proteins at additional developmental stages by in situ hybridization and immunohistofluorescence. To further decipher the roles of *Nedd4-1/2* during cochlear development, we will make use of a conditional knockout strategy: *Nedd4-1lox/lox*; *Nedd4-2lox/lox* mice will be crossed to a *Foxg1:Cre* transgenic mouse line that express the Cre recombinase in the early otocyst to obtain *Nedd4-2-cKO* and *Nedd4-1/2-cKO* mice.

	E14.5	E17.5	P0	P3	P7
Cochlear duct	+++ / +++	++ / ++	++ / -	++ / -	++ / -
Hair cells	NA	++ / ++	++ / -	++ / -	++ / -
Spiral ganglion	+ / ++	+++ / +++	++ / -	++ / -	++ / -
Stria vascularis	NA	++ / ++	++ / -	++ / -	++ / -

Table 1: Developmental pattern of expression of Nedd4.1 and Nedd4.2 in the developing cochlea

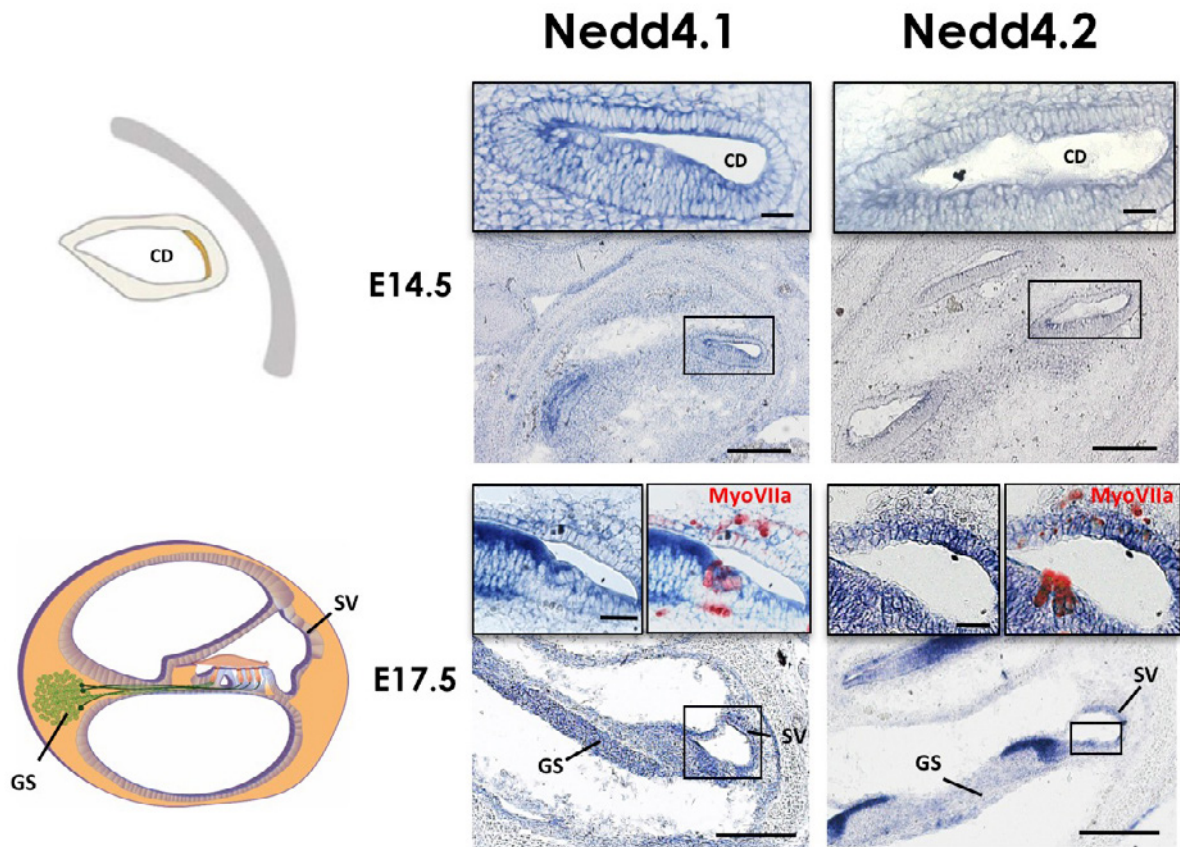


Fig. 4 Nedd4.1 and Nedd4.2 mRNA expression pattern in the developing cochlea. SV=stria vascularis, GS= spiral ganglion, CD= cochlear duct.

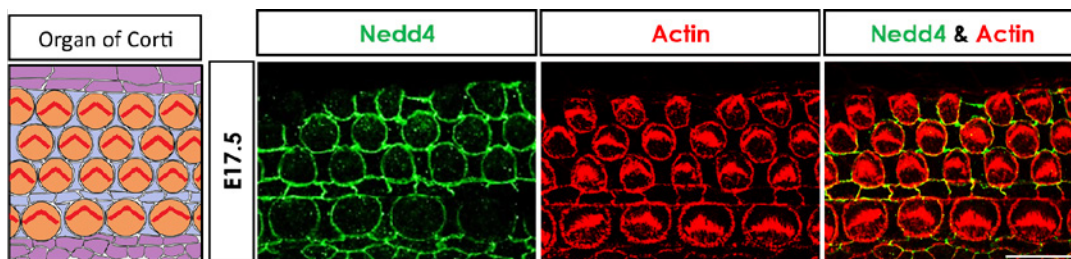


Fig. 5 Nedd4.1/2 are specifically expressed in cell junctions in the developing organ of Corti.

3. Publications of the laboratory in 2016 and 2017 supported by the F.M.R.E.

- Tielens, S.*, Huysseune, S.*, Godin, J.D., Chariot, A., **Malgrange, B.**, and **Nguyen, L.** : Elongator controls cortical migration by regulating actomyosin dynamics. **Cell Research** (2016), 26(10): 1131-1148 (I.F. 2015= 14.812)
- Borgs, L.*, Peyre, E.*, Alix, P., Hanon, K., Grobarczyk, B., Godin, J.D., Purnelle, A., Kruzy, N., Maquet, P., Lefebvre, P.P., Seutin, V., **Malgrange, B.***, and **Nguyen, L.*** : Dopaminergic neurons differentiating from LRRK2 G2019S induced pluripotent stem cells show early neuritic branching defects. **Sci Rep** (2016) Sep 19;6:33377. doi: 10.1038/srep33377 (I.F. 2015= 5.228)
*equal contributions
- Godin, J.D., Creppe, C., Laguesse, S., and **Nguyen, L.**: Emerging Roles for the Unfolded Protein Response in the Developing Nervous System. **Trends Neurosci** (2016) in press, doi: 10.1016/j.tins.2016.04.002 (I.F. 2015= 13.550)
- Morelli, g., Avila, A., Ravanidis, S., Aourz, N., Neve, R.L., Rigo, J.-M.*, **Nguyen, L.***, and Brône, B*. : Cerebral cortical circuitry formation requires functional glycine receptors. **Cereb Cortex** (2017), 27(3):1863-1877 (I.F. 2015= 6.559) *equal contribution
- Van den Ackerveken, P., Mounier, A., Huyghe, A., Sacheli, R., Vanlerberghe, P.-B., Volvert, M.-L., Delacroix, L., **Nguyen, L.**, and **Malgrange, B.**: The miR183/ltgA3 axis is a key regulator of prosensory area during early inner ear development **Cell Death Differ** (2017), 24(12):2054-2065. (I.F. 2016= 8.339)
- Laguesse, S., Close, P., Van Hees, L., Chariot, A., Malgrange, B., and **Nguyen, L.** : Loss of Elp3 impairs the acetylation and distribution of connexin-43 in the developing cerebral cortex. **Front Cell Neurosci** (2017), (11:#122). doi: 10.3389/fncel.2017.00122. eCollection 2017.8 (I.F. 2016=4.555)
- Agirman, G. Broix, L., and **Nguyen L.** : Cerebral cortex development: an outside-in perspective. **FEBS Lett** (2017) 591(24): 3978-3992 (I.F. 2016= 3.623.)

4. Other publications of the laboratory in 2016 and 2017

- Delaunaye, S., Rapino, F., Tharun, L., Zhou, Z., Heukamp, L., Termathe, M., Shostak, K., Klevernic, I., Florin, A., Desmecht A., Desmet, C., **Nguyen L.**, Leidel, S., Willis, A., Büttner, R., Chariot, A., and Close, P. : Elp3 links tRNA modification to IRES-dependent translation of LEF1 to sustain metastasis in breast cancer. *J Exp Med* (2016), 213(11):2503-2523 (I.F. 2015= 11.240)
 - Dwyer, N.D., Chen, B., Chou, S.-j., Hippenmeyer, S., **Nguyen, L.**, and Ghahghaei, H.T. : Neural stem cells to cerebral cortex: Emerging mechanisms regulating progenitor behavior and productivity. *J Neurosci* (2016), 36(45):11394-11401 (I.F. 2015= 5.924)
 - Broix, L., Jagline, H., Ivanova, E., Schmucker, S., Drouot, N., Clayton-Smith, J., Pagnamenta, A. t., Metcalfe, K.A., Isidor, B., Wakther-Louvier, U., Poduri, A., Taylor, J.C., Tilly, P., Poirier, K., Saillour, Y., Lebrin, N., Stemmelen, T., Rudolf, G., Muraca, G., Saintpierre, B., Elmorjani, A., The Deciphering Developmental Disorder study, Bednarek-Weirauch, N., Guerrini, R., Boland, A., Olaso, R., Masson, C., Tripathy, R., Keays, D., Cherif, B., **Nguyen, L.**, Godin, J.D., Kini, U., Nischké, P., Deleuze, J.-F., Bahi Buisson, N., Samara, I., Hinkelmann, M.-V., and Chelly, J. : Mutations in HECT domain of NEDD4L lead to AKT/mTOR pathway deregulation and cause periventricular nodular heterotopia. *Nat Genet* (2016), 48(11):1349-1358 (I.F. 2015= 31.616)
 - Broix, L., Asselin, L., Silva, C. G., Ivanova, E. L., Tilly, P., Gilet, J. G., Lebrun, N., Jagline, H., Muraca, G., Saillour, Y., Drouot, N., Reilly, M. L., Francis, F., Benmerah, A., Bahi-Buisson, N., Belvindrah, R., **Nguyen, L.**, Godin, J. D., Chelly, J., and Hinkelmann, M. V.: Ciliogenesis and cell cycle alterations to KIF2A-related malformations of cortical development *Hum Mol Genet* (2017), in press, Oct 25. doi: 10.1093/hmg/ddx384. (I.F. 2016= 5.340)
1. Rash, B. G. & Grove, E. A. Area and layer patterning in the developing cerebral cortex. *Curr Opin Neurobiol* **16**, 25-34 (2006).
 2. Gupta, A., Tsai, L. H. & Wynshaw-Boris, A. Life is a journey: a genetic look at neocortical development. *Nat Rev Genet* **3**, 342-355 (2002).
 3. Anderson, S. A., Eisenstat, D. D., Shi, L. & Rubenstein, J. L. Interneuron migration from basal forebrain to neocortex: dependence on Dlx genes. *Science* **278**, 474-476 (1997).
 4. Sarnat, H. B. & Flores-Sarnat, L. A new classification of malformations of the nervous system: an integration of morphological and molecular genetic criteria as patterns of genetic expression. *European journal of paediatric neurology : EJPN : official journal of the European Paediatric Neurology Society* **5**, 57-64 (2001).
 5. Sarnat, H. B. & Flores-Sarnat, L. Neuroembryology and brain malformations: an overview. *Handbook of clinical neurology* **111**, 117-128, doi:10.1016/B978-0-444-52891-9.00012-9 (2013).
 6. Spreafico, R. & Tassi, L. Cortical malformations. *Handbook of clinical neurology* **108**, 535-557, doi:10.1016/B978-0-444-52899-5.00047-2 (2012).
 7. Mateo Sanchez, S., Freeman, S. D., Delacroix, L. & Malgrange, B. The role of post-translational modifications in hearing and deafness. *Cell Mol Life Sci*, doi:10.1007/s00018-016-2257-3 (2016).
 8. Nelson, R. F. *et al.* Selective cochlear degeneration in mice lacking the F-box protein, Fbx2, a glycoprotein-specific ubiquitin ligase subunit. *J Neurosci* **27**, 5163-5171, doi:10.1523/JNEUROSCI.0206-07.2007 (2007).
 9. Kazmierczak, M. *et al.* Progressive Hearing Loss in Mice Carrying a Mutation in Usp53. *J Neurosci* **35**, 15582-15598, doi:10.1523/JNEUROSCI.1965-15.2015 (2015).
 10. Narimatsu, M. *et al.* Regulation of planar cell polarity by Smurf ubiquitin ligases. *Cell* **137**, 295-307, doi:10.1016/j.cell.2009.02.025 (2009).



Geneeskundige Stichting Koningin Elisabeth
Fondation Médicale Reine Elisabeth
Königin-Elisabeth-Stiftung für Medizin
Queen Elisabeth Medical Foundation

Progress report
of the research group of

Prof. dr. Timmerman Vincent, PhD

Universiteit Antwerpen (UA)

Principal investigator:

Prof. dr. Timmerman Vincent, PhD
Peripheral Neuropathy Research Group,
University of Antwerp – CDE,
Parking P4, Building V, Room 1.30,
Universiteitsplein 1
2610 Antwerpen
Belgium
E-mail: vincent.timmerman@uantwerpen.be

Unravelling the novel molecular pathways contributing to distal Hereditary Motor Neuropathy caused by mutant HSPB8, with the aim to identify potential therapeutic targets

1. Research report

State of the art: Charcot-Marie-Tooth (CMT) neuropathies comprise a clinically diverse and genetically heterogeneous group of monogenic disorders affecting the peripheral nervous system. The most remarkable group of genes mutated in CMT are those coding for small heat shock proteins (HSPBs). Although regulated by all types of stress, HSPBs are constitutively expressed and responsible for protein quality control and protein folding. The HSPBs are not only molecular chaperones but also involved in many essential cellular processes such as apoptosis, autophagy, splicing and translation, cytoskeleton dynamics and neuronal survival.

Aims of the GSKE project: The development of induced pluripotent stem cells (iPSC) has brought together the genetic accuracy of a patient-derived model and the possibility of having the disease-specific cell type. This model promises to influence modern medicine and drug development particularly for neurological disorders by providing an unlimited access to patient-derived neurons. We will take advantage of the iPSC model along with a knock-in/knock-out mouse model that we have recently developed for distal hereditary motor neuropathy (dHMN), caused by mutations in the small heat shock protein HSPB8, to identify and validate translationally relevant pathway(s) leading to axonal degeneration, and with the ambition to select and test promising therapeutic targets. In this 3-year project we aim to: 1) identify altered molecular pathway(s) responsible for dHMN by differential proteomics, and 2) obtain preclinical evidence to rescue these altered pathways with repurposed drugs.

Results: We first made a survey of all published mutations in three HSPBs; so far 32 mutations occur in HSPB1 and were reported in 169 patients, nine mutations have been described in HSPB8 in 68 patients, and one mutation in HSPB3 in two patients. The phenotypic spectrum of HSPB mutations may not be restricted to axonal CMT disease (CMT2) or distal hereditary motor neuropathy (dHMN), but mutations were also reported in three sporadic patients with amyotrophic lateral sclerosis (ALS). Only recently, a few patients with HSPB mutations were reported to develop distal myopathy at a later stage of the motor neuropathy. This indicates that mutations in multifunctional HSPB's can give rise to multiple neurodegenerative and neuromuscular phenotypes (1).

Since we described the K141N missense mutation in the *HSPB8* gene (2), we and others reported additional patients and families with *HSPB8* mutations (3). Interestingly, most mutations target the same lysine residue (K141E, K141M, K141N, K141T) in the highly conserved α -crystallin domain of the HSPB8 protein. The spectrum of diseases caused by mutations in the *HSPB8* gene was recently expanded to myofibrillar myopathy (MFM) (1, 4, 5). HSPB8 is a molecular chaperone that participates in clearing misfolded poly-Q containing proteins such as mutant *huntingtin* and *ataxin-3* involved in respectively Huntington's disease and spino-cerebellar ataxia. HSPB8 directly interacts with the co-chaperone BAG3 and their role in chaperone-assisted selective autophagy (CASA) and granulostasis is well described (6, 7). To delineate the molecular deficits and functional consequences of *HSPB8* mutations we generated and published our results of a knock-in model for the K141N mutation mimicking the dHMN phenotype (8). We observed that homozygous knock-in mice (*HspB8*^{K141N/K141N}) develop a progressive axonopathy resulting in locomotor deficits. At the ultrastructural level, mice accumulate the mutant HspB8 protein and display degenerative patterns similar to dHMN patients. Interestingly, these animals also develop a progressive MFM as observed in some rare patients with HSPB8 mutations (5).

Additionally, our mouse model allowed us to generate an *HspB8* knock-out using the same targeting construct. Strikingly, the homozygous *HspB8* knock-out animals (*HspB8*^{-/-}) do not show any sign of axonopathy and display a much milder myopathy than the *HspB8* knock-in animals (8). We expect that a therapeutic strategy will be feasible by modulating the expression of HspB8 and thus improve the dHMN and MFM phenotype. This strategy can be beneficial to treat mutations targeting the functional HSPB8-BAG3-HSP70 complex. A new PhD student, L. Vendredy, was attracted thanks to this GSKE project within our research team and she obtained very recently a competitive FWO-SB fellowship (starting from 1/1/2018).

As mentioned in our initial GSKE project description, there is an urgent unmet need to identify molecular signatures that are common to multiple axonal CMT (including CMT2 and dHMN subtypes) representing disease progression that can aid in the development of novel therapeutic strategies and measuring disease outcomes in patients. Our postdoc M. Juneja, PhD performed a differential proteomics based approach on lymphoblasts obtained from patients genetically diagnosed with different gene mutations to identify differentially regulated proteins compared to control lymphoblasts. The results were validated using RT-qPCR and/or western blot analysis on a large axonal CMT patient cohort, motor neurons differentiated from CMT2 patient-derived iPSCs and the sciatic nerves of symptomatic mice (a published *Mfn2* transgenic model and our newly developed *HspB8* knock-in model), to examine the relevance of these proteins in disease progression. The proteomic profiling of patient derived lymphoblasts resulted in the identification of *profilin 2* (PFN2) and *guanidinoacetate methyltransferase* (GAMT) as commonly down-regulated proteins in different genotypes compared to healthy controls. This decrease was also observed at the transcriptional level upon screening 43 CMT2 patients and 22 controls (p=0.005 and p=0.01 respectively). Furthermore, a progressive decrease in the PFN2 expression with age was observed in patients, in contrast to the healthy age-matched controls, wherein PFN2 expression progressively increases with age. The reduced expression of PFN2 was also observed in motor neurons differentiated from patient-derived iPSCs (with missense mutations in the *HSPB1*, *HSPB8*, *MFN2* or *NFL* genes) and in sciatic nerves of the symptomatic *Mfn2* and *HspB8* mouse models when compared to their respective controls. However, no change in GAMT expression levels was observed in the motor neurons and CMT2 mouse-derived sciatic nerves. Our results revealed PFN2 and GAMT as molecular determinants for CMT2 neuropathy, with possible indications of the role of PFN2 in the pathogenesis and disease progression. This is the first study describing biomarkers for axonal neuropathies that can boost the development of therapeutic strategies targeting a larger group of axonal CMT patients with different CMT2 mutations (Juneja et al. 2018, revised manuscript submitted).

In this GSKE project, we also included an extensive review on 'autophagy as an emerging common pathomechanism in inherited peripheral neuropathies' (9), and at the start of this project we revised and completed a research manuscript describing a mutant HSPB1 protein related to dHMN, and which causes loss of translational repression by binding to the poly-C binding protein PCBP1, an RNA binding protein with a possible role in neurodegenerative disease (10).

References to this report:

1. Adriaenssens E, Geuens T, Baets J, Echaniz-Laguna A, Timmerman V. Novel insights in the disease-biology of mutant heat shock proteins in neuromuscular diseases. *Brain*. 2017;140(10):2541-9
2. Irobi J, Van Impe K, Seeman P, Jordanova A, Dierick I, Verpoorten N, et al. Hot-spot residue in small heat-shock protein 22 causes distal motor neuropathy. *NatGenet*. 2004;36(6):597-601.
3. Echaniz-Laguna A, Geuens T, Petiot P, Pereon Y, Adriaenssens E, Haidar M, et al. Axonal Neuropathies due to Mutations in Small Heat Shock Proteins: Clinical, Genetic, and Functional Insights into Novel Mutations. *Hum Mutat*. 2017;38(5):556-68.
4. Echaniz-Laguna A, Lornage X, Lannes B, Schneider R, Bierry G, Dondaine N, et al. HSPB8 haploinsufficiency causes dominant adult-onset axial and distal myopathy. *Acta Neuropathol*. 2017 (E-pub).
5. Ghaoui R, Palmio J, Brewer J, Lek M, Needham M, Evila A, et al. Mutations in HSPB8 causing a new phenotype of distal myopathy and motor neuropathy. *Neurology*. 2016;86(4):391-8.

6. Ganassi M, Mateju D, Bigi I, Mediani L, Poser I, Lee HO, et al. A Surveillance Function of the HSPB8-BAG3-HSP70 Chaperone Complex Ensures Stress Granule Integrity and Dynamism. *Mol Cell*. 2016;63(5):796-810.
7. Crippa V, Sau D, Rusmini P, Boncoraglio A, Onesto E, Bolzoni E, et al. The small heat shock protein B8 (HspB8) promotes autophagic removal of misfolded proteins involved in amyotrophic lateral sclerosis (ALS). *Hum Mol Genet*. 2010;19(17):3440-56.
8. Bouhy D, Juneja M, Katona I, Holmgren A, Asselbergh B, De Winter V, et al. A knock-in/knock-out mouse model of HSPB8-associated distal hereditary motor neuropathy and myopathy reveals toxic gain-of-function of mutant Hspb8. *Acta Neuropathol*. 2018;135:131-48.
9. Haidar M, Timmerman V. Autophagy as an Emerging Common Pathomechanism in Inherited Peripheral Neuropathies. *Front Mol Neurosci*. 2017;10:143.
10. Geuens T, De Winter V, Rajan N, Achsel T, Mateiu L, Almeida-Souza L, et al. Mutant HSPB1 causes loss of translational repression by binding to PCBP1, an RNA binding protein with a possible role in neurodegenerative disease. *Acta Neuropathol Commun*. 2017;5(1):5.

2. Research activities

Articles in International Journals – Acknowledging the GSKE:

1. Bouhy,D., Juneja,M., Katona,I., Holmgren,A., Asselbergh,B., De Winter,V., Hochepped,T., Goossens,S., Haigh,J.J., Libert,C., Ceuterick-de Groote,C., Irobi,J., Weis,J., **Timmerman,V.**: A knock-in/knock-out mouse model of HSPB8-associated distal hereditary motor neuropathy and myopathy reveals toxic gain-of-function of mutant Hspb8. *Acta Neuropathologica* 135:131-148 (2018) Epub: 05-Aug-2017 (PMID: 28780615) (I.F.: 12.213)
2. Adriaenssens,E.*, Geuens,T.*, Baets,J., Echaniz-Laguna,A., **Timmerman,V.** (* equal contribution): Novel insights in the disease biology of mutant small heat shock proteins in neuromuscular diseases. *Brain* 140(10): 2541-2549 (2017) Epub: 01-Oct-2017 (PMID: 28969372) (I.F.: 10.292)
3. Haidar,M., **Timmerman,V.**: Review: Autophagy as an emerging common pathomechanism in inherited peripheral neuropathies. *Frontiers in Molecular Neuroscience* 10: 143- (2017) Epub: 11-May-2017 (PMID: 28553203) (I.F.: 5.076)
4. Echaniz-Laguna,A.*, Geuens,T.*, Petiot,P., Péréon,Y., Adriaenssens,E., Haidar,M., Capponi,S., Maisonobe,R., Fournier,E., Dubourg,O., Degos,B., Salachas,F., Lenglet,T., Eymard,B., Delmont,E., Pouget,J., Morales,R.J., Goizet,C., Latour,P., **Timmerman,V.***, Stojkovic,T.* (* equal contribution): Axonal neuropathies due to mutations in small heat shock proteins: clinical, genetic and functional insights into novel mutations. *Human Mutation* 38(5): 556-568 (2017) Epub: 01-Feb-2017 (PMID: 28144995) (I.F.: 4.601)
5. Geuens,T., De Winter,V., Rajan,N., Achsel,T., Mateiu,L., Almeida-Souza,L., Asselbergh,B., Bouhy,D., Auer-Grumbach,M., Bagni,C., **Timmerman,V.**: Mutant HSPB1 causes loss of translational repression by binding to PCBP1, an RNA binding protein with a possible role in neurodegenerative disease. *Acta Neuropathologica Communications* 5(1): 5 (2017) Epub: 11-Jan-2017 (PMID: 28077174), on line journal of *Acta Neuropathologica* (no I.F. yet).

Awards and fellowships:

- **Leen Vendredy**: FWO-SB PhD fellowship will start on 1st January 2018.
- **Mansour Haidar**: travel fellowship to attend the Annual Meeting of the Peripheral Nerve Society (PNS and CMTR consortium meeting), Sitges-Barcelona, Spain, 8-12 July 2017

PhD theses:

- **Michiel Krols**: Mutations in Atlastin-3: implications for ER membrane fusion and crosstalk with mitochondria; PhD in Biochemistry and Biotechnology, Universiteit Antwerpen, 13/06/2017

Master theses:

- **Kim Claes**: Functional analysis of the interaction between HSPB1 and SLC25A12, Master in Biomedical Sciences, June 2017
- **Lotte Conings**: Investigating the actin cytoskeleton as a common pathomechanism in axonal CMT using iPSC-derived models. Master in Biomedical Sciences, June 2017

Chair and organizational activities:

- **Vincent Timmerman**: secretary of the CMTR consortium meeting and co-chair at the Annual Meeting of the Peripheral Nerve Society (PNS), Sitges-Barcelona, Spain, 8-12 July 2017

- **Manisha Juneja:** co-organizer of the Thermo Fisher Scientific, Technical Stem Cell Workflow and Research Seminar, at the University of Antwerp, with a lecture: Modeling CMT using iPSC derived motor neurons, Antwerp, 19 October 2017

Invited Lectures at international meetings:

- **Vincent Timmerman:** HSPB1/HSPB8 in axonal neuropathy and distal myopathy, 234th ENMC workshop on Chaperone Dysfunction in muscle diseases, Naarden, The Netherlands, 8 - 10 December 2017
- **Vincent Timmerman:** The pathophysiology of small heat shock protein mutations causing peripheral neuropathy. Research Seminar at the Institute of Genetic Medicine, Newcastle University, Newcastle, UK, 14 March 2017
- **Manisha Juneja:** Identifying common molecular determinants of axonal CMT. TREAT-NMD, Freiburg, Germany, 27-29th November 2017

Slide presentations selected at international meetings:

- **Manisha Juneja:** Exploring axonal CMT through iPSC derived neurons. FP7 NeurOmics final meeting, Berlin, Germany, 3-5th May 2017
- **Vincent Timmerman:** A knock-in / knock-out mouse model for small heat shock protein HSPB8 mimicking distal hereditary motor neuropathy and myofibrillar myopathy. Annual Meeting of the Peripheral Nerve Society, Sitges-Barcelona, Spain, 8-12 July 2017
- **Mansour Haidar:** Impairment of autophagy as a possible pathomechanism for CMT causing mutations in HSPB1. Annual Meeting of the Peripheral Nerve Society, Sitges-Barcelona, Spain, 8-12 July 2017

Poster presentations at international meetings:

- **Manisha Juneja:** Identification of common molecular players involved in the prognosis and pathogenesis of axonal CMT subtypes. Annual Meeting of the Peripheral Nerve Society, Sitges-Barcelona, Spain, 8-12 July 2017
- **Elias Adriaenssens:** How does mitochondrial dysfunction contribute to the CMT2F pathogenesis caused by HSPB1 mutations. EMBO/FEBS Course: Mitochondria in life, death and disease, Fasano, Italy, 9-13 October 2017

Slide presentations selected at national meetings:

- **Elias Adriaenssens:** CRISPR/Cas9: Everything you need to know. KVCV seminar Antwerp, 22 February 2017
- **Elias Adriaenssens:** CRISPR/Cas9: recent developments in the field. Thermo Fisher Scientific, Technical Stem Cell Workflow and Research Seminar, at the University of Antwerp, 19 October 2017
- **Elias Adriaenssens:** How does mitochondrial dysfunction contribute to the CMT2F pathogenesis caused by HSPB1 mutations. FBD Faculty Research Day, Universiteit Antwerpen, Antwerp, 27 October 2017
- **Elias Adriaenssens:** CRISPR/Cas9: Everything you need to know. KVCV seminar Ghent, 8 November 2017

Poster presentations at national meetings:

- **Mansour Haidar:** The role of HSPB1 in autophagy and its implications in peripheral neuropathy. VIB Conference: ER Stress, Autophagy & Immune System, Bruges, 26-27 January 2017
- **Elias Adriaenssens:** How does mitochondrial dysfunction contribute to the CMT2F pathogenesis caused by HSPB1 mutations, RBSM2017 symposium (P2N), Antwerp, 7 September 2017
- **Mansour Haidar:** Impairment of Autophagy as a Possible Pathomechanism for CMT Causing Mutations in HSPB1. RBSM2017 symposium (P2N), Antwerp, 7 September 2017

Societal activities:

- **Elias Adriaenssens:** “Het HspB8 muismodel weerspiegelt het ziektebeeld bij de mens”. CMT studie- en contactdag, Antwerpen LO, 4/11/2017

Valorisation of research findings:

- EP17195108: “Biomarkers for Charcot-Marie-Tooth disease” (inventors M. Juneja and V. Timmerman)



Geneeskundige Stichting Koningin Elisabeth
Fondation Médicale Reine Elisabeth
Königin-Elisabeth-Stiftung für Medizin
Queen Elisabeth Medical Foundation

Progress report
of the research group of

Prof. Fadel Tissir, PhD

Université Catholique de Louvain (UCL)

Principal investigator

Prof. Fadel Tissir, PhD, Maître de Recherches FNRS
Institute of Neuroscience, Developmental Neurobiology group
Université Catholique de Louvain
Avenue E. Mounier 73, Box B1.73.16
B1200 Bruxelles
Belgium
Tel.: +32 2 764 73 84
Fax: +32 2 764 74 85
E-mail: Fadel.Tissir@uclouvain.be

Cortical development and malformations

The cerebral cortex is the seat of higher brain functions and its formation requires the production and positioning of the right number and diversity of neurons for intricate circuits assembly. During cortical morphogenesis, neural stem cells (NSC) divide symmetrically in the ventricular zone (VZ) and both daughter cells re-enter the cell cycle, leading to an increased number of NSC. At the onset of neurogenesis, radial or apical neural progenitor cells (aNPC) shift from a symmetric/proliferative to an asymmetric/differentiative/neurogenic mode of division (neurogenic switch). Asymmetric divisions produce aNPC daughter cells as well as neurons, either directly or indirectly through intermediate/basal progenitors (IP/BP) which have limited self-renewal capacity and are committed to an excitatory glutamatergic neuron fate. In the dorsal telencephalon, aNPC give rise sequentially to deep layer (DL: layers 5 and 6), upper layer (UL: layers 2– 4) neurons, and glial cells. Given the remarkable expansion of the cerebral cortex during evolution, but also the tight relationship between dysfunctions of cortical development and neurological disorders, a hot topic of neuroscience is to understand how the proliferation and differentiation of aNPC are orchestrated at the molecular and cellular levels and to identify genes and genetic pathways that control these processes.

During the last year, we have progressed on our understanding of 1) how *Celsr1* regulates the proliferation versus differentiation of NSC and how its loss affects cortical function and behavior (paragraph 1 and appended publication), and 2) how Diaphanous 3 secures cell division of NSC (paragraph 2).

1. *Celsr1* in cortical function/dysfunction

Celsr1 (Cadherin EGF LAG Seven-Pass G-Type Receptor 1) is a member of the flamingo subfamily, part of the cadherin superfamily. The flamingo subfamily consists of 3 nonclassic-type cadherins; a subpopulation that does not interact with catenins. The flamingo cadherins are located at the plasma membrane and have nine cadherin domains, seven epidermal growth factor-like repeats and two laminin G-type repeats in their ectodomain. They also have seven transmembrane domains, a characteristic unique to this subfamily. It is assumed that these chimeric proteins are actually adhesion G protein coupled receptors ‘adhesion GPCRs’ involved in contact-mediated communication, with cadherin domains acting as homophilic binding regions and the EGF-like domains involved in cell adhesion and receptor-ligand interactions. This particular member is a developmentally regulated gene which plays a critical role in early embryogenesis particularly during neural tube closure. Mutations in the *Celsr1* genes have been systematically associated with a variety of neural tube closure defects ranging from the mild forms of spina bifida to “craniorachischis totalis” where the neural tube is completely open. Our expression analysis revealed that the *Celsr1* transcript remains heavily expressed by NPC after neural tube closure. Yet, its function in these cells has never been assessed.

To get insight into the role of *Celsr1* in aNPC, we used a tamoxifen inducible system to label these cells and trace their progeny. Tamoxifen was injected to pregnant females at e13.5, and *Celsr1*^{-/-}; *Nestin*^{CreERT2}; *loxP-stop-loxP-dTomato* embryos were collected at e14.5 and compared to control littermates (*Celsr1*^{+/+}; *Nestin*^{CreERT2}; *loxP-stop-loxP-dTomato*). Mutant aNPC generated more Tomato-positive cells in the ventricular zone (VZ) and less cells in the subventricular zone (SVZ) than controls. This observation was corroborated by *in utero* electroporation of a Gfp coding plasmid at e14.5, which disclosed an accumulation of Gfp- and Pax6-positive cells in the mutant versus control VZ at e15.5. To further investigate the effect of *Celsr1* loss-of-function on fate decision, we injected low concentrations of tamoxifen to mice carrying a floxed allele (*Celsr1*^f) at e10.5, with the aim to inactivate the gene in sparse aNPC and enable a clonal analysis. Examination of the ventricular surface at e14.5 detected

larger clones in conditional mutants (*Celsr1^{ff};Nestin^{CreERT2};loxP-stop-loxP-dTomato*) than in controls (*Celsr1^{+/+};Nestin^{CreERT2};loxP-stop-loxP-dTomato*). These results suggest that *Celsr1*-deficient aNPC undergo more symmetric, proliferative divisions than their control counterparts, leading to accumulation of aNPC (Pax6⁺ cells) in the VZ. Reasoning that this could disrupt the radial *versus* tangential expansion of the developing cerebral cortex, we measured the length of the VZ (which reflects the expansion of the pool of progenitors) and found that it was similar in mutant and control embryos at e10.5, but increased significantly in the mutant from e12.5 onwards. This increase resulted in a local distortion of the VZ at e16.5, and correlated with a higher number of Pax6-positive aNPC in the mutant. During cortical indirect neurogenesis, aNPC produce Tbr2⁺ BP which divide in the SVZ to scale up neuron production. Concomitant to the increased number of aNPC progenitors, the number of Tbr2-positive BP decreased in mutants. The reduction of BPs was significant starting from e12.5 in the lateral pallium, and from e14.5 in the dorsal pallium. This finding was further confirmed by the observation of a decreased number of mitotic, Phospho-Vimentin⁺ cells in the SVZ at e14.5. According to their localization in the developing telencephalon, aNPC cells produce cortical or striatal neurons. To test whether the effect of *Celsr1* on fate decision is restricted to the cerebral cortex, we characterized other neurogenic areas in the developing and adult brain. In absence of *Celsr1*, aNPC in ganglionic eminences, which generate striatal neurons and cortical interneurons, underwent more proliferative divisions than control ones, as illustrated by: 1) higher numbers of Sox2-positive cells; 2) lower numbers of Mash1⁺ BPs; and 3) a narrowing of the intermediate zone containing Dlx5/6⁺ postmitotic neurons. In addition to postmitotic neurons, B1 cells, a pool of neural progenitors that remain quiescent until reactivation in the adult brain, are mainly derived from aNPC during early neurogenesis. In the adult VZ/SVZ, B1 cells display an epithelial apicobasal organization reminiscent of aNPC cells. The morphology of these cells was similar in *Celsr1* mutants and controls. Following electroporation at early postnatal stages, *Gfp*-filled B1 cells extended from the ventricle apically to the VZ/SVZ blood vessel plexuses basally. Similarly, B1 cells exhibited apical processes abutting the ventricle and basal endfeet lining blood vessels at P90. Whole-mount staining of the ventricular lateral wall showed that B1 cells expressing GFAP were surrounded by ependymal GFAP-negative cells, forming the so called pinwheel structure. Contrary to ependymal multiciliated cells, B1 cells are decorated by a single cilium. We used the basal body marker γ -tubulin to visualize the pinwheels and found that these structures were more abundant in mutant than in control mice at P30 and P90. Hence, in *Celsr1* mutants, aNPC produce more adult neural stem cells (B1 cells), and less neurons than in controls.

We measured brain weight at P0, P4, P8, P10, and P12, and found significant differences between *Celsr1^{-/-}* and controls starting from P4. At P90, the hypoplasia was particularly apparent in cerebral cortex and cerebellum, with unmasking of the superior and inferior colliculi. Immunolabeling using layer specific markers showed a reduction in the number of cortical neurons (Foxp2⁺ and Cux1⁺) cortical layers. In addition, histological examination of brain sections revealed that *Celsr1^{-/-}* mice displayed a thicker VZ/SVZ. *Celsr1^{-/-}* adult mice exhibited turning behavior, a distinctive feature of inner ear/vestibular system dysfunction. To investigate further the impact of loss of *Celsr1* on cortical development, we selectively inactivated *Celsr1* in neocortical areas by crossing mice carrying the *Celsr1^f* allele with *Emx1-Cre* mice (*Emx1-Cre* is expressed only in dorsal telencephalon). Like the constitutive mutants, *Celsr1^{ff};Emx1-Cre* conditional knockout mice (*Celsr1^{Emx1cKO}*) displayed smaller cortices than controls (*Celsr1^{+/+};Emx1-Cre*). We assessed the impact of these morphological changes on behavior. *Celsr1^{Emx1cKO}* mice exhibited gender-specific defects in activity, attention, anxiety, spacial learning, and social interactions. Males displayed more spontaneous motor activity and spent more time than controls in exposed areas in open field and elevated plus maze. The hiding behavior defect suggests attention and or anxiety deficit in addition to hyperactivity. Males also exhibited a spatial learning deficit in the water maze setup, but no social behavior defect in the “three chamber” test. Mutant females exhibited a social interaction defect, spending similar time periods in the empty chamber as with the stranger mouse. This combination of traits has been described in rodent models of Attention Deficit/Hyperactivity Disorder (ADHD), and

autism spectrum disorder (ASD), two neurodevelopmental conditions with high co-morbidity. Taken together, these results suggest that the loss of *Celsr1* promotes proliferation of aNPC at the expense of neurogenesis, decreases the number of neurons, leading to cortical hypoplasia and disrupted behavior.

To investigate further how *Celsr1* controls the balance between proliferation and differentiation, we purified aNPC by FACS at e14.5, extracted their mRNA and compared their transcriptome using RNA-Sequencing. 276 genes displayed an altered expression in *Celsr1*-deficient aNPC. Hierarchically clustered gene ontology (GO) terms for biological processes emphasized genes involved in Wnt/planar cell polarity (PCP) signaling, cilia assembly and movement, brain development and generation of neurons, cell proliferation and differentiation, positive regulation of transmembrane receptor protein serine/threonine kinase signaling pathway, and regulation of cellular response to growth factor stimulus. Changes in Wnt/PCP, cilia movement and assembly, and microtubule cytoskeleton were predictable given the established role of *Celsr1* in PCP and cilia biogenesis, and the relationship between Wnt and PCP. On the other hand, several genes involved in Wnt signaling such as *Sulf1*, *Sulf2*, *GPC3*, *Rspo1-3* are also implicated in transmembrane receptor protein serine/threonine kinase signaling. Consistent with the increased proliferation of aNPC in *Celsr1* mutants, we found that 19% of the upregulated genes promote proliferation. Those include *Tmsb4x*, *Rpl34*, *Nsg2*, *Tnc*, *Snhg6*, *Pttg1*, and *Dbi*. Of note, in humans, the extracellular matrix protein TNC (Tenascin C) is highly expressed in the outer SVZ, a region which, in gyrencephalic brains, contains highly proliferative outer radial glia¹. Moreover, Thymosin beta4 (*Tmsb4x*) strongly promotes proliferation of neural progenitors. On the other hand, 13% of the down regulated genes are known tumor suppressors. They include *Sulf1*, *Sostdc1*, *Ccdc67*, *Ptprt*, *Igfbp5*, *Rbm47*, *Sepp1*, *Mamdc2*, *Mecom*, *Zmat4*, *Dab2*, *Gpx3*, *Ptprg*, *Cds1*, and *Spred2*. In addition, *Ptpn6*, *Kank1*, *Lrp1b*, *Lrig3*, *Nkd1*, *Crabp2*, *Igfbp3*, and *Cbx7* have been implicated in glioblastoma progression, supporting a mechanistic link between brain tumors and the proliferation of apical neural progenitors (see point 2 of the report). The most enriched terms in GO for cellular component pointed to cilia, proteinaceous extracellular matrix (ECM), and intrinsic component of plasma membrane, suggesting that *Celsr1* may be instrumental to communication between aNPC and their environment. Indeed, many differentially expressed genes encode extracellular proteins (e.g. *Sulf1*, Metallothionein-3, *Mmp2*, *Adams2*, *Adams18*, *Galnt10*, and *Galnt12*), membrane-bound proteins (*Ptpn6*, *Ptprt*, *Sgms2*, *Tmsb4x*, and *Mamdc2*, ECM components (*Tnc* and *Col1a2*), or growth factor binding proteins (*Igfbp3* and *Igfbp5*). All these molecules can promote and regulate interactions between cell surface receptors, ligands and ECM. Finally, it is worth mentioning that 10% (26/276) of mis-regulated genes are associated with ASD, and 2.5% (7/276) with ADHD.

The phenotype and transcriptional landscape of *Celsr1*^{-/-} mutant aNPC indicate that they fail to perceive critical neurogenic signals. To examine the relationship between the loss of *Celsr1* and the cortical phenotype, we studied the distribution of *Celsr1* protein in the embryonic mouse telencephalon and found that, prior to the onset of neurogenesis, *Celsr1* was confined to the apical junctions of NSC. From e12.5 onwards, *Celsr1* accumulated progressively in basal processes and endfeet of progenitors. Because *Celsr1* is a putative adhesion protein, we investigated the attachment of RG processes to the pia in *Celsr1*^{-/-} mice. Immunohistochemistry with antibodies to the intermediate filament associated protein Nestin showed that mutant aNPC were correctly oriented and reached the basal lamina. Furthermore, we did not observe discontinuities in the basal lamina or neuronal heterotopia in meningeal spaces. However, close scrutiny of the aNPC basal compartment after electroporation of a Gfp encoding plasmid revealed that the number of basal processes was dramatically reduced in *Celsr1*^{-/-} mice. Hence, *Celsr1* redistributes to basal processes of aNPC at the onset of neurogenesis, and its deficiency affects their complexity. As mutant aNPC endfeet were drastically affected, we considered signals emanating from meninges, which were previously proposed to regulate brain development through secreted molecules. Chief among meningeal signals is retinoic acid (RA), which is believed to trigger the switch from proliferative to differentiative divisions at the onset of neurogenesis. Meningeal cells, the main source

of RA in the developing cortex, appear progressively around the telencephalon in a lateral to dorsal gradient between e12.5 and e14.5, which correlates perfectly with the defect in BP production seen in *Celsr1*^{-/-} cortex. Furthermore, *Crabp2*, a cytosol-to-nuclear shuttling protein that facilitates the binding of RA to its cognate nuclear receptor, was concentrated in RG endfeet where it could mediate RA uptake and its relocation to the nucleus. In agreement with this hypothesis, the expression of *Crabp2*, as well as other RA target genes involved in neural differentiation such as *Tnc*, and *Igfbp5* were mis-regulated in *Celsr1*^{-/-} mice. To test further investigate whether RA is involved in the altered neurogenesis observed in mutant mice, we subjected *Celsr1*^{-/-} embryos to RA supplementation *in utero* between e11.5 and e14.5. This treatment restored the expression of *Tnc* and *Igfbp5*. It also rescued the number of Tbr2-positive BP cells, and the length of the VZ. Long term RA supplementation (from e11.5 to e17.5) had profound consequences on the mature brain, and on behavior of adult mice. This treatment rescued the number of cortical neurons, the hyperactivity, hiding behaviors, and social interaction defects in mutant animals. These results have been accepted for publication in *Molecular Psychiatry* (the pdf file of the article is appended).

2. Diaphanous 3 protects NSC in the cerebral cortex

Using a candidate gene approach and expression profiling, we identified five formins as potential regulators of NSC division downstream of the Wnt/planar polarity signaling. Among these, Diaphanous (Diaph)3 is highly and specifically expressed by neural stem cells in telencephalon. To better understand its function in neural stem cells, we generated and analyzed a mouse line carrying a mutation in the *Diaph3* gene. In the knockout mice, cortical progenitor cells undergo apoptosis as early as e10.5. Using flow cytometry analysis, we found a sevenfold increase in the proportion of aneuploid cells in the mutant telencephalon. These cells die therefore depleting progressively the population of progenitors and leading to cortical hypoplasia, as indicated by the marked reduction in all cortical cell types in *Diaph3* ko embryos. Aneuploidy could eventually give rise to neoplastic transformation. Remarkably, mutations in the human *DIAPH3* gene are frequently found in metastatic cancers, and down regulation of *DIAPH3* increases metastatic invasion in xenotransplanted mice^{2,3}. The nuclear asymmetric division we identify could increase chromosomal instability, promoting the emergence of new mutations and facilitating the development of tumors and/or acquisition of metastatic properties.

Investigating the molecular mechanisms of action of Diaph3, we found that Diaph3 co-immunoprecipitates with the mitotic spindle protein BubR1 and its mutation reduces by half the overall level of BubR1. Hence, the lack of Diaph3 weakens the spindle checkpoint and behaves as a BubR1 hypomorphic allele. Consistently, the phenotype of *Diaph3* ko phenocopies that of *BubR1*^h mice in which mitotic slippage, formation of micronuclei, premature chromatid separation, aneuploidy, and decreased number of mitotic cells were described^{4,5}. A link between BUBR1 and chromatid separation was also reported in patients with mosaic variegated aneuploidy, a rare disease associated with intrauterine growth retardation, aneuploidy, microcephaly, and hydrocephalus^{6,7}, further supporting the Diaph3-BubR1-nuclear division axis. In addition to the cortical phenotype, *Diaph3* mutant embryos display growth retardation, twisting neural tube, facial deformities, and increased number and size of brain blood vessels. More than 97% of mutants die before E12.5. The very few animals that survive until young adulthood exhibit smaller brain, hydrocephalus, and growth retardation. These features are common findings in mouse models of microcephaly^{8,9}, and in patients with type II Microcephalic Osteodysplastic Primordial Dwarfism (MOPD-II)¹⁰, whose life is imperiled by modifications of cerebral blood vessels often resulting in stroke or aneurysm. These results provide evidence that Diaph3 protects NSC against mitotic error induced apoptosis, by preserving the activity of the spindle checkpoint. Loss of Diaph3 function does not trigger nuclear division errors in the strict sense. Such events occur physiologically, especially in fast dividing cells like mammalian cortical progenitor cells. Rather, the lack of Diaph3 “relaxes” the spindle

checkpoint enabling a fraction of aberrantly dividing cells, which normally should halt in metaphase, to nevertheless “slip” into anaphase, causing aneuploidy. Because genomic instability often leads to tumorigenesis, we believe that this work uncovers an unanticipated link between the rate of proliferation of NSC and the risk of aneuploidy and may prove valuable to understand the development cortical tumors such as glioblastoma. To explore this, we co-inactivated *Diaph3* and *p53* in the cerebral cortex (to prevent the massive apoptosis owing to *Diaph3* mutation). Our results fully support the hypothesis as the *Diaph3/p53* double mutant exhibit cortical tumors at the age of six months. We are currently using histology, immunohistochemistry, and transcriptomic analysis to gain insight into the tumorigenic process, and identify the cellular changes and molecular signature from the onset to metastasis of brain tumors.

2.1. Function of *Diaph3* in cortical development and function

Diaph3 full knockout mice die as early as e12.5 thus preventing the analysis of the late function *Diaph3* during cortical neurogenesis but and in the adult. To circumvent this, we generated and analyzed conditional knockout mice in which, the gene was specifically inactivated in the cerebral cortex by crossing a floxed allele with mice expressing the recombinase Cre under the control of *Emx1*. In the adult brain, the length of medial longitudinal fissure (Figure 1A) and cerebrum weight (Figure 1B) in *Diaph3^{Emx1-Cre}* conditional knockout (cKO) mice are significantly reduced. The cortical thickness is markedly reduced as well (Figure 1C).

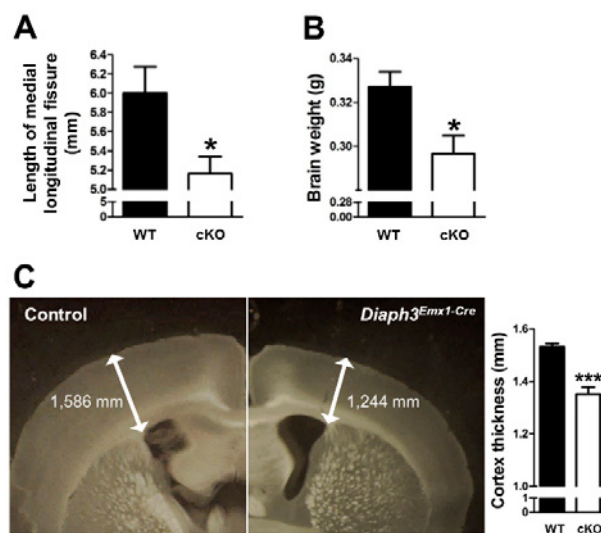


Figure 1 Impact of *Diaph3* deficiency on the cerebral cortex (A) quantification of the length of the medial longitudinal fissure (A), and brain weight (B) showing a significant reduction in *Diaph3^{Emx1-Cre}* conditional knockout (cKO) mice. (C) Coronal sections of the cerebrum showing a marked reduction of cortical thickness in *Diaph3^{Emx1-Cre}* mutant mice. WT (wild-type): $n=6$, cKO: $n=6$, Student's t-test, * $P<0.05$, *** $P<0.001$. Error bars represent: s.e.m.

We performed immunostaining with different cortical layer markers (layer II-III: *Cux1*; layer V: *Ctip2*; and layer VI: *Foxp2*) and found a reduction in the thickness of layer II-III and VI in *Diaph3^{Emx1-Cre}* cKO (Figure 2A-D), along with a decrease in the number of cells in all cortical layers (Figure 2E).

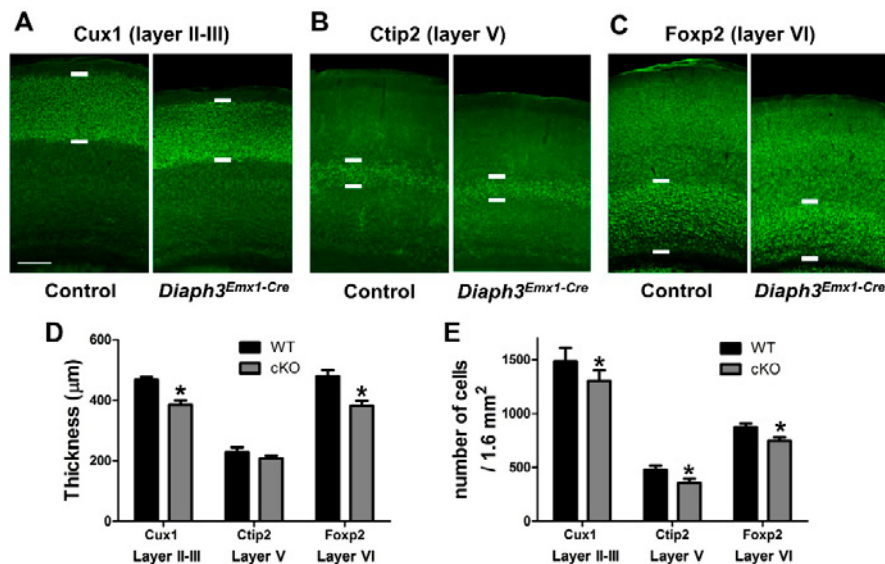


Figure 2 Different cell populations are affected in adult *Diaph3^{Emx1-Cre}* mutant (A-C) Cortex-specific inactivation of *Diaph3* disrupts cortical development. Coronal sections stained with *Cux1* (A), *Ctip2* (B) and *Foxp2* (C) antibodies (green). (D) Thickness of cerebral cortex is quantified. Layer II-III and VI are thickened in *Diaph3^{Emx1-Cre}* cKO. (E) Quantification of *Cux1*-, *Ctip2*- and *Foxp2*-positive cells. Cells were counted in 1.27 mm x 1.27 mm cortical areas from four mutants and four controls. Counts are expressed as number of cells per 1.6 mm². An average of 12%, 26% and 14% decrease in the cell populations in layer II-III (*Cux1*-positive), layer V (*Ctip2*-positive) and layer VI (*Foxp2*-positive) was seen in the mutant cortex. WT (wild-type) ($n=4$), cKO ($n=4$). Student's t-test, * $P<0.05$. Error bars represent s.e.m. Scale bar, 200 μm.

2.2. Cortical hypoplasia in *Diaph3^{Emx1-Cre}* mutant

To better understand how the loss of *Diaph3* impairs cortical development, we immuno-stained neurons (*Tbr1*), intermediate progenitors (*Tbr2*), and aNPC (*Pax6*) at E13.5; and found that the three cell populations are reduced by 37%, 17% and 11% respectively in the cKO mice (Figure 3).

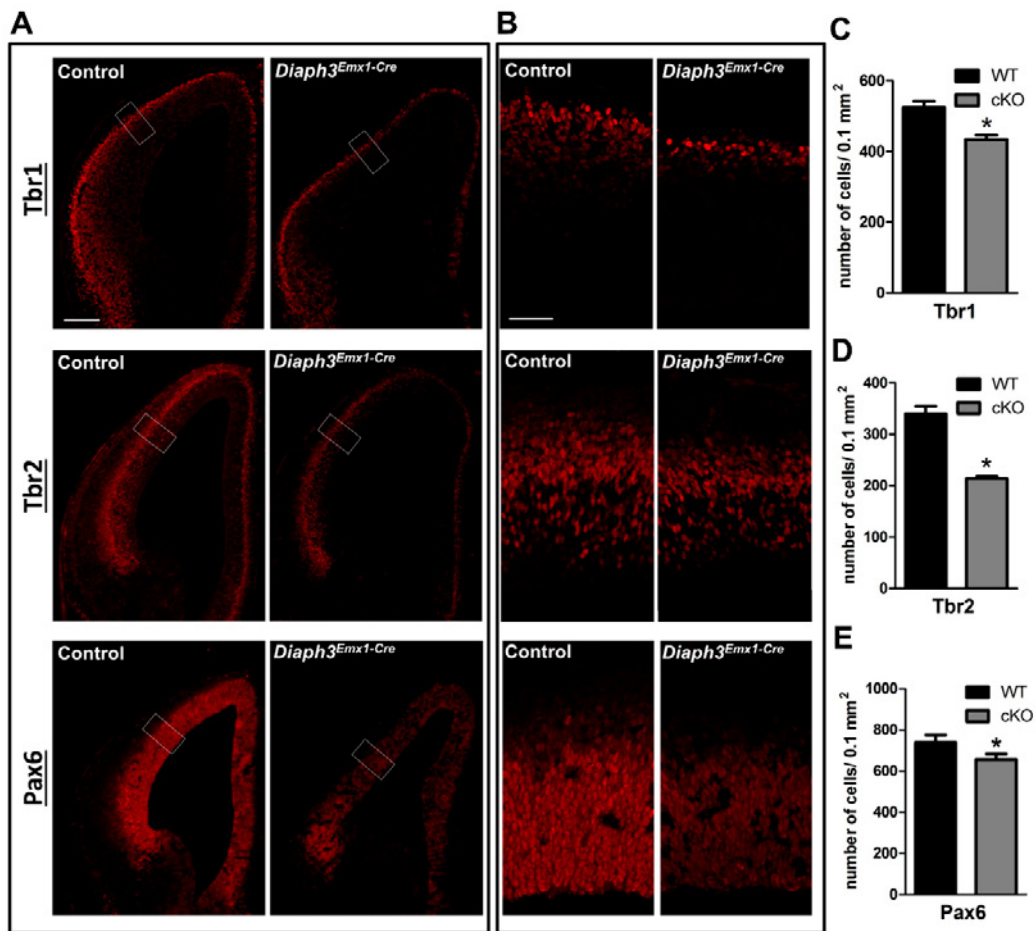


Figure 3 Cortex-specific inactivation of Diaph3 disrupts cortical development. (A) Forebrain coronal sections at e13.5 stained with Tbr1, Tbr2 and Pax6 antibodies (red). (B) Enlargements of the white boxes in (A) emphasising reduced number of the three main cell populations (neuron, Tbr1-positive; intermediate progenitor, Tbr2-positive; radial glial progenitor, Pax6-positive). Quantification are shown in (C-E). Cells were counted in 0.317 mm x 0.317 mm cortical areas from three mutants and three controls, and counts were expressed as cells per 0.1 mm². An average of 37%, 17% and 11% decrease in the cell populations in neuron (Tbr1-positive), intermediate progenitor (Tbr2-positive) and radial glial progenitor (Pax6-positive) was seen in the mutant tissue. WT (wild-type) ($n=3$), cKO (conditional knockout) ($n=3$). Student's t-test, * $P<0.05$. Error bars represent s.e.m. Scale bar, 100 μ m in A, 50 μ m in B.

During cortical development, the plane of cell division relative to the ventricular surface indicates whether the cell is undergoing proliferation or differentiation. Proliferative/symmetric divisions that increase the number of neuronal progenitors are characterized by a plane of cleavage perpendicular to the ventricular zone. In asymmetric division, the plane of cleavage is parallel or oblique to the ventricular zone, giving rise to one aNPC and one IP/BP. The modality of cell division is measured as shown in Figure 4A. Control and *Diaph3^{Emx1-Cre}* sections were immuno-stained with γ -tubulin (red) and DAPI (blue) at e12.5, to visualize centrosome and chromosomes respectively. Angles of cell division relative to the ventricular surface at anaphase were calculated (summarized in Figure 4B). Neural progenitors undergo more Asymmetric /neurogenic division at the expense of proliferation in mutant (neurogenic division: 54 % in mutants versus 26 % in controls; proliferative division: 46% in mutants versus 74 % in controls) (Figure 4C-D).

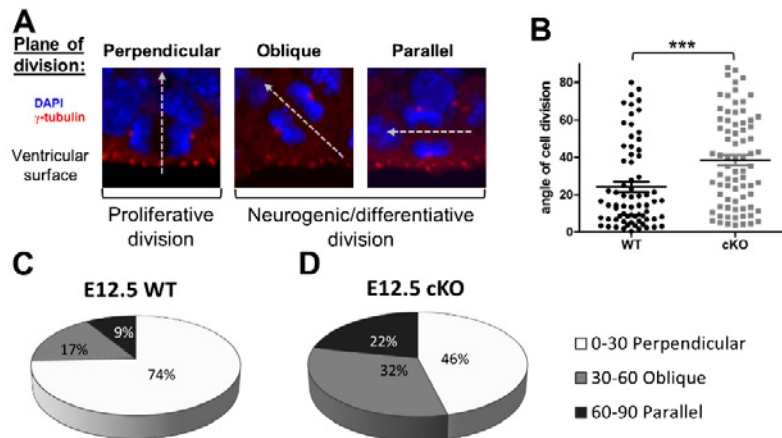


Figure 4 Cell division is disrupted in *Diaph3^{Emx1-Cre}* mutant mice. (A) Cell divisions are categorized into 3 types: perpendicular, oblique or parallel to the ventricular surface. Cell division in perpendicular manner is proliferative, while oblique or parallel is neurogenic/differentiative. E12.5 Cortical sections were stained for γ -tubulin (red) and DAPI (blue) against centrosome and chromosomes at anaphase respectively. (B) Measurement of the angle of spindle orientation of the dividing cells relative to ventricular surface in telencephalon show increased angle of the cleavage plane in *Diaph3^{Emx1-Cre}* mutant. (C-D) At E12.5, *Diaph3^{Emx1-Cre}* mutant mice show reduction of the proliferative and increase in the number of neurogenic/differentiative cell division. WT: $n=70$ from 3 embryos, cKO: $n=76$ from 3 embryos. Student's t-test, *** $P<0.001$. Error bars represent s.e.m.

2.3. Loss of Diaph3 downregulates of Mitotic Spindle-Associated Protein P126 (MAP126)

The mitotic spindle is crucial to cell division and determines whether the cell divides symmetrically or asymmetrically. Astral microtubules connect the centrosome to the cytoplasmic membrane. By cooperating with the cyto-cortical protein complex (including $G\alpha_i$, GoLoco domain protein), the motor protein, dynein-dynactin complex, provides the pulling force to the plus end of the astral microtubule that helps to orient the mitotic spindle. Mitotic Spindle-Associated Protein P126 (MAP126), also called Astrin or Sperm Associated Antigen 5 (Spag5) interacts with SKAP complex at the plus-end of the astral microtubule that balance the spindle positioning force with the help of dynein¹¹. Astrin/SKAP complex also aligned to the centromere or kinetochore and centrosome during metaphase and anaphase to promote stable microtubule-kinetochore attachments¹².

Our data suggests that Pax6 is downregulated in *Diaph3^{Emx1-Cre}* mutant telencephalon at E13.5 (Figure 3A, B and E). Pax6 regulates the expression of Astrin (also known as Spag5)¹³. Hence, we examined Astrin/Spag5 protein levels in the telencephalic lysate from *Diaph3*-deficient mice by Western blotting (tissue from null *Diaph3* knockout is preferred here to avoid contamination of protein from Emx1-cre negative cells in the conditional knockout mice). (Figure 5A, left panel). A 40% reduction of Astrin/Spag5 protein was observed in mutant tissue (Figure 5A-B). Co-immunoprecipitation by Diaph3 antibody shows that Astrin/Spag5 interacted physically with Diaph3 (Figure 5A, right panel). Preliminary studies suggest that dynein may also be down-regulated in *Diaph3* mice. Further studies are ongoing to understand better the relationship between these mitotic spindle regulating proteins and Diaph3.

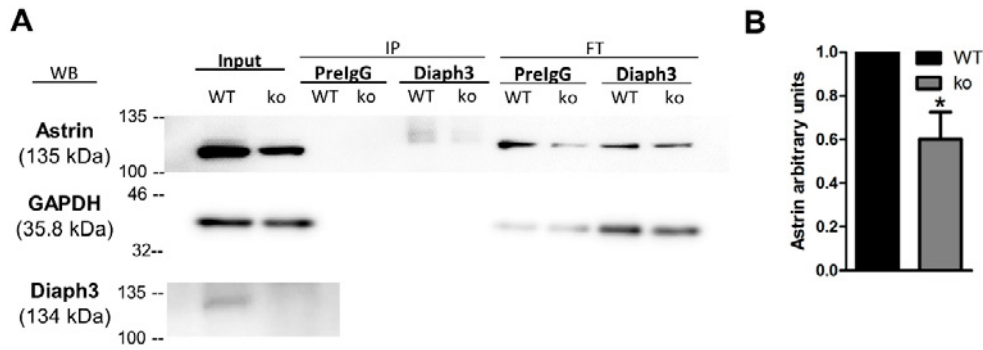


Figure 5 downregulation of Astrin/Spag5 in absence of *Diaph3* (A) Reduction of Astrin/Spag5 protein levels in *Diaph3* ko telencephalon lysate detected by western blotting and quantified relatively to GAPDH (left panel). The same samples were blotted for Diaph3 to confirm the absence of the protein (bottom). Western blotting (WB) detects Astrin/Spag5 on IP with anti-Diaph3 antibodies from WT telencephalon lysates (right panel). WB of Astrin/Spag5 in Input was used as positive control for IP (left panel). Reduced signal was found in the eluted fraction (flow-through, FT) in presence of Diaph3 antibodies in WT when compared to flow-through using PrelgG for IP. (B) The level of Astrin/Spag5 decreased by 40% in the ko (n=3 embryos for each genotype). Student's t-test, * $P < 0.05$ Error bars represent s.e.m.

2.4. Impact of *Diaph3* deficiency on the function of cerebral cortex

Given the defects in cKO cerebral cortex (Figures 1-3), we investigated the behavioral of these mice. Open-field test and elevated plus maze show that cKO mice have lower spontaneous motor activity (Figure 6A-B), but no difference in time spent in exposed area indicating no difference in anxiety level. The 3 chamber test shows that they spend more time in empty chamber than with a stranger mouse (stranger 1) revealing weakened sociability when compared to the control (Figure 6C). When the empty chamber is occupied by a new stranger mouse (stranger 2), cKO mice spend more time with the more familiar stranger mouse (stranger 1), indicating impairment in social novelty. These results indicate an impaired social behavior in the cKO, and are in line with a clinical study that reported on a double hit in *DIAPH3* locus in a patient with autism spectrum disorder¹⁴.

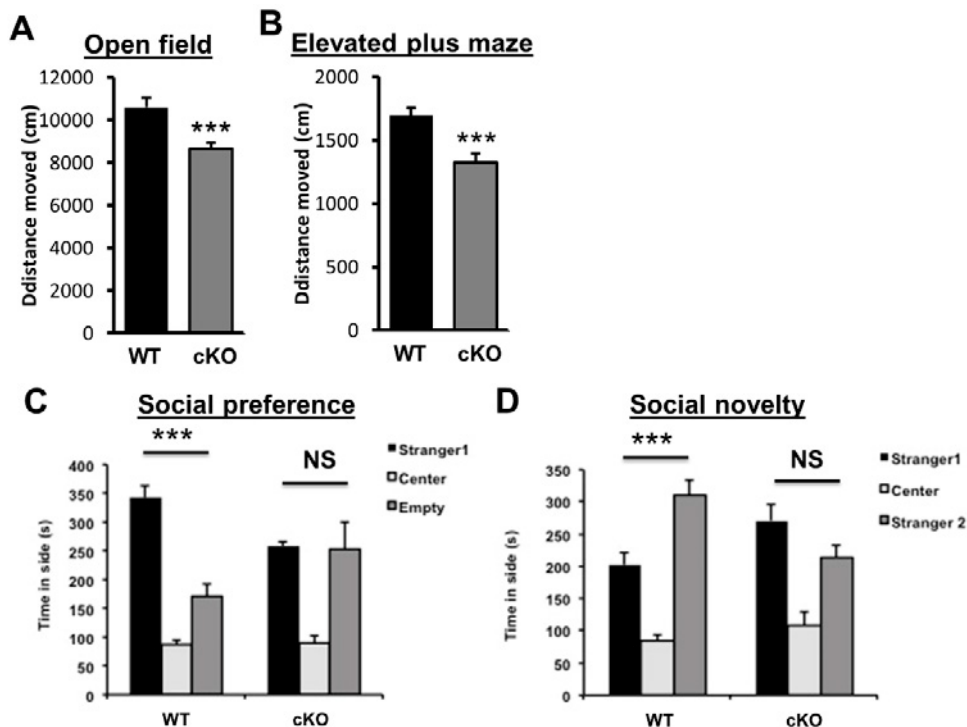


Figure 6 Abnormal behavior in *Diaph3* mutant mice (A) Locomotor activity of males *Diaph3^{Emx1-Cre}* mutant and control mice in open field test. Student's *t* test, *** $P < 0.001$. (B) Distance travelled by the male mice in open areas of elevated plus maze. Student's *t* test, *** $P < 0.001$. (C) Social behavior in the "3 chambers" test for males. One-way ANOVA, *** $P < 0.001$ for both genotypes (stranger versus empty chamber). (D) Social novelty behavior in the "3 chambers" test for males. One-way ANOVA, *** $P < 0.001$ for both genotypes (stranger 1 versus stranger 2 chamber). WT: $n = 10$, cKO: $n = 10$. Error bars represent s.e.m.

3. References

1. Pollen, A. A. *et al.* Molecular identity of human outer radial glia during cortical development. *Cell* **163**, 55-67, doi:10.1016/j.cell.2015.09.004 (2015).
2. Hager, M. H. *et al.* DIAPH3 governs the cellular transition to the amoeboid tumour phenotype. *EMBO Mol Med* **4**, 743-760, doi:10.1002/emmm.201200242 (2012).
3. Morley, S. *et al.* Regulation of microtubule dynamics by DIAPH3 influences amoeboid tumor cell mechanics and sensitivity to taxanes. *Scientific reports* **5**, 12136, doi:10.1038/srep12136 (2015).
4. Dai, W. *et al.* Slippage of Mitotic Arrest and Enhanced Tumor Development in Mice with BubR1 Haploinsufficiency. *Cancer Research* **64**, 440-445, doi:10.1158/0008-5472.can-03-3119 (2004).
5. Baker, D. J. *et al.* BubR1 insufficiency causes early onset of aging-associated phenotypes and infertility in mice. *Nat Genet* **36**, 744-749, doi:10.1038/ng1382 (2004).
6. Matsuura, S. *et al.* Monoallelic BUB1B mutations and defective mitotic-spindle checkpoint in seven families with premature chromatid separation (PCS) syndrome. *American Journal of Medical Genetics Part A* **140A**, 358-367, doi:10.1002/ajmg.a.31069 (2006).
7. Miyamoto, T. *et al.* Insufficiency of BUBR1, a mitotic spindle checkpoint regulator, causes impaired ciliogenesis in vertebrates. *Hum Mol Genet* **20**, 2058-2070, doi:10.1093/hmg/ddr090 (2011).
8. Murga, M. *et al.* A mouse model of ATR-Seckel shows embryonic replicative stress and accelerated aging. *Nat Genet* **41**, 891-898, doi:10.1038/ng.420 (2009).
9. Chen, C. T. *et al.* A unique set of centrosome proteins requires pericentrin for spindle-pole localization and spindle orientation. *Curr Biol* **24**, 2327-2334, doi:10.1016/j.cub.2014.08.029 (2014).
10. Hall, J. G., Flora, C., Scott, C. I., Jr., Pauli, R. M. & Tanaka, K. I. Majewski osteodysplastic primordial dwarfism type II (MOPD II): natural history and clinical findings. *Am J Med Genet A* **130A**, 55-72, doi:10.1002/ajmg.a.30203 (2004).
11. Kern, D. M., Nicholls, P. K., Page, D. C. & Cheeseman, I. M. A mitotic SKAP isoform regulates spindle positioning at astral microtubule plus ends. *J Cell Biol* **213**, 315-328, doi:10.1083/jcb.201510117 (2016).
12. Dunsch, A. K., Linnane, E., Barr, F. A. & Gruneberg, U. The astrin-kinastrin/SKAP complex localizes to microtubule plus ends and facilitates chromosome alignment. *J Cell Biol* **192**, 959-968, doi:10.1083/jcb.201008023 (2011).
13. Asami, M. *et al.* The role of Pax6 in regulating the orientation and mode of cell division of progenitors in the mouse cerebral cortex. *Development* **138**, 5067-5078, doi:10.1242/dev.074591 (2011).
14. Vorstman, J. A. *et al.* A double hit implicates DIAPH3 as an autism risk gene. *Mol Psychiatry* **16**, 442-451, doi:10.1038/mp.2010.26 (2011).



Geneeskundige Stichting Koningin Elisabeth
Fondation Médicale Reine Elisabeth
Königin-Elisabeth-Stiftung für Medizin
Queen Elisabeth Medical Foundation

Progress report
of the research group of

Prof. dr. Vandenberghe Wim, MD. PhD

Katholieke Universiteit Leuven (KU Leuven)

Principal investigator

Prof. dr. Vandenberghe Wim, MD. PhD
University Hospitals Leuven, Department of Neurology
KU Leuven, Department of Neurosciences
Herestraat 49
3000 Leuven
Belgium
Tel.: +32 16 34 42 80
Email: wim.vandenberghe@uzleuven.be

LRRK2, Rab10 and mitochondrial quality control in Parkinson's disease

1. Background

Parkinson's disease (PD) is a highly prevalent, disabling neurodegenerative disorder for which no cure exists yet¹. The number of PD patients in the western world is expected to double over the next two decades, presenting a huge medical, social and economic challenge².

Approximately 5 % of PD cases have a mendelian cause. Familial PD can be caused by recessive mutations in e.g. *PARK2* or *PINK1* or by dominant mutations in e.g. *LRRK2*¹. *LRRK2* mutations are by far the most common monogenic cause of PD, accounting for ~10 % of autosomal dominant familial cases³. *LRRK2* mutations are also found in 3.6 % of apparently sporadic PD cases and have an incomplete, age-dependent penetrance³. In addition, genome-wide association studies (GWAS) identified polymorphisms in the *LRRK2* locus as a risk factor for sporadic PD, indicating that pathogenic pathways may be shared between familial and sporadic forms⁴. *LRRK2* encodes an enzyme with a kinase domain and a GTPase domain⁵. A recent phosphoproteomics study identified Rab10 and several related members of the Rab family as *LRRK2* kinase substrates⁶. The Rab family comprises ~70 small GTPases that cycle between an inactive GDP-bound and an active GTP-bound state as well as between the cytosol and membranes⁷. Rabs regulate vesicle formation, trafficking and fusion⁷. PD-causing *LRRK2* mutations increase phosphorylation of Rab10, which may disturb its membrane-cytosol equilibrium⁶. How this leads to neurodegeneration, is unknown.

Accumulating evidence implicates impairment of mitophagy as a pathogenic mechanism in PD⁸. Mitophagy is a form of selective autophagy in which damaged mitochondria are specifically labeled with ubiquitin and taken up by autophagosomes for degradation in lysosomes⁸. The E3 ubiquitin ligase parkin and the mitochondrial kinase PINK1, encoded by *PARK2* and *PINK1*, respectively, are both critically involved in mitophagy⁸. PINK1 accumulates on damaged mitochondria and phosphorylates both parkin and ubiquitin, thus activating parkin⁹. Parkin-mediated ubiquitination of outer mitochondrial membrane (OMM) proteins in combination with PINK1-mediated ubiquitin phosphorylation triggers recruitment of autophagy receptors, such as optineurin, that tether ubiquitinated mitochondria to LC3 on nascent autophagosomes¹⁰⁻¹². Loss-of-function mutations in *PARK2* or *PINK1* disrupt mitophagy, leading to deficient mitochondrial quality control, accumulation of dysfunctional mitochondria, oxidative stress and apoptosis⁸.

As described in our GSKE research proposal, recent data in my lab demonstrated that fibroblasts from PD patients with the two most common *LRRK2* mutations (G2019S and R1441C) also have a mitophagy defect, which is rescued by a pharmacological inhibitor of *LRRK2* kinase activity and by overexpression of the *LRRK2* substrate Rab10. Moreover, we found that Rab10 translocates from its basal location in the cytosol to depolarized mitochondria in wild-type cells. These findings suggested that the pathogenic effects of *LRRK2*, *PARK2* and *PINK1* mutations may converge on a common pathway.

2. Aim of the project

The aim of this project is to elucidate the mechanisms by which PD-linked *LRRK2* mutations disturb mitophagy.

3. New findings in 2017

3.1. Mitophagy defect in human LRRK2 mutant fibroblasts: confirmation by live mito-Keima imaging

To further validate the mitophagy defect in the *LRRK2* mutant fibroblasts, we transfected them with a mitochondrially targeted form of Keima (mito-Keima), a fluorescent protein that is resistant to lysosomal proteases and exhibits pH-dependent excitation¹³. The peak of the excitation spectrum of mito-Keima shifts from 440 nm to 586 nm when mitochondria are delivered to acidic lysosomes, which allows dual-excitation ratiometric quantification of mitophagy¹³. Indeed, treatment of fibroblasts from healthy controls with valinomycin, a compound that depolarizes mitochondria, resulted in the appearance of punctate structures with high 543 nm/458 nm ratio mito-Keima values that colocalized with the lysosomal dye LysoTracker (Fig. 1A). Emergence of these high 543/458 ratio puncta after valinomycin treatment was inhibited by bafilomycin A1, a lysosomal inhibitor, and by 3-methyladenine, a suppressor of macroautophagy induction (Fig. 1B,D). As expected, emergence of high 543/458 ratio puncta was abrogated in fibroblasts from PD patients with *PARK2* and *PINK1* mutations (Fig. 1C,D). Importantly, mito-Keima imaging confirmed that mitophagy was indeed also defective in cells from the 2 PD patients with the G2019S mutation and the patient with the R1441C mutation (Fig. 1E,F).

3.2. The mitophagy defect of LRRK2 mutant fibroblasts is rescued by LRRK2 knockdown and by LRRK2 kinase inhibitors.

To verify that the mitophagy defect of the *LRRK2* mutant fibroblasts was due to mutant LRRK2, we knocked down LRRK2 using two different siRNAs. Transfection with these 2 LRRK2 siRNAs effectively suppressed LRRK2 protein levels to approximately 30% of control levels (not shown). LRRK2 knockdown with each of these siRNAs corrected the mitophagy defect of the G2019S and R1441C mutant fibroblasts (Fig. 2A-F). Moreover, the LRRK2 kinase inhibitors LRRK2-IN-1 and PF-06447475 both rescued the mitophagy defect of the G2019S and R1441C mutant fibroblasts, indicating that this defect was mediated by LRRK2 kinase activity (not shown).

Mitophagy contributes to mitochondrial quality control. As expected in cells with impaired mitophagy, mitochondrial quality in G2019S and R1441C mutant fibroblasts was impaired as evidenced by reduced average mitochondrial membrane potential and increased mitochondrial production of reactive oxygen species (ROS). These mitochondrial defects were also rescued by LRRK2 kinase inhibition (not shown).

3.3. Non-selective autophagy is preserved in patients with LRRK2 mutations

In addition to selective forms of autophagy such as mitophagy, cells have the capacity for non-selective (bulk) autophagy in which cytosolic components and organelles are degraded indiscriminately via mechanisms that are independent of autophagy receptors¹⁴. A classical trigger for non-selective autophagy is amino acid starvation. Surprisingly, starvation-induced autophagy, as measured by lipidated LC3 (LC3-II)/actin ratios on western blot, was preserved in cells from the 2 G2019S patients and the R1441C patient compared with healthy controls (Fig. 3A,B). As an additional assay for non-selective autophagy, we transfected fibroblasts with Keima, i.e. the same probe as used for mitophagy imaging except that it lacked the mitochondrial targeting sequence¹³. Starvation of control cells induced high 543/458 ratio Keima puncta that colocalized with LysoTracker (not shown) and were suppressed by treatment with bafilomycin A1 and 3-methyladenine (Fig. 3C,D). Strikingly, Keima imaging showed intact starvation-induced autophagy in G2019S and R1441C *LRRK2* mutant patients (Fig. 3E,F), in contrast to the mitophagy defect observed with mito-Keima imaging (Fig. 1E,F). Taken together, these data show that fibroblasts from patients with G2019S and R1441C mutations have impaired mitophagy, but preserved non-selective autophagy.

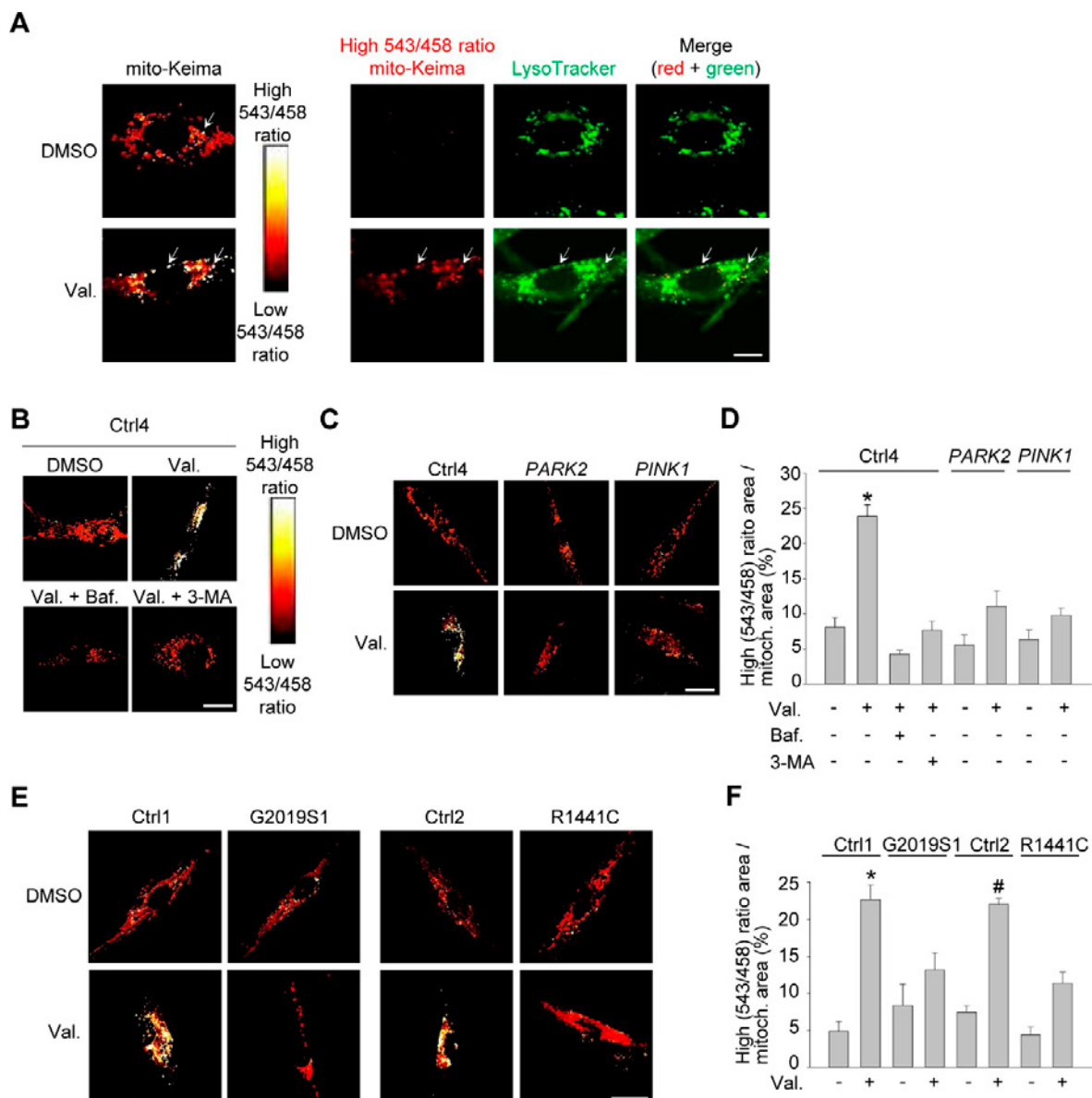


Figure 1. Mito-Keima imaging shows a mitophagy deficit in *LRRK2* mutant fibroblasts. (A) Fibroblasts from a healthy control (Ctrl1) were transfected with mito-Keima. After 24 h cells were treated for 48 h with DMSO or valinomycin (Val., 1 μ M), followed by live ratiometric imaging. High (543/458) signal corresponds to mito-Keima present in lysosomes. LysoTracker Green (50 nM) was added to the medium just before imaging. Arrows indicate high (543/458) ratio mito-Keima puncta that colocalize with LysoTracker. (B–D) Fibroblasts from a control (Ctrl4), a PD patient with compound heterozygous *PARK2* mutations and a PD patient with homozygous *PINK1* mutations were transfected with mito-Keima and treated for 48 h with DMSO, Val., bafilomycin A1 (Baf., 100 nM), or 3-methyladenine (3-MA, 10 mM) as indicated, followed by live ratiometric imaging. (D) High (543/458) ratio area/total mitochondrial area was quantified as an index of mitophagy ($n \geq 4$). * $P < 0.001$ compared with all other conditions. (E, F) Fibroblasts from controls and PD patients with *LRRK2* mutations were transfected with mito-Keima and treated for 48 h with DMSO or Val. (F) Quantification ($n = 4$). * $P < 0.01$ compared with all other Ctrl1 and G2019S1 conditions. # $P < 0.01$ compared with all other Ctrl2 and R1441C conditions. Scale bars, 10 μ m.

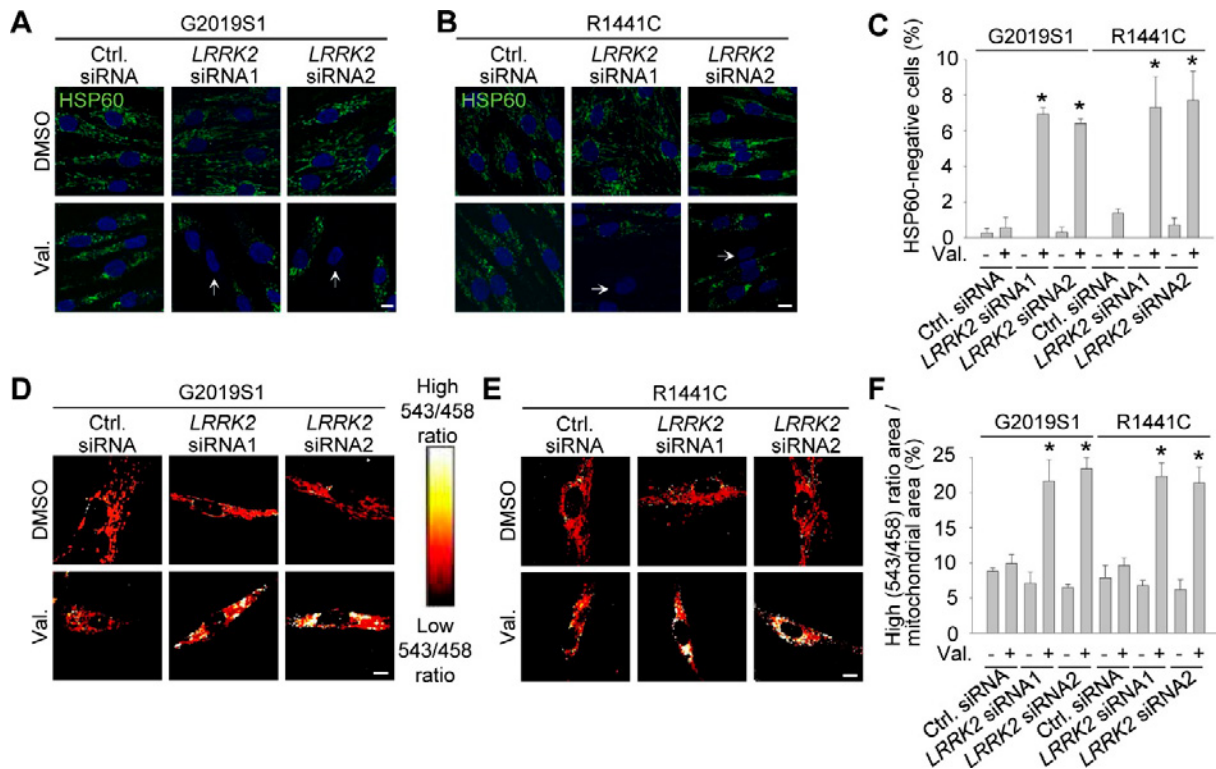


Figure 2. The mitophagy defect of LRRK2 mutant fibroblasts is rescued by LRRK2 knockdown. (A–C) Fibroblasts from a PD patient with the G2019S LRRK2 mutation (G2019S1) and a PD patient with the R1441C LRRK2 mutation were transfected with control siRNA, *LRRK2* siRNA1 or *LRRK2* siRNA2. After 72 h cells were treated with DMSO or valinomycin (Val., 1 μ M) for 48 h and immunostained for HSP60. Nuclei were stained with TOTO-3 (blue). Arrows in **A** and **B** indicate cells without mitochondria. (C) Quantification ($n = 3$). * $P < 0.01$ compared with Val. in control siRNA in the same subject. (D–F) G2019S and R1441C mutant fibroblasts were transfected with mito-Keima and either control siRNA, *LRRK2* siRNA1 or *LRRK2* siRNA2. After 72 h cells were treated with DMSO or Val. for 48 h. (F) Quantification ($n = 3$). * $P < 0.005$ compared with control siRNA after Val. in the same subject. Scale bars, 10 μ m.

3.4. Optineurin recruitment to depolarized mitochondria is impaired in patients with LRRK2 mutations

Once autophagosomes are completely closed around their cargo, they are probably processed similarly along their path to fusion with lysosomes irrespective of whether they have been formed by selective or non-selective autophagy. Our finding of impaired mitophagy and preserved non-selective autophagy in *LRRK2* mutant cells therefore suggested that *LRRK2* mutations disrupted mitophagy at a site upstream of closure of autophagosomal membranes around the mitochondria. To determine at which stage mitophagy was affected by *LRRK2* mutations, we first assessed PINK1-mediated parkin activation at the OMM of depolarized mitochondria using a mitofusin-2 (MFN2) ubiquitination assay. MFN2 is an OMM protein that is ubiquitinated by activated parkin after mitochondrial depolarization¹⁰. Ubiquitinated MFN2 is then extracted from the OMM and degraded by the proteasome¹⁰. Valinomycin treatment for 3 h in control fibroblasts expressing endogenous parkin resulted in ubiquitination of endogenous MFN2 (Fig. 4A,B). This was abrogated in *PARK2* and *PINK1* mutant fibroblasts, as expected, but was fully preserved in G2019S and R1441C LRRK2 mutant cells (Fig. 4A,B), indicating that PINK1 and parkin activity at the OMM of depolarized mitochondria was not affected by *LRRK2* mutations.

PINK1- and parkin-mediated generation of phospho-ubiquitin on depolarized mitochondria induces recruitment of autophagy receptors that tether the mitochondria to nascent autophagosomal membranes¹². Recent work has revealed a critical role for the autophagy receptor optineurin in mitophagy^{11,12}. Optineurin associates with ubiquitinated mitochondria via its ubiquitin-binding domain and recruits LC3 via its LC3 interaction region to promote mitochondria engulfment by autophagosomes. In basal conditions GFP-tagged optineurin was predominantly cytosolic both in control and *LRRK2* mutant fibroblasts (Fig. 4C–F). After mitochondrial depolarization optineurin accumulated on mitochondria in control cells. However, in G2019S and R1441C mutant cells optineurin recruitment to depolarized

mitochondria was severely reduced (Fig. 4C-F). Thus, although PINK1 and parkin activity at depolarized mitochondria was preserved in *LRRK2* mutant fibroblasts, these mutations interfered with optineurin recruitment.

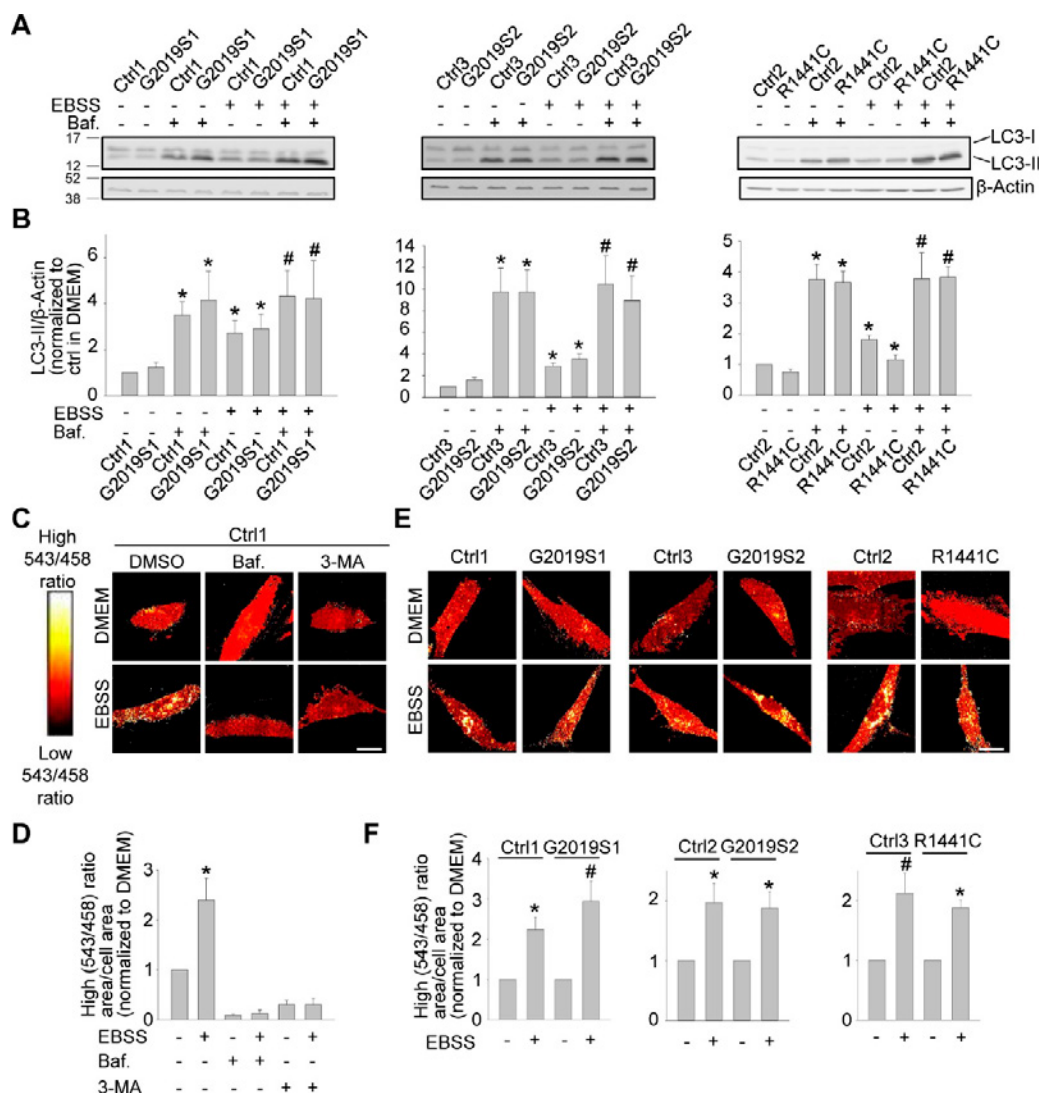


Figure 3. Non-selective autophagy is preserved in *LRRK2* mutant cells. (A, B) Fibroblasts from 2 PD patients with the G2019S mutation, a PD patient with the R1441C *LRRK2* mutation and 3 controls were incubated either in Earle's balanced salt solution (EBSS) for 4 h to trigger starvation-induced autophagy, or in standard culture medium (DMEM), in the presence or absence of bafilomycin A1 (Baf., 100 nM). (A) Western blot showing LC3-I, LC3-II and β -actin levels. (B) Quantification of LC3-II/ β -actin, normalized to the DMEM condition in the corresponding control ($n = 5-8$). * $P < 0.05$ compared with DMEM without Baf. in the same subject. # $P < 0.05$ compared with EBSS without Baf. in the same subject. (C, D) Fibroblasts from Ctrl1 were transfected with Keima and incubated for 4 h in DMEM or EBSS in the presence or absence of Baf. (100 nM) and 3-methyladenine (3-MA, 10 mM), as indicated, followed by ratiometric live imaging. High (543/458) signal corresponds to Keima present inside lysosomes. (D) Quantification ($n = 3$). * $P < 0.001$ compared with all other conditions. (E-F) Control and *LRRK2* mutant fibroblasts were transfected with Keima and incubated in DMEM or EBSS for 4 h. (F) High (543/458) ratio area/total cell area was quantified as an index of autophagy ($n = 4$). # $P < 0.01$ compared with DMEM in the same subject. * $P < 0.05$ compared with DMEM in the same subject. Scale bars, 10 μ m.

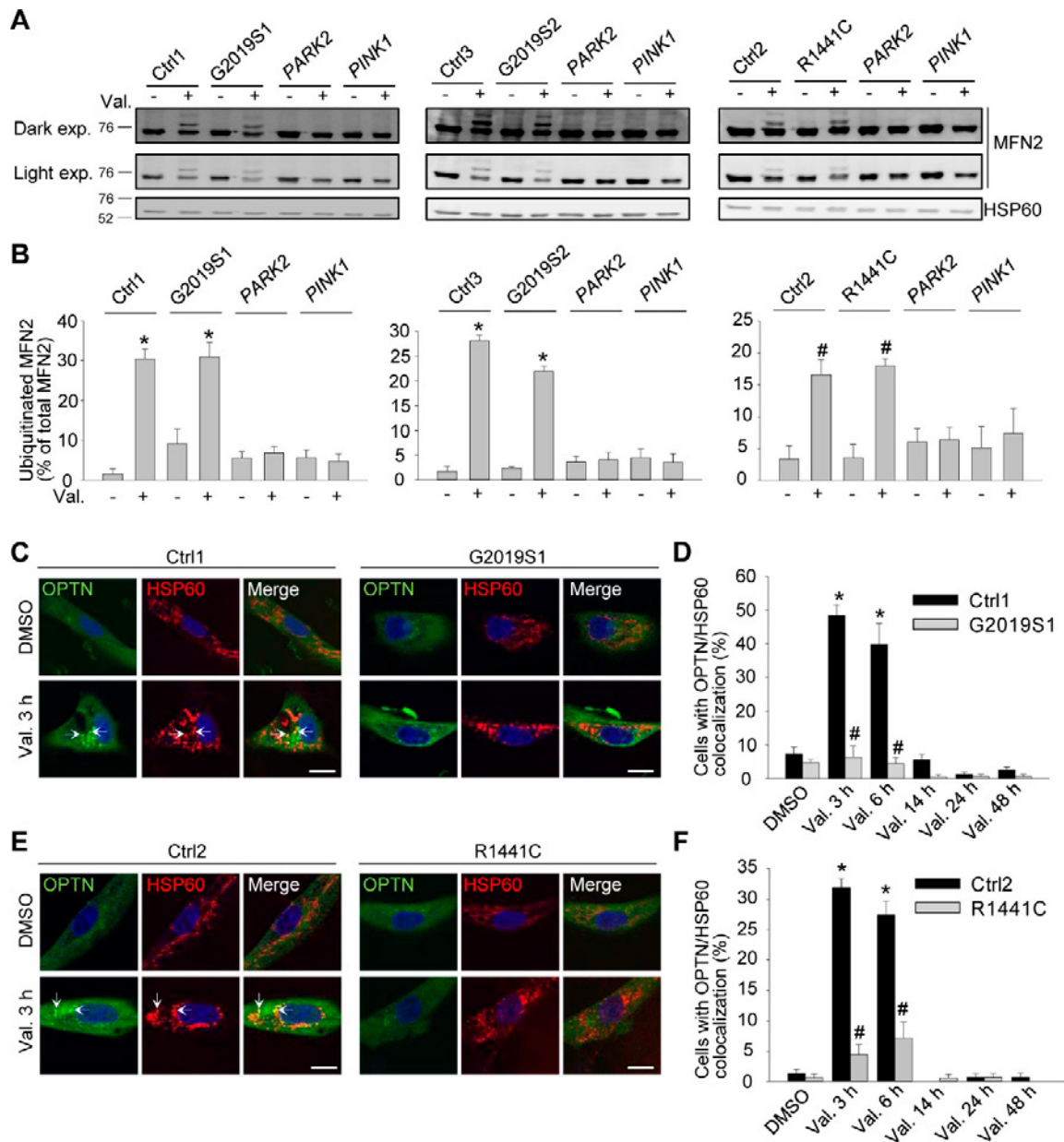


Figure 4. Optineurin recruitment to depolarized mitochondria is impaired in PD patients with *LRRK2* mutations despite preserved mitochondrial ubiquitination. (A, B) Untransfected control, *LRRK2*, *PARK2* and *PINK1* mutant fibroblasts were treated with DMSO or valinomycin (Val., 1 μ M) for 3 h. (A) Western blot of mitochondrial fractions for mitofusin-2 (MFN2) and HSP60. The same MFN2 blots are shown after either light or dark exposure (exp.). (B) Quantification of ubiquitinated MFN2 relative to total MFN2 ($n = 3-4$). * $P < 0.001$ and # $P < 0.05$ compared with DMSO condition in the same subject. (C-F) Control and *LRRK2* mutant fibroblasts were transfected with GFP-tagged optineurin (OPTN). After 24 h cells were treated with DMSO or Val. (1 μ M) for 3, 6, 14, 24 or 48 h. Fibroblasts were immunostained for HSP60 and nuclei were stained with TOTO-3. Arrows in C and E indicate mitochondria that colocalize with OPTN. (D, F) Quantification of the percentage of cells with OPTN/HSP60 colocalization ($n = 3$). * $P < 0.001$ compared with DMSO in the same subject. # $P < 0.001$ compared with the corresponding Val. condition in the control subject. Scale bars, 10 μ m.

3.5. Rab10 specifically rescues defects in mitophagy and mitochondrial function in *LRRK2* mutant cells

Rab10 and several related members of the Rab GTPase family were recently identified as substrates of the *LRRK2* kinase⁶. As already described in our GSKE research proposal, overexpression of Rab10 rescued the mitophagy defect of the *LRRK2* mutant fibroblasts. To assess how specific this effect was for Rab10, we overexpressed Rab10 and several other Rab substrates of *LRRK2* (Rab3A, Rab5B, Rab7L1 and Rab12) in the *LRRK2* mutant fibroblasts. We also overexpressed Rab7 because of its reported functional link with *LRRK2*¹⁵. Interestingly, overexpression of Rab10 had by far the strongest

rescuing effect (Fig. 5). Overexpression of Rab3A also had a significant, although smaller, rescuing effect, whereas Rab5B, Rab7, Rab7L1 and Rab12 had no effect (Fig. 5). Rab10 overexpression in G2019S and R1441C fibroblasts also improved mitochondrial membrane potential and mitigated mitochondrial ROS production (not shown).

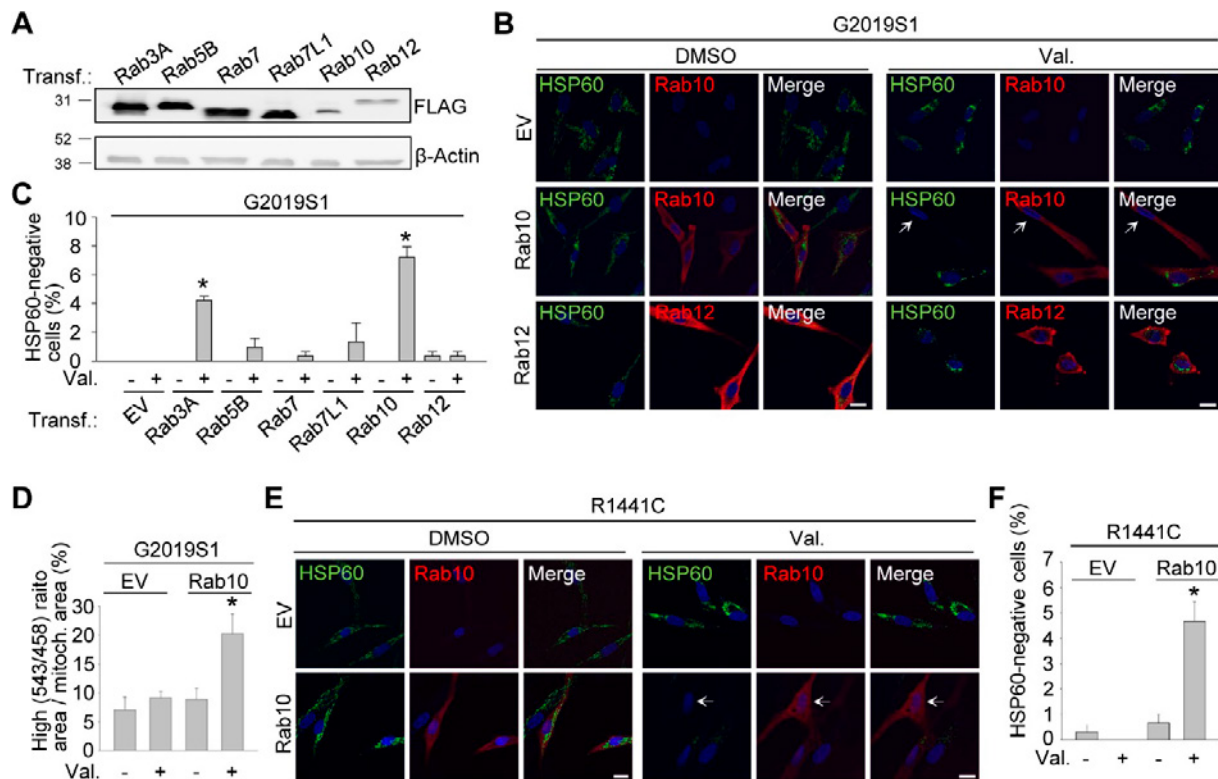


Figure 5. Overexpression of Rab10 mitigates the mitophagy defect of *LRRK2* mutant cells. (A-C) Fibroblasts were transfected (Transf.) with empty vector (EV) or FLAG-Rab3A, -Rab5B, -Rab7, -Rab7L1, -Rab10 or -Rab12. (A) Western blot showing expression levels of overexpressed FLAG-Rab proteins. (B, C) G2019S1 fibroblasts transfected with the indicated Rab were treated with DMSO or valinomycin (Val., 1 μ M) for 48 h, followed by immunostaining for FLAG and HSP60. Nuclei were stained with TOTO-3 (blue). Arrows in B indicate cell without detectable HSP60. (C) Quantification ($n = 3-8$). * $P < 0.001$ compared with Val. EV. (D) G2019S1 fibroblasts were transfected with mito-Keima and either EV or GFP-Rab10 and treated with DMSO or Val. (1 μ M) for 48 h, followed by live ratiometric imaging. High (543/458) ratio area/total mitochondrial area was quantified ($n \geq 3$). * $P < 0.05$ compared with all other conditions. (E, F) R1441C fibroblasts were transfected with EV or FLAG-Rab10, treated with DMSO or Val. (1 μ M) for 48 h and immunostained for FLAG and HSP60. Arrows in E indicate cell without detectable HSP60. (F) Quantification ($n = 3$). * $P < 0.001$ compared with all other conditions.

3.6. Rab10 facilitates mitophagy and accumulates on depolarized mitochondria in wild-type cells

Next we used RNAi-mediated knockdown of Rab10 (Figure 6A-D) to determine whether endogenous Rab10 regulated mitophagy. Transfection with 2 different *Rab10* siRNAs effectively suppressed Rab10 protein levels to approximately 40% of control levels (not shown). Rab10 knockdown in wild-type cells impaired valinomycin-induced mitophagy, as shown by HSP60 immunocytochemistry (Fig. 6A,B) and live mito-Keima imaging (Fig. 6C,D). Conversely, overexpression of Rab10 enhanced mitophagy in wild-type cells (Fig. 6E).

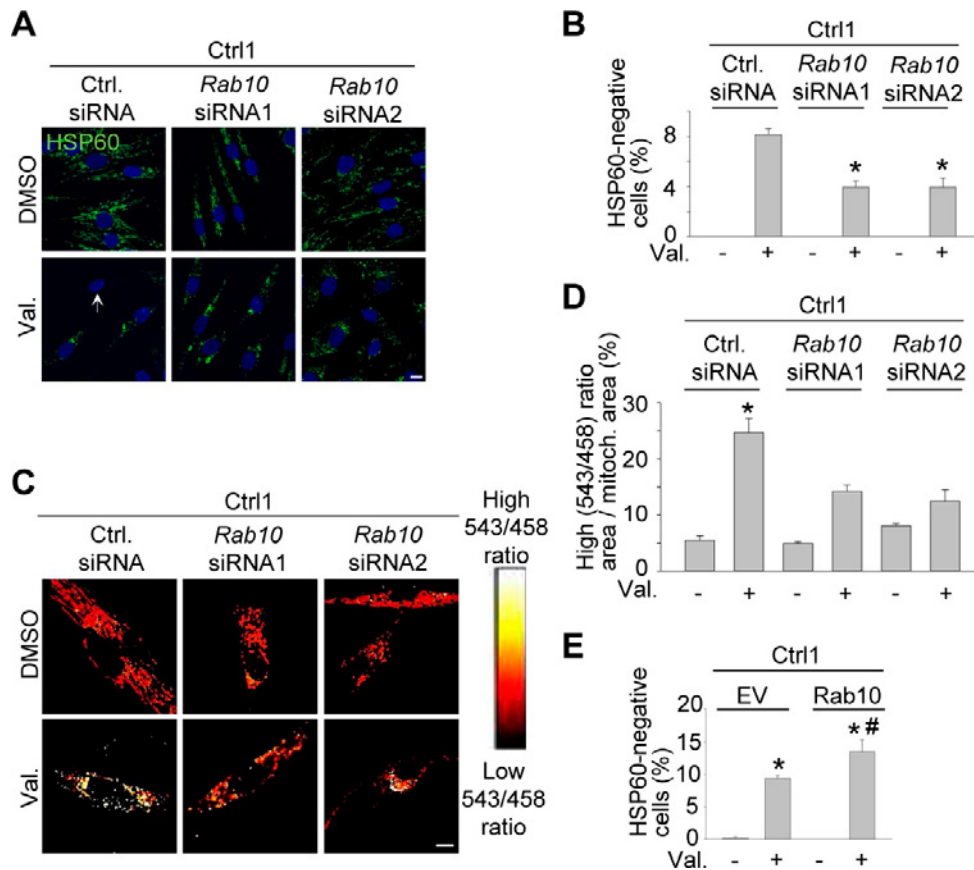


Figure 6. Endogenous Rab10 facilitates mitophagy in wild-type cells. (A-B) Control fibroblasts were transfected with control siRNA, *Rab10* siRNA1 or *Rab10* siRNA2. After 72 h cells were treated with DMSO or valinomycin (Val., 1 μ M) for 48 h and immunostained for HSP60. Nuclei were stained with TOTO-3 (blue). Arrow in B indicates cell without mitochondria. (C) Quantification ($n = 3$). $*P < 0.005$ compared with Val. in control siRNA. (C, D) Control fibroblasts were transfected with mito-Keima and either control siRNA, *Rab10* siRNA1 or *Rab10* siRNA2. After 72 h, cells were treated with DMSO or Val. (1 μ M) for 48 h, followed by ratiometric imaging. (D) Quantification ($n = 3$). $*P < 0.01$ compared with all other conditions. (E) Control fibroblasts were transfected with empty vector (EV) or FLAG-Rab10, treated with DMSO or Val. (1 μ M) for 48 h and immunostained for HSP60 and FLAG. The percentage of cells without HSP60 staining was quantified ($n = 4$). $*P < 0.001$ compared with the corresponding DMSO condition. $\#P = 0.02$ compared with Val. in EV. Scale bars, 10 μ m.

As already described in our GSKE research proposal, immunocytochemical experiments showed that mitochondrial depolarization triggered translocation of FLAG-tagged Rab10 from its basal, predominantly cytosolic localization to mitochondria in wild-type fibroblasts (Fig. 7A). We now characterized the time course of Rab10 translocation after mitochondrial depolarization in control fibroblasts in more detail (Fig. 7B). In addition, we now confirmed accumulation of FLAG-Rab10 on depolarized mitochondria by western blotting after mitochondrial fractionation (Figure 7D,E). Overexpressed untagged Rab10 (not shown) and endogenous Rab10 (Figure 7F,G) also accumulated on mitochondria after valinomycin treatment. By contrast, FLAG-tagged Rab12 did not show detectable translocation to depolarized mitochondria (Fig. 7C).

Interestingly, the mitochondrial Rab10 puncta after depolarization strongly colocalized with optineurin in wild-type cells (Figure 7H,I).

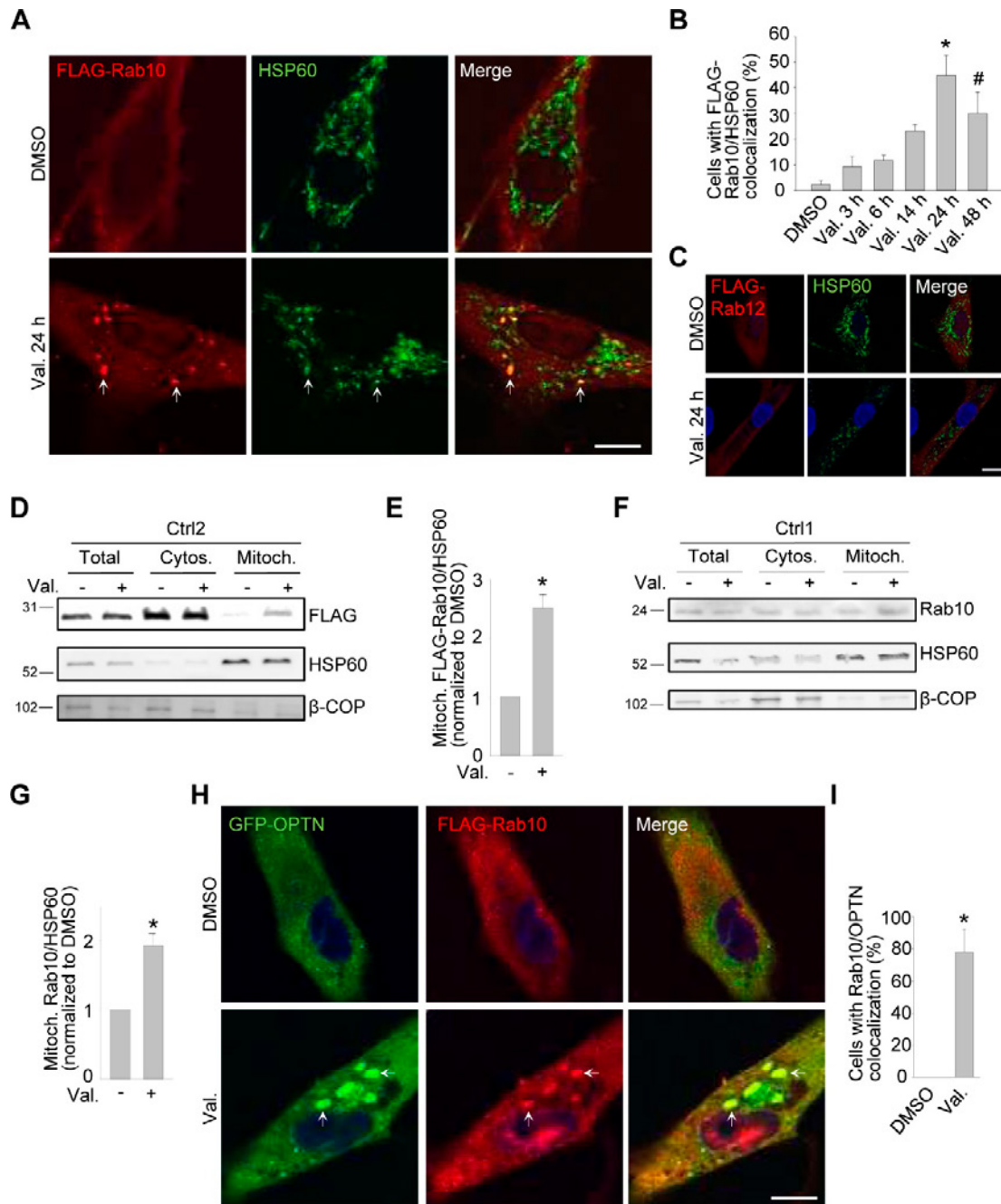


Figure 7. Rab10 accumulates on depolarized mitochondria in wild-type fibroblasts. (A-C) Control fibroblasts were transfected with FLAG-Rab10 (A, B) or FLAG-Rab12 (C). After 24 h cells were treated with DMSO or valinomycin (Val., 1 μ M) for the indicated time and immunostained for FLAG and HSP60. (B) Quantification of the percentage of cells with colocalization of FLAG-Rab10 and HSP60 ($n = 4$). $*P < 0.001$ and $\#P = 0.02$ compared with DMSO. Arrows in A indicate examples of Rab10 puncta that colocalize with mitochondria. (D, E) Control fibroblasts transfected with FLAG-Rab10 were treated with DMSO or Val. for 14 h, followed by subcellular fractionation and western blotting of total, cytosolic (Cytos.) and mitochondrial (Mitoch.) fractions for FLAG, HSP60 and the non-mitochondrial protein β -COP. (E) Quantification of FLAG-Rab10/HSP60 in the mitochondrial fraction, normalized to DMSO ($n = 3$). $*P < 0.005$ compared with DMSO. (F, G) Untransfected control fibroblasts were treated with DMSO or Val. for 14 h, followed by western blotting of subcellular fractions for endogenous Rab10, HSP60 and β -COP. (G) Quantification of endogenous Rab10/HSP60 in the mitochondrial fraction, normalized to DMSO ($n = 10$). $*P < 0.001$ compared with DMSO. (H, I) Control fibroblasts were transfected with GFP-tagged optineurin (OPTN) and FLAG-Rab10, treated with DMSO or Val. for 3 h and immunostained for FLAG. Arrows in H indicate examples of colocalization of GFP-OPTN and FLAG-Rab10. (I) Quantification of the percentage of cells with colocalization of GFP-OPTN and FLAG-Rab10 ($n = 3$). $*P = 0.002$ compared with DMSO. Scale bars, 10 μ m.

3.7. Accumulation of Rab10 on depolarized mitochondria is impaired in patients with LRRK2 mutations and is rescued by LRRK2 knockdown and LRRK2 kinase inhibition

In G2019S and R1441C LRRK2 mutant fibroblasts Rab10 accumulation on depolarized mitochondria was substantially reduced, as shown by immunocytochemistry and mitochondrial fractionation followed by western blotting (Fig. 8A-F). Interestingly, Rab10 accumulation on depolarized mitochondria was also largely abrogated in fibroblasts from PD patients with *PINK1* and *PARK2* mutations (not shown). Thus, recruitment of Rab10 to depolarized mitochondria requires intact function of PINK1 and parkin and is inhibited by PD-causing *LRRK2* mutations.

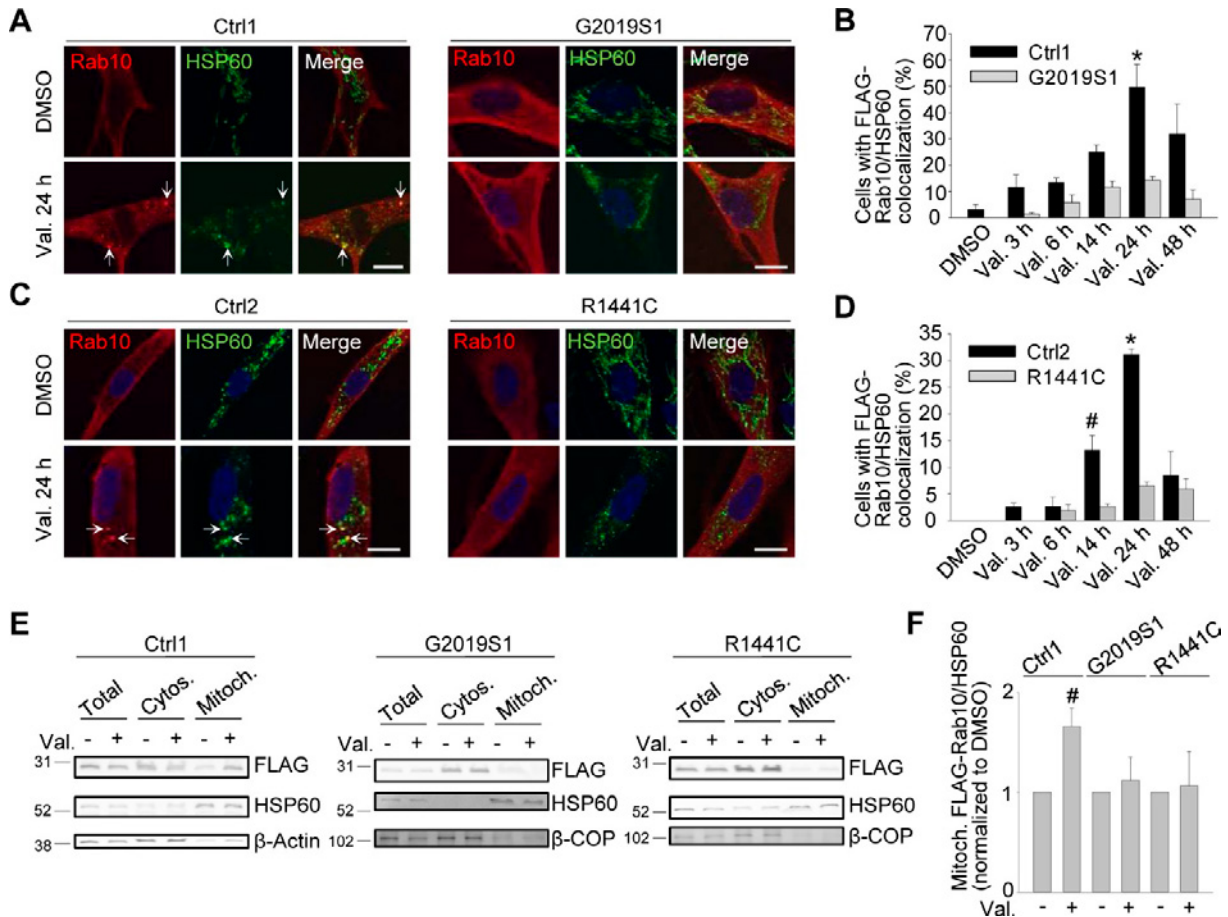


Figure 8. Rab10 accumulation on depolarized mitochondria is impaired in patient fibroblasts with *LRRK2* mutations. (A-D) Control and *LRRK2* mutant fibroblasts were transfected with FLAG-Rab10, treated with DMSO or valinomycin (Val., 1 μ M) for the indicated time periods and immunostained for FLAG and HSP60. Nuclei were stained with TOTO-3. Arrows in A and C indicate puncta with FLAG-Rab10/HSP60 colocalization. (B, D) Quantification of the percentage of cells with FLAG-Rab10/HSP60 colocalization ($n = 3$). * $P < 0.005$, # $P = 0.02$ compared with DMSO in the same subject. (E, F) Control and *LRRK2* mutant fibroblasts transfected with FLAG-Rab10 were treated with DMSO or Val. for 14 h, followed by subcellular fractionation and western blotting of total, cytosolic (Cytos.) and mitochondrial (Mitoch.) fractions for FLAG, HSP60 and the non-mitochondrial proteins β -actin or β -COP. (F) Quantification of FLAG-Rab10/HSP60 in the mitochondrial fraction, normalized to DMSO ($n \geq 3$). # $P = 0.02$ compared with DMSO in the same subject.

Importantly, *LRRK2* kinase inhibition with two different pharmacological inhibitors and *LRRK2* knockdown with two different siRNAs rescued the mitochondrial accumulation of Rab10 (Fig. 9A-H) and optineurin (not shown) in valinomycin-treated G2019S or R1441C mutant fibroblasts, in parallel with the rescue of the mitophagy defect (Fig. 2).

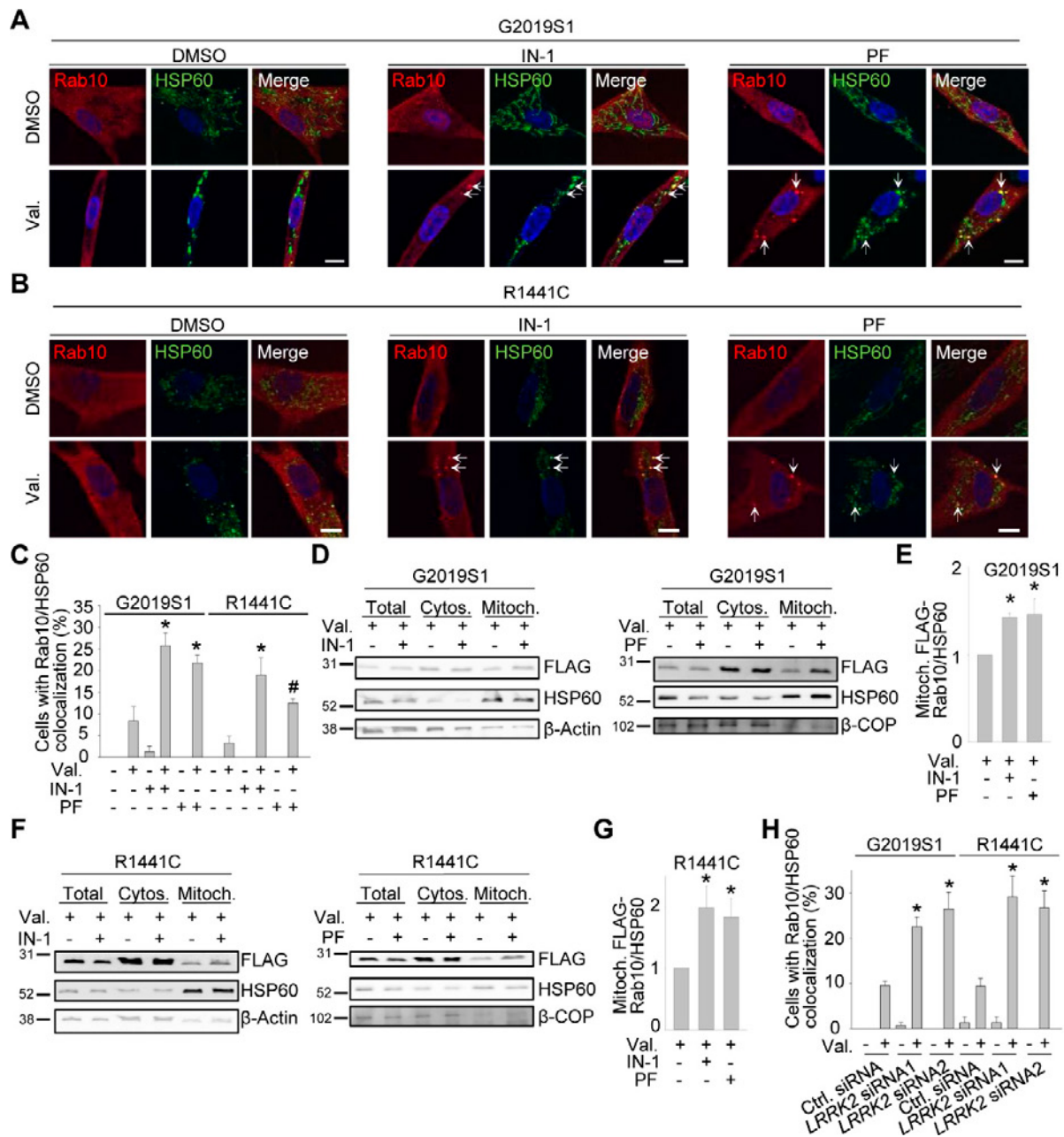


Figure 9. LRRK2 kinase inhibitors and LRRK2 knockdown rescue accumulation of Rab10 on depolarized mitochondria in patient fibroblasts with *LRRK2* mutations. (A-C) G2019S and R1441C mutant fibroblasts were transfected with FLAG-Rab10. After pre-treatment for 24 h with DMSO or the LRRK2 kinase inhibitors LRRK2-IN-1 (IN-1, 1 μM) or PF-06447475 (PF, 0.5 μM), cells were treated for 24 h with DMSO or valinomycin (Val., 1 μM) in the continued presence or absence of the LRRK2 kinase inhibitors, and immunostained for FLAG and HSP60. Arrows in **A** and **B** indicate puncta where FLAG-Rab10 and HSP60 colocalize. (C) Quantification of the percentage of cells with colocalization of FLAG-Rab10 and HSP60 ($n = 3$). * $P < 0.005$ and § $P = 0.03$ compared with Val. alone in the same subject. (D-G) G2019S and R1441C mutant fibroblasts were transfected with FLAG-Rab10. After pre-treatment for 24 h with DMSO, LRRK2-IN-1 (1 μM) or PF-06447475 (0.5 μM), cells were treated for 14 h with DMSO or Val. (1 μM) in the continued presence or absence of the LRRK2 kinase inhibitors, followed by western blotting of subcellular fractions for FLAG, HSP60 and the non-mitochondrial proteins β-actin or β-COP. (E, G) Quantification of FLAG-Rab10/HSP60 (normalized to Val. alone) in the mitochondrial fraction, normalized to DMSO ($n = 3-5$). * $P < 0.05$ compared with Val. alone. (H) G2019S and R1441C mutant fibroblasts were transfected with FLAG-Rab10 and control or *LRRK2* siRNA1 or 2. After 72 h cells were treated with DMSO or Val. for 24 h and immunostained for FLAG and HSP60. The percentage of cells with Rab10/HSP60 colocalization was quantified ($n = 3$). * $P < 0.005$ compared with Val. in control siRNA in the same subject.

3.8. Summary of the findings

Our findings show that the recently identified LRRK2 substrate Rab10 accumulates on depolarized mitochondria in a PINK1/parkin-dependent fashion and facilitates mitophagy. Rab10 recruitment to depolarized mitochondria and mitophagy are disrupted in PD patient cells expressing endogenous mutant LRRK2, and LRRK2 knockdown as well as inhibition of LRRK2 kinase activity rescue these deficits. LRRK2 mutations enhance the phosphorylation of Rab10⁶, which may inhibit Rab10 recruitment to depolarized mitochondria, leading to impairment of mitophagy. These results indicate that the pathogenic effects of PD-causing *LRRK2*, *PARK2* and *PINK1* mutations converge on a common pathway.

A manuscript describing these findings has recently been submitted for publication.

4. Further plans

4.1. Analysis of mechanisms of Rab10 association with depolarized mitochondria

We will analyze the biochemical events that mediate the association of Rab10 with depolarized mitochondria. In general, Rab GTPases cycle between cytosolic and membrane-bound pools⁷. Membrane association of Rabs is ensured by posttranslational modification of C-terminal cysteine (Cys) residues with lipophilic geranylgeranyl groups that act as hydrophobic membrane anchors⁷. Geranylgeranylation is mediated by Rab geranylgeranyl transferase (RABGGT) in collaboration with Rab escort protein (REP). REP chaperones the newly geranylgeranylated, GDP-bound Rab to its appropriate membrane. After insertion into the membrane guanine nucleotide exchange factors (GEFs) activate Rabs by promoting the exchange of bound GDP with GTP. Active, GTP-bound Rab then organizes a distinct protein scaffold on the membrane by recruiting specific binding partners called Rab effectors. Interaction with Rab effectors can further stabilize the active Rab on its membrane. Rabs are inactivated by GTPase-activating proteins (GAPs) that stimulate the ability of Rabs to hydrolyze GTP. The GDP-bound Rab is then extracted from the membrane by Rab GDP dissociation inhibitor (GDI), which escorts the geranylgeranylated Rab back to the cytosol⁷.

Given these general principles it seems very likely that geranylgeranylation of the 2 C-terminal Cys residues of Rab10 (C199 and C200) by the RABGGT/REP pathway may be required for association of Rab10 with the OMM of depolarized mitochondria. To test this we will construct versions of Rab10 in which C199 and C200 are singly or doubly mutated to serine. We will transfect these constructs in control fibroblasts and compare their translocation to depolarized mitochondria with that of wild-type Rab10, using immunocytochemistry as well as western blotting on isolated mitochondrial fractions. Also, we will assess whether siRNA-mediated knockdown of the α - and β -subunits of RGGT and REP1 in control fibroblasts impairs translocation of Rab10 to depolarized mitochondria.

4.2. Identification of binding partners of Rab10 in the mitophagy pathway

To identify potential novel binding partners of Rab10 that may be relevant for its association with depolarized mitochondria and mitophagy we will use a proteomics approach in collaboration with Prof. E. Waelkens and Prof. R. Derua (Laboratory of Protein Phosphorylation and Proteomics, KU Leuven). We will transiently express FLAG-tagged Rab10 in control fibroblasts and treat them either with valinomycin or with DMSO. FLAG-Rab10 and its binding partners will be immunoprecipitated with anti-FLAG beads, followed by elution of bound proteins with free FLAG peptides and mass spectrometric identification of the eluted proteins. The abundance of identified interactors will be normalized to the abundance of eluted Rab10 in each condition. We are particularly interested in proteins that show enhanced interaction with Rab10 after mitochondrial depolarization. Newly identified interactions will be verified by coimmunoprecipitation. We will also perform these coimmunoprecipitation experiments in *LRRK2* mutant cells. If the interactions are affected by *LRRK2* mutations, we will test whether they can be rescued by treatment of the cells with LRRK2 kinase inhibitors or by siRNA-mediated knockdown of

LRRK2. We will use our well-established mitophagy assays and cell biological approaches to explore the roles of the newly identified, validated Rab10 binding partners in mitophagy.

4.3. Analysis of Rab10 activation during mitophagy

In general, Rab GTPases are in an inactive, GDP-bound state when localized in the cytosol. Activation of Rabs only takes place during their association with membranes⁷. The observed accumulation of Rab10 on depolarized mitochondria in control fibroblasts suggests that Rab10 may become activated after mitochondrial depolarization. Rab10 activation after mitochondrial depolarization may be impaired in *LRRK2* mutant fibroblasts, in line with its reduced mitochondrial association. We will assess whether Rab10 becomes activated during mitophagy and via which mechanisms.

4.4. Validation of key findings from the fibroblast studies in human dopaminergic neurons

It will be important to confirm novel findings from the fibroblast studies in neurons. We will determine whether human dopaminergic (DA) neurons with PD-causing *LRRK2* mutations also have a mitophagy defect. In collaboration with the group of Prof. C. Verfaillie (Stem Cell Institute, KU Leuven) we successfully reprogrammed fibroblasts from the 2 G2019S mutant patients and the R1441C mutant patient to iPSCs via Sendai virus overexpression of pluripotency-related transcription factors. At least 3 iPSC clones have been generated from each patient. These iPSCs have undergone state-of-the-art quality controls. We will use CRISPR/Cas9 paired nickases to correct the point mutations in the *LRRK2* locus to create 3 isogenic control iPSC lines. In collaboration with the lab of C. Verfaillie we also optimized methods to differentiate iPSCs to DA neurons. In our hands the protocol of Kriks et al.¹⁶ yields cultures in which more than 50 % of cells are DA neurons based on staining for the marker tyrosine hydroxylase. The cells also express other midbrain DA neuron markers such as LMX1A or FOXA2. Functionality of iPSC-derived DA neurons has already been confirmed via electrophysiological recording.

We will differentiate the G2019S and R1441C mutant iPSCs as well the isogenic control iPSCs to DA neurons. We will compare mitophagy between the control and *LRRK2* mutant neurons in basal conditions and after mitochondrial depolarization. To detect mitophagy we will assess colocalization of mitochondria with the endogenous autophagosomal marker LC3 and the lysosomal marker LAMP1. In addition, we will transiently transfect mito-Keima and assess mitophagy by live imaging. In preliminary experiments we already found that cDNA transfection of adherent iPSC-derived neurons using the 4D-Nucleofector™ System (Lonza) is feasible. In addition, we will transfect FLAG-Rab10 into the neurons and assess Rab10 translocation after mitochondrial depolarization. If mitophagy or mitochondrial translocation of Rab10 are abnormal in the *LRRK2* mutant neurons, we will determine whether treatment with *LRRK2* kinase inhibitors rescues these abnormalities.

5. References

1. Poewe, W. *et al.* Parkinson disease. *Nat. Rev. Dis. Primers* **3**, 17013 (2017).
2. Kowal, S. L. *et al.* The current and projected economic burden of Parkinson's disease in the United States. *Mov. Disord.* **28**, 311-318 (2013).
3. Corti, O. *et al.* What genetics tells us about the causes and mechanisms of Parkinson's disease. *Physiol. Rev.* **91**, 1161-1218 (2011).
4. Nalls, M. A. *et al.* Large-scale meta-analysis of genome-wide association data identifies six new risk loci for Parkinson's disease. *Nat. Genet.* **46**, 989-993 (2014).
5. Rudenko, I. N. & Cookson M. R. Heterogeneity of leucine-rich repeat kinase 2 mutations: genetics, mechanisms and therapeutic implications. *Neurotherapeutics* **11**, 738-750 (2014).
6. Steger, M. *et al.* Phosphoproteomics reveals that Parkinson's disease kinase LRRK2 regulates a subset of Rab GTPases. *eLife* **5**, e12813 (2016).
7. Zhen, Y. & Stenmark, H. Cellular functions of Rab GTPases at a glance. *J. Cell Sci.* **128**, 3171-3176 (2015).
8. Pickrell, A. M. & Youle, R. J. The roles of PINK1, parkin and mitochondrial fidelity in Parkinson's disease. *Neuron* **85**, 257-273 (2015).
9. Koyano, F. *et al.* Ubiquitin is phosphorylated by PINK1 to activate parkin. *Nature* **510**, 162-166 (2014).
10. Chan, N. C. *et al.* Broad activation of the ubiquitin-proteasome system by Parkin is critical for mitophagy. *Hum. Mol. Genet.* **20**, 1726-1737 (2011).
11. Wong, Y. C. & Holzbaur, E. L. Optineurin is an autophagy receptor for damaged mitochondria in parkin-mediated mitophagy that is disrupted by an ALS-linked mutation. *Proc. Natl. Acad. Sci. USA* **111**, E4439-E4448 (2014).
12. Lazarou, M. *et al.* The ubiquitin kinase PINK1 recruits autophagy receptors to induce mitophagy. *Nature* **524**, 309-314 (2015).
13. Katayama, H. *et al.* A sensitive and quantitative technique for detecting autophagic events based on lysosomal delivery. *Chem. Biol.* **18**, 1042-1052 (2011).
14. Mizushima, N. & Komatsu, M. Autophagy: renovation of cells and tissues. *Cell* **147**, 728-741 (2011).
15. Gomez-Suaga, P. *et al.* LRRK2 delays degradative receptor trafficking by impeding late endosomal budding through decreasing Rab7 activity. *Hum. Mol. Genet.* **23**, 6779-6796 (2014).
16. Kriks, S. *et al.* Dopamine neurons derived from human ES cells efficiently engraft in animal models of Parkinson's disease. *Nature* **480**, 547-551 (2011).



Geneeskundige Stichting Koningin Elisabeth
Fondation Médicale Reine Elisabeth
Königin-Elisabeth-Stiftung für Medizin
Queen Elisabeth Medical Foundation

Progress report
of the research group of

Prof. dr. Vangheluwe Peter, PhD

Katholieke Universiteit Leuven (KU Leuven)

Principal investigator

Prof. dr. Vangheluwe Peter, PhD
Laboratory of Cellular Transport Systems (LCTS)
Department Cellular & Molecular Medicine
Faculty of Medicine, KU Leuven
Campus Gasthuisberg, ON1 box 802
Herestraat 49
B-3000 Leuven
Belgium
Tel.: +32 16 33 07 20
Fax: +32 16 34 59 9.
E-mail: Peter.Vangheluwe@kuleuven.be
gbiomed.kuleuven.be/english/research/50000618

Neuroprotection by lysosomal transport mechanisms in Parkinson's disease

1. Aims of the Project

Parkinson's disease (PD) is the second most common neurodegenerative disorder. The neurons in PD patients accumulate protein aggregates and impaired mitochondria, which contributes to cell death. In healthy neurons, endo-/lysosomal pathways provide protection by the efficient removal of damaged proteins and mitochondria, while in PD the endo-/lysosomal system is disturbed. Genetic evidence points to two novel lysosomal transport systems that are impaired in PD, which are the subject of this project: ATP13A2/PARK9 and ATP10B, a novel, candidate PD gene. Both ATP10B and ATP13A2 belong to the P-type ATPase family of active transporters.

The overall aim of the study is to unravel and compare the transport function and cellular implications of ATP13A2 and ATP10B in endo-/lysosomes, establish their role in PD onset and assess their value as therapeutic targets.

2. Progress report of ATP10B

2.1. Results

- Dr. C. Van Broeckhoven (University of Antwerp), an international leader in genetics of neurodegenerative disorders, identified five recessive mutations in the *ATP10B* gene as a likely cause for early onset PD (EOPD). First, *ATP10B* compound heterozygous mutations were found via massive parallel sequencing in a Belgian EOPD case with unaffected parents. Secondly, compound heterozygous *ATP10B* mutations were identified in affected individuals of two unrelated EOPD families.
- We optimized new biochemical methods to measure the ATPase activity, autophosphorylation activity and lipid translocation activity of *ATP10B* WT and mutants. With these assays, we established *ATP10B* WT as a phospholipid flippase in the late endo-/lysosomal compartment. Using ATPase and lipid translocation assays, we obtained convincing evidence for the loss of function nature of the disease mutations. Proving the functional loss of *ATP10B* disease mutations represents an important milestone to establish *ATP10B* as a PD-associated gene.
- We generated several cell lines to study *ATP10B* gain and loss of function. We phenotypically analyzed these cell lines and we demonstrated that *ATP10B* provides cellular protection against environmental PD risk factors. We confirmed the protective phenotype of *ATP10B* in isolated cortical neurons.
- Based on these results, we submitted a manuscript to report *ATP10B* as a novel candidate PD gene: Shaun Martin[#], Aline Verstraeten[#], Chris Van den Haute, Bavo Heeman, Igor Beletchi, Stefanie Smolders, Sarah van Veen, David Crosiers, Géraldine Gelders, Norin Hamouda, Sebastiaan Engelborghs, Jean-Jacques Martin, Jan Eggermont, Peter P De Deyn, Patrick Cras, Veerle Baekelandt, **Peter Vangheluwe***, Christine Van Broeckhoven* Familial early-onset Parkinson's disease caused by *ATP10B* mutations. Submitted. # shared first authorship; * **shared last authorship and corresponding authorship**
- Based on these results, we also submitted a patent with Dr. C. Van Broeckhoven where we claim *ATP10B* as a novel PD gene. (www.google.com/patents/WO2016166373A1?cl=en)

2.2. Ongoing work and perspectives

- We're investigating the role of *ATP10B* in autophagy and lysosomal function in our cell models.
- We will investigate the link between *ATP10B* and α -synuclein aggregation, and work together with Veerle Baekelandt (KU Leuven).

- We consider ATP10B as an interesting drug target for PD, which will be explored together with the Centre for Drug Design and Discovery (CD3, KU Leuven).

3. Progress report of ATP13A2

3.1. Results

- We obtained strong data demonstrating that ATP13A2 protects against mitochondrial stress conditions by controlling the levels of reactive oxygen species. A manuscript describing these results is currently in preparation (Martin S, et al.).
- We screened for possible transported substrates of ATP13A2 by screening for substrate induced ATPase activity on purified human ATP13A2. We identified candidate substrates that are currently further explored by biochemical analysis, including transport assays.
- We established cell models of ATP13A2 overexpression, knockdown and more recently also CRISPR/Cas9 mediated knockout. We also rescued the ATP13A2 KO by re-expressing ATP13A2 WT or disease mutants. These cell models are important to study the ATP13A2-dependent phenotype and establish a link between ATP13A2 and the candidate substrates. We already observed that ATP13A2 overexpression reduces, while knockdown increases cell toxicity towards the candidate substrates.
- Towards the mechanism of ATP13A2 activation, we made important progress by demonstrating that ATPase activity is stimulated by the lipids phosphatidic acid and phosphatidylinositol (3,5) bisphosphate, which bind to the N-terminus. We screened for the N-terminal binding site on ATP13A2 and found a possible interaction site that is currently subjected to mutagenesis.

3.2. Ongoing work and perspectives

- We're setting up a transport assay to conclusively demonstrate that ATP13A2 transports the candidate substrates.
- We will finalize our cellular experiments to establish the precise role of ATP13A2 in lysosomal health and functionality (autophagy, exosome production, ...).

4. Implications of our findings and opportunities for therapy

Our work on ATP13A2 and ATP10B has the potential to transform the PD field:

- we will establish ATP10B as a novel PD-associated gene
- we will reveal the function and substrate of two (candidate) PD-associated genes
- we will report on two novel lysosomal transport modalities.
- we will provide strategies to target ATP13A2 and ATP10B as a possible therapeutic strategy

This research is timely, since the endo-/lysosomal compartment is now considered to take a central position in PD pathology, while lysosomal based therapies are currently evaluated for PD treatment. Our study will also advance the existing knowledge on how lysosomes control α -synuclein and mitochondrial toxicity, two hallmarks of PD.

These exciting data provide new insights in the disease mechanism of PD, which will offer new therapeutic strategies. We consider ATP13A2 and ATP10B as interesting drug targets, which will be explored together with the Centre for Drug Design and Discovery (Dr. P. Chaltin), where these targets will be prioritized.

5. Budget information and request for additional resources

We are grateful that the Medical Foundation Queen Elisabeth supports our work, and our project critically depends on this funding. Despite our exciting preliminary work and fast progress, we did not yet acquire additional funding from other funding agencies like FWO to further establish the transport roles of ATP13A2 and ATP10B in the lysosomes. This puts a limit on our budget for staff, so we decided to use the GSKE budget of 2017 to pay the salary of a PhD-student involved in the project.

To report on two novel lysosomal transport systems in high impact factor journals, we will need strong and independent confirmations of the role of ATP13A2 and ATP10B in neurodegeneration. We therefore would like to follow an independent and unbiased approach using a state of the art mass-spectrometry based lipidomics and metabolomics analysis. We would analyze available gain and loss of function cell models of ATP10B and ATP13A2. These lipidomics and metabolomics analysis will be performed in specialized facilities, and require the following budget:

- **Metabolomics** (Metabolomics Expertise Center, Bart Ghesquière, VIB/KU Leuven)
Expenditures: 30€/sample
→ 48 samples x 30€/sample = 1440 € (free of VAT)
- **Lipidomics** (Research Institute for Chromatography, RIC, Kortrijk)
Expenditures: 150€/sample for full spectrum, incl. sphingo- and phospholipids
→ 36 samples x 150€/sample = 5400 € (excl VAT); 6534 € (incl VAT)
→ Purification of lysosomes with nanoparticles: 12x 120€/purification = 1440€ (free of VAT)

The total expenditures for this analysis will be 9414 €.

We would be grateful if the Foundation may consider supporting these additional expenses to support our project.

6. Publications and Activities

6.1. Visit of Princess Astrid to the Laboratory of Cellular Transport Systems

On November 23rd 2017, Princess Astrid visited the Laboratory of Cellular Transport Systems of Prof. Dr. Peter Vangheluwe and the Laboratory of Ion Channel Research of Prof. Dr. Thomas Voets in the Department of Cellular and Molecular Medicine, KU Leuven. Both professors are awardees of the Queen Elisabeth Medical Foundation for Neurosciences 2017-2019. This event has been covered by the press to inform the broad public about our research activities. Several press links are listed below:

<http://www.robtv.be/nieuws/leuven/prinses-astrid-bezoekt-laboratoria-ku-leuven>

http://www.nieuwsblad.be/cnt/dmf20171123_03203478

<https://www.hln.be/regio/leuven/prinses-astrid-bezoekt-gasthuisberg~aeaaf126/>

<https://nieuws.kuleuven.be/nl/2017/prinses-astrid-bezoekt-leuvense-labos>

<https://www.facebook.com/ROBtv.be/videos/10154952286531825/>

<https://www.monarchie.be/nl/agenda/vib-center-for-brain-disease-research>

<http://www.fmre-gske.be/pages/nl/bezoekKULeuven3.html>

6.2. Patents related to the project

- Screening Methods and Pharmaceutically active compounds for neurodegenerative diseases; inventors: Peter Vangheluwe, Veerle Baekelandt, Patrizia Agostinis, Chris Van den Haute, Sarah van Veen, Shaun Martin, Jan Eggermont. Filing date: July 3rd 2017; ZL916077
- PCT/EP2016/058558: A novel gene in neurodegenerative disease; inventors: Christine Van Broeckhoven, Jessie Theuns, Aline Verstraeten, Bavo Heeman, Peter Vangheluwe, Filing date: April 18th 2016

6.3. Publications in 2017 (* directly related to the project)

- * Estrada-Cuzcano A., Martin S., Chamova T., Synofzik M., Timmann D., Holemans T., Andreeva A., Reichbauer J., De Rycke R., Chang D., van Veen S., Samuel J., Schöls L., Pöppel T., Sorensen D., Asselbergh B., Klein C., Zuchner S., Jordanova A., **Vangheluwe P.**, Tournev I., Schüle R. (2017). Loss-of-function mutations in the ATP13A2/PARK9 gene cause complicated hereditary spastic paraplegia (SPG78). *Brain*, 140 (2), 287-305 (most recent IF: 10.29). #, **shared last authorship**
- * Demirsoy S., Martin S., Motamedi s., van Veen S., Holemans T., Van den Haute C., Jordanova A., Baekelandt V., **Vangheluwe P.**, Agostinis P. (2017). ATP13A2/PARK9 regulates endo-/lysosomal cargo sorting and proteostasis through a novel PI(3,5)P2-mediated scaffolding function. *Human Molecular Genetics*, 26 (9), 1656-1669 (most recent IF: 5.34). #, **shared corresponding author**
- * Martin S., Dudek-Peric A., Garg A., Roose H., Demirsoy S., Van Eygen S., Mertens F., **Vangheluwe P.**, Vankelecom H., Agostinis P. (2017). An autophagy-driven pathway of ATP secretion supports the aggressive phenotype of BRAF(V600E) inhibitor-resistant metastatic melanoma cells. *Autophagy*, 13 (9), 1512-1527 (most recent IF: 8.59).
- * Tharkeshwar A., Trekker J., Vermeire W., Pauwels J., Sannerud R., Priestman D., Te Vrucchte D., Vints K., Baatsen P., Decuyper J., Lu H., Martin S., **Vangheluwe P.**, Swinnen J., Lagae L., Impens F., Platt F., Gevaert K., Annaert W. (2017). A novel approach to analyze lysosomal dysfunctions through subcellular proteomics and lipidomics: the case of NPC1 deficiency. *Scientific Reports*, 7, 41408 (most recent IF: 4.26).
- * Martin S, Dudek-Peric AM, Garg AD, Roose H, Demirsoy S, Mertens F, **Vangheluwe P**, Vankelecom H & Agostinis P. An autophagy-dependent ATP secretion potentiates migration and invasion of BRAF-inhibitor resistant melanoma cells. *Autophagy* 13 (9), 1512-1527 (most recent IF: 8.59).
- Chen J., De Raeymaecker J., Hovgaard J., Smaardijk S., Vandecaetsbeek I., Wuytack F., Møller J., Eggermont J., De Maeyer M., Christensen S., **Vangheluwe P.** (2017). Structure/activity Relationship of Thapsigargin Inhibition on the Purified Golgi/secretory Pathway Ca²⁺/Mn²⁺ Transport ATPase (SPCA1a). *Journal of Biological Chemistry*, 292 (17), 6938-6951 (most recent IF: 4.13).
- Smaardijk S, Chen J, Wuytack F, **Vangheluwe P.** SPCA2 couples Ca²⁺ influx via Orai1 to Ca²⁺ uptake into the Golgi/secretory pathway. *Tissue Cell*. 2017 49(2 Pt A):141-149.
- Bittremieux M., Gerasimenko J., Schuermans M., Luyten T., Stapleton E., Alzayady K., De Smedt H., Yule D., Mikoshiba K., **Vangheluwe P.**, Gerasimenko O., Parys J., Bultynck G. (2017). DPB162-AE, an inhibitor of store-operated Ca²⁺ entry, can deplete the endoplasmic reticulum Ca²⁺ store. *Cell Calcium*, 62, 60-70 (most recent IF: 3.71).

6.4. Publications in revision or in preparation

- Danny Møllerup Sørensen*, Tine Holemans*, Sarah van Veen, Shaun Martin, Tugce Arslan, Ida Winther Haagendahl, Henrik Waldal Holen, Norin Hamouda, Jan Eggermont, Michael Palmgren, **Peter Vangheluwe**. Parkinson disease related ATP13A2 evolved early in animal evolution. *Plos One*. In revision.
- Shaun Martin#, Aline Verstraeten#, Chris Van den Haute, Bavo Heeman, Igor Beletchi, Stefanie Smolders, Sarah van Veen, David Crosiers, Géraldine Gelders, Norin Hamouda, Sebastiaan Engelborghs, Jean-Jacques Martin, Jan Eggermont, Peter P De Deyn, Patrick Cras, Veerle Baekelandt, **Peter Vangheluwe***, Christine Van Broeckhoven* Familial early-onset Parkinson's disease caused by ATP10B mutations. Submitted. # shared first authorship; * **shared last and corresponding authorship**
- Fieke Wauters, Tom Cornelissen, Shaun Martin, Brianada Koentjoro, Carolyn Sue, Peter Vangheluwe, Wim Vandenberghe. LRRK2 mutations impair mitophagy through inhibition of mitochondrial accumulation of Rab10. Submitted.
- Sarah van Veen, Shaun Martin, Chris Van den Haute, Jianmin Si, Tugce Arslan, Johan Swinnen, Wim Annaert, Patrizia Agostinis, Veerle Baekelandt, Jan Eggermont, Peter Vangheluwe. The substrate of ATP13A2. In preparation.
- Shaun Martin, Jeffry Zielich, Chris Van den Haute, Sarah van Veen, Patrizia Agostinis, Veerle Baekelandt, Jan Eggermont, Erik Lambie, Peter Vangheluwe. ATP13A2 activity mediates the mitochondrial unfolded protein response. In preparation.



Geneeskundige Stichting Koningin Elisabeth
Fondation Médicale Reine Elisabeth
Königin-Elisabeth-Stiftung für Medizin
Queen Elisabeth Medical Foundation

Progress report
of the research group of

Prof. Vanhollebeke Benoit, PhD

Université Libre de Bruxelles (ULB)

Principal investigator

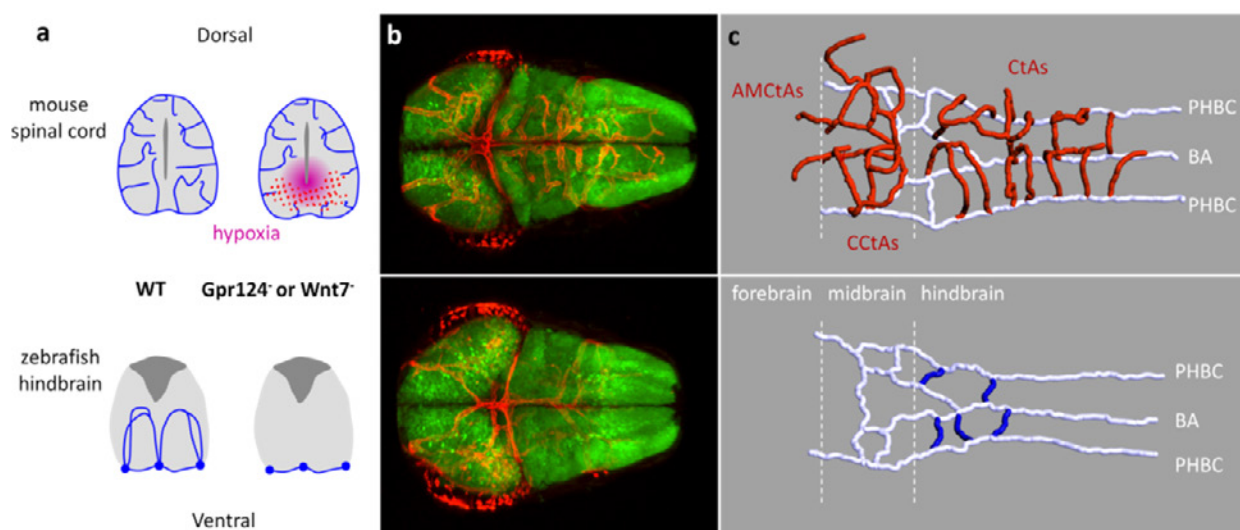
Prof. Vanhollebeke Benoit, PhD
Head of the Laboratory of Neurovascular Signaling
Department of Molecular Biology
Neuroscience Institute Faculty of Sciences
University of Brussels (ULB)
Tel.: +32 2 650 97 61
Fax: +32 2 650 97 50
E-mail: Benoit.Vanhollebeke@ulb.ac.be
nvasc.ulb.be/vanhollebekelab/

Organ-wide analysis of brain neurovascular communication in real-time and at single-cell resolution

1. State of the Art

Blood vessels are more than passive conduits for blood flow and that tissue-specific vascular beds not only match the metabolic demands of the perfused organs, but also act as important signaling centers releasing angiocrine factors that contribute to organ development, maintenance and repair. Accordingly, proper brain function relies on elaborate communications between the neural and vascular system and this organ serves as a paradigm for extensive crosstalk between the vascular system and its local microenvironment. Central nervous system (CNS) neurovascular development has been best studied in the developing mouse CNS and a number of genetic regulators of neurovascular development have been uncovered, with a subset of them further organized into networks. Despite this progress, an integrated picture of how, when and to what extent neural and vascular development are coordinated is lacking. Building this model will critically rely on the combined capacity to (i) scrutinize the cellular modalities of the intrinsically highly dynamic processes of vascular and neural development in real-time and to (ii) identify experimental settings where the signaling and circulatory functions of the intracerebral blood vessels can be, at least partially, uncoupled. Every aspect of neurovascular development and function, from blood vessels morphogenesis and BBB formation to neural cell metabolism, is indeed exquisitely sensitive to reduced tissue oxygen tension. The hypoxia response that invariably accompanies defective vascular development is a confounding factor severely blunting the scope of approachable investigations in the field.

Our previous work identified and validated the optically-clear zebrafish embryonic brain as uniquely endowed with these distinctive attributes, through the startling observation that zebrafish brains remain normoxic throughout organogenesis even in the total absence of intracerebral blood vessels and that, after prolonged periods of impaired vascular development, blood vessels invade and branch within the neural system in stereotypical patterns, implying long-prevailing physiological conditions.



A normoxic and transparent setting to explore CNS neurovascular interactions. (a) Cross-section through the mouse and zebrafish central nervous system with or without impaired vascular development. (b) z-projection of a dorsal confocal scan through the zebrafish brain, with post-mitotic neurons labeled in green and endothelial cells in red. (c) Wire-diagram representation of WT and mutant zebrafish brain vasculature in dorso-lateral views. Red vessels represent the intra-cerebral BBB network.

Through the combined increase in spatio-temporal resolution, best suited to comprehend the intrinsically dynamic processes of neurovascular development and function, and the absence of confounding hypoxic signaling cascades, some fundamental questions seem now within reach: Through which cellular and molecular mechanisms is CNS vascular invasion and maturation controlled by neural signals? Reciprocally, how does the developing vascular system impact on brain patterning and function?

The physical and genetic constraints imposed to the study of the dynamic cellular mechanisms governing sprouting angiogenesis have restricted their investigation to a limited number of *in vivo* settings, most notably the postnatal mouse retina and the zebrafish ISVs. In recent years, a coherent model integrating controlled behaviors of VEGF-selected tip cells and notch-induced stalk cells within nascent sprouts has been derived from those prototypical settings. Hierarchical organization of differentially-fated endothelial cells (ECs) during sprouting angiogenesis and organ-specific adaptations are viewed as consecutive, and hence distinct, aspects of vascular development. However, through live imaging of mosaic animals, an integrated control was recently shown to operate under the control of CNS-derived signals. Neural progenitor-derived Wnt7 ligands, well-known inducers of brain EC maturation, govern CNS EC invasion through selective modulation of tip cell function within the parental perineural vessels.

2. Objectives

The major aim of our project in 2017 was to address how perineural endothelial cells (ECs) selectively respond to neural-derived Wnt7 ligands during the process of brain angiogenesis.

From the initial discovery of Frizzled as Wnt receptors two decades ago to the recent crystallographic insights into their interaction mechanism, it has remained unknown how cells discriminate between multiple Wnt ligands within complex biological systems. The Wnt/Frizzled interaction chemistry is indeed incompatible with mono-specific recognition and, accordingly, when tested in pair-wise combinations, multiple Wnt ligands compete for binding to various Frizzled receptors. We are exploring a novel molecular mechanism that enables cells to bind and respond to Wnt7 ligands with strict specificity.

Our previous findings indeed identified Adgra2/Gpr124, an orphan member of the adhesion class of G protein-coupled receptors as an essential co-factor of Wnt7 signaling in CNS ECs. Adhesion G protein-coupled receptors (aGPCRs) constitute the second largest group of GPCRs in humans. Most aGPCRs are orphan receptors with no identified ligands that function through remarkably diverse mechanisms. They differ from other GPCRs by long N-terminal extensions preceding a membrane-proximal GPCR autoproteolysis-inducing (GAIN) domain containing the highly conserved GPCR proteolytic site (GPS). These N-terminal sequences typically comprise multiple protein-protein interaction domains involved in cell-cell and cell-matrix contacts. This structural hallmark significantly broadens the signaling potential and complexity of this class of GPCRs that, context-dependently, behave as adhesion molecules or signal transducing GPCRs. Gpr124, a member of this branch of GPCRs has gained considerable interest since the discovery of its essential role in brain vascular development (Kuhnert et al., 2010). Upon genetic inactivation, vascularization and blood-brain barrier maturation are impaired in all or parts of the zebrafish and mouse central nervous system, respectively (Anderson et al., 2011; Cullen et al., 2011; Kuhnert et al., 2010; Vanhollebeke et al., 2015). This receptor promotes angiogenic sprouting through endothelial cell (EC)-autonomous Wnt/ β -catenin signaling stimulation upon contact with neural progenitor-derived Wnt7 ligands (Posokhova et al., 2015; Vanhollebeke et al., 2015; Zhou and Nathans, 2014).

Genetic studies in zebrafish have shown that in order to recognize these ligands, and hence to be competent for brain invasion, ECs must additionally express Reck, a GPI-anchored glycoprotein (Ulrich

et al., 2016; Vanhollebeke et al., 2015). Consistently, EC-specific invalidation of RECK in the mouse leads to CNS-specific vascular defects, thereby demonstrating the evolutionary conserved role of RECK in cerebrovascular development (de Almeida et al., 2015). Gpr124 and Reck have been proposed to interact at the plasma membrane to assemble a potent and Wnt7-specific Wnt/ β -catenin co-activator complex (Vanhollebeke et al., 2015). The complex also operates in neural crest-derived cells to promote dorsal root ganglia (DRG) neurogenesis in zebrafish embryos (Vanhollebeke et al., 2015). Defective DRG neurogenesis is accompanied by metamorphic pigmentation alterations in the adult Gpr124 mutant skin (Vanhollebeke et al., 2015).

While the genetic interaction between *gpr124* (also known as *adgra2*) and *reck* is well supported by studies in the zebrafish model as well as cell culture experiments, their activation and signaling mechanisms are poorly characterized, in part as a result of a lack of *in vivo* models where structure-function relationships can be probed.

3. Results

3.1. Identification of an *in vivo* model of *gpr124/adgra2*-dependent neurovascular dysfunction (Bostaille et al. Development)

Malmquist *et al.* (2013) phenotypically characterized the *ouchless* mutant that was recovered from an F3 forward genetic screen for defective dorsal root ganglion (DRG) neurogenesis in zebrafish. While the initial dorsoventral migration of neural crest-derived cell clusters towards presumptive DRG locales appears unaffected in *ouchless* mutants, the neurogenic program leading to the generation of *neurog1:EGFP+* cells within the ganglion is defective, resulting in a severe reduction of DRG numbers in 72 hours post fertilization (hpf) *ouchless* mutants. *ouchless* mutants are viable but exhibit reduced growth rates and interrupted melanophore stripes in the adult skin. The *ouchless* mutation was mapped by bulk segregation analysis to a 342 kb genomic region of chromosome 8, harboring the *sorbs3* gene. No causative mutation could be identified within the coding sequence of *sorbs3*, but a mutation was suspected to reside within cis-regulatory elements, accounting for the reduced *sorbs3* transcript levels observed in *ouchless* mutants. Antisense *sorbs3* morpholino knockdown experiments, as well as BAC and mRNA rescue experiments, further supported the model that *sorbs3* regulates DRG neurogenesis and that *sorbs3* dysfunction drives the *ouchless* phenotypes (Malmquist et al., 2013).

The *ouchless* phenotypes are remarkably analogous to the DRG defects reported in *gpr124* knock-out mutants (Vanhollebeke et al., 2015). Of note *gpr124* has been renamed to *adgra2*. Along with Reck, Gpr124/Adgra2 has been shown to control DRG formation by activating Wnt signaling in neural crest-derived *sox10:mRFP+* ganglion cells (Vanhollebeke et al., 2015). Given the phenotypic similarities, we therefore set out to test whether *adgra2* and *ouchless* (presumably *sorbs3*) co-operate during the process of DRG neurogenesis and brain vascularization.

We first demonstrated that *adgra2/gpr124* and *ouchless* genetically interact by functional gene dosage experiments (**Figure 1**).

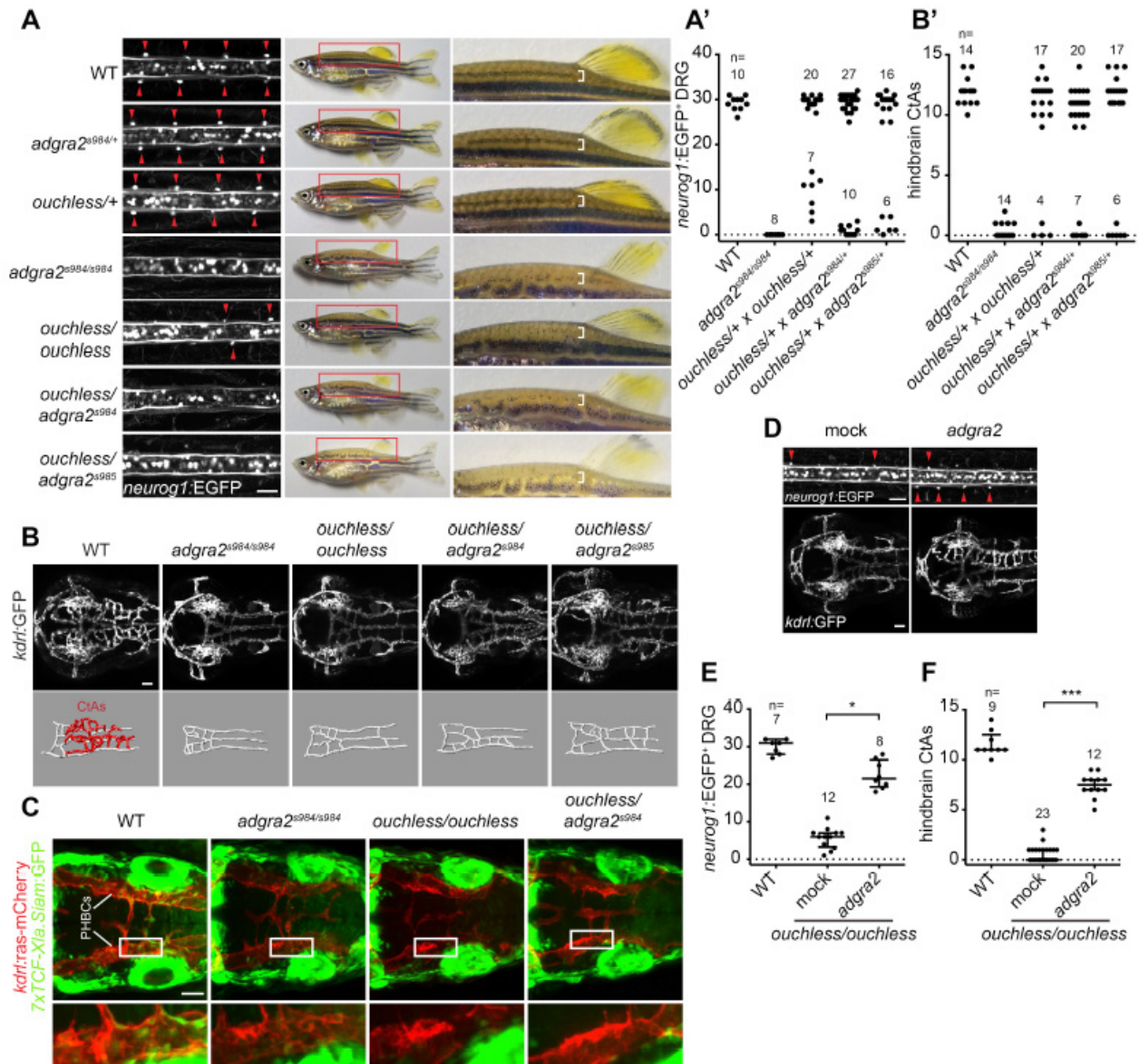


Figure 1 *gpr124/adgra2* and *ouchless* mutations fail to complement. (A and A') Fish heterozygous for *ouchless* were crossed with the previously described *adgra2* heterozygotes, *adgra2*^{s984/+} and *adgra2*^{s985/+}, and the offspring were assessed at 72 hpf for defects in DRG neurogenesis. From these crosses, ~25% of the offspring (annotated as *ouchless/adgra2*^{s984} and *ouchless/adgra2*^{s985}) showed an almost complete lack of *neurog1*:EGFP⁺ DRG. When raised to adulthood, these fish could be distinguished from their siblings by discontinuous dorsal melanophore stripes on their skin (brackets). (B and B') Cerebral vasculatures of 60 hpf embryos derived from *ouchless* heterozygotes incrosses and outcrosses to *adgra2* heterozygotes. 25% of the offspring of each of the crosses displays highly penetrant brain vascular defects, characterized by a complete absence of central arteries (CtAs), similar to *adgra2* mutants. (C) Defective endothelial Wnt/ β -catenin signaling in the perineural primordial hindbrain channel (PHBC) ECs. (D-F) When *ouchless* mutants are injected at the one-cell stage with mRNA encoding wild-type (WT) *Adgra2*, significant restoration of *neurog1*:EGFP⁺ DRG and cerebral blood vessels is observed.

The lack of complementation between *ouchless* and *adgra2*, together with the discovery of vascular phenotypes in *ouchless* mutants that mimic those of *adgra2* mutants, indicates that *ouchless* constitutes a new allele of *adgra2*. The re-evaluation of the genomic region known to harbour the *ouchless* mutation revealed that the *adgra2* gene resides within the critical interval, spanning the ca-48 and ca-37 genomic markers. In *ouchless* mutants, *adgra2* displays an essential splice site mutation inactivating *Adgra2* through the in-frame deletion of a single LRR in the ectodomain of this adhesion G-protein coupled receptor (Figure 2).

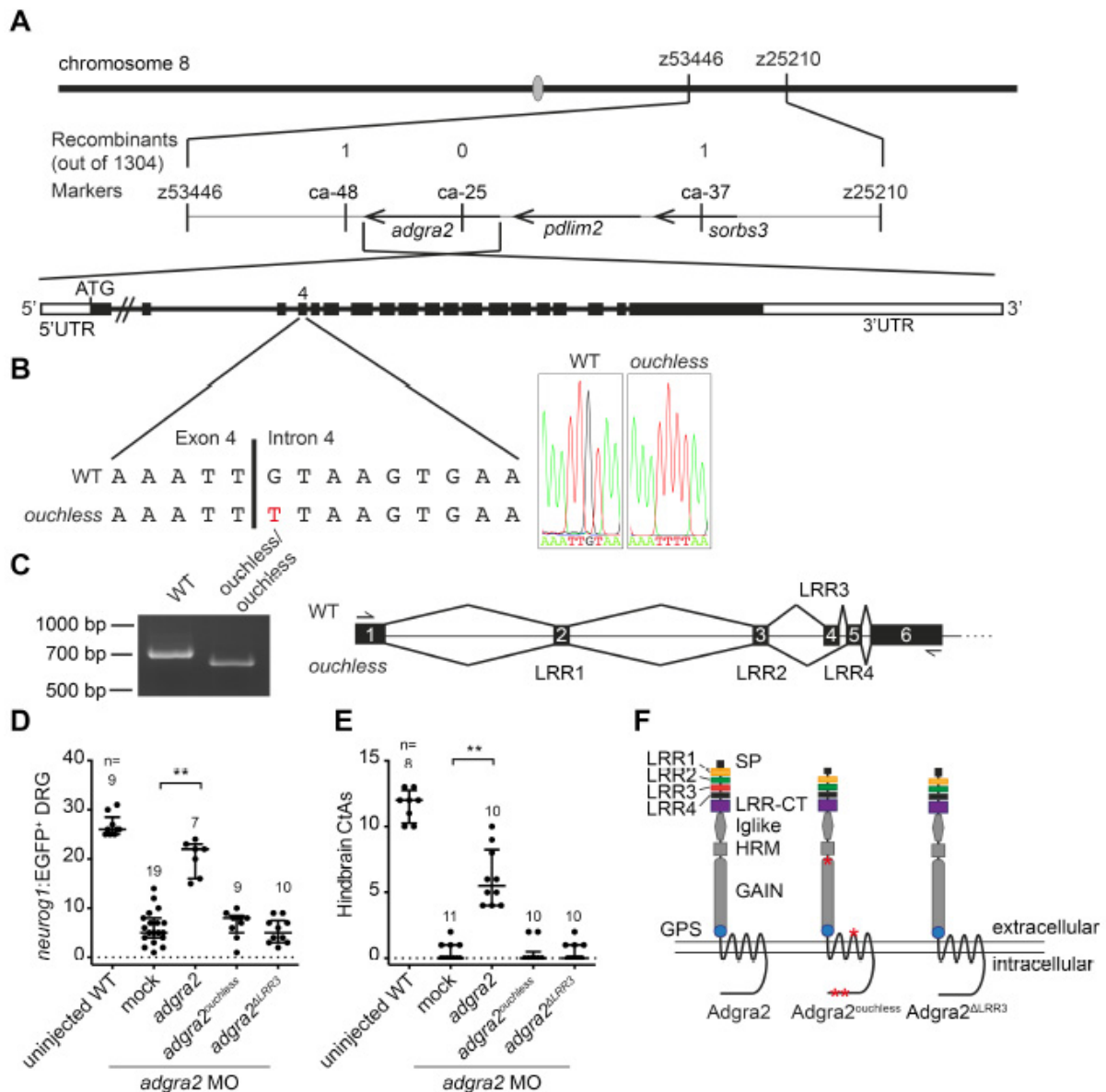


Figure 2 *adgra2* is mutated in *ochless* mutants. (A) Representation of the *ochless* locus genetic map on chromosome 8. The number of recombinants among 1304 meioses as determined by Malmquist et al. (2013) is indicated above the markers utilized for mapping. (B) Sanger sequencing of the exon 4-intron 4 boundary of *adgra2* in WT and *ochless* mutant embryos. The G→T change in the *ochless* 5' splice donor sequence appears in red. (C) RT-PCR splicing analysis of *adgra2* in 48 hpf WT and *ochless* mutant embryos. The amplification primers hybridize to exon 1 and exon 6, as illustrated in the panel on the right. (D, E) The capacity of the full-length *adgra2* coding sequence from *ochless* mutants to rescue DRG and CtA defects in *adgra2* morphants was evaluated by mRNA injection at the one-cell stage. While mRNA encoding the WT receptor (annotated as *adgra2*) partially suppressed both phenotypes, the *ochless* variant (annotated as *adgra2^{ochless}*) did not affect either. (F) Comparison of a reference WT *adgra2* allele with the *adgra2* coding sequence recovered from *ochless* mutant embryos. Four non-synonymous single nucleotide polymorphisms (SNPs; M429V, S895P, A1282V and A1302G) as well as an in-frame 72 bp deletion corresponding to exon 4 are found in *ochless*. While all four *adgra2* SNPs identified in *ochless* mutants had been previously identified in functionally validated *adgra2* alleles derived from mixed AB/TL genetic backgrounds, alternative splicing resulting in exon 4 skipping is absent from any known zebrafish, mouse or human *ADGRA2* isoform. When probed in zebrafish, alternative splicing of the exon 1-exon 6 sequences is undetectable by RT-PCR (C). Exon 4 corresponds precisely to the third leucine-rich repeat (LRR) unit of the LRR/CT domain of Adgra2, which comprises an array of four 24-residue-long LRR units followed by a LRR cysteine-rich C-terminal motif (LRR-CT).

Altogether, this work reveals that *ochless* and *adgra2* mutants are allelic and that the *ochless* phenotypes result from an essential splice site mutation inactivating Adgra2 through the in-frame deletion of a single LRR in the ectodomain of this adhesion G-protein coupled receptor (GPCR). The zebrafish *ochless* mutant thereby constitutes the first *in vivo* model of *adgra2* N-terminal domain-specific variation.

3.2. Molecular insights into Adgra2/Gpr124 and Reck intracellular trafficking (Bostaille et al. Biology Open)

Taking advantage of the above-described mutation in *adgra2*, we undertook to better define the cellular and molecular modalities of the Gpr124/Reck synergistic interaction. In particular, the stoichiometry of the Gpr124/Reck complex and the molecular determinants of its trafficking, assembly and signal transduction still needed to be investigated. The N-terminal domains of Gpr124 are likely contributors to several, if not all, of these processes. Indeed, cell culture and *in vivo* experiments have revealed that Gpr124 function critically relies on its extracellular domain architecture. N-terminal truncations or substitution of the ectodomain of Gpr124 with the equivalent domain derived from the closely related Gpr125, abrogate receptor signaling (Posokhova et al., 2015; Vanhollebeke et al., 2015). Moreover, the Gpr124 potential interaction interface with Reck, a cell surface exposed GPI-anchored glycoprotein, is restricted to the extracellular parts of the receptor.

As is typically found in aGPCRs, the extracellular N-terminus of Gpr124 comprises multiple protein-protein interaction domains whose contributions to receptor function remain largely elusive. Specifically, the Gpr124 ectodomain is sequentially composed of an N-terminal LRR/CT domain, an Ig-like domain and a hormone receptor motif (HRM) preceding the membrane-proximal GPS-containing GAIN domain. The Gpr124 LRR/CT domain contains four leucine-rich repeat (LRR) units which are 20-29 residue-long structural units that assemble in a superhelical manner with tandemly arranged repeats to form curved solenoid structures acting as protein interaction frameworks. As found in Gpr124, extracellular LRR motifs are often flanked by cysteine-rich C-terminal domains (LRR-CTs) that are integral parts of the LRR domain and shield the hydrophobic core of the last LRR motif. Building a proper understanding of Gpr124 function will benefit from delineating the contribution of each N-terminal domain to receptor function.

The *adgra2* variant found in *ouchless* mutants differs from *adgra2* reference sequences by four non-synonymous SNPs as well as a 72 bp deletion corresponding to exon 4 (**Figure 3A**). While the SNPs represent naturally occurring variations, the exon 4 skipping event is caused by an ENU-induced essential splice-site mutation at the exon 4–intron 4 boundary and was shown to result in Adgra2^{ouchless} inactivation (Bostaille et al., 2017). Exon 4 encodes the third LRR motif (LRR3) of the LRR/CT domain. In order to determine how the absence of LRR3 mechanistically impairs Adgra2 function, we generated C-terminal EGFP-tagged versions of wild-type (WT) Adgra2 as well as *ouchless* (Adgra2^{ouchless}) and Δ LRR3 (Adgra2 ^{Δ LRR3}) variants. This latter variant reproduces the exon 4 deletion found in *ouchless* in a WT allele of *adgra2*, and hence lacks the *ouchless*-associated SNPs (Bostaille et al., 2017). We first evaluated the functionality of the fusion proteins in brain angiogenic assays in zebrafish by mRNA injections at the one-cell stage. While ectopic restoration of either EGFP-tagged or untagged versions of WT Adgra2 could restore angiogenic sprouting in *adgra2*^{s984/s984} hindbrains (red arrowheads in **Figure 3C**), the equivalent Adgra2^{ouchless} and Adgra2 ^{Δ LRR3} variants were inactive (**Figure 3B,C**). These observations extend and confirm previous findings indicating that C-terminal fusions are compatible with receptor function *in vivo* and that, in the absence of LRR3, Adgra2 is non-functional (Vanhollebeke et al., 2015, Bostaille et al., 2017).

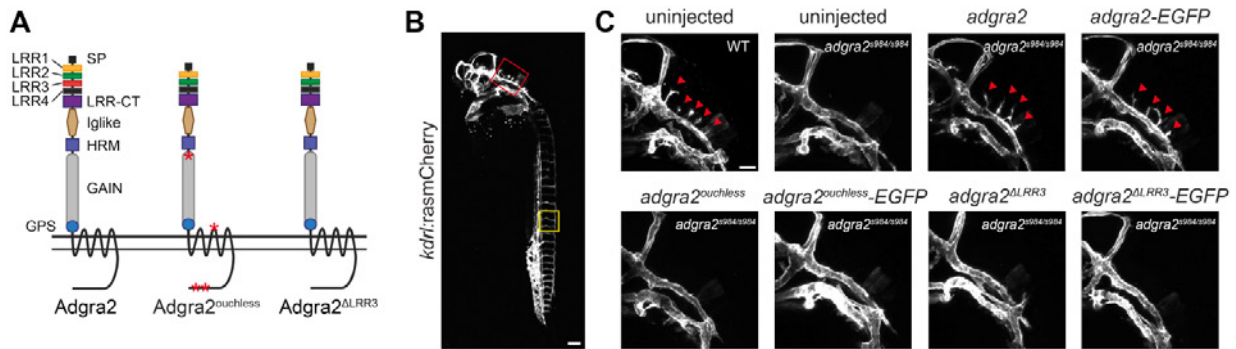


Figure 3. *Adgra2*^{ouchless} mislocalizes to the endoplasmic reticulum. (A) Schematic representation of *Adgra2*, *Adgra2*^{ouchless} and *Adgra2*^{ΔLRR3} topology and domain organization. *Adgra2*^{ouchless} and *Adgra2*^{ΔLRR3} lack the third LRR motif (red rectangle). The positions of the residue variations resulting from naturally occurring SNPs in *adgra2*^{ouchless} are designated by red asterisks. (B) Maximal intensity projection of a confocal z-stack of a WT *Tg(kdrl:ras-mCherry)* embryo at 36 hpf in lateral view. The red and yellow boxes define, respectively, the magnified areas of the hindbrain vasculature shown in C and the intersegmental vessels shown in E. Scale bar: 100 μm. (C) Maximal intensity projection of a confocal z-stack of WT and *adgra2*^{ouchless} *Tg(kdrl:ras-mCherry)* embryos at 36 hpf in lateral view after injection of 100 pg of *adgra2*, *adgra2*-EGFP, *adgra2*^{ouchless}, *adgra2*^{ouchless}-EGFP, *adgra2*^{ΔLRR3} or *adgra2*^{ΔLRR3}-EGFP mRNA at the one-cell stage. The red arrowheads point to the CtAs invading the hindbrain rhombomeres. Scale bar: 50 μm.

We then analyzed the stability and subcellular distribution of the EGFP-tagged variants in different cell types. When examined in the large and cobblestone-shaped enveloping layer cells of the 5 h post fertilization (hpf) zebrafish blastula, WT *Adgra2*-EGFP labeled the plasma membrane where it colocalized with a membrane-tethered lyn-RFP marker. By contrast, the mutant fusion proteins accumulated in an intracellular reticulate compartment reminiscent of the ER. Similarly, when analyzed in ECs of mosaic transgenic zebrafish, the WT fusion decorated the EC plasma membranes, including the numerous filopodial extensions of the tip cells, while the mutant variants showed strong intracellular and perinuclear signals that did not colocalize with the *ras-mCherry* EC membrane marker. Finally, in order to streamline quantitative colocalization studies, we imaged the cellular distribution of the EGFP fusion proteins in cultured HEK293T cells. Whereas the WT fusion protein accumulated at the plasma membrane marked by GPI-RFP as anticipated, the mutant versions failed to reach this compartment but instead accumulated intracellularly. The accumulating compartment was identified as the ER with the help of the mCherry-fused ER protein translocation apparatus component SEC61β. This was further quantitatively evaluated by Pearson's colocalization coefficient (PCC) analysis. Moreover, a perfect correlation was observed between the capacity of the LRR chimera variants to reach the plasma membrane and their ability to support vascular sprouting in the zebrafish hindbrain or to induce the formation of DRG neurons.

When overexpressed in cultured cells, *Adgra2* and *Reck* colocalize at the plasma membrane and proximity ligation assays further suggest that the proteins may directly interact within this compartment to assemble a receptor complex (Vanhollebeke et al., 2015). It remains to be determined whether the partners recognize and assist each other during their progression within the secretory pathway or instead meet at the plasma membrane after independent trafficking events. We took advantage of the ER retention of the LRR/CT variants to address this question. As revealed by indirect immunofluorescence assays in non-permeabilized HEK293T cells, HA-*Reck* reached the plasma membrane independently of the nature and trafficking status of the co-expressed *Adgra2* receptor (Figure 4A). In addition, when expressed individually in HEK293T cells, *Reck* and *Adgra2* localized to the plasma membrane (Vanhollebeke et al., 2015). These results suggest that *Reck* does not require *Adgra2* in order to reach the plasma membrane and vice versa. However, as HEK293T cells express low levels of endogenous *ADGRA2* and *RECK* (Vanhollebeke et al., 2015; Zhou and Nathans, 2014), this endogenous protein pool might be sufficient to accompany ectopic *Reck* and/or *Adgra2* during secretion. We therefore engineered *ADGRA2*^{-/-} and *RECK*^{-/-} HEK293T cells through CRISPR/Cas9 approaches and re-evaluated *Adgra2* and *Reck* trafficking in these genetic backgrounds (Figure 4B). As in WT cells, both proteins

accumulated at the plasma membrane when expressed individually, indicating that each partner can reach its final destination independently (**Figure 4C,D**).

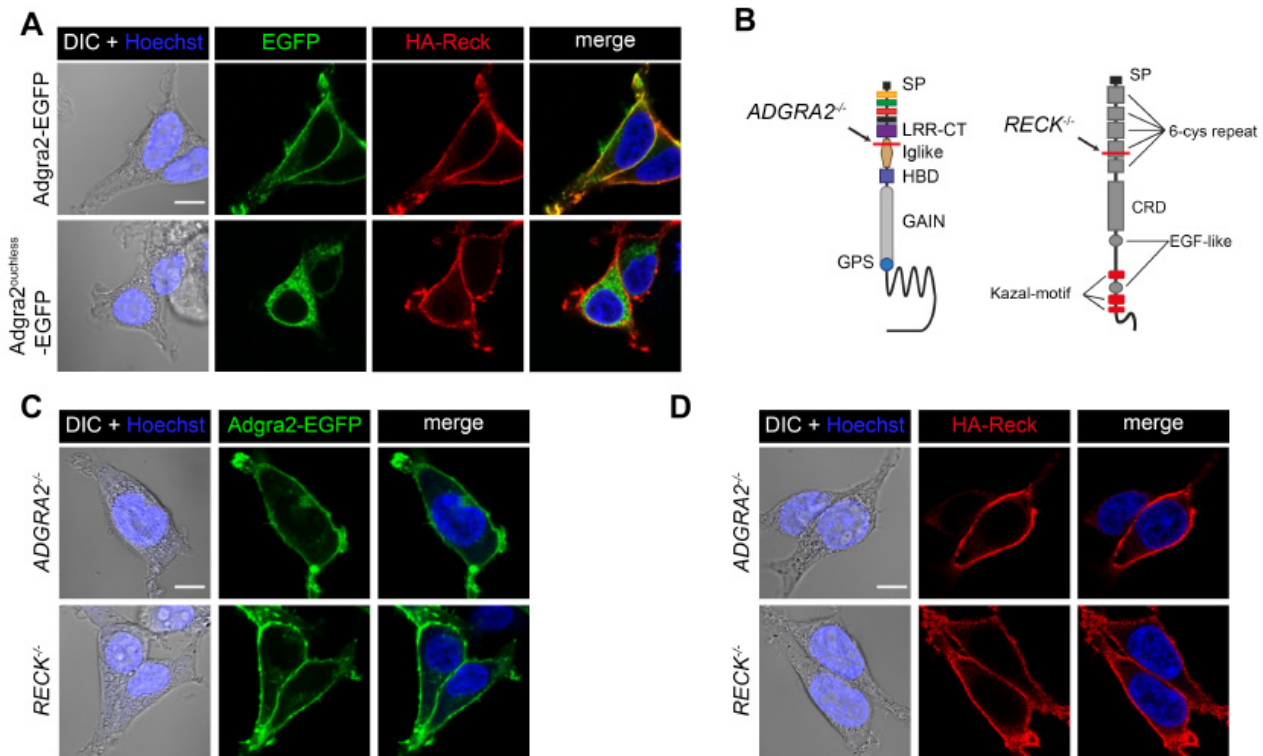


Figure 4 Independent trafficking of Reck and Adgra2 to the plasma membrane. **(A)** Single-plane confocal images of non-permeabilized HEK293T cells 48 h after transfection with HA-reck and adgra2-EGFP variants, as indicated. **(B)** Schematic representation of the genetic lesions of ADGRA2^{-/-} and RECK^{-/-} cells. The position of the frame-shift mutation is indicated by the red line. **(C,D)** Single-plane confocal images of non-permeabilized ADGRA2^{-/-} and RECK^{-/-} HEK293T cells 48 h after transfection with adgra2-EGFP **(C)** and HA-reck **(D)** constructs. In all panels, EGFP is detected by direct fluorescence and the HA-Reck fusion by anti-HA indirect immunofluorescence. Cells were additionally transfected with a *Wnt7a* (mouse gene) expression construct. Nuclei were counterstained with Hoechst. Scale bars: 10 μ m.

When assessed 48 h post transfection in saponin-permeabilized HEK293T cells, a minor fraction of HA-Reck can be immunodetected in the ER and as such co-distributes with Adgra2^{ouchless} (**Figure 5A**, arrows) and presumably with a fraction of WT Adgra2 transiting through this compartment. To test whether Adgra2 is able to interact with Reck under these conditions, we performed proximity ligation assays as described previously (Vanhollebeke et al., 2015). As shown in **Figure 5B**, no interaction could be detected between HA-Reck and FLAG-Adgra2^{ouchless}, in contrast to the plasma membrane-localized signal readily detected in HA-Reck and FLAG-Adgra2 co-expressing cells. These results suggest that either the ER is not permissive for the formation of the complex or that the LRR deletion in Adgra2 impairs its interaction with Reck.

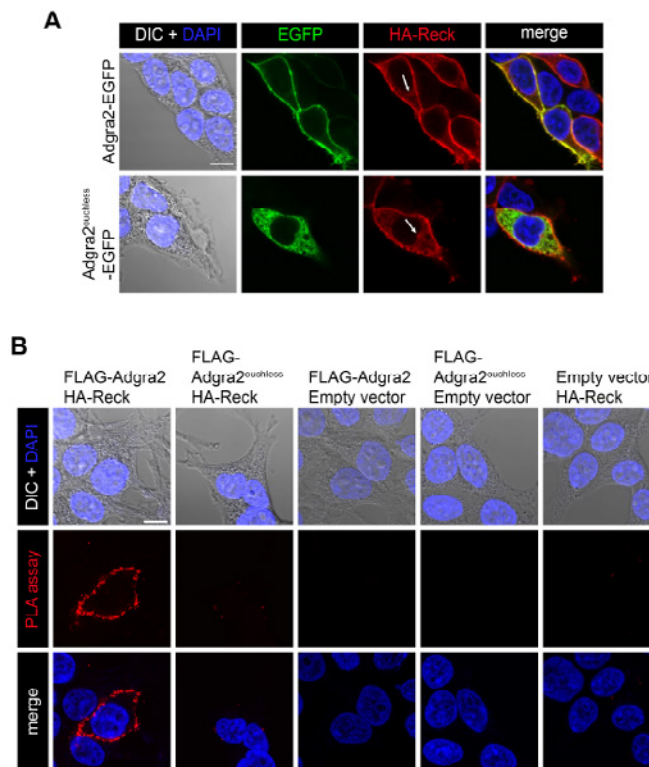


Figure 5 Cellular distribution of Adgra2 and Reck interaction. (A) Single-plane confocal images of saponin-permeabilized HEK293T cells 48 h after transfection with *HA-reck* and *adgra2-EGFP* variants, as indicated. Nuclei were counterstained with DAPI. EGFP is detected by direct fluorescence and the HA-Reck fusion by anti-HA indirect immunofluorescence. Arrows point to the ER. (B) Proximity ligation assays in HEK293T cells 48 h after transfection with *FLAG-adgra2*, *FLAG-adgra2^{ouchless}* and *HA-reck* constructs, as indicated. Nuclei were counterstained with DAPI. In all panels, cells were additionally transfected with a *Wnt7a* (mouse gene) expression construct. Scale bar: 10 μ m.

This study characterized the functionally null mutation of *adgra2* recently identified in zebrafish *ouchless* mutants. The genetic lesion results in *adgra2* alternative splicing and we show that this receptor variant localizes to the ER instead of the plasma membrane. This unprecedented occurrence of an aberrantly routed Adgra2 prompted us to evaluate whether the intracellular trafficking of Reck and Adgra2 are interdependent. When co-expressed with the ER-retained Adgra2 variant, Reck still reached the plasma membrane. Extending this analysis in CRISPR/Cas9 engineered cells, Reck was shown to accumulate at the plasma membrane in both WT and *ADGRA2*^{-/-} HEK293T cells and, similarly, Adgra2 trafficking to the plasma membrane was unaffected by the presence or absence of RECK. These data indicate that the partners, when expressed individually, are able to traffic independently. When co-expressed in HEK293T cells, their close proximity can be detected by PLA assays at the plasma membrane but not within the endomembrane compartments of the secretory pathway through which they transit. These combined observations indicate that the partners first meet at the plasma membrane and that their synergy is likely restricted to the events occurring subsequently at the cell surface, in agreement with the current model (Vanhollebeke et al., 2015). It is conceivable that the interaction between Adgra2 and Reck is only made possible within plasma membrane microdomains of specific proteolipidic composition or that a yet to be defined component induces complex formation within this compartment. The selective association of Reck and Adgra2 at the plasma membrane could also result from the higher concentrations reached within this final membrane compartment favoring the potentially transient encounters of the partners.

While this study describes the role of the LRR/CT domain in promoting Adgra2 progression through the ER, it does not exclude additional roles for this domain in the Adgra2/Reck signaling pathway. The LRR/CT domain might, for instance, be additionally implicated in the interactions with Reck, Wnt7 or Fzd/Lrp5/6 occurring at the plasma membrane.

By extension, the contribution of the other extracellular domains of Adgra2 and Reck to Adgra2/Reck signaling will require further investigation. These future studies will be important not only for their insights into the molecular mechanisms governing essential developmental processes, but also because they hold the key to understanding the thus-far elusive mechanisms of Wnt ligand-specific signaling pathways. These efforts will be extended in the upcoming years.

4. Publications

- Bostaille N, Gauquier A, Stainier DY, Raible DW, Vanhollebeke B. Defective *adgra2* (*gpr124*) splicing and function in zebrafish *ouchless* mutants. *Development*. 2017 Jan 1;144(1):8-11.
- Bostaille N, Gauquier A, Twyffels L, Vanhollebeke B. Molecular insights into Adgra2/Gpr124 and Reck intracellular trafficking. *Biol Open*. 2016 Dec15;5(12):1874-1881.
- Fontaine F, Lecordier L, Vanwalleghem G, Uzureau P, Van Reet N, Fontaine M, Tebabi P, Vanhollebeke B, Büscher P, Pérez-Morga D, Pays E. APOLs with low pH dependence can kill all African trypanosomes. *Nat Microbiol*. 2017 Nov;2(11):1500-1506.
- Horáková E, Changmai P, Vancová M, Sobotka R, Van Den Abbeele J, Vanhollebeke B, Lukeš J. The Trypanosoma brucei TbHrg protein is a heme transporter involved in the regulation of stage-specific morphological transitions. *J Biol Chem*. 2017 Apr 28;292(17):6998-7010.
- De Muylder G, Vanhollebeke B, Caljon G, Wolfe AR, McKerrow J, Dujardin JC. Naloxonazine, an Amastigote-Specific Compound, Affects Leishmania Parasites through Modulation of Host-Encoded Functions. *PLoS Negl Trop Dis*. 2016 Dec 30;10(12):e0005234.

5. Additional References

- Anderson K. D., Pan L., Yang X., Hughes V. C., Walls J. R., Dominguez M. G., Simmons M. V., Burfeind P., Xue Y., Wei Y. et al. (2011). Angiogenic sprouting into neural tissue requires Gpr124, an orphan G protein-coupled receptor. *Proc. Natl. Acad. Sci. USA* 108, 2807-2812. 10.1073/pnas.1019761108
- Bostaille N., Gauquier A., Stainier D. Y. R., Raible D. W. and Vanhollebeke B. (2017). Defective *adgra2* (*gpr124*) splicing and function in zebrafish *ouchless* mutants. *Development*, doi:10.1242/dev.146803. 10.1242/dev.146803
- Bostaille N, Gauquier A, Twyffels L, Vanhollebeke B. Molecular insights into Adgra2/Gpr124 and Reck intracellular trafficking. *Biol Open*. 2016 Dec15;5(12):1874-1881.
- Cullen M., Elzarrad M. K., Seaman S., Zudaire E., Stevens J., Yang M. Y., Li X., Chaudhary A., Xu L., Hilton M. B. et al. (2011). GPR124, an orphan G protein-coupled receptor, is required for CNS-specific vascularization and establishment of the blood-brain barrier. *Proc. Natl. Acad. Sci. USA* 108, 5759-5764. 10.1073/pnas.1017192108
- de Almeida G. M., Yamamoto M., Morioka Y., Ogawa S., Matsuzaki T. and Noda M. (2015). Critical roles for murine Reck in the regulation of vascular patterning and stabilization. *Sci. Rep.* 5, 17860 10.1038/srep17860
- Kuhnert F., Mancuso M. R., Shamloo A., Wang H.-T., Choksi V., Florek M., Su H., Fruttiger M., Young W. L., Heilshorn S. C. et al. (2010). Essential regulation of CNS angiogenesis by the orphan G protein-coupled receptor GPR124. *Science* 330, 985-989. 10.1126/science.1196554
- Malmquist, S. J., Abramsson, A., McGraw, H. F., Linbo, T. H. and Raible, D. W. (2013). Modulation of dorsal root ganglion development by ErbB signaling and the scaffold protein Sorbs3. *Development* 140, 3986-3996. doi:10.1242/dev.084640
- Posokhova E., Shukla A., Seaman S., Volate S., Hilton M. B., Wu B., Morris H., Swing D. A., Zhou M., Zudaire E. et al. (2015). GPR124 functions as a WNT7-specific coactivator of canonical β -catenin signaling. *Cell Rep.* 10, 123-130. 10.1016/j.celrep.2014.12.020
- Ulrich F., Carretero-Ortega J., Menendez J., Narvaez C., Sun B., Lancaster E., Pershad V., Trzaska S., Veliz E., Kamei M. et al. (2016). Reck enables cerebrovascular development by promoting canonical Wnt signaling. *Development* 143, 147-159. 10.1242/dev.123059
- Vanhollebeke B., Stone O. A., Bostaille N., Cho C., Zhou Y., Maquet E., Gauquier A., Cabochette P., Fukuhara S., Mochizuki N. et al. (2015). Tip cell-specific requirement for an atypical Gpr124- and Reck-dependent Wnt/ β -catenin pathway during brain angiogenesis. *eLife* 4, e06489 10.7554/eLife.06489
- Zhou Y. and Nathans J. (2014). Gpr124 controls CNS angiogenesis and blood-brain barrier integrity by promoting ligand-specific canonical Wnt signaling. *Dev. Cell* 31, 248-256. 10.1016/j.devcel.2014.08.018



Geneeskundige Stichting Koningin Elisabeth
Fondation Médicale Reine Elisabeth
Königin-Elisabeth-Stiftung für Medizin
Queen Elisabeth Medical Foundation

Progress report
of the research group of

Prof. dr. Geert van Loo, PhD

Universiteit Gent (UGent)

Principal investigator

Prof. dr. Geert van Loo, PhD

Co-investigators

Prof. Dr. Mohamed Lamkanfi

Inflammation Research Center
VIB – Gent University
Technologiepark 927
9052 Gent-Zwijnaarde
Belgium
Tel.: +32 9 331 37 61
Fax: +32 9 221 76 73
E-mail: geert.vanloo@irc.vib-ugent.be

Microglia, inflammasomes and multiple sclerosis

Multiple sclerosis (MS) is the most common chronic inflammatory disease of the central nervous system (CNS). MS is prevalent in Caucasians, where it affects about 0.1 % of the population (Trapp and Nave (2008) *Annu Rev Neurosci* 31, 247-269), which means for a country like Belgium that about 10.000 patients suffer from the disease. The cause of degeneration in MS remains largely enigmatic, but the disease is generally considered to be the result of an autoimmune inflammatory reaction characterized by activated auto-reactive myelin-specific lymphocytes that home to the CNS where they initiate a vicious cycle of inflammation, oligodendrocyte loss, demyelination, and axonal damage. The major targets in MS pathology are oligodendrocytes, the myelin-producing cells of the CNS, and neurons, and their loss is directly associated with clinical manifestations of the disease, including speech disturbances, sensation deficits and paralysis. Astrocytes and microglia, the other CNS resident cell types, are considered to act as effector cells during pathology, since more and more evidence indicates that both cell types actively contribute to the inflammatory reactions in MS (Dendrou *et al.* (2015) *Nat Rev Immunol.* 15, 545-558). An important experimental model to study the human disease is the model of Experimental Autoimmune Encephalomyelitis (EAE), which can be induced in rodents by immunization with myelin-specific antigens. Important knowledge concerning the molecular mechanisms driving MS pathology came from studies using this model (Baxter (2007) *Nat Rev Immunol* 7, 904-912).

1. NF- κ B in MS pathology

NF- κ B transcription factors localize to the cytoplasm but translocate to the nucleus after an inflammatory stimulus. Upon activation, NF- κ B shapes the immune response as it regulates expression of both pro- and anti-inflammatory cytokines and chemokines. In addition, NF- κ B controls the expression of protective anti-apoptotic genes (Oeckinghaus *et al.* (2011) *Nat. Immunol.* 12, 695-708). Suggestive for a role in MS, activation of NF- κ B in the CNS of MS patients and EAE animals has been described (Mc Guire *et al.* (2013) *Trends Mol. Med.* 19, 604-613). In addition, genome wide association studies and transcriptional studies identified several genes involved in NF- κ B signalling as MS susceptibility loci (De Jager *et al.* (2009) *Nat. Genet.* 41, 776-782; Sawcer *et al.* (2011) *Nature* 476, 214-219). Moreover, gene targeting studies in mice have confirmed an important role for NF- κ B in EAE, not only in controlling peripheral immune responses, but also an important role for CNS-restricted NF- κ B activation in EAE pathogenesis has been demonstrated (Mc Guire *et al.* (2013) *Trends Mol. Med.* 19, 604-613). Mice lacking IKK2 or NEMO, essential signalling proteins controlling NF- κ B activation, in all cells of neuroectodermal origin are protected from EAE as a result of the inability of astrocytes to sustain an inflammatory environment (van Loo *et al.* (2006) *Nat. Immunol.* 7, 954-961). In addition, mice expressing an astrocyte-specific dominant-negative NF- κ B super-repressor transgene (GFAP-I κ B α -dn) are also protected from EAE due to defective astrocyte expression of pro-inflammatory cytokines and chemokines (Brambilla *et al.* (2009) *J. Immunol.* 182, 2628-2640).

One critical NF- κ B response gene, induced under inflammatory conditions, is A20 (also referred to as tumor necrosis factor-alpha induced protein 3, TNFAIP3). A20 encodes a zinc finger protein which acts as a potent inhibitor of NF- κ B activation, but also has strong anti-apoptotic activities (Catrysse *et al.* (2014) *Trends Immunol.* 35, 22-31). As a consequence, mice deficient in A20 die prematurely due to systemic multi-organ inflammation (Lee *et al.* (2000) *Science* 289, 2350-2354). Conditional deletion of A20 in B cells, DCs or myeloid cells results in a spontaneous autoimmune phenotype (Catrysse *et al.* (2014) *Trends Immunol.* 35, 22-31), further emphasizing the role of A20 in controlling inflammatory immune responses. Interestingly, A20 has been identified in humans as a susceptibility locus for

multiple immunopathologies (Catrysse *et al.* (2014) *Trends Immunol.* 35, 22-31), including MS (De Jager *et al.* (2009) *Nat. Genet.* 41, 776-782). Finally, expression of A20 is downregulated in peripheral blood mononuclear cells of MS patients (Gilli *et al.* (2010) *PLoS One* e8962), further suggesting a role for A20 in MS pathology.

2. A20 critically controls microglia activation and neuroinflammation

Given the evidence for a role of NF- κ B in MS and EAE pathogenesis, and taken into account that A20 acts as a strong inhibitor of both NF- κ B and apoptosis signalling, we sought to clarify the role of A20 in specific CNS cell types in EAE. We therefore generated mice lacking A20 specifically in all cells of neuroectodermal origin ($A20^{CNS-KO}$), in astrocytes ($A20^{Astr-KO}$), in oligodendrocytes ($A20^{ODC-KO}$) and in neurons ($A20^{Neur-KO}$). To our surprise, incidence nor severity of EAE differed between $A20^{CNS-KO}$, $A20^{Astr-KO}$, $A20^{ODC-KO}$ or $A20^{Neur-KO}$ and their respective control littermate mice (Figure 1).

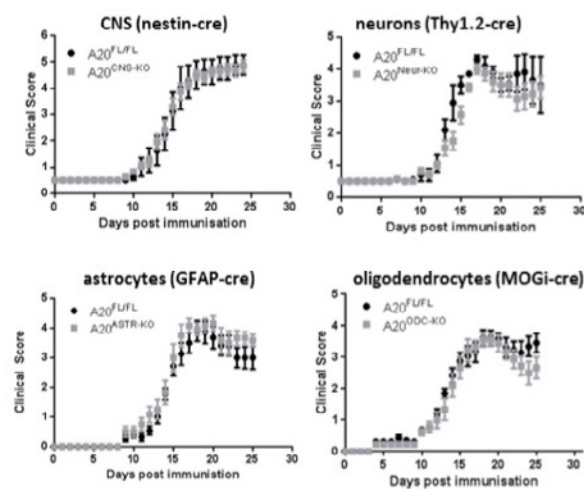


Fig. 1. EAE was induced by active immunization of CNS-specific A20 deficient ($A20^{CNS-KO}$, $n=7$), neuron-specific A20 deficient ($A20^{Neur-KO}$, $n=7$), astrocyte-specific A20 deficient ($A20^{Astr-KO}$, $n=6$), oligodendrocyte-specific A20 deficient ($A20^{ODC-KO}$, $n=9$) mice and respective control littermate $A20^{FL/FL}$ mice ($n=7, 6, 11$ and 13 respectively) with MOG peptide, and clinical disease development was followed over time. Each data point represents the mean \pm SEM. Representative experiment from three independent experiments.

However, A20 turned out to be very important in microglia, the CNS resident myeloid cells. Microglia act as immune sentinels which constantly scan the CNS to detect signs of pathogenic invasion or tissue damage. Under pathological conditions, however, microglia can acquire a detrimental pro-inflammatory phenotype that actively contributes to the chronicity of inflammatory brain diseases, including MS (Shemer *et al.* (2015) *Trends Immunol.* 36, 614-624; Biber *et al.* (2016) *Nat Rev Drug Discov.* 15, 110-124). To assess the function of A20 *in vivo*, we crossed mice carrying a floxed A20 allele (Vereecke *et al.* (2010) *J. Exp. Med.* 207, 1513-1523) to $Cx3Cr1CreErt2$ transgenic mice allowing Cre-mediated gene deletion following tamoxifen (TAM) treatment. Targeting of microglia using this system is based on microglia longevity and capacity of self-renewal without any appreciable input from circulating blood cells (Goldmann *et al.* (2013) *Nat. Neurosci.* 16, 1618-1626; Tay *et al.* (2017) *Nat. Neurosci.* 20, 793-803). Microglia A20 deficient mice ($A20^{Cx3Cr1-KO}$) and control littermates were immunized with MOG peptide and disease progression was monitored by assessing clinical disease symptoms and body weight. Although both $A20^{Cx3Cr1-KO}$ and control mice develop EAE, $A20^{Cx3Cr1-KO}$ mice demonstrate earlier disease onset and a more severe disease course as compared to control mice (Figure 2 and Table 1), demonstrating a crucial role for microglia A20 activity in EAE pathogenesis.

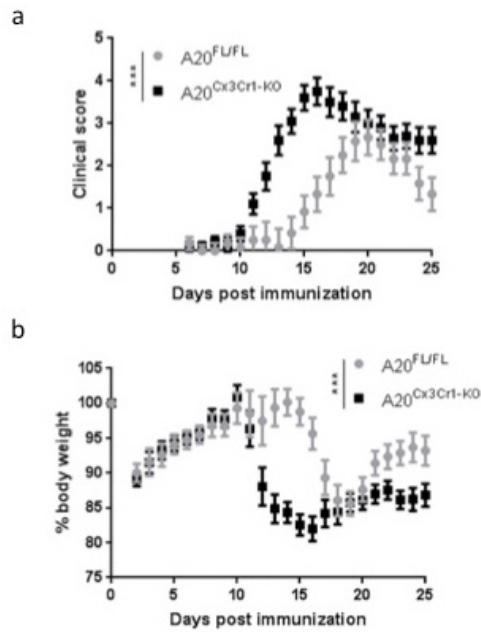


Fig. 2. EAE was induced by active immunization of control A20^{FL} (n=6) and A20^{Cx3Cr1-KO} mice (n=10) with MOG peptide, and clinical disease development (a) and body weight (b) was followed over time. Each data point represents the mean ± SEM as estimated by the REML analysis. Changes in clinical score and relative body weight differ significantly (***) p < 0.001; F-test) between genotypes across the time span. Data are representative of three independent experiments.

Genotype	Incidence	Day of onset (p < 0.001)	Mean max score (p = 0.012)
A20 ^{FL}	100% (6/6)	16,2 ± 0,5	2,8 ± 0,3
A20 ^{Cx3Cr1-KO}	100% (10/10)	11,9 ± 0,3	3,9 ± 0,2

Table 1. Clinical features of MOG-induced EAE in A20^{FL} and A20^{Cx3Cr1-KO} littermates showing disease incidence (at least a score of 2), day of onset and mean maximal clinical score. Results are displayed as mean ± SEM.

Clinical pathology in A20^{Cx3Cr1-KO} was confirmed by histology on spinal cord sections at start of the clinical manifestations, showing extensive demyelination, axonal damage, inflammation and immune cell infiltration in A20^{Cx3Cr1-KO} mice, while nearly no immune cell infiltration, demyelination or axonal loss could be detected in the spinal cord of control mice at this early time-point (Figure 3). Also the expression of inflammatory cytokines, chemokines and Th1-, Th17- and Treg-linked factors, confirmed the hypersensitivity of A20^{Cx3Cr1-KO} mice to EAE (Figure 4).

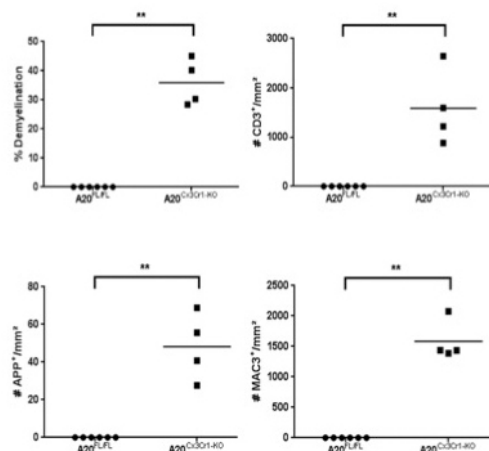


Fig. 3. Quantification of immune cell infiltration, demyelination and neuronal damage in the spinal cord of control (A20^{FL}) and A20^{Cx3Cr1-KO} mice 13 days post-immunization. Each symbol indicates the mean of one mouse. Significant differences are determined by a Mann-Whitney U statistical test (** p < 0.01).

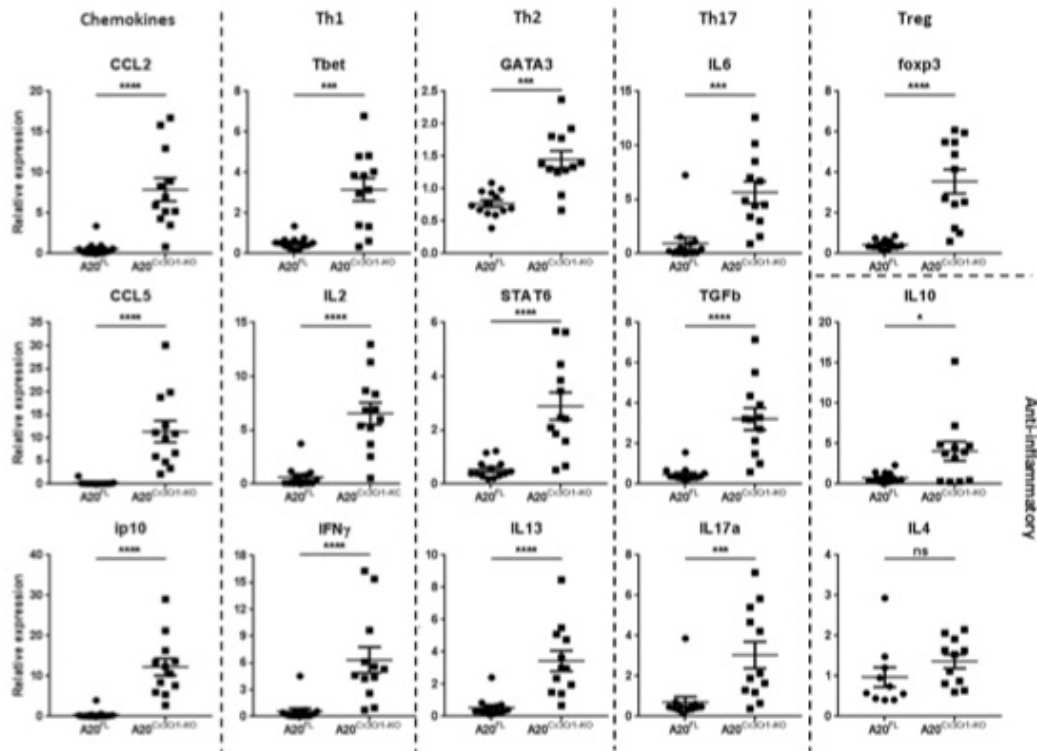


Fig. 4. Expression of chemokines, Th1-, Th17-, Th2-, and Treg-related factors, and anti-inflammatory cytokines in the spinal cord of control ($A20^{FL}$) and $A20^{Cx3Cr1-KO}$ mice 12 days post immunization. Each symbol represents one mouse. Data are expressed as the ratio of the mRNA expression normalized to endogenous housekeeping genes and expressed as mean \pm SEM. Significant differences are determined by a Mann-Whitney U statistical test (* $p < 0.05$, *** $p < 0.001$, **** $p < 0.0001$).

Although the $Cx3Cr1$ promoter is not thought to target lymphocytes in $Cx3Cr1CreErt2$ mice, we confirmed that the enhanced sensitivity in EAE was caused by the CNS-specific ablation of A20 and not by an impaired peripheral T-cell response. Lymphocytes from immunized mice were isolated and tested *in vitro* for their response upon secondary exposure to MOG peptide, showing similar responses in $A20^{Cx3Cr1-KO}$ and control mice, thereby demonstrating that peripheral immune functions are not affected in $A20^{Cx3Cr1-KO}$ mice (Figure 5).

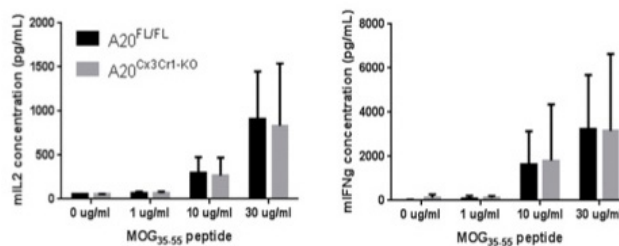


Fig. 5. Recall assay in $A20^{Cx3Cr1-KO}$ mice. Splenocytes from MOG-immunized $A20^{FL}$ and $A20^{Cx3Cr1-KO}$ mice were cultured and stimulated with indicated MOG peptide concentrations. Supernatants were analyzed for IL-2 and IFN γ 48h after stimulation using ELISA. Data represent mean \pm SEM of 4 mice per group.

Microglia, like other macrophages, express multiple innate immune receptors including inflammasome receptors. Inflammasomes are large cytosolic protein complexes that function as intracellular sensors for infectious agents and host-derived danger signals. Inflammasomes thus serve critical functions in host defence, however, aberrant inflammasome activation has been linked to many inflammatory and (neuro) degenerative diseases, including MS (Lamkanfi and Dixit (2014) *Cell* 157, 1013-1022; Walsch *et al.* (2014) *Nat Rev Neurosci* 15, 84-97). We have strong evidence that the clinical phenotype of microglia-

specific A20 knockout mice in EAE critically relies on inflammasome hyperactivation in microglia, in agreement with our previous finding identifying A20 as a critical control on Nlrp3 inflammasome activation in macrophages (Vande Walle *et al.* (2014) *Nature* 512, 69-73). Indeed, primary microglial cells derived from A20 deficient mice show inflammasome hyperactivation when stimulated with soluble and crystalline Nlrp3 inducing agents, as evidenced by enhanced caspase-1 activation and IL-1 β /IL-18 secretion (Figure 6).

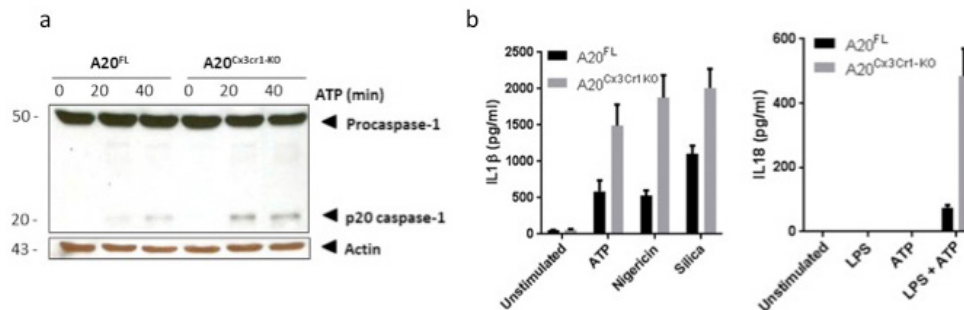


Fig. 6. (a) Immunoblot for procaspase-1 and cleaved caspase-1 (p20) in primary cultured microglia from control (A20^{FL}) and A20^{Cx3Cr1-KO} mice stimulated with LPS and/or ATP. Actin is shown as loading control. Data are representative of two independent experiments. (b) IL1 β and IL18 protein levels in the supernatant of primary cultured microglia stimulated with LPS alone or together with ATP, Silica or Nigericin. Data represent the mean \pm SD of three technical replicates of pooled microglial cells from control (A20^{FL}) and A20^{Cx3Cr1-KO} mice. Data are representative of three independent experiments.

To test the hypothesis that the hyperactivation of the Nlrp3 inflammasome is responsible for the aggravated EAE phenotype in A20^{Cx3Cr1-KO} mice, Nlrp3^{-/-} mice were crossed with A20^{Cx3Cr1-KO} mice and EAE disease development was monitored. In contrast to A20^{Cx3Cr1-KO} mice, which develop a more severe pathology, A20^{Cx3Cr1-KO}-Nlrp3^{-/-} mice show a significantly reduced clinical pathology, comparable to control A20^{FL} littermate mice (Figure 7).

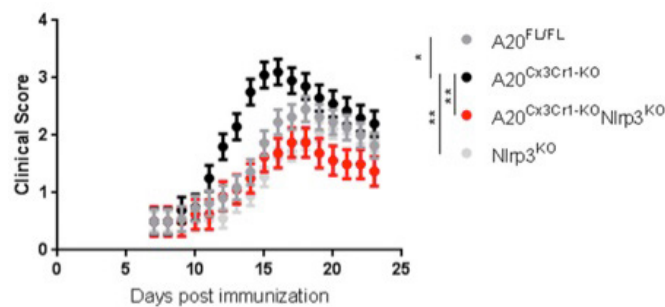


Fig. 7. Active immunization of control (A20^{FL}, n=11), A20^{Cx3Cr1-KO} (n=10), Nlrp3^{KO} (n=18) and A20^{Cx3Cr1-KO}-Nlrp3^{KO} (n=8) mice and clinical disease development over time. Each data point represents the mean \pm SEM as estimated by the REML analysis. Changes in clinical score and relative body weight differ significantly between genotypes across the time span (* p < 0.05, ** p < 0.01; F test). Graph represents combined data from three independent experiments.

Nlrp3^{-/-} mice lack the Nlrp3 protein ubiquitously, and the specific contribution of inflammasome signaling inside the CNS to EAE pathogenesis is unknown. To study the specific function of inflammasomes within microglia during EAE, caspase-1 conditional knockout mice having a floxed allele (caspase-1^{FL}) were generated (Van Gorp *et al.* (2016) *Proc Natl Acad Sci USA* 113, 5-10) and crossed with A20^{Cx3Cr1-KO} mice to produce mice lacking both A20 and caspase-1 in microglia (caspase-1-A20^{Cx3Cr1-KO}). These mice are currently challenged in EAE in order to clarify the involvement of inflammasome activation locally in microglia in the EAE phenotype of A20^{Cx3Cr1-KO} mice.

Results obtained from mouse studies need to be translated to humans. We could obtain through collaborations human samples (tissue and cerebrospinal fluid (CSF)) from MS patients and controls allowing the validation of our findings. Published studies have shown that the levels of IL-1 β and IL-18 are elevated in CSF and brain tissue of MS patients. Also, the expression of caspase-1 and NLRP3 have been shown to be elevated in samples of MS patients (Inoue and Shinohara (2013) *Autoimmune Dis* 859145). In agreement, we could demonstrate elevated expression of IL-1 β and NLRP3, and a trend, albeit not significant, in enhanced IL-18 and caspase-1 in MS plaques compared to NAWM (normal appearing white matter) (Figure 8a). Higher IL-18 and IL-1 β protein levels were also detected in CSF of MS patients compared to controls, suggestive of inflammasome activation in microglia, although also other immune cells may have contributed to this (Figure 8b). Finally, we could demonstrate enhanced expression of *A20/TNFAIP3* in MS plaques compared to NAWM (Figure 8c). Together, our data analysing the expression levels of inflammasome mediators in brain plaques isolated from normal and MS patients show that brain tissue affected by MS clearly exhibits enhanced activation of the NLRP3 inflammasome.

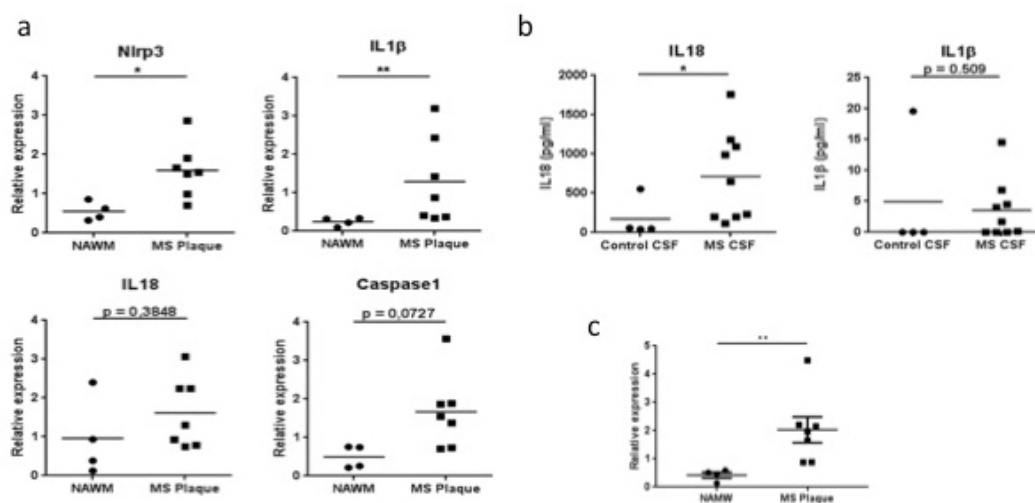


Fig. 8. (a) Relative gene expression levels of inflammasome-associated factors in plaques of post-mortem MS patients (Plaque) or post-mortem control tissue (NAWM). Each symbol represents one patient. Data are expressed as the ratio of the mRNA expression normalized to endogenous housekeeping genes and expressed as mean \pm SEM. (b) IL1 β and IL18 cytokine levels in the CSF of post-mortem MS patients or control samples. Each symbol represents one CSF sample. (c) Relative gene expression levels of *A20/TNFAIP3* in plaques of post-mortem MS patients or control NAWM. Significant differences are determined by Mann-Whitney U statistical test (* p < 0.05, ** p < 0.01).

3. Ongoing studies

Microglia function as CNS-specific immune sentinels, but also support and monitor synaptic function, control synaptogenesis and are vital for the survival of neurons during development (Shemer *et al.* (2015) *Trends Immunol.* 36, 614-624; Biber *et al.* (2016) *Nat Rev Drug Discov.* 15, 110-124). Since *A20* deficient primary microglia display an 'activated' phenotype characterized by inflammasome hyperactivation (Figure 6), ongoing studies now focus on the spontaneous phenotypes of *A20*^{Cx3Cr1-KO} mice (*viz.* in the absence of any inflammatory insult).

Besides their role in the activation and secretion of IL-1 β and IL-18, the major effector mechanism of inflammasomes is the induction of pyroptosis. Pyroptosis, a pro-inflammatory and lytic mode of cell death, is the dominant response upon caspase-11 activation and Gasdermin D cleavage, occurring mainly in myeloid cells including microglia. Pyroptosis induces cell swelling and rupture of the plasma membrane, causing massive leakage of cytosolic contents provoking inflammatory reactions. Caspase-11 expression is also required for non-canonical caspase-1 activation and secretion of IL-1 β and IL-18. Early studies on the role of caspase-11 in EAE identified caspase-11 as a crucial mediator of oligodendrocyte death and EAE pathogenesis (Hisahara *et al.* (2001) *J Exp Med.* 193, 111-22). However,

the specific role of caspase-11 in microglia in neuroinflammation and MS/EAE pathology has never been addressed. Ongoing research investigates the specific role of caspase-1 and of caspase-11 in microglia by analysing unique microglia-specific caspase-1 and caspase-11 knockout mice. These mice have recently been generated in the research group and will allow to address the differential importance of caspase-1 and -11 in microglia activation, pyroptosis and CNS inflammation in EAE. In a parallel *in vitro* approach, microglial cell cultures from these mice are being isolated allowing biochemical studies.

4. Impact

Microglial cells are the key immune effector cells of the CNS and are increasingly being recognized as targets for therapeutic intervention in CNS diseases (Biber *et al.* (2016) *Nat. Rev. Drug Discover.* 15, 110-124). With our studies we hope to identify the importance of inflammasome activation in microglia, and provide new fundamental knowledge helping us to better understand the pathways and molecular mechanisms that control autoimmune inflammation in the brain, especially in the context of MS pathogenesis. However, these findings may also broaden our knowledge on the mechanisms behind other neuroinflammatory diseases. With this knowledge we hope to contribute to the development of new and better therapies to treat patients suffering from these diseases. Proposed research is thus of great importance, not only for the scientific community, but especially for the many patients (and relatives) confronted with MS.

5. Publications van Loo group 2017 (acknowledging GSKE support)

- Catrysse, L. and van Loo, G. (2017) Inflammation and the metabolic syndrome : the tissue specific functions of NF- κ B. *Trends Cell Biol.*, 27(6), 417-429. (IF:11.5)
- De Wilde, K., Martens, A., Lambrecht, S., Jacques, P., Drennan, M.B., Debusschere, K., Coudenys, J., Verheugen, E., Windels, F., Beyaert, R., van Loo, G. and Elewaut, D. (2017) A20 inhibition of STAT1 signaling in myeloid cells: a novel endogenous regulatory mechanism preventing development of enthesitis. *Annals of the Rheumatic Diseases*, 76(3), 585-592. (IF : 12.4)



Geneeskundige Stichting Koningin Elisabeth
Fondation Médicale Reine Elisabeth
Königin-Elisabeth-Stiftung für Medizin
Queen Elisabeth Medical Foundation

Progress report
of the research group of

Prof. dr. Verfaillie Catherine

Katholieke Universiteit Leuven (KU Leuven)

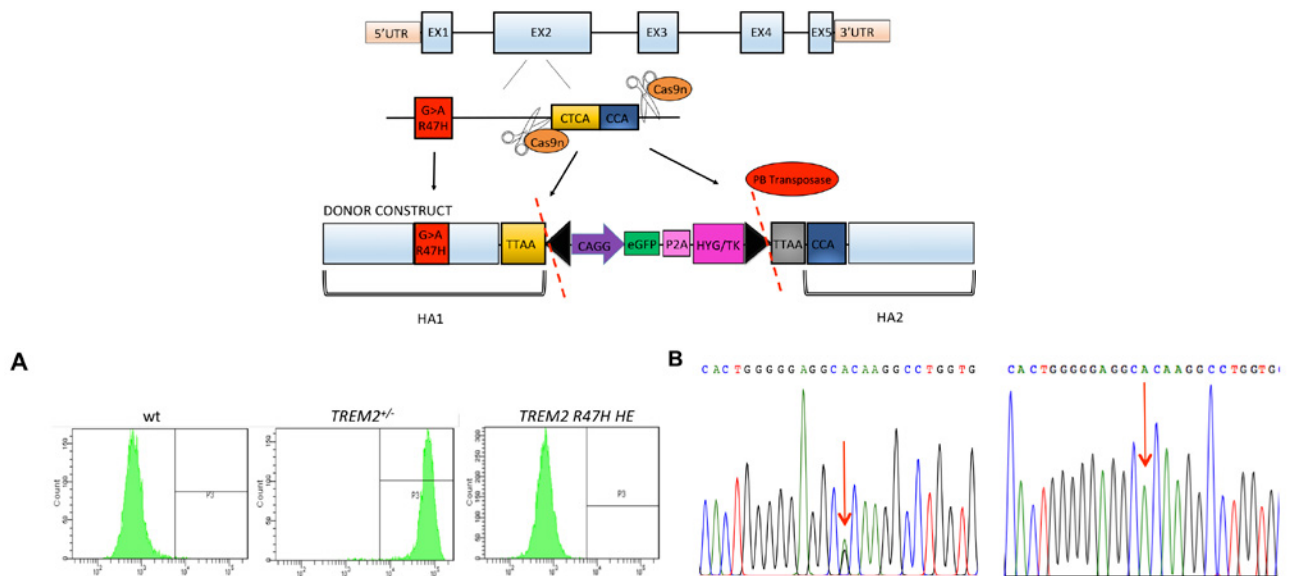
Principal investigator

Prof. dr. Verfaillie Catherine
Interdepartementaal Stamcel Instituut
Katholieke Universiteit Leuven
UZ Gasthuisberg
Herestraat 49
3000 Leuven
Belgium
Tel.: +32 16 33 02 95
Fax: +32 16 33 02 94
E-mail: catherine.verfaillie@med.kuleuven.be

Unraveling the role of TREM2 mutations in Alzheimer's disease using human Pluripotent Stem Cells

1. Genome engineering of TREM2 mutant lines

To assess the role of *TREM2* mutations or loss of *TREM2* on human monocyte/microglia function, we created, using CRISPR/Cas9 mediated genome engineering human ESC (H9) with a *TREM2* R47H HE mutation (risk factor for Alzheimer's disease (AD)), with a heterozygous (*TREM2*^{+/-}) and a homozygous (*TREM2*^{-/-}) loss of *TREM2*. We inserted by homologous recombination a donor construct, encompassing the R47H HE point mutation and a 6 kb hygromycin/thymidine kinase selection cassette, in exon 2 of *TREM2*^{+/-}, either in one allele (CRISPR/dCas-nickase + sgRNA A and B) or both alleles (CRISPR/Cas9 + sgRNA B) (schematic). This resulted in *TREM2*^{+/-} and *TREM2*^{-/-}H9-hESC cells. Following excision of the selection cassette via piggyBac Transposase, the R47H HE line was created from the *TREM2*^{+/-} cells. As outlined in Figure 1 A, demonstration of successful targeting and subsequent removal of the selection cassette from the *TREM2*^{+/-} line to create the *TREM2* R47H HE mutant line, was based on GFP expression before and after piggyBac excision. For all lines, correct targeting was confirmed by PCR genotyping (5'JA, 5'RI and Cell PCR) (data not shown), and sequencing of *TREM2* exon 2 (G>A, R47H) (Figure 1B), sequencing of the top 3 predicted off-target sites of each gRNA, array comparative genome hybridization (aCGH), and pluripotency assays (immunohistochemistry and score card) (data not shown).

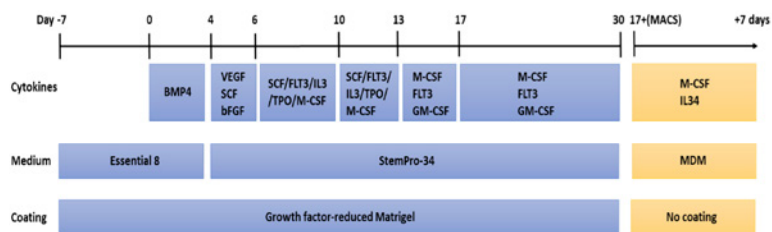


Schematic: Genomic targeting of exon 2 of the human *TREM2* gene by means of CRISPR/Cas9 nickases; The donor construct encompasses the R47H HE mutation and a silent TTA A mutation in the homology arm (HA)1, a selection cassette, an additional TTA A and HA2. Removal of the cassette, between the TTA A sequences and inverted terminal repeats (ITR)(black triangles), was performed by transfection with piggyBac transposase. **Figure 1: (A)** Representative FACS plot for % FITC⁺ cells after positive selection with hygromycin; left to right: H9wt (0% FITC⁺) - H9 *TREM2*^{+/-} clone M16 (100% FITC⁺) - and after subsequent removal of the selection cassette, *TREM2* R47H HE (0% FITC⁺); **(B)** Left: Sequencing of HA1 demonstrating presence of the R47H mutation (G>A) in 1 allele of *TREM2*; Right: After HO targeting of the H9wt line sequencing reveals the presence of the R47H mutation (G>A) in both alleles.

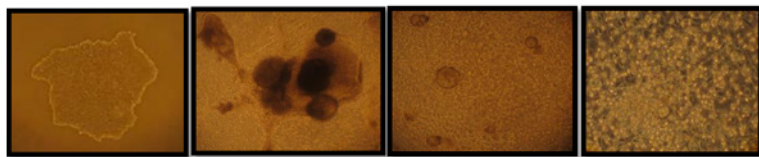
Conclusion: We successfully created *TREM2* R47H HE, *TREM2*^{+/-} and *TREM2*^{-/-} hPSC lines

2. Differentiation of TREM2 mutant hPSC lines towards monocytes and microglia-like cells

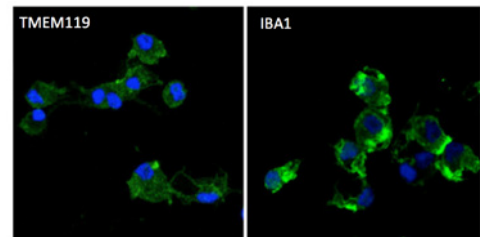
Differentiation to monocytes of all hPSC lines (*TREM2 wt*, *TREM2 R47H HE*, *TREM2^{+/-}* and *TREM2^{-/-}*) was performed using the Yanagimachi protocol (1) (schematic). From D17 onwards, non-attached hPSC progeny (Figure 2a) was subjected to MACS to purify CD14⁺ monocytes. FACS analysis demonstrated that hPSC-monocytes were nearly 100% positive for *CX3CR1* and *CD14* (Figure 2c), and qRT-PCR demonstrated that the cells no longer expressed *OCT4*, but expressed *CD14*, *CD45*, *CCR2*, *TREM2*, *DAP12* and *CX3CR1* (Fig.2d). Differences in *TREM2* expression levels in the different cell lines was confirmed by qRT-PCR (Fig.2d). To transdifferentiate monocytes to microglia-like cells (transdifferentiated microglia-like cells or t-MG), monocytes were plated in microglia differentiation medium (MDM) adapted from Muffat *et al.*, 2016 (2), for 1 week (schematic), a method similar to what has recently been described by Douvaras *et al.*, 2017 (3). t-MG stained positive for *TMEM119* and *IBA1*, and qRT-PCR demonstrates upregulation of multiple microglia related genes including *TMEM119*, *C1Q*, *CST3*, *ApoE*, amongst others, compared to monocytes (Fig.2b,e).



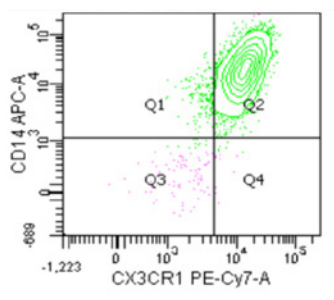
A



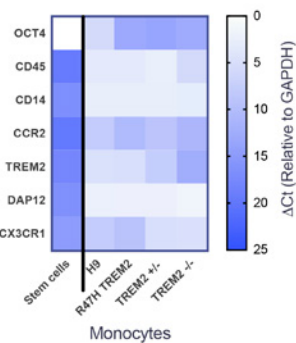
B



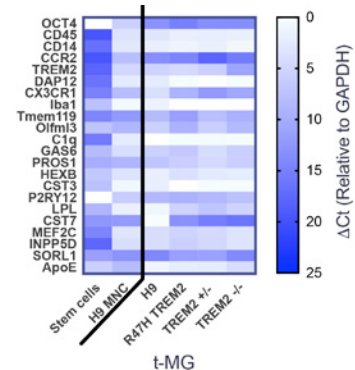
C



D



E



Schematic: Protocol to differentiate hPSC-derived monocytes (based on Yanagimachi *et al.*, 2013) and subsequent differentiation of MACS sorted CD14⁺ cells to tMG, based on medium adapted from Muffat *et al.*, 2016. **Figure 2:** (A) Brightfield images of hPSC-derived monocytes overtime, left to right: D0-D13-D17-D30; (B) ICC confirms expression of *TMEM119* and *IBA1* by tMG after 7 days of culture in supplemented MDM; (C) Representative FACS plot after MACS to purify CD14⁺mo reveals a 97% pure population; MACS can be performed 5 times between D17 and D30; (D) qRT-PCR for *OCT4*, *CD45*, *CD14*, *CCR2*, *TREM2*, *DAP12* and *CX3CR1* confirms expression of monocyte-related genes for mo derived from each line compared to H9wt stem cells. Levels were normalized based on the housekeeping gene *GAPDH*, *N*=3; (E) qRT-PCR of multiple microglia and monocyte-related genes reveals higher expression of microglia specific genes for tMG derived from each line including *C1q*, *ApoE*, *IBA1*, *CST3*, *TMEM119* and *OLFML3* and lower expression of *CCR2* vs. mo. Levels were normalized based on the housekeeping gene *GAPDH*, *N*=3

Conclusion: We successfully differentiated *TREM2 R47H HE*, *TREM2^{+/-}* and *TREM2^{-/-}* hPSC lines to monocytes and microglia-like cells

3. Phagocytosis of pHrodo-linked E.Coli particles by TREM2 mutant hPSC-derived monocytes and microglia-like cells

To test whether human *TREM2* mutant monocytes/t-MGs have abnormal phagocytic function, we studied the ability of the different cells to phagocytose red-labeled *E.Coli* fragments (pHrodo fragments) by FACS. We observed decreased phagocytosis of *TREM2* mutant compared to *TREM2*wt monocytes, with the strongest defects observed for the *TREM2*^{+/-}H9 and *TREM2*^{-/-}H9 monocytes (Fig.3a). Likewise, *TREM2*^{+/-}H9 and *TREM2*^{-/-}H9 tMG, but not *TREM2* R47H HE H9 t-MG displayed a decreased ability to phagocytose pHrodo fragments compared to wt-tMG (Fig.3b). Finally, overall we observed an increased phagocytic efficiency for tMG vs. their monocytic counterpart derived from the same line (Fig.3c).

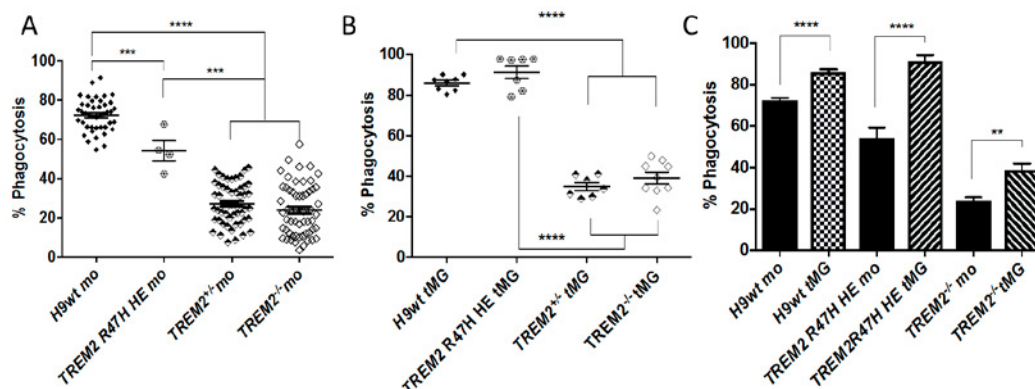


Figure 3: (A,B) Uptake of pHrodo labelled E.Coli fragments by *TREM2*wt, *R47H HE*, *TREM2*^{+/-} and *TREM2*^{-/-} mo (A) and tMG (B); (C) *TREM2*wt, *R47H HE* and *TREM2*^{-/-} tMG phagocytosed significantly more fragments compared to their monocytic counterpart in the same period of time; For each cell line, N≥2. Data represents means with SEM and p-value by unpaired t-test; **p<0.005; ***p<0.001; ****p<0.0001.

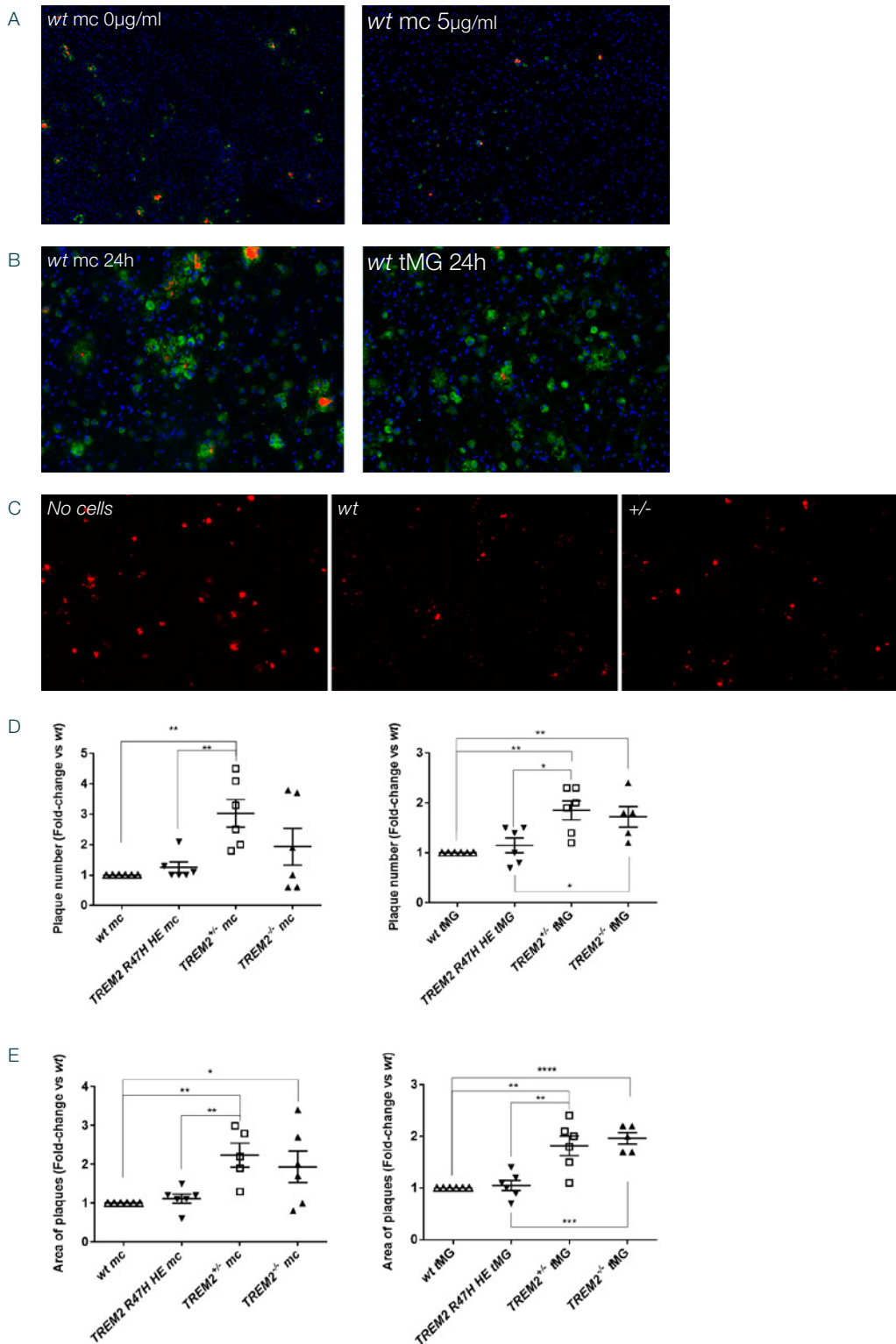
Conclusion: *TREM2*^{+/-} and *TREM2*^{-/-} hPSC-derived monocytes and tMG reveal a severe reduction of phagocytic capacity compared to wt, in contrast to minimal effects observed for *R47H HE* hPSC-derived monocytes and tMG.

4. Amyloid plaque clearance by TREM2 mutant hPSC-derived monocytes and microglia-like cells

To demonstrate a phagocytic defect more relevant to *TREM2*-linked pathologies, we compared the ability of monocytes and t-MG generated from the different hPSC lines to remove amyloid plaques from brain slices of 6 month-old *APP/PS1*^{+/-} mice. Brain slices were cut from snap-frozen material and solely used as a platform to provide human amyloid plaques. To attract monocytes/t-MG to the plaques, we incubated the slices with 5µg/ml mAb11, a murine IgG2a antibody with similar amyloid binding properties as the therapeutically used anti-Ab antibody, Gantenerumab, using the protocol from Xiang et al. 2016 (Fig. 4a). (4) Monocytes or t-MG derived from *TREM2*wt, *TREM2* *R47H HE*, *TREM2*^{+/-} and *TREM2*^{-/-} hPSC were subsequently cultured on the brain slices. To visualize the plaques, we stained the slices with thiazin red, while phagocytic active monocytes and t-MG were labeled with an anti-LAMP1 antibody. (5) Following an initial time-course analysis we conclude that the optimal time point to visualise differences in phagocytosis by wt- and mutant-monocytes was 24h after co-culture, and for wt- vs. mutant-t-MG 16h (Fig. 4b). To analyse amyloid plaque removal, multiple images were taken in the cortex from consecutively cut slices to ensure equal initial plaque load. As a control, no cells were added. Comparative quantification was done for the total number of plaques (bright thiazin red signal) as well as the area correlating with this number (total area of the plaques), between slice sections incubated either with no cells, or with *TREM2*-wt or-mutant monocytes and t-MG (Fig. 4c). Data indicates that cells derived from all lines were able to reduce the total number and area of plaques compared to the control.

However, again, a highly significant decrease in phagocytic ability of *TREM2*^{+/-} and *TREM2*^{-/-} derived monocytes and t-MG, compared to *TREM2*^{wt}, was observed whereas more plaques, correlating with a bigger area, remained present when co-cultured with *TREM2*^{+/-} and *TREM2*^{-/-} -derived cells (Fig.4 d,e). An example of representative images of a thiazine staining used for this analysis, after adding either no cells, wt or *TREM2*^{+/-} monocytes on consecutively cut slices are shown in Figure 4f. This research was conducted in collaboration with the lab of Dr. Tahirovic at the DZNE in Munich, Germany.

Conclusion: This is to our knowledge the first evidence for defective amyloid phagocytosis caused by heterozygous or homozygous loss of *TREM2* in hPSC-derived monocytes and t-MG.



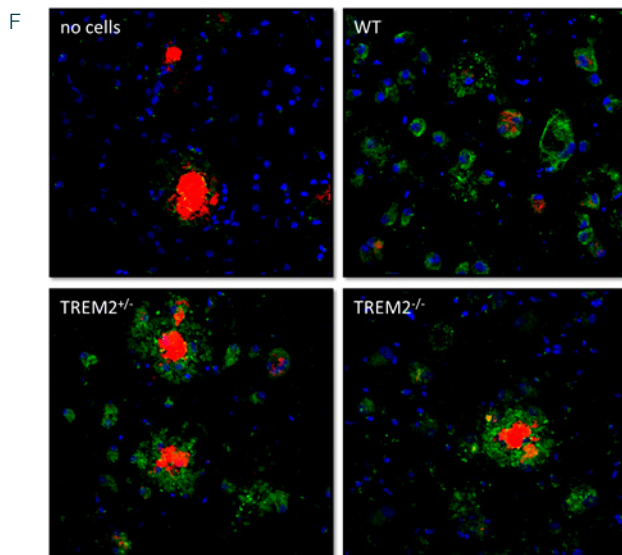


Figure 4: **A)** *APP/PS1^{+/+}* Brain slices were incubated with 0 or 5µg/ml mAb11 and analyzed after 48 hours of culturing with wt monocytes. We observed that wt monocytes degraded amyloid plaques (thiazine red stained) and their halo (3552-stained, green) more efficiently when pre-incubated with the mAb11 antibody; **B)** Staining of amyloid plaques (thiazine red) reveals a lower number of plaques, reflecting enhanced clearance, upon co-culturing of brain slices with LAMP1-stained (green) t-MG compared to monocytes after 24h; **C)** Representative images of amyloid plaques (thiazine red stained) after 24 hours in culture. A clear reduction in the amount of amyloid plaques can be observed after co-culturing of brain slices with wt or *TREM2^{+/+}* monocytes, in comparison to the control where no cells were added; **D-E)** Quantification analysis of amyloid plaque numbers (D) or area (E) based on thiazine red staining upon co-culturing of brain slices with wt, *TREM2 R47H HE*, *TREM2^{+/+}* and *TREM2^{-/-}*-derived monocytes (24h) and microglia-like cells (16h). We detected a higher number of amyloid plaques and larger plaque areas upon co-culturing of brain slices with *TREM2^{+/+}* and *TREM2^{-/-}*-derived monocytes and microglia-like cells compared to wt, reflecting their reduced phagocytic capacity. No difference in number of plaques and plaque area was observed upon co-culture of brain slices with *TREM2 R47H HE* monocytes and tMG compared to wt; Data represents N=3 with duplicates, means with SEM and p-value by unpaired t-test; *p<0.05; **p<0.005; ***p<0.001; ****p<0.0001; **F)** Increased amyloid plaque (thiazine red stained) clearance is observed upon co-culturing of brain slices with wt LAMP1 stained monocytes (green) after 24h compared to *TREM2^{+/+}* and *TREM2^{-/-}*-derived monocytes;

5. Future work

Samples for RNA sequencing were taken from monocytes and microglia-like cells derived from either *wt* or *TREM2^{-/-}* hPSC at different timepoints, with or without co-culturing with the amyloid plaque bearing brain slices. The RNA sequencing data is currently being analyzed. Further work will include deciphering the mechanism of *TREM2*-mediated phagocytic clearance including verification of the data that will be obtained by RNA sequencing. Finally, transplantation of tMG derived from *TREM2* mutant lines in *Rag2^{-/-}CSF1^{h/h}APP/PS1^{+/+}* mice will be performed to establish an improved humanized mouse model to study the contribution of *TREM2* mutated microglia-like cells to AD.

6. References

1. Yanagimachi MD, Niwa A, Tanaka T, Honda-Ozaki F, Nishimoto S, Murata Y, Yasumi T, Ito J, Tomida S, Oshima K, Asaka I, Goto H, Heike T, Nakahata T & Saito MK. Robust and Highly-Efficient Differentiation of Functional Monocytic Cells from Human Pluripotent Stem Cells under Serum- and Feeder Cell-Free Conditions. *PLoS ONE* (2013) **8**: e59243
2. Muffat J, Li Y, Yuan B, Mitalipova M, Omer A, Corcoran S, Bakiasi G, Tsai L-H, Aubourg P, Ransohoff RM & Jaenisch R. Efficient derivation of microglia-like cells from human pluripotent stem cells. *Nature Medicine* (2016) **22**: 1358
3. Douvaras, P. *et al.* Directed Differentiation of Human Pluripotent Stem Cells to Microglia. *STEMCR* **8**, 1516–1524 (2017).
4. Xiang X, Werner G, Bohrmann B, Liesz A, Mazaheri F, Capell A, Feederle R, Knuesel I, Kleinberger G & Haass C. *TREM2* deficiency reduces the efficacy of immunotherapeutic amyloid clearance. *EMBO Molecular Medicine* (2016) **8**: 992
5. Barrachina, M., Maes, T., Buesa, C. & Ferrer, I. Lysosome-associated membrane protein 1 (LAMP-1) in Alzheimer's disease. *Neuropathol Appl Neurobiol* **32**, 505–516 (2006).



Geneeskundige Stichting Koningin Elisabeth
Fondation Médicale Reine Elisabeth
Königin-Elisabeth-Stiftung für Medizin
Queen Elisabeth Medical Foundation

Progress report
of the research group of

Prof. Voets Thomas

Katholieke Universiteit Leuven (KU Leuven)

Principal investigator

Prof. Thomas Voets
Laboratory of Ion Channel Research
VIB-KU Leuven Center for Brain & Disease Research
KU Leuven, Department of Cellular and Molecular Medicine
Herestraat 49 bus 802
3000 Leuven
Belgium
Tel.: +32 16 33 02 17
E-mail: Thomas.voets@kuleuven.vib.be

Table of contents

1. Research program summary
2. Results
3. Identification of the relative role of TRPM3 in acute heat sensing
4. Novel approaches to study the role of TRPM3 in persistent pain
5. Outlook
6. Budget
7. References

Unraveling the role of TRPM3 in neuropathic and inflammatory pain

1. Research program summary:

About 1 in 5 adult Europeans suffer from moderate-to-severe chronic pain, and about half of these chronic pain sufferers report inadequate pain control. Indeed, over-the-counter analgesics such as paracetamol or nonsteroidal anti-inflammatory drugs show limited efficacy in the treatment of severe chronic pain. Opioids such as morphine, hydrocodone or fentanyl are increasingly used as potent analgesic drugs to treat moderate to severe pain, but these cause tolerance and addiction and can have severe adverse effects including the risk of overdose (Reid et al., 2011). Of note, a dramatic increase in the use of prescription and non-prescription opioids has been observed in the last two decades, referred to as the “opioid epidemic”, resulting in an alarming rise in the number of fatalities from prescription opioids and heroin (Wilson-Poe and Moron, 2017). Therefore, there is a large unmet need for newer and safer treatments for pain, which requires identification of potential druggable targets in the pain pathway (Grayson, 2016).

The objective of this project is to better understand the molecular and cellular mechanisms underlying persistent pain in the contexts of nerve damage and inflammation. In particular, we focus on the role of TRPM3, an ion channel expressed in sensory neurons that we have recently identified as a key sensor for acute heat pain and a master regulator of thermal and mechanical hypersensitivity during pathological pain (Vriens et al., 2011; Held et al., 2015; Vriens and Voets, 2018). With this research, we not only aim at a better understanding of fundamental pain mechanisms but also anticipate to provide essential pre-clinical evidence that TRPM3 antagonists may be further developed as novel analgesic drugs for human use.

2. Results

During the first year of the project, we have made important progress in identifying the relative role of TRPM3 in acute pain sensing in relation to other pain receptors, and have established important novel experimental approaches to elucidate how TRPM3 contributes to the altered stimulus sensitivity in sensory neurons and pain behavior in mice.

2.1. Identification of the relative role of TRPM3 in acute heat sensing

At the onset of the project, it was well established that TRPM3 acts as a heat sensor involved in the detection of noxious heat. However, pharmacological inhibition or genetic elimination of TRPM3 in mice provokes only a minor reduction of heat responses in sensory neurons and a moderate increase in response latencies to painful heat stimuli *in vivo*, indicative of the co-existence of multiple heat sensors in these neurons (Vriens et al., 2011; Straub et al., 2013; Vriens et al., 2014).

To understand how TRPM3 contributes to thermal hypersensitivity in pathological conditions such as inflammation or nerve injury, it was essential to first identify the full set of heat sensors in sensory neurons and their relative role in heat-induced pain. We initially focused on TRPV1, also known as the capsaicin/vanilloid receptor, an extensively studied heat-activated channel in sensory neurons. To this aim, we first produced and analyzed double knockout (DKO) mice lacking expression of both TRPM3 and TRPV1 (DKO^{M3/V1} mice). Whereas the number of heat-sensitive sensory neurons was further reduced, we still observed robust heat responses in ~40% of DKO^{M3/V1} neurons. Moreover, DKO^{M3/V1} mice still showed robust behavioral avoidance responses to noxious heat (**Figure 1**).

An important breakthrough was our discovery that the remaining heat responses in $DKO^{M3/V1}$ neurons are mediated by TRPA1, a channel that in mammals has been implicated in the detection of noxious chemicals such as acrolein, mustard oil and H_2O_2 (Bautista et al., 2006), but was not associated with heat sensing. Strikingly, simultaneous pharmacological inhibition of TRPM3, TRPV1 and TRPA1 leads to a nearly complete elimination of heat responses in sensory neurons (**Figure 1DA-C**), and triple knockout (TKO) mice lacking all three TRP channels show a dramatic and specific deficiency in the avoidance of noxious heat (**Figure 1D**). Indeed, in tail flick or hot plate experiments, TKO mice would not withdraw from the noxiously heat stimulus and obtain burn injuries unless the experiment was terminated by the experimenter (**Figure 1D**). In contrast, the TKO mice showed normal pain responses to cold or mechanical stimuli and normal thermal preference. Taken together, these data indicate that TRPM3 is one of three redundant noxious heat sensors - as long as one of these three channels is functional, acute heat sensing is conserved.

These findings are of high importance for the future development of TRPM3 antagonists for chronic pain. In particular, it has been questioned whether TRPM3 inhibition could lead to hyposensitivity to noxious heat, leading to a high risk of burn injury. However, our data indicate that as long as TRPM3 antagonists do not inhibit TRPV1 and TRPA1, acute heat sensing remains largely preserved. A manuscript describing these findings and acknowledging the support of the Queen Elisabeth Medical Foundation is currently under review at *Nature* (Vandewauw et al., 2018).

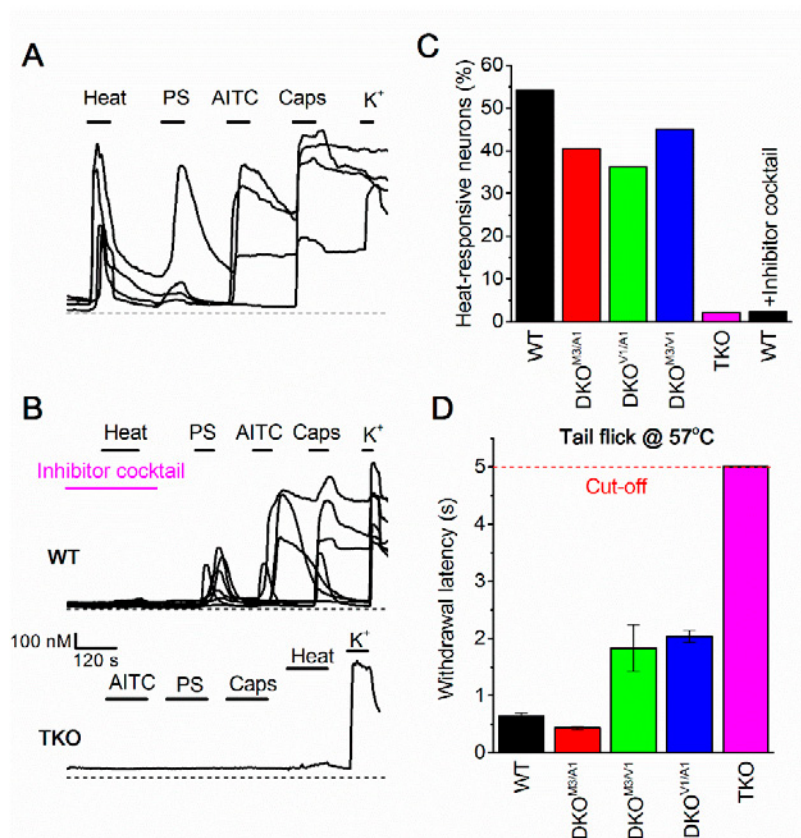


Figure 1: (A) Intracellular calcium responses in mouse sensory neurons stimulated with heat (45 °C) and with agonists of TRPM3 (Pregnenolone sulphate; PS), TRPV1 (Capsaicin) and TRPA1 (Allyl Isothiocyanate; AITC). (B,C) Heat responses are eliminated by combined pharmacological inhibition of the three TRP channels (using isosakuranetin, AMG9810 and HC030031) or by combined genetic elimination in TKO mice. Different DKO mice show robust heat responses. (F) TKO mice lack a withdrawal response to noxious heat.

2.2. Novel approaches to study the role of TRPM3 in persistent pain

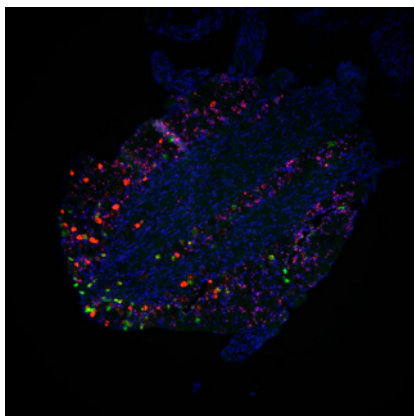


Figure 2: Multiplex fluorescent *in situ* hybridization using RNAscope probes against TRPM3 (magenta), TRPM8 (red) and TRPV1 (green) in a mouse dorsal root ganglion. Nuclei are stained using DAPI (blue).

Based on published and unpublished data showing that pharmacological inhibition or genetic ablation of TRPM3 eliminates thermal hypersensitivity in the context of inflammation and peripheral nerve injury (Vriens et al., 2011; Jia et al., 2017; Vriens and Voets, 2018), we hypothesize that these disease states leads to an upregulation of TRPM3 expression in nociceptor neurons, leading to increased excitability. Alternatively, inhibition of TRPM3 expression and function may modulate the expression and function of other ion channels involved in mechano- and thermosensation.

In the first year of the project, we have established and fine-tuned approaches to assess TRPM3 expression in sensory neurons, and to address whether inhibition of TRPM3 function influences the expression of other genes. First, we have implemented the RNAscope-technology (Wang et al., 2012) to detect the expression at the mRNA level of TRPM3 along with other sensory TRP channels in dorsal root ganglia (DRG; **Figure 2**). In further studies, this approach will allow us to investigate changes in the expression profile of these channels in sensory ganglia innervating inflamed/injured tissue.

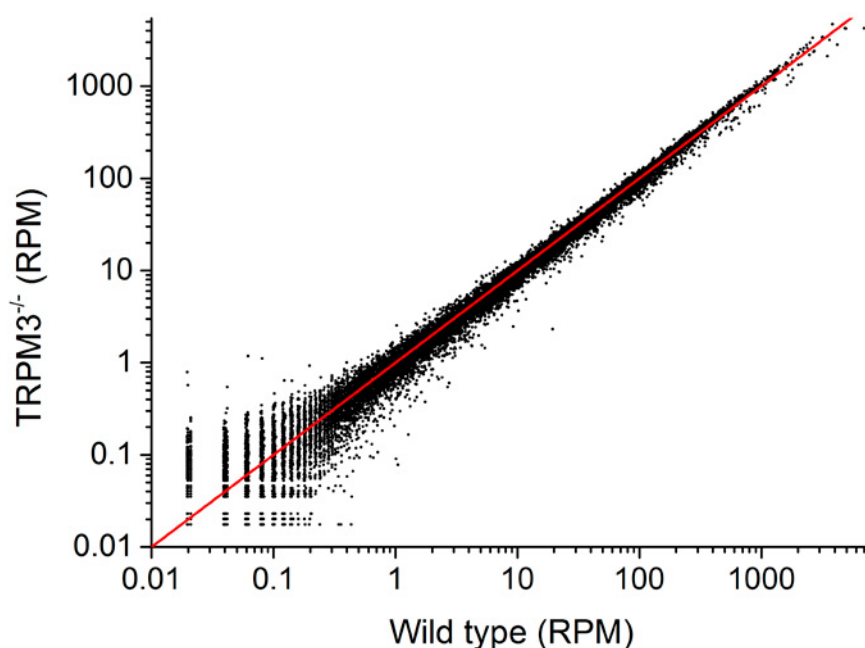


Figure 3: Comparative transcriptome analysis of DRG neurons from wild type and TRPM3^{-/-} mice. Dots represent the number of reads for individual genes, expressed as reads per million reads (RPM), from three mice per genotype.

Second, we have initiated RNA-seq experiments to assess whether TRPM3 deficiency affects the DRG transcriptome. A comparison of wild type and TRPM3^{-/-} neurons of uninjured mice did not reveal any significant changes in the mRNA expression of genes known to be involved in sensory neuron function or other genes that are highly expressed in this tissue (**Figure 3**). In further studies, this approach will be used to assess how inflammation or nerve injury affect the sensory neuron transcriptome, and whether this is influenced by TRPM3 deficiency or inhibition.

Third, we have implemented a Dynamic Weight Bearing (DWB) assay, which allows us to better characterize and automatically quantify ongoing pain in mice (Tetreault et al., 2011). In this assay, mice are allowed to move freely on a surface covered with pressure sensors while they are continuously video-monitored. This allows automated and operator-independent monitoring of the weight on each paw, paw surface, posture and activity. In particular, differences in weight bearing between the ipsi- and contralateral paws provides a good measure of discomfort/pain in the injured paw. In initial experiments, we have shown that injection of the TRPM3 agonist PS into one hind paw leads to a significant reduction in the weight on that paw, thus representing a measure of ongoing TRPM3-dependent pain.

3. Outlook

With the support of the GSKE, our lab has been able to delineate the role of TRPM3 in acute heat sensing, and to establish several new lines of research and novel technology to further decipher the role of TRPM3 in persistent pain.

Ongoing research is now focusing on alterations in expression and function during inflammation and nerve injury, as well as in addressing the full consequences of TRPM3 inhibition on ongoing pain in animal models. In this respect, it is important to note that our research group has recently joined forces with the Centre for Drug Design and Discovery (www.cd3.eu/) and a pharmaceutical company (confidential) to further develop a novel class of TRPM3 antagonists for analgesic treatment in patients. This opens new possibilities to translate the outcomes of the ongoing research towards actual novel therapeutic options for patients with chronic pain.

4. Budget

The 2017 budget received from the Queen Elisabeth Medical Foundation was used for the purchase of an automated Dynamic Weight Bearing system (as outlined in the Results section), as well as to cover part of the costs related to the housing and genotyping of wild type and the different single, double and triple knockout mouse lines used for experiments as described in **Figure 1** and **Figure 3**.

5. References

- Bautista DM, Jordt SE, Nikai T, Tsuruda PR, Read AJ, Poblete J, Yamoah EN, Basbaum AI, Julius D (2006) TRPA1 mediates the inflammatory actions of environmental irritants and proalgesic agents. *Cell* 124:1269-1282.
- Grayson M (2016) Pain. *Nature* 535:S1.
- Held K, Kichko T, De Clercq K, Klaassen H, Van Bree R, Vanherck JC, Marchand A, Reeh PW, Chaltin P, **Voets T**, Vriens J (2015) Activation of TRPM3 by a potent synthetic ligand reveals a role in peptide release. *Proceedings of the National Academy of Sciences of the United States of America* 112:E1363-1372.
- Jia S, Zhang Y, Yu J (2017) Antinociceptive Effects of Isosakuranetin in a Rat Model of Peripheral Neuropathy. *Pharmacology* 100:201-207.
- Reid KJ, Harker J, Bala MM, Truyers C, Kellen E, Bekkering GE, Kleijnen J (2011) Epidemiology of chronic non-cancer pain in Europe: narrative review of prevalence, pain treatments and pain impact. *Current medical research and opinion* 27:449-462.
- Straub I, Krugel U, Mohr F, Teichert J, Rizun O, Konrad M, Oberwinkler J, Schaefer M (2013) Flavanones that selectively inhibit TRPM3 attenuate thermal nociception in vivo. *Molecular pharmacology* 84:736-750.
- Tetreault P, Dansereau MA, Dore-Savard L, Beaudet N, Sarret P (2011) Weight bearing evaluation in inflammatory, neuropathic and cancer chronic pain in freely moving rats. *Physiology & behavior* 104:495-502.
- Vandewauw I, De Clercq K, Mulier M, Held K, Pinto S, Van Ranst N, Segal A, Voet T, Vennekens R, Zimmermann K, Vriens J, **Voets T** (2018) A TRP channel triad mediates acute noxious heat sensing. *Nature* **Under review** (revised version).
- Vriens J, **Voets T** (2018) Sensing the heat with TRPM3. *Pflugers Archiv : European journal of physiology*. **In press**.
- Vriens J, Nilius B, **Voets T** (2014) Peripheral thermosensation in mammals. *Nature reviews Neuroscience* 15:573-589.
- Vriens J, Owsianik G, Hofmann T, Philipp SE, Stab J, Chen X, Benoit M, Xue F, Janssens A, Kerselaers S, Oberwinkler J, Vennekens R, Gudermann T, Nilius B, **Voets T** (2011) TRPM3 is a nociceptor channel involved in the detection of noxious heat. *Neuron* 70:482-494.
- Wang F, Flanagan J, Su N, Wang LC, Bui S, Nielson A, Wu X, Vo HT, Ma XJ, Luo Y (2012) RNAscope: a novel in situ RNA analysis platform for formalin-fixed, paraffin-embedded tissues. *The Journal of molecular diagnostics* : JMD 14:22-29.
- Wilson-Poe AR, Moron JA (2017) The dynamic interaction between pain and opioid misuse. *British journal of pharmacology*.



Geneeskundige Stichting Koningin Elisabeth
Fondation Médicale Reine Elisabeth
Königin-Elisabeth-Stiftung für Medizin
Queen Elisabeth Medical Foundation

Progress report
of the research group of

Prof. dr. Vonck Kristl

Universiteit Gent (UGent)

Principal investigator

Prof. dr. Vonck Kristl
Reference Center for Refractory Epilepsy
Laboratory for Clinical and Experimental Neurophysiology
Institute for Neuroscience
Department of Neurology
Ghent University Hospital
De Pintelaan 185
9000 Gent
Belgium
Tel.: +32 50 61 06 51
E-mail: Kristl.Vonck@UGent.be
www.uzgent.be
H-index: 28

The role of locus coeruleus noradrenergic neurons in the mechanism of vagus nerve stimulation and the effect of selective activation of these neurons in epilepsy.

1. Achieved results 2017

Workpackage 1: Chemogenetic modulation of the locus coeruleus: effect on *normal* hippocampal activity

2. Task 1.1 Validation of DREADD-based modulation of the locus coeruleus (LC)

2.1. Induction of DREADD expression in LC neurons in rats

To selectively induce expression of DREADDs in LC neurons, titration experiments were performed in male rats with different volumes (10nl and 50nl) and concentrations of the adeno-associated viral vector AAV2/7-Prsx8-hM3Dq-mCherry (5.99E12 genome copies/ml) or the control viral vector AAV2/7-Prsx8-eGFP (6.72E12 genome copies/ml) that were injected in the LC (AP +3.9; ML 1.15; DV -6 mm relative to Lambda) using Nanoject II Auto-Nanoliter Injector. Three weeks later, rats were anesthetized and transcardially perfused to extract the brain and to investigate the level of transgene expression by immunofluorescence staining. Expression was reached within the LC but also in more ventral regions in rats injected with 10nl (undiluted) of the mCherry viral vector. To further optimize the expression level and location, this experiment was repeated after adjustment of the injection coordinates (DV -5.7mm below dura) and making use of a different injection method (Quintessential Stereotaxic Injector, Hamilton 1 μ l) with a flow rate of 2nl/min to slow down the diffusion process. Immunofluorescence staining revealed a higher expression rate localized in the dorsal LC. To target the ventral locus coeruleus, a different condition was tested in the left LC of three rats. AAV2/7-Prsx8-hM3Dq-mCherry was injected at -5.7 and -5.9 mm below the dura (10nl undiluted at each location) using the Quintessential Stereotaxic Injector, Hamilton 1 μ l with a flow rate of 2nl/min. Analysis of the expression levels using immunofluorescence staining is currently ongoing.

2.2. Recording of neuronal single unit activity in DREADD expressing LC neurons in anesthetized rats

To validate the functionality of hM3Dq receptors expressed in LC neurons, rats were systemically injected with clozapine-N-Oxide (CNO) (1 mg/kg) or clozapine (0.01,0.03,0.1 mg/kg) to activate the hM3Dq receptor and induce an increase in neuronal firing. Tungsten microelectrodes were positioned in the LC in anesthetized rats (1.5 % isoflurane) three weeks after viral vector injection and single unit activity was recorded.

LC neurons are characterized by particular firing rates for which standard criteria have been defined (see also fig1A). Following the recording of a stable baseline period of 300s, different doses of CNO or clozapine were injected, starting with the lowest dose. Epochs of 300s unit recording data (0.1 Hz, number of spikes/10s) were analyzed after clozapine or CNO injections compared to baseline. Systemic CNO injection (1 mg/kg, s.c., n=3 rats) increased the firing rate in 2 hM3Dq-rats. Systemic clozapine administration with different concentrations (0.01, 0.03, 0.1 mg/kg, s.c., n=2 rats) led to a significant increase in the firing rate in one LC-hM3Dq rat. The lowest dose of clozapine (0.01 mg/kg) increased the firing rate significantly (208.87 spikes/10s \pm 2.08) compared to baseline activity (157 spikes/10s \pm 1.86) ($p < 0.001$, one way repeated measures ANOVA) (fig.1). Administration of higher doses of clozapine (0.03 mg/kg, 0.1 mg/kg) did not lead to an additional increase in firing rate.

To exclude activation of LC-neurons through endogenous receptors after Clozapine injection, rats injected with the AAV2/7-Prsx8-GFP viral vector were used as a control. In all rats, the highest clozapine dose (0.1 mg/kg, s.c.) significantly increased the firing rate compared to baseline. The lowest dose (0.01 mg/kg, s.c.) led to a statistically significant increase in the firing rate (15.17 spikes/10s \pm 0.27, $p < 0.001$) compared to baseline (10.8 spikes/10 s \pm 0.22) in one rat, and decreased the firing rate (16.7 spikes/10s \pm 0.71, $p < 0.001$) compared to baseline (20.3 spikes/10s \pm 1.37). More animals are needed to determine whether these statistical changes are biological significant, as the differences in firing rate appear to be in the normal biological variance of LC neurons.

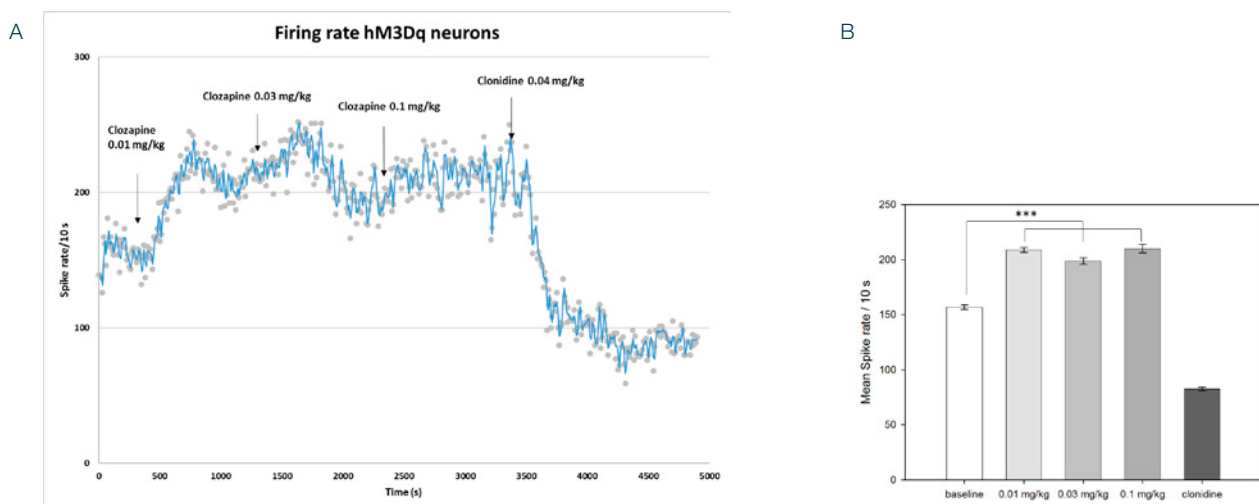


Fig. 1: A. In vivo unit recording data from hM3Dq-expressing LC neurons demonstrating increased firing rate in response to systemic clozapine injections (0.01, 0.03, 0.1 mg/kg, s.c.). The spike rate /10 s is averaged for 5 neurons responsive to a foot pinch. Each point represents the number of spikes per 10s (grey dots, trendline in blue). To have a confirmation that the neurons are LC neurons, clonidine (40µg/kg, s.c.) was injected to evaluate whether the firing rates decreased. B. Mean spike rate/10s for LC-hM3Dq rat (5 cells) for baseline and after clozapine 0.01 mg/kg, 0.03 mg/kg, 0.1 mg/kg and clonidine s.c. injections. We observed a significant increase after 0.01 mg/kg (208.8 spikes/10s \pm 2.08), 0.03 mg/kg (198.8 spikes/10s \pm 2.82) and 0.1 mg/kg (210.17 \pm 3.74) compared to baseline (157 spikes/10s \pm 1.86) ($p < 0.001$, one way ANOVA). No significant difference between the doses of clozapine were observed.

2.3. Measuring hippocampal noradrenalin levels from activation of DREADD expressing LC neurons in anesthetized rats

In a next experiment, the aim was to investigate whether chemogenetic activation of DREADD expressing LC neurons induces significant increases in hippocampal noradrenaline levels. The AAV2/7-Prsx8-hM3Dq-mCherry was injected bilaterally in the LC (n=3, 10 nl, undiluted). Rats injected with AAV2/7-Prsx8-eGFP were used as a control (n=2, 10 nl, undiluted). After a recovery period of three weeks, a microdialysis guide cannula was stereotactically implanted in the left hippocampus. The microdialysis probe was continuously perfused with Ringer's solution at a flow-rate of 0.5 µl/min and hippocampal dialysate samples (10µl) were collected every 20 min. After a baseline period of 4h (12 samples), CNO was injected subcutaneously (1mg/kg) followed by a 4h post-CNO sampling period. Samples are currently being analysed at the Center for Neurosciences using Ultra High Performance Liquid Chromatography (UHPLC) analysis to determine noradrenaline levels.

3. Future Experiments

- Optimizing the expression levels of hM3Dq DREADD in LC neurons

The expression levels of the last injection method, two injections at different DV sites (described in 1.1.1), is currently being analyzed. If this technique is not sufficient to target the whole LC, a different approach will be investigated before performing the microdialysis experiments.

- **Dose-response curve determination for clozapine to activate hM3Dq-LC neurons**
- **Role of the locus coeruleus in hippocampal electrophysiology and noradrenaline levels**

In a next step, we want to investigate whether there is a relationship between LC-induced changes in hippocampal noradrenaline levels and hippocampal electrophysiology. We will inject the AAV2/7-Prsx8-hM3Dq-mCherry or AAV2/7-Prsx8-GFP bilaterally in the LC (10 nl, undiluted) and stereotactically implant a microdialysis guide cannula in the hippocampus to measure hippocampal NA levels. A bipolar recording electrode and bipolar stimulation electrode will be implanted respectively in the dentate gyrus and perforant path to assess the effect of chemogenetic activation of the locus coeruleus (clozapine 0.01 mg/kg, s.c.) on hippocampal electrophysiology and excitability (perforant path evoked potentials).

- **Chemogenetic activation of the locus coeruleus: effect on hippocampal electrophysiology in a model for temporal lobe epilepsy**

As a final experimental step, we aim to investigate the effect of modulating the LC-NA system in the Status Epilepticus (SE) rat model for temporal lobe epilepsy to investigate a potential therapeutic role of chemogenetic LC activation. We know from previous research that hippocampal noradrenaline concentrations are related to VNS-induced anti-epileptic and anti-depressant effects. For these reasons, we will directly modulate the LC, to assess whether this can reproduce the antiepileptic and anti-depressant effects. If the LC plays a role in regulating the hippocampal excitability, it is likely that LC activation has anti-epileptic and anti-depressant effects, whereas LC inhibition leads to proconvulsive and depressive symptoms. We will start by assessing whether chemogenetic LC modulation of hippocampal NA levels and EEG is feasible in epileptic rats. The induction of SE by intraperitoneal injection of KA has been performed many times in our laboratory. Multiple doses of KA (5 mg/kg/hour) are administered until the animals display a behavioral SE characterized by continuous head nodding and salivation and repeated tonic-clonic seizures. In the weeks following SE, rats develop spontaneous seizures that exponentially increase in number up to a plateau phase. This plateau phase is generally reached around 20 weeks after SE. At this time, rats will be bilaterally injected with the AAV-PRsx8-DREADD-mCherry or AAV-PRsx8-mCherry viral vector in the LC. Microdialysis cannulas and bipolar recording/stimulation electrodes can be implanted in the hippocampus to measure hippocampal NA and EEG. After a recovery period, a baseline period will be followed by chemogenetic activation of the LC (clozapine 0.01 mg/kg, s.c.) to determine its effect on epileptic spikes and fast ripples on the EEG, the hippocampal excitability (evoked potentials) in combination with NA levels. Finally, we will evaluate the effects of DREADD-based LC modulation on the frequency of spontaneous seizures. Continuous (24h/7d) video-EEG monitoring will be performed to determine baseline seizure frequency in the SE model. This will be followed by repeated CNO injections (dependent on the duration of the effect seen in 2.1.1) for two weeks to determine the effects on seizure frequency.

4. Publications

- Latoya Stevens, Robrecht Raedt, Wouter Van Lysebettens, Paul Boon, Kristl Vonck. Induction of DREADD expression in LC rats and its effects on neuronal firing. (Abstract in preparation for submission to SWO, Amsterdam, The Netherlands and submission ECE, Vienna, Austria)
- Latoya Stevens*, Wouter Van Lysebettens*, Kristl Vonck, Paul Boon, Robrecht Raedt. Noradrenergic modulation of brain excitability. (Review in preparation)



Geneeskundige Stichting Koningin Elisabeth
Fondation Médicale Reine Elisabeth
Königin-Elisabeth-Stiftung für Medizin
Queen Elisabeth Medical Foundation

Geneeskundige Stichting Koningin Elisabeth – G.S.K.E.

Fondation Médicale Reine Elisabeth – F.M.R.E.

Queen Elisabeth Medical Foundation – Q.E.M.F.

Mailing address:

The scientifique director:

Prof. dr. Jean-Marie Maloteaux
3, avenue J.J. Crocq laan
1020 Bruxelles - Brussel
Belgium
Tel.: +32 2 478 35 56
E-mail: jean-marie.maloteaux@uclouvain.be

and

Secretary:

Mr. Erik Dhondt
3, avenue J.J. Crocq laan
1020 Bruxelles - Brussel
Belgium
Tel.: +32 2 478 35 56
E-mail: fmre.gske@skynet.be
E-mail: erik.dhondt@skynet.be, e.l.dhondt@skynet.be
www.fmre-gske.be
www.fmre-gske.eu
www.fmre-gske.com